UNIVERSITY OF SOUTHAMPTON

School of Electronics and Computer Science

Type-Spread and Multiple-Access Molecular Communications

by

Weidong Gao

BEng, MSc

ORCiD:0000-0002-3361-9614

February 2023

SUPERVISOR: Professor Lie-Liang Yang and Dr Terrence Mak

BEng, MEng, PhD, FIEEE, FIET

Professor of Communications, Southampton Wireless Group

School of Electronics and Computer Science University of Southampton

Southampton SO17 1BJ

United Kingdom

Dedicated to my family

UNIVERSITY OF SOUTHAMPTON

ABSTRACT

School of Electronics and Computer Science
Faculty of Physical Science and Engineering

Doctor of Philosophy

Type-Spread and Multiple-Access Molecular Communications

by Weidong Gao

Molecular communications (MC) is a communication paradigm inspired by biology, which employs chemical molecules to convey information. Owing to its tiny transceivers, energy-efficient propagation, and biocompatibility, MC has been regarded as a promising nano/micro-scale communication method that is feasible for information transmission in some scenarios challenging to the conventional electromagnetic communications, such as, inter/intra living cells and other organisms. In this thesis, all the researches are based on diffusive molecular communications (DMC), because of the fact that free diffusion is the most common propagation mechanism in natural occasions.

More specifically, the thesis first introduces the motivation and challenges of DMC, as well as the retrospect background and related work of DMC, including channel modeling, modulation schemes, multiple access techniques, interference mitigation, and signal detection. In DMC, inter-symbol interference (ISI) is recognized as one of the important hindrances to the practical deployment of DMC. Therefore, in the thesis, an information modulation scheme called type-spread molecular shift keying (TS-MoSK) is firstly proposed for DMC, which is characterized by introducing extra types of molecules for ISI mitigation (ISIM). In order to mitigate ISI further, two ISIM methods are introduced to the TS-MoSK modulated DMC systems, which are the active ISIM and passive ISIM. Furthermore, the TS-MoSK modulated DMC scheme is extended to support multiple nano-machines (NMs) to simultaneously transmit information to a common access point (AP) or an information fusion center (FC), forming the multi-access type-spreading molecular shift keying (MTS-MoSK) DMC system.

In the context of the MTS-MoSK DMC systems, firstly, two detection schemes, namely, the maximum selection assisted majority vote detection (MS-MVD) and equal gain combining detection (EGCD), are proposed to achieve signal detection. To compare the error performance of the MTS-MoSK DMC systems with both detection schemes, the bit-error rate (BER) performance of MTS-MoSK DMC systems is studied based on both the analytical results and simulations. In MTS-MoSK DMC systems, there exist different types of interference, including multiple-access Interference (MAI), ISI and noise, in which MAI and ISI may severely impact the achievable performance. Hence, in order to mitigate MAI and achieve more reliable communications, a range of MAI cancellation schemes are designed based on two fundamental detectors, namely threshold-assisted majority vote detector (TMVD) and EGCD. These MAI cancellation schemes are the

TMVD-assisted minimum-distance decoding based interference cancellation (TMVD-MDDIC), TMVD-assisted iterative interference cancellation (TMVD-IIC), the EGCD-assisted N-order iterative interference cancellation (EGCD-NIIC) and EGC-based interference mitigation (EGC-IM). Moreover, following the principle of maximum likelihood detection, a simplified approximate maximum likelihood (SAML) detection scheme is proposed to provide a near-optimal criteria for measuring the achievable error performance. The BER performance of the MTS-MoSK DMC systems employing respectively the considered detection schemes is comprehensively studied and compared. Furthermore, the complexity of these detection schemes is analyzed and compared.

Our studies with the MTS-MoSK DMC systems demonstrate that the MTS-MoSK DMC with an effective interference mitigation scheme is efficient for MAI and ISI mitigation and hence, achieving promising performance. However, the MTS-MoSK DMC schemes are relied on multiple types of molecules for supporting multiple-access transmission, which may be hard to implement in some practical DMC environments. To mitigate this problem and furthermore, to address the practical DMC environments where the distances between NMs and AP may be different, a molecular code-division multiple-access (MoCDMA) scheme relying only on two types of molecules is proposed and studied. As different distances result in the 'near-far' effect, the uniform and channel-inverse based molecule-emission schemes are proposed for NMs to emit molecules. For signal detection at AP, different representations of received signals are derived. Correspondingly, three symbol-by-symbol detectors with low-complexity are proposed following the principles of matched-filtering (MF), zero-forcing (ZF) and minimum mean-square error (MMSE), respectively. Furthermore, the complexity and reliability of various detection schemes are analyzed and compared with the motivation to attain a good trade-off.

Finally, continuing on the MoCDMA with the motivation to mitigate ISI (called inter-chip interference (ICI) specifically in MoCDMA) and MAI, three frequency-domain equalizers (FDEs) in the principles of MF, ZF, and MMSE are proposed for ICI mitigation. Furthermore, the one/two-stage decision-feedback successive interference cancellation (DF-SIC) schemes are proposed to mitigate MAI.

Overall, the thesis motivates to propose and investigate the multiple-access schemes for operation in DMC environments and the associated detection schemes of relatively low-complexity. Two multiple-access schemes, namely MTS-MoSK and MoCDMA, and corresponding detection schemes are proposed and studied. The error performance of the multiple-access systems with various detection schemes are comprehensively studied and compared. The studies show that both MTS-MoSK and MoCDMA are effective for supporting multiple-access transmissions in DMC. Depending on a DMC environment, MTS-MoSK or MoCDMA with an appropriate detection scheme is capable of striking a good trade-off between detection reliability and implementational complexity.

Declaration of Authorship

I, **Weidong Gao**, declare that the thesis entitled **Type-Spread and Multiple-Access Molecular Communications** and the work presented in it are my own and has been generated by me as the result of my own original research. I confirm that:

- This work was done wholly or mainly while in candidature for a research degree at this University;
- Where any part of this thesis has previously been submitted for a degree or any other qualification at this University or any other institution, this has been clearly stated;
- Where I have consulted the published work of others, this is always clearly attributed;
- Where I have quoted from the work of others, the source is always given. With the exception of such quotations, this thesis is entirely my own work;
- I have acknowledged all main sources of help;
- Where the thesis is based on work done by myself jointly with others, I have made clear exactly what was done by others and what I have contributed myself;
- Parts of this work have been published.

Signed: ..... Date: .....

Acknowledgements

First of all, I would like to give my sincere gratitude to my supervisor Prof. Lie-Liang Yang for his excellent and careful supervision and support. His patience, encouragement, guidance, and inspiration helped me at the research and writing of this thesis. Secondly, I would like to thank my colleagues in NGW group, and the university staff for their help. I also thank all my friends. In particular, I would like to expressly mention Lu Shi and Yuankun Tang, for their invaluable help and advice on every occasion needed and for making my study more enjoyable. Last but not the least, I would like to thank my family, and especially my parents, for their constant love and support during my study. Their endless support was a key factor for me in completing this degree.

List of Publications

Journal Papaers

1. **Weidong Gao**, Terrence Mak, Lie-liang Yang, Molecular Type Spread Molecular Shift Keying for Multiple-Access Diffusive Molecular Communications, ***IEEE Transactions on Molecular, Biological and Multi-Scale Communications***, vol. 7, no. 1, pp. 51-63, March 2021, doi: 10.1109/TMBMC.2020.3041182.

2. **Weidong Gao**, Terrence Mak, Lie-liang Yang, Equal-gain combining with interference mitigation for molecular type hopping assisted molecular shift keying systems, ***ITU Journal on Future and Evolving Technologies***, Volume 2 (2021), Issue 2, Pages 157-164, December 2021, doi: https://doi.org/10.52953/NMLF1506.

3. **Weidong Gao**, Lie-liang Yang, Interference Mitigation Enabled Signal Detection in Molecular Type Spreading Assisted Molecular Shift Keying Systems, (submitted to ***IEEE Internet of Things Journal***).

4. **Weidong Gao**, Lu Shi, Lie-liang Yang, Molecular Code-Division Multiple-Access: Signaling, Detection and Performance, (submitted to ***IEEE Internet of Things Journal***).

5. **Weidong Gao**, Lu Shi, Lie-liang Yang,Frequency-Domain Detection and Interference Cancellation for Molecular Code-Division Multiple-Access

Conference Papers

1. **Weidong Gao**, Lie-liang Yang, Type-Spread Molecular Communications: Principles and Inter-Symbol Interference Mitigation, ***ICC 2019 - 2019 IEEE International Conference on Communications (ICC)***, 2019, pp. 1-6, doi: 10.1109/ICC.2019.8761545.

Contents

Glossary

3D: 3-dimensional

AP: access point

ASK: amplitude shifting keying

BCSK: binary concentration shifting keying

BDSK: binary direction shift keying

BER: bit error ratio

BMoSK: binary molecular shift keying

BPSK: binary phase-shift keying

BTC: best-to-closest

BTF: best-to-furthest

CDF: cumulative density function

CDMA: code-division multiple-access

CIR: channel impulse response

CP: cyclic prefix

CSK: concentration shifting keying

DF: decision feedback

DFE: decision-feedback equalizer

DMC: diffusion-based molecular communication

DMCs: diffusion-based molecular communications

EGCD: equal-gain combining detection

FC: fusion center

FDEs: F-domain equalizers

FDMA: frequency-division multiple-access

FFH: fast frequency-hopping

FFT: fast Fourier transform

FoCQ: fairness of communication quality

FSK: frequency shift keying

IBI: inter-block interference

ICI: inter-chip interference

IIC: iterative interference cancellation

IM: interference mitigation

IoBNT: internet of bio-nano things

IoMT: internet of medical things

IoT: internet of things

ISI: inter-symbol interference

ISIC: ISI cancellation

ISIM: ISI mitigation

LEQ: linear equalizer

MA: multiple-access

MAI: multiple-access interference

MAMC: multiple-access molecular communication

MAP: maximum a-posteriori

MCSK: molecular concentration shift keying

MDDIC: minimum-distance decoding based interference cancellation

MDMA: molecular division multiple-access

MF: matched-filtering

MFSK: molecular frequency shift keying

MIMO: multiple-input multiple-output

ML: maximum likelihood

MLS: maximum length sequence

MMSE: minimum mean-square error

MoCDMA: molecular code-division multiple-access

MoSDMA: molecular space-division multiple-access

MoSK: molecular shifting keying

MoTDMA: molecular time-division multiple-access

MPPM: molecular pulse position modulation

MRC: maximal ratio combining

MSE: mean-square error

MSN: molecular sensor network

MTS: molecular type-spread

MS-MVD: maximum selection assisted majority vote detection

MSIC: multistage successive interference cancellation

NIIC: N-order iterative interference cancellation

NMs: nano-machines

NUs: nano-users

OFDM: orthogonal frequency-division multiplexing

OOK: on-off keying

PDF: probability density function

PMF: probability mass function

PPM: pulse position modulation

PSK: phase-shift keying

RdCDMA: radio-based CDMA

RS: Reed-Solomon

SAML: simplified approximate maximum likelihood

SNR: signal-to-noise ratio

SIC: successive interference cancellation

SINR: signal to interference-plus-noise ratio

TDMA: time-division multiple-access

TMVD: threshold-assisted majority vote detector

TS: type-spread

ZF: zero-forcing

List of Symbols

Special Operation

$\lvert\cdot\rvert$:	Absolute value.
$\lVert\cdot\rVert^2$:	Euclidean norm operation.
$(\cdot)^H$:	Hermitian transpose of a matrix.
$(\cdot)^T$:	Transpose of a matrix.
$(\cdot)^*+$:	Pseudo inversion
$(\cdot)^*$:	Conjugate of a complex symbol/vector/matrix.
$\lfloor\cdot\rfloor$:	Rounding a numerical value to the nearest integer lower than the value.
$\oplus$:	Addition in the Galois field.
$\sum$:	Summation operation.
$\prod$:	Product operation.
$\int$:	Integration.
$E[\cdot]$:	Expectation operation.
$\exp(\cdot)$:	Exponential function.
$\log(\cdot)$:	Logarithm function.
$\ln(\cdot)$:	Natural logarithm function.
$\max(\cdot)$:	Maximum function.
$\min(\cdot)$:	Minimum function.
$\mathbf{Var}(\cdot)$:	Variance of a random variable.
$\mathrm{diag}(\cdot)$:	Diagonalizing operation.

Chapter 1

Introduction and Backgrounds

1.1 Motivation

The speech of Richard Feynman on the nanotechnology concept first drew researchers' attention to producing and controlling molecular or atomic scale devices to complete some particular tasks at microscopic dimensions [1]. Referring to Moore's Law, the component density has increased rapidly in the last several decades and nano-machines (NMs) have reduced in size and been capable of accomplishing simple tasks. Since the global pandemic of COVID-19, the attention of researchers in the field of internet of things (IoT) has emphasised on the internet of medical things (IoMT) [2, 3], where nano-devices, such as NMs, have the potential to play important roles [4]. However, due to the limited storage space and computing power of individual NMs [5], a number of, or even many NMs are expected to be able to collaborate with each other to accomplish complicated tasks and to conduct network communications in nano-/micro-scale [6]. This kind of bio-related IoT at the microscopic scale is classified as the internet of bio-nano things (IoBNT) in literature [7], which has been regarded as one of the important technologies in the future 6G/7G communications.

When IoBNT is capable of conducting the intra-body communication networking, it will undoubtly revolutionize numerous intelligent medical applications, such as targeted drug delivery [8, 9], disease diagnosis and treatment [10, 11], and health monitoring [12, 13], etc. For instance, unlike conventional vascular injection and oral medication, the targeted drug delivery aims at leading NMs to emit drugs precisely at pathological organ tissues. Therefore, a feasible solution to the targeted drug delivery is that the NMs carrying drugs are capable of exchanging information for positioning and pathfinding via the intra-body fluid medium (channel) [14]. The targeted drug delivery can not only transport specific drugs to the target organisms or tissues with high efficiency, but also prevent drugs from spreading to the other irrelevant locations to reduce side effects.

IoBNT is a paradigm applied to the microscopic scale communication scenarios, where chan-

nels are usually the fluid environments. Explicitly, the conventional electromagnetic communication methods are not suitable for implementation in this kind of nano-scale environment due to their large size, high power consumption and complexity [15], and bio-imcompatibility [16]. Inspired by the existing communication phenomena happening in nature, molecular communication (MC) whose information carrier is molecules conveys information between NMs [17]. To be specific, the advantages of MC can be summarized in literature as follows:
1) Compatibility: NMs embedded in biology implement communications by transmitting and receiving molecular chemical signals, similar to the existing communication paradigms between living cells. In addition, biological cells are likely to be modified to form the foundation for designing MC transceivers that are friendly for operation intra-body [17].
2) Low power consumption: A large number of MC examples in nature are based on free diffusion, which does not require additional power supplements. On the other hand, NMs designed from biological cells are able to consume chemical energy (such as glucose, ATP), which can be directly drawn from the intra-body environment [18].
3) Small size: As NMs designed in the principle of MC do not rely on long antennas to transmit or receive signals, the size of nano-transceivers can be reduced significantly.

However, the implementation of MC systems still meets a lot of challenges, some of which are as follows:
1) Validity of channel modeling: First, in most researches on MC, the transceivers are assumed to be in static locations, which ignore the mobility of molecular transceivers. This static model is not suitable for numerous practically complex scenarios [19]. Moreover, in most investigations on diffusive MC (DMC), the diffusion coefficient is assumed to be stable and unchanged. However, the fluid medium is very complicated in realistic, in which the diffusion coefficient of information molecules is relied on the environment and is likely to be time-variant. Thus, time-varying diffusive channel models are required to be considered in some MC scenarios [20]. What is more, in literature, a large number of researches assume MC channels as a 3-D space without boundaries, which is also impractical in many MC environments. Thus, the modelling of MC channels by considering various application scenarios needs further investigating. [21]
2) Limitations of nano-devices: Due to the tiny size of nano-devices, nano-transmitters have very limited spaces for molecule storage and the power supplementation for signalling, on the other side, nano-receivers cannot bear the signal processing with high complexity and provide the completely accurate recognition because of manufacturing constraints. [5]

Overall, while MC has great potential for implementation of IoBNT on the microscopic scale, there are still many challenging issues that are very different from the conventional radio-based communications. The theme of this thesis is MC at micro-/nano-scale, which tries to address some challenges as above-mentioned.

1.2 Background for Research

The state-of-art researches in the field of MC focus mainly on the physical layer techniques at the microscopic scale, including channel modelling, modulation, channel coding, signal detection, and performance of MC systems. In the following subsections, we review channel modelling, modulation schemes, multiple-access techniques, and signal detection for MC systems and with an emphasis on the multiple-access techniques as well as the associated signal detection.

1.2.1 Channel Modeling

MC transmits information via the propagation of information molecules. According to the different molecular propagation ways in nature, some molecular propagation mechanisms have been investigated in association with the channel modelling in MC, which include free diffusion [22, 23], diffusion with drift [24], molecular motors [25], gap junctions [26], and bacterial motors [27]. In more detail, free diffusion-based MC drives molecules to propagate in fluid medium by Brownian motion, which is the most common and essential molecular propagation in nature [28]. Compared to the MC systems based on the other propagation mechanisms, diffusion-based molecular communication (DMC) systems have some advantages. First, unlike the MC based on molecular motors, no external power supplement is needed to transport molecules in DMC [25]. Second, different from the MC based on gap junctions, the special fundamental infrastructure is not required [26]. Third, in comparison with the MC based on bacterial motors, some inducers like a food concentration gradient are not needed [27]. Based on these advantages, therefore, our works in this thesis are all based on the DMC system model, owing to its wide application opportunities in MC.

As the research of other communication techniques, at the very beginning, the investigation in DMC focused mainly on the physical channel modelling. To model DMC channels, not only the characteristics of the molecular propagation process need to be considered, but some other details such as influences of transmitter mechanisms and receiver mechanisms considering the whole end-to-end channel modelling also need to analyze.

For example, in DMC, the receptions can in general be categorized into passive reception and active absorptive reception. The passive reception does not affect the movement of molecules and is capable of sensing the molecular concentration without reaction or absorption [29, 30]. By contrast, the active reception detects signal molecules by fully or partially absorbing the information molecules via chemical reaction or binding to the receptors of receiver [23, 31, 32]. In literature, the closed-form expression of ligand-receptor noise was given in [23]. In [31, 32], the authors derived the closed-form expressions for the channel impulse response (CIR) for the DMC systems with reactive receptions, where the reactions of binding of signal molecules are reversible. This CIR takes account of the diffusion and reaction processes jointly.

Some properties of transmitter in DMC can also affect the CIR of DMC channels, which in-

clude the geometric features of transmitter and the molecular emission mechanisms implemented in transmitter. In literature, the most widely used assumption for transmitter is deeming it as a point source for the sake of its simplicity. In this case, the effect of geometric features, including the volume and shape of the transmitter, does not need to be considered. Moreover, it is usually assumed that the point transmitter emits every impulse of molecules instantaneously into medium. By contrast, the volume transmitter takes the distribution of molecules produced within the transmitter into account. For example, the authors of [33] provided the CIR of the volume transmitter with molecules uniformly distributed in the transmitter. The above transmitter models are also under the assumption that the boundaries of transmitters are transparent and do not affect molecules moving through them. However, in some transmitter models, the emission mechanisms are very different from the above-mentioned. For example, in [34], the authors introduced the model for the ion-channel-based transmitters, where a so-called gating parameter controls whether molecules can leave transmitters to the medium. In [35], a novel modulation scheme referred to as direction shift keying was designed based on the assumption that the transmitters are capable of pumping molecules in some specific directions. In the same reference, the concentration of molecules in the 3-D DMC channel was analyzed, when the direction shift keying is employed.

In DMC systems, the CIR is also likely to be influenced by the different factors of physical channels, including the velocity vector of flow in fluid medium, the geometry of channels, and the degradation during the diffusive process. In the unbounded diffusion channels without advection, the CIR is only related to diffusion and is simply described by Fick's second law. In [36], a circular duct-bounded channel model with uniform advection was considered, which is useful to model the blood vessel networks. An analytical equation for the CIR of a partially absorptive rectangular-duct channel is derived in [37]. In [38], the authors took the Michaelis-Menten reaction mechanism into consideration and derived a CIR for the degraded diffusive channel, where signal molecules react with enzymes.

Besides the above factors affecting the CIR of DMC channels, DMC channels also experience various types of noise, such as counting noise and sampling noise [39, 40]. In this thesis, only the counting noise is considered, which is because of the Brownian motion of molecules resulting in the uncertainty of observation. In more detail, due to the uncertainty of diffusive process, there is a difference between the observed concentration of molecules (or the number of molecules) within the detection space of receiver and the expected concentration of molecules (or the number of molecules) evaluated according to the CIR equation. Thus, the counting noise in DMC is relevant to the number of molecules emitted by transmitter and that of residual molecules in the diffusive medium. In other words, the counting noise is dependent on both the pulse of molecules emitted for the current symbol transmission and that emitted for the previous symbol transmission. This property of DMC is sharply different from the radio-based communications, where additive Gaussian noise is added at receiver, which is usually different from the transmission process.

In this thesis, our focus is on the multiple-access transmission in DMC, we assume the relatively

simple channel models consisting of passive receiver, point transmitter, unbounded propagation channels, and counting noise.

1.2.2 Modulation Schemes

After the early stage research on DMC channel models, various molecular modulation schemes have been designed and investigated. According to the different information carriers employed, molecular modulation schemes can be divided into three categories: molecular type-based, concentration-based, and releasing time-based modulations. Specifically, in the type-based modulation schemes, different symbols are mapped to the corresponding molecular types. Molecular Shift Keying (MoSK) is a primary type-based modulation scheme that employs M types of molecules to represent $log_2 M$ bits per symbol [41]. In the concentration-based modulation schemes, information is encoded into the amplitude of molecular concentration [41]. For instance, on-off keying (OOK) modulation transmits binary information by either no transmission or emitting a pulse of molecules. In the general concentration shift keying (CSK), concentration thresholds are used to distinguish the different levels of concentrations representing different symbols. Compared to the CSK modulation scheme, MoSK usually achieves better error performance, because it naturally has some capability to overcome inter-symbol interference (ISI) by employing several types of molecules to transmit information. However, relying on multiple types of molecules for transmission, MoSK modulation scheme results in a relatively high complexity of transceiver design. Finally, pulse position modulation (PPM), which is releasing time-based, controls the emitting time of molecular pulses to encode information to various time shifts of the molecular pulses [42]. To implement this type of modulation schemes, precise time synchronizations between transmitter and receiver are required. Note that in DMC, the most popular modulation schemes are the molecular type and concentration based modulation schemes. In this thesis, we mainly consider the MoSK and CSK.

1.2.3 Multiple Access Techniques

Due to the limited storage space and computing power, an individual NM is usually unable to accomplish complicated tasks [43]. Relatively complex tasks can only be accomplished by the nano-networks relying on the collaboration among individual NMs, where multiple access techniques play a crucial role. Inspired by the numerous multiple access techniques studied in conventional radio-based communications, multiple access in MC has also been investigated from different domains [44–52]. Specifically, inspired by the principle of neural network, [53–55] employed the mechanism of neurons to implement multiple access. On the other hand, many researchers have proposed, the multiple-access schemes by exploiting the characteristic of DMC channels, which can be categorized into multiple-access diffusion molecular communication (MADMC). First, the most straightforward one is the molecular division multiple-access (MDMA) [44, 45], which is more or less an analogy to the frequency division multiple-access (FDMA) in the conventional

radio-based wireless communications. With MDMA, different NMs sharing a common DMC environment simultaneously communicate with a common receiver via orthogonal channels explained by the different types of molecules. Hence, in MDMA systems, there is no multiple access interference (MAI). However, the receiver is required to be capable of sensing numerous different types of molecules, when there are many NMs transmitting messages simultaneously. In this case, a high MDMA demands complexity for implementation. Multiple-access DMC can also be achieved in the time-domain using molecular time-division multiple-access (MoTDMA) [46–48]. To conduct MoTDMA, frames are formed in the time domain, and each frame is divided into some time slots. These time slots are allocated to different NMs for individual transmissions to achieve multiple access transmission. In this way, within one time slot, there is only one NM transmitting messages relying on one type of molecule. However, MoTDMA is highly relied on the time schedules to achieve good synchronization so as to mitigate MAI, which is often difficult to achieve in practical DMC systems. This is because in DMC systems, the channel impulse response (CIR) is highly sensitive to the transmission distance, resulting in the shapes of received pulses from different nano-transmitters being extremely different if the nano-transmitters have different distances from the receiver [56]. Furthermore, DMC channels are highly dispersive, which have very long tails, resulting in MAI and ISI. In addition, molecular space-division multiple-access (MoSDMA) can also be an alternative technique supporting multiple-access DMC [49, 50]. In principle, MoSDMA exploits the tremendous impact of transmission distance on the CIR in DMC. With MoSDMA, the receiver can distinguish the information pulses sent from different NMs based on the shapes of CIRs. However, MoSDMA relies significantly on the instantaneous information about the channels from different NMs, which are hard to estimate due to the MAI and ISI. Furthermore, the principle of CDMA can also be applied to achieve multiple-access DMC, implementing the MoCDMA [51, 52]. Like the conventional CDMA in the radio-based wireless systems, MoCDMA assigns different NMs different signatures to spread messages, which are also used by the receiver to de-spread and distinguish the information conveyed by the different NM. MoCDMA has the advantage that it does not require a large number of molecular types and also strict synchronization. However, the receiver is required to employ certain computing power to mitigate interference and detect information. In this thesis, two types of multiple access schemes are proposed and studied, which are the time-hopping MoSK and MoCDMA.

1.2.4 Interference Mitigation and Signal Detection

Due to the slow diffusion process in DMC, the transmission of information in DMC system experiences severe ISI. Hence, along with the signal detection in DMC, the mitigation of ISI has been a hotspot investigated by many researchers. Specifically, following the philosophy of conventional wireless communications, maximum *a-posteriori* (MAP), maximum likelihood (ML), etc., have been introduced to DMC systems to design the sequence detections [30, 57, 58]. Though MAP or ML is able to achieve optimal detection, its complexity increases exponentially with the length of

ISI, which is infeasible for implementation with the nano-devices having low computing power. Instead, it is usually used as a criterion to evaluate the other detection schemes. In literature, the adaptive decision-feedback equalizer (DFE) and minimum mean-square error (MMSE) equalizer with relatively lower complexity have also been considered [30, 59]. However, all these are coherent detectors, which are highly dependent on the acknowledgement of channel impulse response (CIR). As shown in [60], even a small channel estimation error is likely to cause a severe decline in reliability. Theoretically, the CIR can be estimated in some simple models according to some given system parameters. However, in the more realistic DMC channels, accurate channel estimation is difficult to achieve. Without the acknowledgement of CIR, non-coherent detectors have to be implemented, which conduct detection at relatively low complexity by exploiting the characteristics of received signals. As some examples, in [61], an adaptive threshold detection scheme was proposed for OOK modulation, which uses the observation of the previous signal as a threshold to detect the current signal. Furthermore, by exploiting the transient features of molecular signals, in [62], a high-dimensional metric for received signals is generated, which transfers the original signal to a new domain that is relatively insensitive to the ISI. In general, due to the lack of CIR acknowledgement, the error performance of non-coherent detectors is usually inferior to that of coherent detectors. On the other hand, the characteristics that non-coherent detectors rely on for signal detection are likely to attenuate or even disappear at a high transmission rate.

Although there are numerous techniques proposed for ISI mitigation and signal detection in single-user DMC systems, little research has been done on the MAI mitigation and single-/multiple-user detection for multiple-access DMC systems. In literature, the Reed Solomon error correction coding assisted method proposed in [63] for combating MAI and ISI ought to be classified as a channel coding method. Recently, the authors of [64] proposed a novel modulation scheme referred to as the binary direction shift keying (BDSK), which encodes one bit of information into two different pumping directions. Employing the BDSK modulation scheme, adjacent transmitters can pump the same type of information molecules in two opposite azimuth angles directed to their corresponding receivers to mitigate MAI. However, this method requires the details of transceivers, including, the spherical transceivers of considerably large sizes compared to the transmission distance, the fixed pair of non-rotatable transceivers, and the reflective surfaces of transmitters and fully absorbing receivers. Therefore, one of the research emphases in this thesis is to propose a range of interference mitigation and signal detection schemes for the receiver design in multiple-access MC.

1.2.5 Design of Nano-Machines

Because the practical experiments have not been applied to the nano-scale and are still at the macroscopic validation phase. To the best of our knowledge, there are insufficient references attempting to specify the architecture and computational complexity of single NMs employed as transmit-

ter/receiver.

In literature, the encoding process at the transmitter NMs was summarized in [17]. Information can be loaded in various aspects of the information particles, like in the spatial structure of the information particle (a specific molecular type), in the permutation of some information molecules (a specific sequence of nucleotides composing a DNA fragment), or in the concentration/number of the information particles (the number of molecules per unit volume around the receiver). The principle and practical structure of the receiver NM was also detailed in [17]. A solution for a receiver NM to catch information particles is to rely on a membrane structure only open to the valid information particles. For example, a living cell has a plasma membrane selectively permeable to some signal particles and the receptors inside the cell can recognize these signal particles in the cytoplasm. Another scheme is to use different receptors which are able to bind to various corresponding types of molecules or react with information particles. Gated channels are another method to permit the specific signal particles to pass and enter the receiver NM.

[43] is one of few references which provide a framework to specify the computational capabilities of single nano-machines precisely. In retrospect of [43], present CPUs are designed to have considerable computational power by combining huge amounts of basic building blocks, which is still not feasible at the nano-scale. Though the current CPUs are minimising their sizes constantly with few-nanometers-big transistors, they are still in the size of centimetres due to their complex structure. Thus, [43] mainly illustrates what the lower bound on the complexity requirement of an individual nano-machine to be capable of executing all necessary operations is. In [43], the computational complexity of NMs is classified into three complexity classes L, AC^0, and NC^1 and the NM problems corresponding to different scenarios can be categorized in relation to one another in the complexity hierarchy.

1.3 Contributions

This thesis focuses mainly on the design of transceivers and the evaluation of the error performance of DMC systems. Our motivation is to design the methods that are efficient to improve the error performance of MADMC systems, while at the cost of relatively low complexity. Our designs include mainly the signalling, signal detection schemes, and interference cancellation schemes. Specifically, the contributions of this thesis are portrayed as follows.

In Chapter 2, we first propose an information modulation scheme for DMC, which is referred to as the type-spread molecular shift keying (TS-MoSK). Considering that DMC signals usually experience severe ISI, our TS-MoSK is characterized by introducing extra types of molecules for ISI mitigation (ISIM). Furthermore, we introduce two ISIM methods to the TS-MoSK modulated DMC systems, namely, the active ISIM and passive ISIM. We detail their operation principles and investigate as well as compare their achievable performance. Our studies show that aided by the

extra types of molecules, TS-MoSK outperforms the MoSK without type-spreading. Both ISIM approaches are effective for further improving the performance of TS-MoSK systems.

To accomplish complex tasks, several NMs may need to communicate via multiple-access channels with one access point (AP), where information fusion is carried out. Multiple access is an important technique for multiple NMs to send information to one AP or fusion center (FC). Built on the MoSK modulation, Chapter 2 also extends the novel Molecular Type Spread MoSK (MTS-MoSK) scheme to support multiple-access transmission in DMC systems. Correspondingly, two detection schemes are introduced and investigated, which are the maximum selection assisted majority voter detection (MS-MVD) and equal-gain combining detection (EGCD). The error performance of the MTS-MoSK DMC systems with respectively the two detection schemes is analyzed, when both MAI and ISI are taken into account. Furthermore, the performance of MTS-MoSK DMC systems is investigated and compared with the aid of analytical results as well as Monte-Carlo and particle-based simulations. Our studies and performance results show that MTS-MoSK constitutes a promising candidate for implementing multiple-access DMC, and MS-MVD has the potential to outperform EGCD for signal detection in DMC.

Since multiple-access DMC systems suffer from severe MAI and ISI, which should be effectively mitigated at the receiver in order to achieve acceptable detection performance, we investigate the interference cancellation schemes for the MTS-MoSK MADMC systems in Chapter 3. Built on two fundamental single-user detection schemes, namely threshold-assisted majority vote detection (TMVD) and equal gain combination detection (EGCD), we first propose four low-complexity interference cancellation schemes, which are the TMVD-assisted iterative interference cancellation (TMVD-IIC), TMVD-based minimum-distance decoding assisted interference cancellation (TMVD-MDDIC), the EGCD-assisted N-order iterative interference cancellation (EGCD-NIIC) and EGCD-based interference mitigation (EGCD-IM). Then, following the principle of maximum likelihood detection, we propose a simplified approximate maximum likelihood (SAML) detection scheme. The error performance of the MTS-MoSK DMC systems employing respectively the considered detection schemes is comprehensively investigated and compared. Furthermore, the complexities of the detection schemes are analyzed and discussed in terms of the complexity-performance trade-off. Our studies and results show that, compared with the single-user TMVD and EGCD schemes, the proposed interference cancellation schemes are capable of efficiently mitigating the effect of MAI and enabling significant performance improvement at a slightly increased complexity.

Although MTS-MoSK is able to support multiuser communications in DMC, there are still some shortcomings, such as requiring a large number of molecular types, similar transmission distance between NMs and AP, etc. These shortcomings may hinder it from some applications in practical DMC environments. In order to overcome these limitations, in Chapter 4, based on two types of molecules, a molecular code-division multiple-access (MoCDMA) scheme is designed for multiple NMs to simultaneously send information to a fusion center (FC) in a DMC environment. In our

considered MoCDMA system, different NMs may have different distances from FC, which generates 'near-far' effect. Correspondingly, the uniform and channel-inverse based molecule-emission schemes are proposed for NMs to emit information molecules. To facilitate signal detection, the received signals by FC are represented in different forms, based on which a range of detection schemes are derived. Specifically, by considering the limited computational power of NMs, a range of relatively low complexity detectors are derived in the principles of matched-filtering (MF), zero-forcing (ZF) and minimum mean-square error (MMSE). The noise characteristics in MoCDMA systems and the complexity of various detection schemes are analyzed. The error performance of the MoCDMA systems with various molecule-emission and detection schemes are demonstrated and compared. Our studies and performance results demonstrate that MoCDMA constitutes a promising scheme for supporting multiple-access transmission in DMC, while the channel-inverse based transmission can ensure the fairness of communication quality (FoCQ) among different NMs. Furthermore, different detection schemes can be implemented to attain a good trade-off between implementation complexity and communication reliability.

In chapter 5, we continue to study the MoCDMA by introducing the frequency-domain equalizers (FDEs) in order to mitigate interference and reduce complexity. Specifically, the FDEs in the principles of MF, ZF and MMSE are proposed to combat inter-chip interference (ICI). Furthermore, the one- and two-stage decision-feedback successive interference cancellation (DF-SIC) schemes are proposed to mitigate multiple-access interference (MAI). We also analyze the complexity of the proposed detection schemes and compare the error performance of the MoCDMA systems with these proposed detection schemes, when different factors are considered. Our investigation and performance results show that the FDE based on MMSE is a highly promising equalization scheme in most operational cases. The FDE assisted by one-stage DF-SIC is capable of providing a significant performance improvement in contrast to the original FDE without using DF-SIC. In addition, our studies demonstrate that Walsh codes are the mostly recommended spreading code for the MoCDMA assisted by FDE.

Finally, we summarize our main conclusions obtained from research, and suggest some potential future research issues in Chapter 6.

Chapter 2

Type-Spread Molecular Shift Keying: Signalling Principle, Interference and Multiple-Access

According to the retrospection of DMC channels and the related works in the last chapter, MC signals over DMC channels usually experience severe inter-symbol interference (ISI). Hence, in order to mitigate ISI, in this chapter, we first propose an information modulation scheme for DMC, which is referred to as the Type-Spread Molecular Shift Keying (TS-MoSK). Our TS-MoSK is characterized by introducing extra types of molecules for ISI mitigation (ISIM). Furthermore, we introduce two ISIM methods to the TS-MoSK modulated DMC systems, which are the active ISIM and passive ISIM. Subsequently, as the review in Chapter 2 depicts, in nano-networking, many nano-machines need to share common communication media, in order to achieve information exchange and data fusion. Multiple-access is an important technique for multiple nano-machines to send information to one access point (AP) or fusion center (FC). Built on the Molecular Shift Keying (MoSK) modulation, the second half of this chapter proposes a novel Molecular Type Spread MoSK (MTS-MoSK) scheme for achieving multiple-access transmission in DMC. Correspondingly, two detection schemes are introduced and investigated, which are the Maximum Selection assisted Majority Voter Detection (MS-MVD) and Equal-Gain Combining Detection (EGCD).

2.1 Type-Spread Molecular Shift Keying (TS-MoSK): Principles and Inter-Symbol Interference Mitigation

2.1.1 Introduction

Diffusion-based Molecular Communication (DMC) is an essential information transmission approach between the nano-machines deployed in gas or in liquid medium environments [41, 65]. In these communications environments, at macro-scale, information molecules relying on the Brownian motion always migrate from a higher concentration region to a lower concentration region following Fick's law. Correspondingly, in literature, there are a range of contributions considered the channel modeling in DMC. For example, in [65, 66], the noise modeling in DMC has been addressed. The studies show that noise in DMC cannot be considered separately from transmitted signal as done in the conventional radio-wave based communications systems, but is dependent on the transmitted signal. Furthermore, noise in DMC is non-stationary.

Based on the channel characteristics and noise models derived for DMC, three fundamental data modulation schemes have been developed in references for DMC, namely the Concentration Shift Keying (CSK), Pulse Position Modulation (PPM), and the Molecular Shift Keying (MoSK). First, CSK makes use of the concentration levels to convey information [67]. PPM restores received information based on the different time shifts of the concentration pulses appearing at receiver [68]. Finally, information in MoSK is encoded to a type of molecules via activating one out of several types of molecules [41]. In DMC, all these modulation schemes may experience inter-symbol interference. However, MoSK has certain capability to mitigate ISI, owing to the employment of multiple types of molecules, and hence the probability of continuously activating the same type of molecules is less than one, which becomes smaller as the number of types increases. In this section, on the basis of MoSK, we further enhance its ISI mitigation (ISIM) capability by introducing some extra types of molecules, and hence spreading the original MoSK signal. Therefore, the proposed scheme is referred to as the Type-Spread MoSK (TS-MoSK). Following the principles of MoSK, our studies show that TS-MoSK is able to improve the ISIM capability of MoSK, and hence enhance its error performance, especially in the case that there is severe ISI. The cost for this performance improvement is the increased types of molecules, which may be exploit for other purpose, such as, to simultaneously support multiple communication links.

A main challenge in DMC is that the slow molecular diffusion process results in significant propagation delay spread, generating serious ISI. Therefore, a lot of effort has been made to design the detection techniques for DMC systems, which are robust to ISI or have the capability to mitigate ISI. As some examples, the traditional signal processing methods, such as Maximum *A-Posteriori* (MAP), Maximum Likelihood (ML), etc., have been introduced to equalize the DMC channels [57, 58], in order to achieve optimum performance. In order to reduce the implementational complexity of the optimum equalizers, adaptive Decision-Feedback Equalizer (DFE) and

Minimum Mean-Square Error (MMSE) equalizer have been considered [30, 59]. In terms of ISIM and detection reliability, these detection (equalization) algorithms are efficient. However, it is highly challenging to implement them at nano-scale. Considering the research background and the feasibility of implementation in practice, in this section, we consider only low low-complexity detection and introduce two ISIM methods, namely, the passive ISIM and active ISIM. As shown in our forthcoming discourses, the passive ISIM is implemented at receiver, which is the extension of the ISIM approach proposed in [58] and improved in [69, 70]. By contrast, the proposed active ISIM is operated at transmitter, which controls the number of molecules emitted for transmitting a symbol with reference to the expected ISI experienced by the symbol. Our studies show that the TS-MoSK enhanced by the active ISIM is efficient in short-distance communication scenarios, but is invalid if the communication distance is too long. By contrast, the passive ISIM has the capability to boost the error performance of the TS-MoSK assisted DMC systems in any communication scenarios addressed in this section.

The rest of this section introduces a novel modulation scheme Type-Spread Molecular Shift Keying (TS-MoSK) and proposes two ISI mitigation methods. Section 2.1.2 introduces the DMC system model and the principles of TS-MoSK. In Section 2.1.3, we present principles of the two ISIM techniques. The performance results and their analysis are addressed in Section 2.1.4. Finally, the main conclusions from research are summarized in Section 2.1.5.

2.1.2 System Model of Type-Spread Molecular Communication

The idea behind TS-MoSK is that Q $(Q > M)$ types of molecules are used to transmit $\log_2 M$ bits per symbol using MoSK modulation. Hence, information is spread on the types of molecules, and the use of extra types of molecules makes the probability that the same type of molecules is continuously emitted becomes smaller, which naturally mitigates the effect of ISI. Below we describe the principles of TS-MoSK.

2.1.2.1 Transmitter Scheme

Let us assume that there is a binary data sequence to be transmitted. At the transmitter, this binary data sequence can be divided into symbols, forming a symbol sequence $\boldsymbol{x}^T = \left[x_0, x_1, \ldots, x_j, \ldots, x_N\right]$, where N is the number of symbols, $x_i \in \{0, 1, \ldots, M-1\}$ is an integer, representing $\log_2 M$ bits of the ith symbol in the binary data sequence. Then, when the M-ary MoSK modulation [71] is employed, these N symbols are transmitted one-by-one in serial based on the principles of MoSK. Specifically, for transmitting x_i, a pulse of x_i-th type of molecules is emitted by the molecular transmitter.

When the TS-MoSK is considered, we assume that there are Q $(Q > M)$ types of molecules are used to transmit the M-ary symbols. In order to configure the M-ary symbols to the Q types of

molecules, let us introduce a periodic spreading sequence, expressed as $\boldsymbol{q}^T = [q_0, q_1, \ldots, q_i, \ldots, q_N]$, where $q_i \in \{0, 1, \ldots, Q-1\}$. With the aid of this spreading sequence, then, the M-ary symbols can be mapped to the Q-ary symbols by a simple operation, such as,

$$\begin{aligned} \boldsymbol{y} &= [y_0, y_1, \ldots, y_i, \ldots, y_N]^T \\ &= (\boldsymbol{x} + \boldsymbol{q}) \mod Q \end{aligned} \tag{2.1}$$

where $\mod Q$ means modulo-Q operation. Hence, y_i is an integer taking a value in $[0, Q-1]$. For instance, if a 4-ary symbol sequence $\boldsymbol{x}^T = [1,0,3,2,2,0,3,1]$ is transmitted and a 7-ary spreading sequence $\boldsymbol{q}^T = [0,2,1,6,4,5,3,0]$ is employed, the 7-ary symbol sequence can be obtained as $\boldsymbol{y} = [1,2,4,1,6,5,6,1]^T$. Finally, the elements of $\boldsymbol{y}$ are transmitted one-by-one in the principles of a Q-ary MoSK. In detail, for the ith element of $\boldsymbol{y}$, a pulse of the y_i-th type of molecules is emitted at the beginning of a symbol interval, while all the other types of molecules maintain inactive.

2.1.2.2 Channel Model

We assume that information molecules released by the transmitter are propagated over a DMC channel. As shown in [38], given a spherical receiver having a fixed distance r from the transmitter, the concentration observed in the receiver meets the Fick's law, having the time-dependent function of

$$c(t) = \frac{A}{(4\pi D t)^{\frac{3}{2}}} \exp\left(-\frac{r^2}{4Dt}\right), \; t \geq 0 \tag{2.2}$$

when a pulse of A molecules is emitted at time zero. In (2.2), D in $[m^2 s^{-1}]$ is the diffusion coefficient of communication medium which can be derived based on the Einstein relation [72]

$$D = \frac{k_B Te}{6\pi\eta R} \tag{2.3}$$

where $k_B = 1.38 \times 10^{-23} JK^{-1}$ is Boltzmann's constant, Te is the temperature in kelvin, η is the viscosity of the fluid, and R is the radius of the propagation particle. In addition, t is the propagation time.

Fig. 2.1 demonstrates the concentration function in one symbol interval for given values of D, A and r, as shown in the figure. In this concentration function, the peak point can be found from the extremum point of (2.2) by solving the equation of $dc(t)/dt = 0$, which gives $t_o = r^2/6D$. Substituting this point into (2.2), we obtain the maximum value of concentration of

$$c_o = \left(\frac{3}{2\pi e}\right)^{\frac{3}{2}} \frac{A}{r^3} \tag{2.4}$$

As shown in Fig. 2.1, the received pulse is not constrained within one symbol duration, but extend, in theory, to infinity. Hence, when symbols are continuously transmitted, as shown in

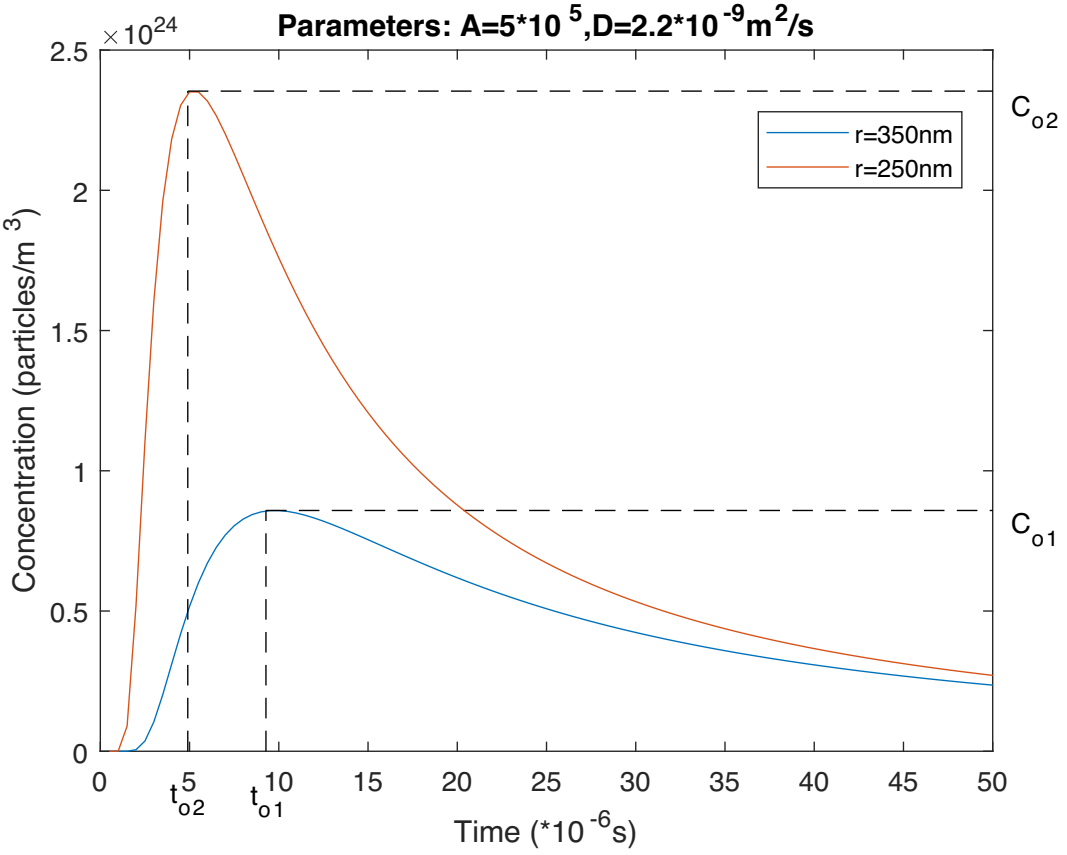

Figure 2.1: Function of molecular concentration.

Fig. 2.2, the pulses corresponding to different symbols overlap with each other, generating ISI. Explicitly, the strength of ISI is dependent of the symbol rate, or on the symbol duration, higher symbol rate has higher ISI. However, from Figs. 2.1 and 2.2, we can be implied that the ISI on a specific symbol is dominated by the several pulses (or symbols) transmitted right in the front of the symbol. Hence, in order to mitigate ISI, we should try to avoid transmitting the same type of molecules continuously. MoSK modulation has this embedded merit, and a higher modulation order, i.e., the value of M, yields a lower probability of transmitting the same type of molecules continuously. In this section, we enhance this by introducing some extra types of molecules for information transmission, which can further reduce the above-mentioned probability, and hence the ISI.

2.1.2.3 Received Signal

In order to detect the data, the observation about the molecular concentration at the receiver can be utilized. Specifically, for detecting the kth symbol, the decision variables can be obtained by

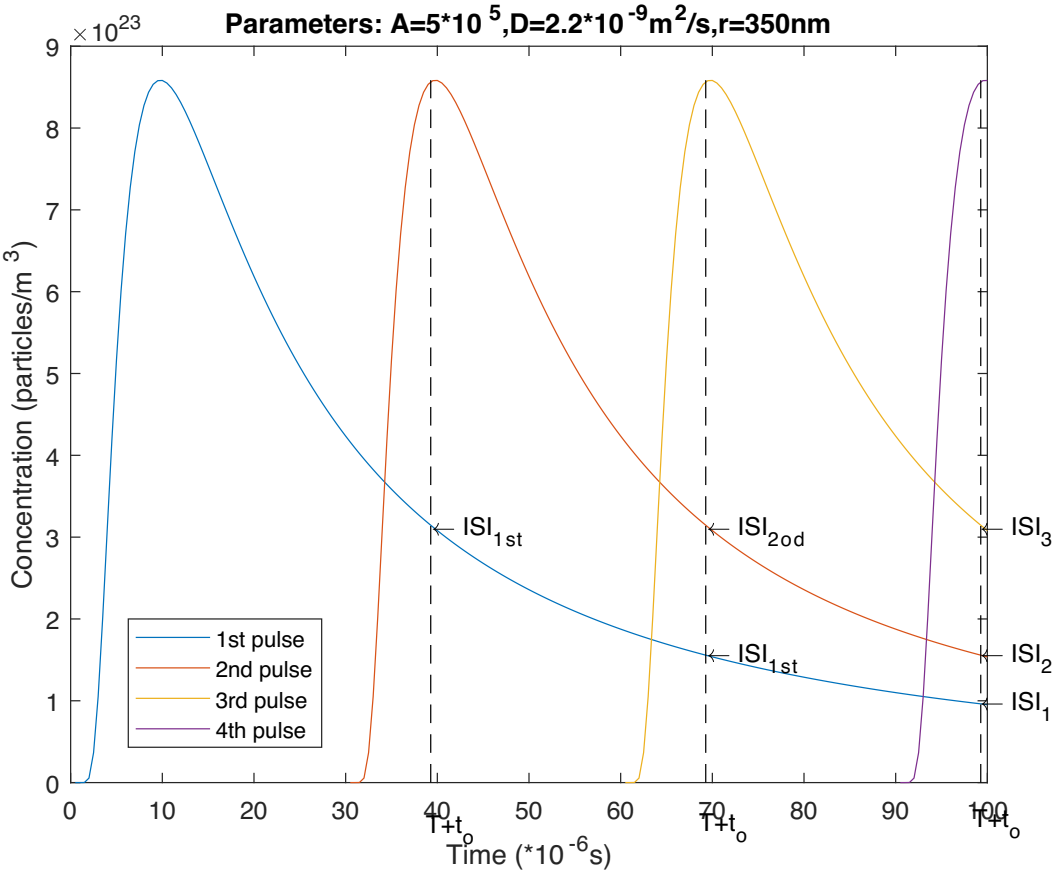

Figure 2.2: Demonstration of inter-symbol interference.

sampling the concentrations of the Q types of molecules at $t = kT + t_o$, which can be expressed as

$$\begin{aligned} r_q(k) =& r_q(t = kT + t_o) \\ =& \sum_{i=0}^{\min\{I,k\}} l_{q,k-i} c_q(iT + t_o) + n_q(kT + t_o) \\ =& l_{q,k} c_{q,o} + \underbrace{\sum_{i=1}^{\min\{I,k\}} l_{q,k-i} c_{q,i}}_{\text{ISI}} + n_{q,k}, \\ & q = 0, 1, \ldots, Q-1;\ k = 0, 1, \ldots, N \end{aligned} \tag{2.5}$$

for the Q types of molecules. In (2.5), the ISI length is assumed to be I, $l_{q,i}$ is a logic value, which is '1', if the qth type of molecules is activated during the ith symbol duration, and is '0', if the qth type of molecules is inactive during the ith symbol duration. In (2.5), $c_{q,i}$ is the expected concentration of the qth type of molecules at $t = iT + t_o$, when a pulse of A molecules was sent at $t = 0$. T is a symbol-duration. Finally, $n_q(k)$ is the noise resulted from Brownian motion of the q type of molecules, which can be approximately treated as the Gaussian noise, obeying the distribution with

mean zero and a variance of [38]

$$n_{q,k} \sim \mathcal{N}\left(0, \frac{1}{V} \sum_{i=0}^{\min\{I,k\}} l_{q,k-i} c_{q,i}\right) \tag{2.6}$$

where $V = \frac{4}{3}\pi\rho^3$ is the volume of a spherical receiver with a radius ρ.

Based on the decision variables shown in (2.5), the detection of the kth symbol can be carried out as follows. First, by comparing the Q decision variables as shown in (2.5), the type of molecules activated for transmitting the kth symbol can be identified as the one having the highest concentration, which can be formulated as

$$S_k = \arg \max_{q \in \{0,1,\ldots,Q-1\}} \{r_q(k)\},\ k = 0, 1, \ldots, N \tag{2.7}$$

Then, corresponding to the modulo addition of (2.1) carried out at the transmitter, an estimate to the M-ary symbol x_k can be obtained by a modulo subtraction operation on S_k, which can be expressed as

$$\hat{x}_k = (S_k - q_k) \mod Q,\ k = 0, 1, \ldots, N \tag{2.8}$$

Finally, upon mapping $\{\hat{x}_0, \hat{x}_1, \ldots, \hat{x}_N\}$ to binary, we obtain the estimates to the transmitted binary sequences.

From the operation of (2.8), we can know that the recovered $\hat{x_k}$ may not be in the range of $[0, M-1]$. In this case, there is an error occurred, and the receiver may either throw away the detected symbol, or randomly take a value in $[0, M-1]$ as the estimate to the received symbol.

2.1.3 Inter-Symbol Interference Mitigation

From our discussion in Section 2.1.2.2, we can know that the proposed TS-MoSK may also experience ISI, which becomes more serious, when transmission rate increases. For instant, if the same type of molecules, such as Type i, is continuously transmitted several times, before the transmission of another type, say Type j, the accumulated concentration of Type i molecules may be higher than that of Type j molecules, hence resulting in error detection. Therefore, ISI mitigation in TS-MoSK is also important. In this section, we introduce two approaches for ISI mitigation (ISIM), namely, the passive ISIM approach operated at receiver, and the active ISIM approach executed at transmitter.

2.1.3.1 Passive ISI Mitigation

A simple passive ISIM technique has been proposed in [58] for the DMC systems with On-Off Keying (OOK) modulation. This ISIM scheme can be directly extended to our TS-MoSK. In detail, instead of making the decision solely relying on the observations obtained at $t = kT + t_o$, which yields the decision variables as shown in (2.5), when the passive ISIM is employed, the receiver

makes the decision depending on the observations at both $t = kT + t_o$ and $t = kT$, giving the decision variables to be

$$\begin{aligned} Z_q(k) =& r_q(t = kT + t_o) - r_q(t = kT) \\ =& \sum_{i=0}^{\min\{I,k\}} l_{q,k-i} c_q(iT + t_o) + n_q(kT + t_o) \\ & - \left(\sum_{i=1}^{\min\{I,k\}} l_{q,k-i} c_q(iT) + n_q(kT) \right) \\ & q = 0, 1, \ldots, Q-1;\ k = 0, 1, \ldots, N \end{aligned} \tag{2.9}$$

where $r(t = kT + t_o)$ is as the same as (2.5), while $r(t = kT)$ is the concentration observed at $t = kT$.

As shown in Fig. 2.1, $t = kT + t_o$ is time instant generating the peak molecular concentration, if a pulse of molecules is sent for the kth symbol. By contrast, $r(t = kT)$ is the molecular concentration presenting at the beginning of the kth symbol duration, at which point the pulse of molecules for the kth symbol has not been emitted yet. Therefore, $r(t = kT)$ includes only the ISI from the molecules sent before $t = kT$, which can be used to approximate the ISI suffered by the kth symbol at the sampling time $t = kT + t_o$. Consequently, after the ISIM as shown in (2.9), the detection can be expected to me more reliable.

From Figs. 2.1 and 2.2, we can be implied that the value of $r(t = kT)$ obtained at $t = kT$ may be slightly higher than the actual ISI experienced by the kth symbol at $t = kT + t_o$, which results in excessive cancellation. This phenomenon becomes more declared, when the transmission rate becomes higher, making received pulses close to each other. Furthermore, as shown in (2.9), the ISIM operation introduces extra noise and hence yields noise amplification. In [70], an improved ISIM scheme has been proposed, which mitigates these side effects via downscaling the ISI estimated at $t = kT$.

2.1.3.2 Active ISI Mitigation

The passive ISIM is operated at receiver without any impact on the signal transmission and propagation. By contrast, active ISIM approaches are operated at the transmitter side via the corresponding adjustment of transmitted signals. In this section, we propose a novel active ISIM technique for the TS-MoSK, which can also be applied to many other DMC systems with various data modulation schemes.

In all our previous analysis and discussion, the number of molecules per pulse emitted by transmitter is a constant A, as seen in (2.2), which determines that the expected peak concentration c_o, if only single molecular pulse is emitted. When there is ISI, this peak value will change depending on the actual ISI. Since transmitter has the information to be transmitted, and hence knows exactly which and when the pulses are transmitted, the transmitter is capable of modifying the correspond-

ing number of molecules to be emitted, so that the expected peak concentration is always c_o. Our active ISIM technique is based on this observation. Instead of always emitting A molecules, the numbers of molecules actually emitted by the transmitter for sending the kth symbol is adjusted to

$$A_{q,k} = \begin{cases} A, & \text{when } k = 0 \\ A - \dfrac{\sum_{i=1}^{\min\{I,k\}} l_{q,k-i} A_{q,k-i} c_{q,i}}{c_{q,o}}, & \text{when } k > 0 \end{cases}, \quad k = 0, 1, \ldots, N;\ q = 0, 1, \ldots, Q-1 \tag{2.10}$$

where $c_{q,0}, c_{q,1}, \ldots, c_{q,I}$ are the concentration obtained from (2.2), when the number of molecules with a pulse if A.

It can be shown that, when the transmitter emits the pulses of molecules with the numbers of molecules of the pulses as shown in (2.10), the expected concentration of the type of molecules activated during the kth symbol duration is always c_o at the sampling instant of $t = kT + t_o$. This can be demonstrated as follows by assuming $k > I$. Let us assume that the qth type of molecules is activated during the kth symbol duration. Let the numbers of the qth type of molecules sent corresponding to the symbols x_{k-I}, $x_{k-I+1}, \ldots, x_k$ be expressed as $l_{q,k-I} A_{q,k-I}$, $l_{q,k-I+1} A_{q,k-I+1}, \ldots, A_{q,k}$, where $l_{q,k} = 1$ as the qth type is assumed to be activated during the kth symbol duration. Then, at the sampling time of $t = kT + t_o$, the expected concentration is

$$\bar{c}_{q,k} = \frac{A_{q,k} c_{q,o}}{A} + \sum_{i=1}^{I} l_{q,k-i} \frac{A_{q,k-i} c_{q,i}}{A} \tag{2.11}$$

Upon substituting $A_{q,k}$ with $k > I$ from (2.10) into the above equation, we can readily show that

$$\bar{c}_{q,k} = c_{q,o} \tag{2.12}$$

In comparison with the passive ISIM scheme introduced in Section 2.1.3.1, we realize that the active ISIM technique has the following characteristics. First, the ISIM operation is carried out at transmitter, which shifts the complexity from receiver to transmitter. This is practically useful in the communications scenarios, where receivers are more capable than transmitters. Second, by making use of the expected ISI, the total number of molecules emitted is reduced, which in return, can be used to increase the signal-to-noise ratio (SNR), and ultimately improve reliability. Additionally, the reduced number of molecules also reduces the counting noise associated with both the current and following detection.

Below we provide some simulation results to characterize the performance of the TS-MoSK, as well as that of the TS-MoSK with respectively the passive and positive ISIM schemes.

2.1.4 Performance Results

In this section, the error performance of the TS-MoSK assisted DMC systems is depicted against the SNR per bit. This SNR is defined as the ratio between the power received from a single pulse

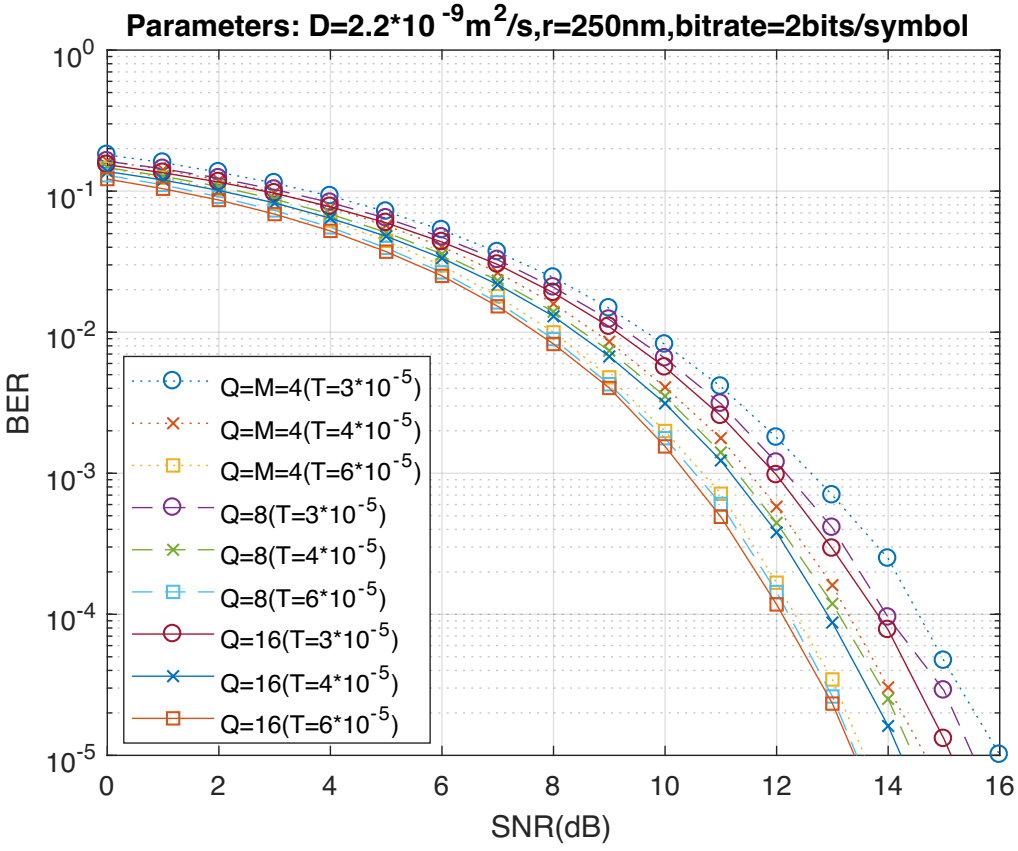

Figure 2.3: BER versus SNR per bit performance of the DMC systems with 4-ary MoSK modulation and different TS levels at the same bit rate of 2 bits/symbol.

of molecules emitted for transmitting one bit and the noise power, formulated by [70, 73]

$$\text{SNR} = \frac{c_o^2}{c_o/V} = Vc_o \tag{2.13}$$

In our simulations, for a given SNR per bit and the volume V of a receiver, we can obtain c_o from (2.13). Then, when the communications distance r is given, from (2.4), we can derive the corresponding number of molecules A_b for transmitting one bit. As M-ary MoSK is used in the TS-MoSK, the total number of molecules emitted for transmitting a symbol is $A = \log_2 M \times A_b$.

In our simulations, some parameters are fixed, which are $D = 2.2 \times 10^{-9}\ m^2/s$ and $V = \frac{4}{3}\pi\rho^3$ with $\rho = 1$ nm. The length of ISI is obtained via the measurement of

$$I \triangleq \arg_i \left\{ \frac{c_i}{c_o} \leq 0.01\% \right\} \tag{2.14}$$

meaning that only the ISI with the strength above 0.01% of the present desired signal is considered, the ISI weaker than this value is ignored. This is reasonable, as the ignored ISI is at least 80 dB lower than the desired signal.

First, in Fig. 2.3 we compare the BER performance of the DMC systems with the TS-MoSK operated with different levels of spreading, when a fixed 4-ary MoSK, and hence the bit rate of 2

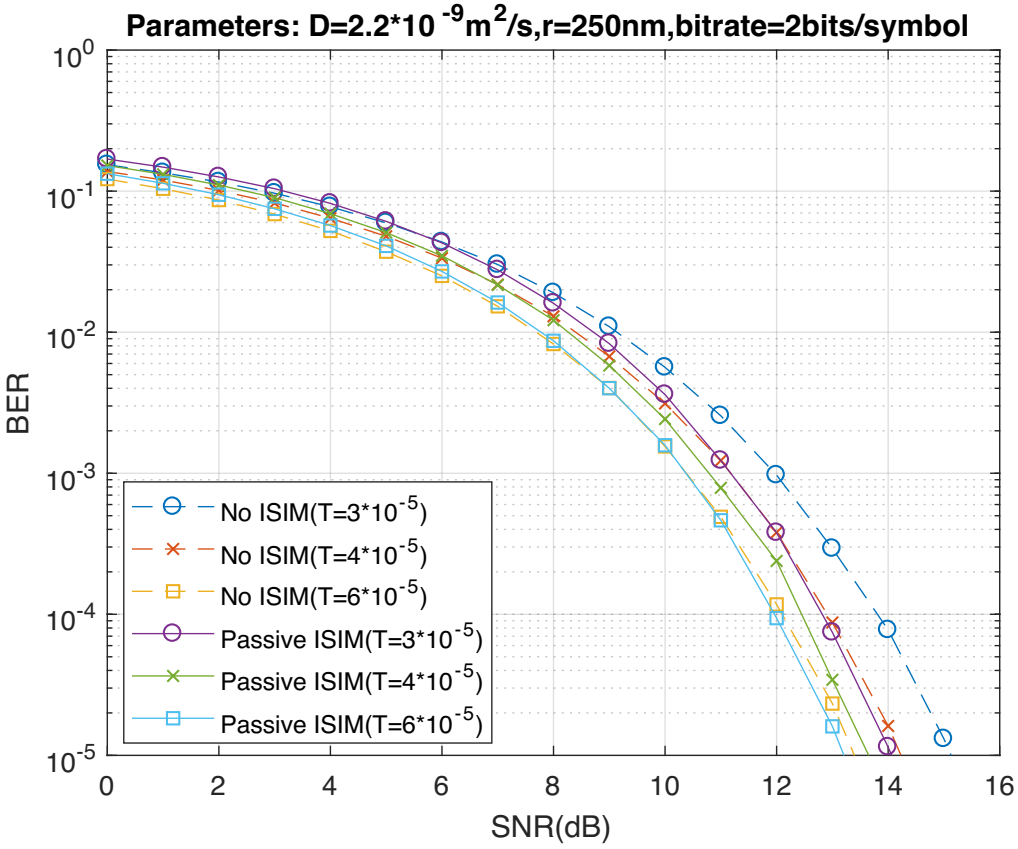

Figure 2.4: BER versus SNR performance of DMC systems with the TS-MoSK supported by $Q = 16$ types of molecules, when $4 - ary$ MoSK is employed with/without passive ISIM.

bits/symbol, is considered. Furthermore, in the figure three symbol durations of T are considered, which correspond to three symbol rates given by $R = 1/T$. From Fig. 2.3 we can have the following observations. First, the BER performance of the DMC systems improves, as the number of the types of molecules used for TS increases. Specifically, in the case of $T = 3 \times 10^{-5}$ s, explicit performance improvement can be observed, when the number of types is increased from $Q = 4$ to $Q = 8$, and then to $Q = 16$. By contrast, when $T = 6 \times 10^{-5}$ s, only slight performance improvement is observed at relatively high SNR. Furthermore, we can be implied from the results that the performance improvement becomes less, as the symbol duration T increase. The reason behind the above observation is that: a) MoSK modulation itself has certain capability to mitigate ISI, as previously mentioned, and b) as T increases, ISI becomes shorter, making the effect of TS less observable. Second, in the case of $Q = M = 4$, the BER performance improves, as the symbol duration increases, due to the reduced transmission rate. From this we can also be implied that, for a given value of Q, the BER performance improves, as the symbol duration increases.

Fig. 2.4 depicts the BER versus SNR performance of the TS-MoSK assisted DMC systems with $Q = 16$ types of molecules to transmit 4-ary MoSK symbols. Both the DMC systems without

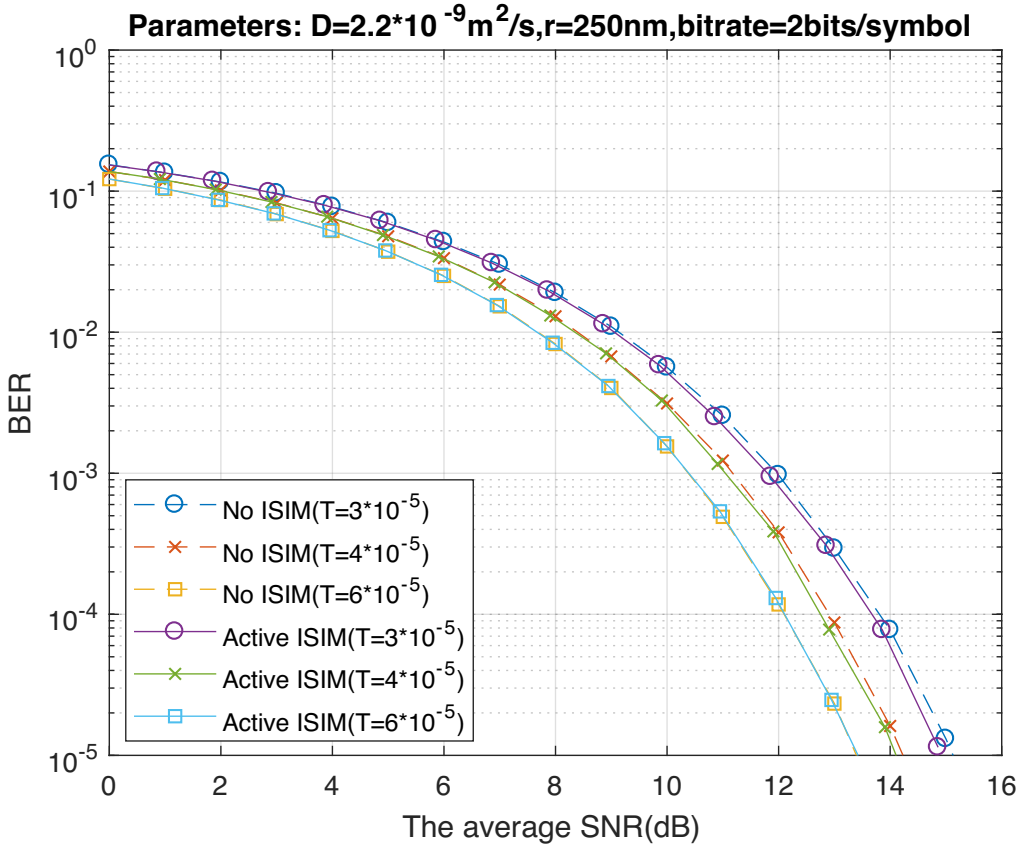

Figure 2.5: BER versus SNR performance of DMC systems with the TS-MoSK supported by $Q = 16$ types of molecules, when $4 - ary$ MoSK is employed with/without passive ISIM.

ISIM and that with passive ISIM are considered. Similar to the observations in Fig. 2.3, when the data rate is relatively high, yielding relatively severe ISI, employing passive ISIM is capable of generating noticeable performance gain. By contrast, when data rate becomes lower, ISI also becomes weak. Straightforwardly, the performance improvement resulted from passive ISIM becomes less significant.

In contrast to Fig. 2.4, in Fig. 2.5 we show the BER versus SNR performance of the TS-MoSK assisted DMC systems with $Q = 16$ types of molecules to transmit 4-ary MoSK symbols, when without employing ISIM or with active ISIM. Note that, when the active ISIM is implemented, the number of molecules released per symbol is time variant, which is depended on the ISI. Hence, the SNR shown in the figure is the average SNR per bit, computed based on the actual number of molecules emitted by the transmitter. Specifically, in our simulations for the case of active ISIM, we set the number of molecules released during the first symbol period to be the same as that for the cases without ISIM or with passive ISIM. Therefore, the average SNR should be slightly lower than the SNR of the first symbol. The same as Fig. 2.4 for using passive ISISM, as demonstrated in Fig. 2.5, the active ISIM is capable of attaining some performance gain, when data

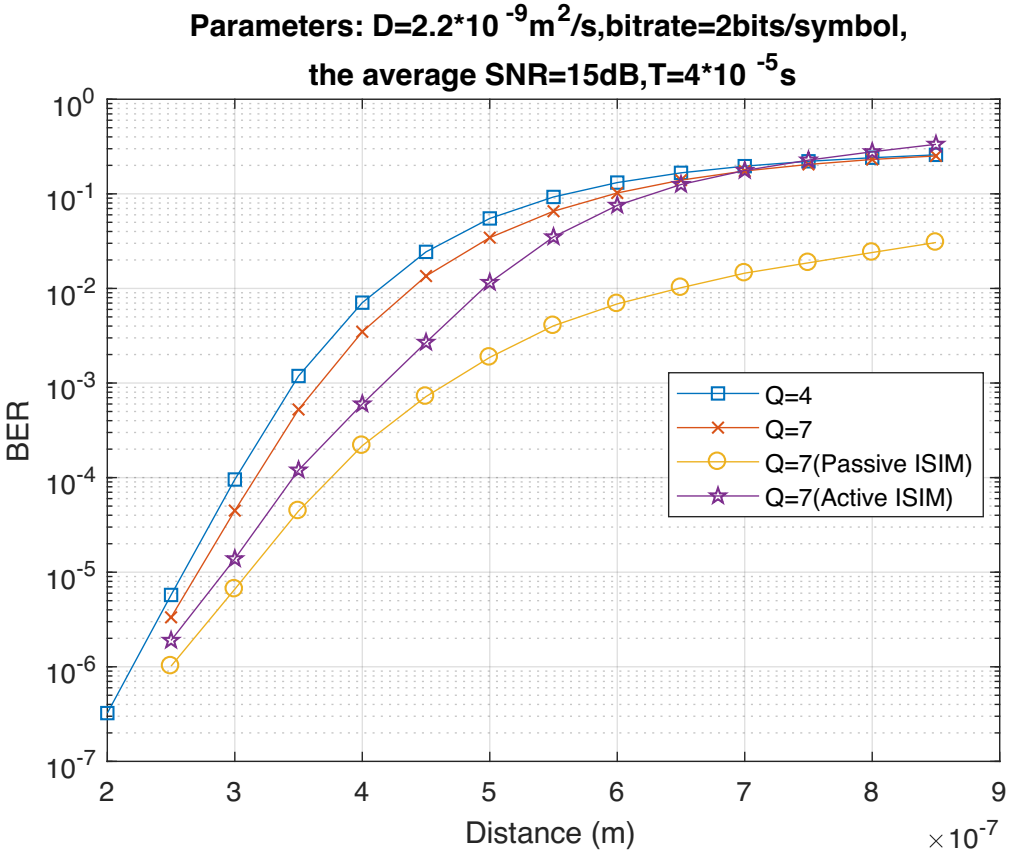

Figure 2.6: Performance comparison of the 4-ary MoSK modulated DMC systems with various signaling and detection schemes considered.

rate is high, meaning that there is strong ISI. By contrast, when data rate is low, yielding smaller ISI, as expected, there performance gain also becomes smaller, and finally, there is no performance gain, when data rate is very low, making ISI ignorable.

Finally, in Fig. 2.6, we compare the BER versus transmission distance performance of the DMC systems employing the various transmission and ISIM schemes, when the SNR per bit is fixed to 15 dB and the symbol interval to $T = 4 \times 10^{-5}$ s, while adjusting the transmission distance r from 200 nm to 900 nm. From the results of Fig. 2.6 we may have the following observations. First, as the propagation distance increases, the error performance of the DMC systems in any case degrades, due to the increased ISI. Second, at low to moderate transmission distance, we can observe that the TS-MoSK, TS-MoSK with passive ISIM and the TS-MoSK with active ISIM all outperform the pure MoSK. Third, when the transmission distance becomes sufficiently long, the performance of the TS-MoSK converges to that of the original MoSK, implying that the benefit from TS disappear. This is because the severe ISI introduced by long transmission distance overwhelms the benefit obtained from TS. Fourth, at high transmission distance, such as $r > 700$ nm, the active ISIM is even outperformed by the original MoSK, meaning that ISIM is useless. This is true because the received concentration pulse, as shown in Fig. 2.1, becomes flatter, as transmission distance

increases. In this case, the reduced number of emitted molecules makes the detection hard. Finally, as shown in Fig. 2.6, at any transmission distance, the passive ISIM method is efficient, which significantly outperforms the active ISIM, if transmission distance is relatively long, and has a big performance gain over TS-MoSK for any transmission distance.

2.1.5 Conclusions

In this section, we have first proposed a TS-MoSK scheme for improving the error performance of the MoSK by spreading the transmitted information over more types of molecules, and hence reducing the ISI. In order to further mitigate the ISI, we have introduced a passive ISIM operated at receiver, and proposed an active ISIM operated at transmitter. Both their advantages and disadvantages have been discussed. The performance of the MoSK modulated DMC systems employing respectively these schemes has been investigated. Our studies demonstrate that, with proper design and system settings, the capability of ISIM can be improved by the TS operation, which can be further, usually significantly, enhanced by either the active ISIM or the passive ISIM. When comparing active ISIM with passive ISIM, we find that the passive ISIM is usually more efficient than the active ISIM in terms of error performance. Active ISIM is only effective in short-distance communication scenario. However, active ISIM has the advantage that its impact on the communication environment is less than passive ISIM, owing to the reduced number of molecules emitted by the active ISIM into the communication environment. Our future research will consider the practical implementation of TS-MoSK, and analyze the performance of the TS-MoSK assisted DMC systems with active/passive ISIM.

2.2 Molecular Type Spread Molecular Shift Keying (MTS-MoSK) for Multiple-Access Diffusive Molecular Communications (MADMC)

2.2.1 Introduction

In order to boost the capability of nano-networks, the individual nano-machines of each being only able to complete simple tasks are required to cooperate with each other and/or to exchange information, so that more complex mission can be fulfilled. For example, in a molecular sensor network, each molecular sensor has only limited storage space and computation potential, and can only observe a very limited region. In order to monitor a relatively large region, multiple and, possibly, many molecular sensors may have to be distributed over the region in order to attain a seamless coverage. Furthermore, considering the limited storage and computation capabilities of individual sensors, the observations obtained by individual sensors may need to be conveyed to a fusion center, where the final decision about the monitored event is made. In the above described process, one of the important challenges is how to send the observations obtained by individual

sensors to the fusion center, efficiently and reliably. Explicitly, this task can be achieved with the aid of the multiple-access techniques, which deal with information transmission between multiple transmit nodes (like molecular sensors) and one common receive node (like fusion center). Hence, significant research effort is required for designing the efficient multiple-access schemes for supporting nano-networking. In this section, we propose and investigate a multiple-access scheme for Diffusion-based Molecular Communications (DMC) by extending type-spreading to multiple access.

In literature, there are several multiple-access transmission techniques having been proposed in the context of DMC. Specifically, the Molecular Code-Division Multiple-Access (MCDMA) introduced in [51, 74] allows multiple nano-machines to simultaneously transmit information to a receiver by assigning different nano-machines unique signature codes. These transmitter-specific signature codes are used by the receiver to distinguish the information received from different transmit nano-machines. In [52–54], Molecular Time-Division Multiple-Access (MoTDMA) has been considered to support multiple nano-machines communicating with a receiver. With MoTDMA, the transmission of different nano-machines is arranged to occur within different time slots, and the information conveyed from a specific nano-transmitter is then recovered from the corresponding time-slots. Furthermore, multiple-access molecular communications can be implemented via Molecule Division Multiple Access (MDMA) [75]. With this multiple-access technique, every nano-machine is employed a particular type of molecules or a set of unique types of molecules for it to transmit information to a receiver. Hence, MDMA uses molecular types to distinguish different nano-machines.

As in the conventional radio-based communications, multiple-access communications often experiences interference, referred to in general as Multiple-Access Interference (MAI). This demands particular attention in DMC's transceiver design, because of the nature of DMC, where interference can hardly be avoided via signaling design, such as, spreading codes in MCDMA. Hence, multiple-access scheme and corresponding receiver design in DMC become highly challenging. In the context of multiple-access DMC, there are a range of detection schemes introduced and studied in references, e.g., [51, 52, 54, 75]. Specifically for the MCDMA considered in [51], since the multiple-access scheme is based on On-Off Keying (OOK) modulation, the authors developed a chip-based detection scheme with the adaptive threshold obtained by referring to the concentrations of previous chips. In [52], the detection algorithm proposed in [61] was introduced for MoTDMA detection, which is also a threshold-based detector, with the threshold directly set to the number of molecules of the same type that are received during the previous impulse period. In [54], three genetic detection methods were considered, namely the roulette-wheel selection, stochastic universal sampling and tournament selection for artificial neuronal networks. Finally, [75] considered to use different types of molecules to support multiple-access transmission. Correspondingly, the ligand-receptors matched to the different types of molecules are used to aid information detection.

In the conventional radio-based wireless communications, there is a Fast Frequency-Hopping

M-ary Frequency Shift Keying (FFH-MFSK) scheme [76, 77], which exploits multiple frequencies to simultaneously support both frequency-hopping and data transmission of multiple users. Based on the observation that frequencies in conventional radio-based communications are analogous to the different types of molecules in DMC, in this section, we design a Molecular Type Spread MoSK (MTS-MoSK) scheme to allow DMC to simultaneously support multiple nano-machines. In MTS-MoSK DMC systems, MTS is implemented by assigning different nano-machines unique spreading codes. For a given nano-machine to send data, it first signatures the data using its unique spreading code, yielding the outputs that control the release of different types of molecules. At the receiver, different types of molecules and their numbers (densities) are measured, which are used to recover the data sent by these nano-machines with the aid of their spreading codes. In this section, we investigate two types of low-complexity detection schemes [78], namely the Maximum Selection assisted Majority Vote Detector (MS-MVD) and the Equal Gain Combining (EGC) assisted Detector (EGCD). When MS-MVD is employed, some candidate molecular types are first identified, followed by the molecular-type de-spreading and majority voting. By contrast, with EGCD, molecular-type de-spreading is first carried out. Then, the sum of concentration of each type is calculated, based on which final decision is made to give the estimate to the transmitted data. Both detection approaches have the advantage that no threshold is required, which is usually difficult to be set to a near-optimum value, because of the Brownian motion of molecules and severe ISI in DMC.

In this section, we also analyze the error performance of the MTS-MoSK DMC systems. Specifically, when MS-MVD is employed, we derive a lower-bound for the Bit Error Rate (BER) of MTS-MoSK DMC systems. By contrast, when EGCD is employed, we derive the approximate BER of MTS-MoSK DMC systems, when both the Poisson approximation [29, 79, 80] and Gaussian approximation [81, 82] are considered, respectively. Finally, the error performance of MTS-MoSK DMC systems is investigated with the aid of analytical results, Monte-Carlo simulation and particle-based simulation. It is demonstrated that the performance results obtained from analytical results and that from simulations agree with each other, which valid our analysis. The error performance of MTS-MoSK DMC systems is also compared with that of the on-off keying (OOK)-assisted DMC system, where each nano-machine is exclusively supported by one type of molecules. Furthermore, we demonstrate the impact of different parameters on the error performance of MTS-MoSK DMC systems, showing the design trade-off between performance and complexity.

The contribution of the work can be summarized as follows.

- A MTS-MoSK multiple-access scheme is proposed for DMC to support multiple nano-machines simultaneously communicating with a receiver.
- Two low-complexity detection schemes, namely MS-MVD and EGCD, are proposed for information detection in MTS-MoSK DMC systems.

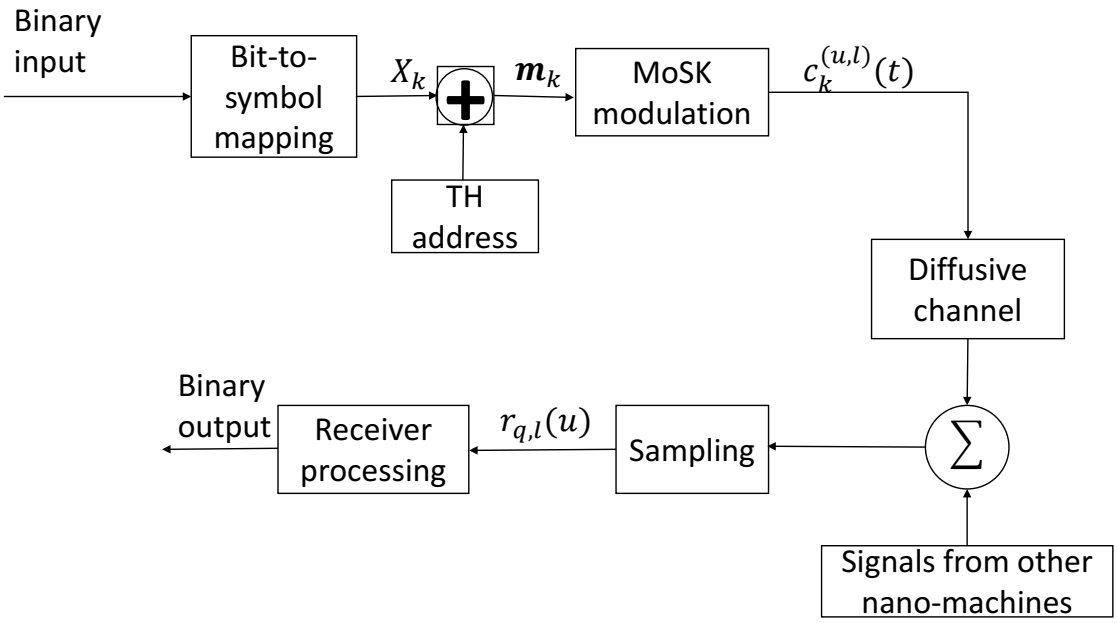

Figure 2.7: System diagram showing the components of the MTS-MoSK DMC systems.

- An BER lower-bound is derived for the MTS-MoSK DMC systems with MS-MVD, and the approximate BER expressions are derived, respectively, based on the Poisson- and Gaussian approaches for the MTS-MoSK DMC systems with EGCD.
- The error performance of MTS-MoSK DMC systems is investigated based on both analytical results and simulations. Both model- and particle-based simulations are invoked for performance studies. Furthermore, the error performance of the MTS-MoSK DMC system with EGCD is compared with that of the OOK-assisted DMC system.

The remainder of this section is arranged as follows. Section 2.2.2 introduces the MTS-MoSK DMC system model. In Section 2.2.3, the principles of two detection schemes are introduced. Section 2.2.4 details the analysis of error performance. Performance results are demonstrated in Section 2.2.6. Finally, the main conclusions from research are summarized in Section 2.2.7.

2.2.2 System Model

The MTS-MoSK DMC system proposed has the structure as shown in Fig. 2.7. The details about the system structure and operations are provided in the following subsections.

2.2.2.1 Description of Transmitter and Channel Model

We assume a MTS-MoSK DMC system, which employs M types of information molecules to supports $K \leq M$ nano-machines communicating with a common access point (AP). We assume that the locations of nano-machines and AP are fixed. For simplicity, all nano-machines are assumed to

have a similar distance from AP. However, we should note that in practice, this may be the case in a molecular sensor network (MSN), where multiple sensors communicate with a fusion center, deployed for monitoring an event. The transmitter of a nano-machine in the MTS-MoSK DMC system is shown as the above part of Fig. 2.7. Assume that M types of molecules are employed by each of the nano-machines for information transmission. Then, $b = \log_2 M$ bits per symbol can be delivered by a nano-machine. Assume that T_s is the symbol-duration, which is divided into $L = T_s/T_h$ chips of each having the duration of $T_h = T_s/L$ seconds referred to as chip-duration. We assume that the transmissions of K nano-machines are synchronous at chip-level. In practice, this can be achieved via synchronizing the transmissions of different nano-machines with the pilot signals periodically sent from AP. During a symbol-duration of T_s seconds, b bits of information to be transmitted by the kth nano-machine is first mapped to a M-ary symbol expressed as $X_k \in \{0, 1, \ldots, M-1\}$, as shown in Fig. 2.7. Let the MTS code of the kth nano-machine be expressed as $\boldsymbol{a}_k = [a_k^{(0)}, a_k^{(1)}, \ldots, a_k^{(L-1)}]$, $k = 1, 2, \ldots, K$, where $a_k^{(i)} \in [0, M-1]$. In practice, the MTS codes should be designed and assigned to nano-machines in favor of distinguishing the symbols transmitted by different nano-machines. As shown in Fig. 2.7, the M-ary symbol X_k is signed by the kth nano-machine's MTS code, with the operation expressed as

$$\begin{aligned}\boldsymbol{m}_k =& [m_k^{(0)}, m_k^{(1)}, \ldots, m_k^{(L-1)}] \\ =& X_k \cdot \mathbf{1}_{(1\times L)} \oplus \boldsymbol{a}_k \\ =& [X_k \oplus a_k^{(0)}, X_k \oplus a_k^{(1)}, \ldots, X_k \oplus a_k^{(L-1)}], \\ & k = 1, 2, \ldots, K \end{aligned} \tag{2.15}$$

where $\oplus$ is the addition operation in the Galois field GF(M) [83], and $\mathbf{1}_{(1\times L)}$ is an all-one row vector of length L. After the signature operation, it can be known that the elements of $\boldsymbol{m}_k$ have the integer values in $[0, M-1]$, which can be directly processed by the M-ary MoSK modulation block as seen in Fig. 2.7, to emit the corresponding types of molecules within the L chip-durations.

For example, assume that there are two nano-machines in the MTS-MoSK DMC system employing $M = 8$ types of molecules and using $L = 6$ chips per symbol for information transmission. Let the first and second nano-machines' MTS codes be $\boldsymbol{a}_1 = [4, 3, 7, 6, 2, 5]$ and $\boldsymbol{a}_2 = [2, 0, 1, 6, 4, 7]$, and their data symbols to be transmitted be $X_1 = 5$ and $X_2 = 3$, respectively. Then, to transmit X_1 and X_2, they are first extended to the L-length vectors of $X_1 \cdot \mathbf{1}_{(1\times L)} = [5, 5, 5, 5, 5, 5]$ and $X_2 \cdot \mathbf{1}_{(1\times L)} = [3, 3, 3, 3, 3, 3]$, respectively. Then, by executing the addition operation with $\boldsymbol{a}_1$ and $\boldsymbol{a}_2$, respectively, in the Galois field $GF(8)$, we obtain two vectors of $\boldsymbol{m}_1 = X_1 \cdot \mathbf{1}_{(1\times L)} \oplus \boldsymbol{a}_1 = [1, 6, 2, 3, 7, 0]$ and $\boldsymbol{m}_2 = X_2 \cdot \mathbf{1}_{(1\times L)} \oplus \boldsymbol{a}_2 = [1, 3, 2, 5, 7, 4]$, where a value represents the type of molecules to be activated within the corresponding chip-duration. Note that in $\boldsymbol{m}_1$ and $\boldsymbol{m}_2$, the colored elements illustrate that the transmissions from two nano-machines collide with each other and generate interference, as they emit the same type of molecules within the same chip-duration.

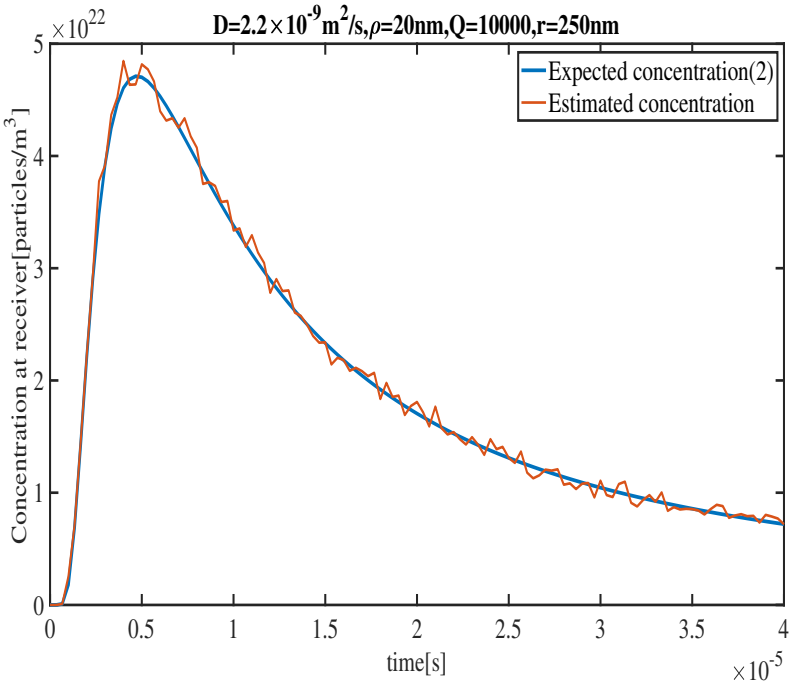

Figure 2.8: Comparison between the expected concentration given by Fick's law of (2.16) and the concentration obtained from the average of 1000 particle-based simulations, when assuming that one pulse of molecules is emitted at $t = 0$.

We assume that the M types of molecules belong to a family of the isomers, which hence have a similar diffusion coefficient denoted by D when propagating within a fluid medium [84]. Then, after the MoSK modulation, if a molecular type is activated within a given chip-duration, a pulse of molecules of this type is emitted at the beginning of the chip. Let at the lth chip of the uth symbol-duration, the qth molecular type is activated by the kth nano-machine. Then, following the Fick's diffusion law [42, 69], the concentration of molecules observed by AP at time t for the qth type of molecules emitted by the kth nano-machine can be formulated as

$$c_{k,q}^{(u,l)}(t) = \frac{A}{\left[4\pi D\left(t - uT_s - lT_h\right)\right]^{3/2}} \times \exp\left(\frac{-r^2}{4D\left(t - uT_s - lT_h\right)}\right), \; t \geq \left(uL + l\right) T_h \tag{2.16}$$

where Q is the number of molecules emitted per pulse and r is the distance between a transmit nano-machine and AP.

Given a molecular pulse with $Q = 10000$ molecules emitted at $t = 0$, Fig. 2.8 compares the expected concentration of (2.16), which is a given function, and the estimated concentration obtained from the average of 1000 particle-based simulations. It is shown that the estimated concentration agrees well with the expected concentration given by Fick's law. However, the estimated concentration still slightly fluctuates around the expected concentration, which is due to the randomness of particles' Brownian motion. Note that, according to [66], the desired signal in DMC is given by the expected value, such as, the expected concentration of (2.16), while the difference between the

actual and expected values is unexpected and treated as noise.

From the characteristics of diffusion process, we can easily conceive that there are different kinds of interference in the MTS-MoSK DMC system. First, as shown in many references, such as in [30, 58], the same type of molecules transmitted corresponding to different symbols may overlap with each other, generating ISI. Second, there is background noise generated by the randomness of molecules' Brownian motion. Third, when a MTS-MoSK DMC system supports multiple nano-machines simultaneously transmitting signals to a common AP using the same M types of molecules, the signals transmitted by these nano-machines in the current chip-duration interfere with each other. Furthermore, the molecules transmitted previously in the adjacent chips by the different nano-machines also interfere the signals transmitted in the current chip. These kinds of interference generated by the interfering nano-machines can be referred to as multiple-access interference (MAI). Therefore, in order to achieve reliable communication in MTS-MoSK DMC system, the detector operated at AP should be carefully designed.

2.2.2.2 Observations Obtained by Receiver

After a pulse of molecules is transmitted at the beginning of a chip, it is feasible for the receiver at AP to sample at the expected peak concentration, which can be derived from (2.16) and occurs at $t_d = r^2/(6D)$. Assume that this is the case in this paper, meaning the assumption of $T_h > t_d$. The concentration sampled within the lth chip of the uth symbol-duration can be expressed as

$$\begin{aligned} r_{q,l}(u) =& r_q(t = uT_s + lT_h + t_d), \\ & l = 0, 1, \ldots, L-1;\ u = 0, 1, \ldots; \\ & q = 0, 1, \ldots, M-1 \end{aligned} \tag{2.17}$$

When taking account of the Brownian motion noise, ISI from the same type of molecules transmitted previously, and the MAI from the other nano-machines, the received signal $r_{q,l}(u)$ can be expressed as

$$\begin{aligned} r_{q,l}(u) &= \sum_{k=1}^{K} \sum_{i=0}^{\min\{I, uL+l\}} \ell_{k,q}^{uL+l-i} c_{k,q}(iT_h + t_d) \\ &\quad + n_q(uT_s + lT_h + t_d) \\ &= \sum_{k=1}^{K} \sum_{i=0}^{\min\{I, uL+l\}} \ell_{k,q}^{uL+l-i} c_{k,q}(i) + n_{q,l}(u) \end{aligned} \tag{2.18}$$

where the ISI length is assumed to span I chip-durations, $\ell_{k,q}^{i}$ is a logic value, which is '1', if the qth type of molecules is activated by the kth nano-machine in the ith chip, or is '0', otherwise. In (2.18), $c_{k,q}(i)$ is the expected concentration of the qth type of molecules at $t = iT_h + t_d$, i.e., $c_{k,q}(iT_h + t_d)$, when an impulse of A molecules of this type was sent at $t = 0$. It is worth noting that here only the component with $i = 0$ contributes to the detection of the desired signal, while

all the other components corresponding to $i \neq 0$ generate interference. Finally in (2.18), $n_{q,l}(u)$ is the counting noise introduced due to the transmission of the qth type of molecules, which can be approximated as the Gaussian noise [58], with the probability density function (PDF) expressed as

$$n_{q,l}(u) \sim \mathcal{N}\left(0, \frac{1}{V}\sum_{k=1}^{K}\sum_{i=0}^{\min\{I,uL+l\}} \ell_{k,q}^{uL+l-i} c_{k,q}(i)\right) \tag{2.19}$$

where V is the volume of the space that the receiver used to measure the concentration of information molecules. From (2.19), we can conceive that the noise is due to the transmission of signals. In other words, whenever a signal for conveying information is transmitted, there is added noise power, and higher signal power also gives higher noise power. Hence, the noise in DMC is very different from that in the conventional radio frequency communications, where background noise is not related to transmitted signals, but added at receiver.

2.2.3 Signal Detection in MTS-MoSK DMC Systems

From (2.17) we are inferred that during a symbol-duration, there are in total ML observations available for detecting the symbols transmitted by the K nano-transmitters during this symbol-duration. For convenience of description of our proposed detectors, these ML observations obtained during the uth symbol-duration are arranged as an observation matrix $\boldsymbol{R}_u$, which has M rows corresponding to the M types of molecules and hence the M possible symbols, and L columns representing the L chips within the uth symbol-duration. The (q,l)th element of $\boldsymbol{R}_u$, i.e., $r_{q,l}(u)$, represents the concentration sample of the qth type of molecules in the lth chip-duration of the uth symbol, which is given in (2.18). Explicitly, the observation matrix $\boldsymbol{R}_u$ can be expressed as

$$\boldsymbol{R}_u = \begin{bmatrix} r_{1,1}(u) & r_{1,2}(u) & \cdots & r_{1,l}(u) & \cdots & r_{1,L}(u) \\ r_{2,1}(u) & r_{2,2}(u) & \cdots & r_{2,l}(u) & \cdots & r_{2,L}(u) \\ \vdots & \vdots & \ddots & \vdots & \ddots & \vdots \\ r_{q,1}(u) & r_{q,2}(u) & \cdots & r_{q,l}(u) & \cdots & r_{q,L}(u) \\ \vdots & \vdots & \ddots & \vdots & \ddots & \vdots \\ r_{M,1}(u) & r_{M,2}(u) & \cdots & r_{M,l}(u) & \cdots & r_{M,L}(u) \end{bmatrix}$$

Based on the observation matrix $\boldsymbol{R}_u$, below we introduce two detection approaches to detect the uth symbols received from the K nano-machines. The first approach implements the Maximum Selection followed by Majority Vote based Detection, which is the MS-MVD. By contrast, the second detection approach is designed in the principle of Equal-Gain Combining (EGC), which is the EGCD. Let us first describe the MS-MVD in detail.

2.2.3.1 Maximum Selection Assisted Majority Vote Detection

The MS-MVD can be well explained with the aid of the schematic block diagram shown in Fig. 2.9. This detector includes two main operations. The first main operation is the Maximum Selection

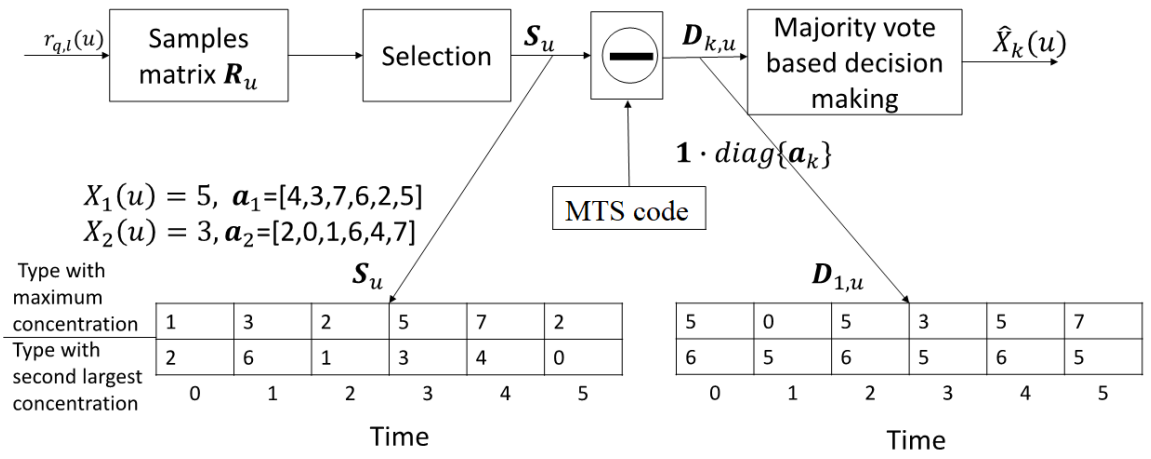

Figure 2.9: Schematic block diagram for the MS-MVD.

(MS), which selects a number of entries that have the largest concentration from each of the L columns of $\boldsymbol{R}_u$. The second main operation is the Majority Vote based Detection (MVD), which makes the decision of a symbol to be detected based on the number of times that a specific symbol appears, and the symbol appears the most number of times is decided to be the desired one detected.

In detail, the principle of the MS-MVD can be described as follows with reference to Fig. 2.9. First, from each of the L columns in the observation matrix $\boldsymbol{R}_u$, K elements having the highest concentration values are selected, the corresponding row indices of these selected elements are used to form a $(K \times L)$ candidate matrix $\boldsymbol{S}_u$, as shown in Fig. 2.9 for the case of $K = 2$. In $\boldsymbol{S}_u$, the first row accommodates the largest elements, the second row stores the second largest elements, and so on. Note that, the reason why the K largest elements in each column are chosen is that the number of nano-machines supported is K and hence, each column has at most K active types.

The above MS scheme has the advantage that no threshold is required for selection, as threshold is sometimes hard to determine due to the lack of channel knowledge. However, it has the disadvantage that some inactive types may be selected, as K elements have to be selected from each column, while there is possibility that two or more nano-machines may activate the same type of molecules during one chip, as shown in the example below (2.15). Hence, although our performance results for the MS-MVD in Section 2.2.6 are obtained by applying the above MS scheme, below we provide some discussion about the possible schemes modified from the above selection scheme. One modified selection scheme is the joint maximum-threshold selection (JMTS). With the JMTS scheme, based on $\boldsymbol{R}_u$, the receiver first forms a $(K \times L)$ candidate matrix $\boldsymbol{S}_u$ as the above described, i.e., by selecting the K largest elements from each of the L columns of $\boldsymbol{R}_u$. Then, each of the selected elements in $\boldsymbol{S}_u$ is compared with a threshold Th. If the element value is lower than Th, the corresponding element is emptied or counted as an erasure. Otherwise, if the element value is higher than Th, the element is left as it is. During the following type de-spreading operation and MVD, the empty elements will not be processed. The JMTS scheme is depended on the threshold

setting, which is sometimes hard to determine, as above mentioned. One approach for the JMTS approach to circumvent this problem is to compare only a given number of the smallest elements in $\boldsymbol{S}_u$ to the threshold. The objective of this improved approach is to retain the activated elements in the candidate matrix but remove the inactive elements from the candidate matrix with a high probability.

After $\boldsymbol{S}_u$ is obtained, the detector proceeds to the molecular type de-spreading operation by exploiting the knowledge about the MTS code assigned to the nano-machine being detected. Specifically for the kth nano-machine, using its MTS code $\boldsymbol{a}_k$, the molecular type de-spreading procedure generates a $(K \times L)$ detection matrix expressed as

$$\boldsymbol{D}_{k,u} = \boldsymbol{S}_u \ominus (\mathbf{1}_{(K\times L)} \cdot \mathrm{diag}\{\boldsymbol{a}_k\}),\ k = 1, 2, \ldots, K \tag{2.20}$$

where $\mathbf{1}_{(K\times L)}$ is an all-one matrix with K rows and L columns. Therefore, $\mathbf{1}_{(K\times L)} \cdot \mathrm{diag}\{\boldsymbol{a}_k\}$ just copies the kth nano-machine's MTS code $\boldsymbol{a}_k$ to each of the K rows. In (2.20), the symbol $\ominus$ represents the element-by-element subtraction operation between $\boldsymbol{S}_u$ and $\mathbf{1}_{(K\times L)} \cdot \mathrm{diag}\{\boldsymbol{a}_k\}$ in the Galois field GF(M). As shown in Fig. 2.9, the detection matrix obtained by de-spreading $\boldsymbol{S}_u$ using the first nano-machine's MTS code is expressed as $\boldsymbol{D}_{1,u}$.

Finally, based on the detection matrix $\boldsymbol{D}_{k,u}$, the estimate to the uth symbol sent by the kth nano-machine is decided in the principle of majority vote, which makes the decision in favor of the symbol appearing most frequently in the detection matrix $\boldsymbol{D}_{k,u}$. However, if there are two or more than two symbols having the same number of times appearing in $\boldsymbol{D}_{k,u}$, the detector can randomly select one from them to represent the estimate to the received symbol. Specifically for the example considered, as shown in Fig. 2.9, symbol '5' appears the most number of times. Hence, according to the majority vote rule, $\hat{X}_1(u) = 5$ is the estimated symbol received from the first nano-machine. Similarly, the symbol sent by the second nano-machine can be estimated, which is $\hat{X}_2(u) = 3$, as expected.

The complexity of MS-MVD can be analyzed as follows. After the observation matrix $\boldsymbol{R}_u$ is prepared, for each of the L columns, the detector needs to identify the K largest among the M types of molecules. When the quick-sort algorithm [85] is used, the average number of comparisons required to sort M real numbers is $2M \ln M$. It is known that the number of comparisons required to find the maximum among M real numbers using binary-search is $(M-1)$. Hence, when K is small, lower number of computations than the quick-sort algorithm may be obtained by using direct comparison to find the K largest among M real numbers, which requires $K(M - [K+1]/2)$ comparisons. Hence, to form the candidate matrix $\boldsymbol{S}_u$, $A_c = 2LM \ln M$ (in average) or $A_c = KL(M - [K+1]/2)$ comparisons are required, when the quick-sort algorithm or direct comparison is employed. Note that, the above operations are common for all nano-machines. By contrast, after obtaining the candidate matrix, the following computations for deriving the detection matrices and the decision making are specific to individual nano-machines. Specifically, for the kth nano-machine, KL number of element-by-element subtraction in GF(M) is required for molecular type

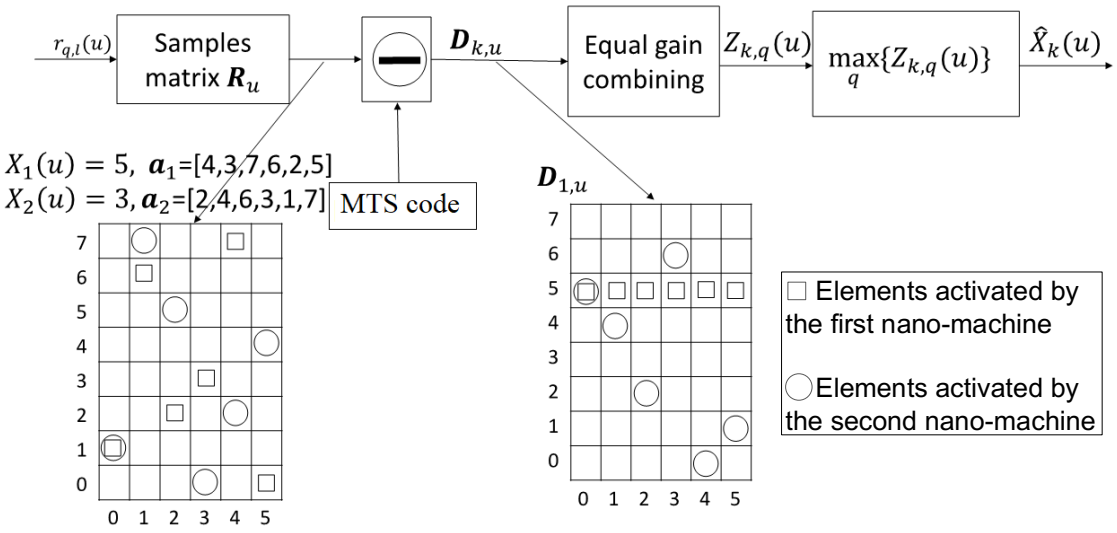

Figure 2.10: Schematic block diagram showing the EGC assisted detection.

de-spreading. Finally, finding the number of times of the M possible elements appearing in $\boldsymbol{D}_{k,u}$ and then selecting the one with the highest number of times require about $KL + M$ operations. Therefore, the total operations for detecting a symbol of one nano-machine is about $A_c/K + 2KL + M$.

2.2.3.2 Equal-Gain Combining (EGC) Assisted Detection

The principle of the equal-gain combining assisted detection (EGCD) can be well understood with the aid of Fig. 2.10. As done in the MS-MVD, the receiver first forms the observation matrix $\boldsymbol{R}_u$ based on the concentrations of the M types of molecules and of the L chips. In Fig. 2.10, those marked elements in $\boldsymbol{R}_u$ represent the elements activated by the $K = 2$ nano-machines. These active elements contain both signals and noise as well as interference. By contrast, those un-filled elements in $\boldsymbol{R}_u$ contain only noise and interference. As shown in Fig. 2.10, to detect the symbol received from the kth nano-machine, the observation matrix $\boldsymbol{R}_u$ is de-spreaded using the MTS code $\boldsymbol{a}_k$ of the kth nano-machine, yielding the detection matrix $\boldsymbol{D}_{k,u}$. To be more specific, after the type de-spreading, the (q,l) th element $r_{q,l}(u)$ in $\boldsymbol{R}_u$ is moved to the location $(q \ominus a_k(l), l)$ of $\boldsymbol{D}_{k,u}$, i.e.,

$$d^{(k)}_{(q\ominus a_k(l),l)}(u) = r_{q,l}(u),\ q = 0,1,\ldots,M-1;$$
$$l = 0,1,\ldots,L-1;\ k = 1,2,\ldots,K \tag{2.21}$$

As an example, in Fig. 2.10, when $\boldsymbol{R}_u$ is de-spreaded using the first nano-machine's MTS code $\boldsymbol{a}_1 = (4,3,7,6,2,5)$, yielding the detection matrix $\boldsymbol{D}_{1,u}$. It can be seen that all the $L = 6$ elements activated by the first nano-machine are de-spreaded to the fifth row, inferring that the received symbol is $\hat{X}_1(u) = 5$. By contrast, the elements activated by the undesired nano-machine scatter randomly over the matrix, forming MAI.

Based on the detection of $\boldsymbol{D}_{k,u}$, then, EGC can be carried out to form M decision variables as

$$Z_q^{(k)}(u) = \sum_{l=0}^{L-1} d_{(q,l)}^{(k)}(u),\ q = 0, 1, \ldots, M-1; \quad k = 1, 2, \ldots, K \tag{2.22}$$

for each of $u = 0, 1, \ldots$. Finally, the decision on the symbol to be detected is made by choosing the largest among $\{Z_0^{(k)}(u), Z_1^{(k)}(u), \ldots, Z_{M-1}^{(k)}(u)\}$, and its subscript represents the detected symbol. This decision making procedure can be described as

$$\hat{X}_k(u) = \arg\max_q \{Z_q^{(k)}(u)\},\ k = 1, 2, \ldots, K \tag{2.23}$$

The complexity of the EGCD can be analyzed as follows. The $M \times L$ elements of observation matrix $\boldsymbol{R}_u$ are directly operated in the de-spreading process. To be more specific, the detector operates the $GF(M)$ subtraction between the elements' locations and desired nano-machine's MTS code on the element-by-element basis, which transforms the observation matrix $\boldsymbol{R}_u$ to the detection matrix $\boldsymbol{D}_{k,u}$ by assigning every element a new location. Hence, the total number of operations in the de-spreading procedure is $(M \times L)$. Note that, because the first stage of EGCD is operated with a single MTS code, all the operations in the whole detection process are for one nano-machine. After the detection matrix $\boldsymbol{D}_{k,u}$ is attained, according to the principle of EGCD, the sum of the elements in each of the M rows is required to be calculated. For each row, there are $(L-1)$ additions. Therefore, to generate the decision variables $Z_q^{(k)}(u)$, $M(L-1)$ additions are required. Finally, finding the largest one from the M decision variables needs $(M-1)$ operations. Consequently, when considering all the operations, the total number of computations required for detecting a symbol of one nano-machine using EGCD is approximately $2ML$.

2.2.4 Error Probability Analysis

In this section, we attempt to analyze the error performance of the MTS-MoSK DMC systems. In our analysis, we assume that the M-ary symbols transmitted by K nano-machines are randomly selected with a uniform probability of $P(0) = P(1) = \cdots = P(M-1) = 1/M$, and that the random MTS codes with each of their elements obeying the discrete uniform distribution in $[0, M-1]$ are employed. Let us first analyze the MTS-MoSK DMC system with MS-MVD.

2.2.4.1 Error Probability of MS-MVD: A Lower-Bound

Due to the ISI and counting noise, it is extremely hard to mathematically analyze the error rate of the MTS-MoSK DMC system with MS-MVD. Therefore, we analyze for a lower bound by assuming that there is no ISI and also that the SNR is sufficiently high, so that there are no false-alarm and miss identifications of the active elements in the candidate matrix $\boldsymbol{S}_u$. In this case, an erroneous detection occurs only because of the interference among nano-machines.

Without any loss of generality, let us assume that the 1st nano-machine is the reference one, whose transmitted symbol $X_1 = 0$ is detected. Hence, in the detection matrix $\boldsymbol{D}_{1,u}$ of size $(K \times L)$, there should be L and only L elements being 0. Erroneous detection occurs only when there is one or more than one symbol other than symbol 0 appearing L times in $\boldsymbol{D}_{1,u}$ and appearing once in each column.

Since both data symbols and MTS codes are randomly and uniformly distributed, the probability that a given symbol value other than 0, such as $i \in \{1, 2, \ldots, M-1\}$, appears in a column is

$$P_A = 1 - \left(1 - \frac{1}{M}\right)^{K-1} \tag{2.24}$$

As the events with all the columns are independent, the probability that the same symbol i appears L times in $\boldsymbol{D}_{1,u}$ is

$$P_A^L = \left[1 - \left(1 - \frac{1}{M}\right)^{K-1}\right]^L \tag{2.25}$$

Furthermore, it can be shown that the probability that there are j symbols other than symbol 0, each of which appears L times in $\boldsymbol{D}_{1,u}$ is

$$\begin{aligned} P(j) =& \binom{K-1}{j} (P_A^L)^j \left(1 - P_A^L\right)^{K-1-j}, \\ & j = 0, 1, \ldots, K-1 \end{aligned} \tag{2.26}$$

When the above event occurs, there are $j+1$ symbols appearing the same L times in $\boldsymbol{D}_{1,u}$, and the detector has to randomly choose one of them as the estimate $\hat{X}_1$ to the symbol X_1 transmitted by the reference nano-machine. Hence, the average symbol error probability (SEP) is

$$P_s = 1 - \sum_{j=0}^{K-1} \frac{1}{j+1} \times P(j) \tag{2.27}$$

Furthermore, following the principle of the M-ary modulation, the bit error rate (BER) is given by [86]

$$P_b = \frac{M/2}{M-1} P_s \tag{2.28}$$

which is a lower-bound for the MTS-MoSK DMC system with MS-MVD.

2.2.5 Error Probability of EGCD

To analyze the error probability of the MTS-MoSK DMC systems with EGCD, below we consider two approaches to model the distributions of the elements in the detection matrices of K nano-machines, namely, Poisson-approach and Gaussian-approach. In our analysis, again, we assume that the first nano-machine is the reference one, whose transmitted symbol $X_1(u) = 0$ is to be

detected. Hence, our analysis is based on $\boldsymbol{D}_{1,u}$. For simplicity, the index 1 of the reference nano-machine is ignored in the analysis.

First, let us consider the Poisson approach. Assume that the volume of the space used by the receiver to measure the molecular concentration is V. Then, when the ISI symbols and the symbols sent by the K nano-machines during the uth symbol-duration are given, the number of molecules of $D_{m,l}(u) = Vd_{m,l}(u)$ obtained based on (2.21) obeys the Poisson distribution with the PMF expressed as

$$f_{D_{m,l}(u)}(n|\mathcal{X}_I(u), X_1(u)=0) = \frac{\lambda_{m,l}^n(u)e^{-\lambda_{m,l}(u)}}{n!}, \quad n = 0,1,\ldots, \tag{2.29}$$

where $\mathcal{X}_I(u)$ contains all the ISI symbols from the K nano-machines as well as the $K-1$ interfering symbols sent by the $(K-1)$ interfering nano-machines during the uth symbol-duration, $\lambda_{m,l}(u)$ is the mean value of $D_{m,l}(u)$ under the above conditions. From (2.21), we can conceive that

$$\lambda_{m,l}(u) = \lambda_{q,l}(u),\ l = 0,1,\ldots,L-1 \tag{2.30}$$

with $q = m \oplus a_1^{(l)}$, where $\lambda_{q,l}(u)$ can be obtained from (2.18) as

$$\begin{aligned}\lambda_{q,l}(u) =& E[Vr_{q,l}(u)] \\ =& V\sum_{k=1}^{K}\sum_{i=0}^{\min\{I,uL+l\}} \ell_{k,q}^{uL+l-i} c_{k,q}(i)\end{aligned} \tag{2.31}$$

When the EGCD is employed, the M decision variables for the reference nano-machine are given by (2.22). Since the sum of Poisson distributed random variables is still Poisson distributed, the PMF of $D_m(u)$ can be expressed as

$$f_{D_m(u)}(n|\mathcal{X}_I, X_1(u)=0) = \frac{\Lambda_m^n(u)e^{-\Lambda_m(u)}}{n!}, \quad n = 0,1,\ldots;\ m = 0,1,\ldots,M-1 \tag{2.32}$$

where $\Lambda_m(u) = \sum_{l=0}^{L-1}\lambda_{m,l}(u)$.

With the PMFs of the decision variables prepared, the conditional probability that the uth sym-

bol of the reference nano-machine is correctly detected can be derived as

$$\begin{aligned}
&P_c^{(1)}(\mathcal{X}_I, X_1(u)=0)\\
&=P(D_0(u)>D_1(u),\ldots,D_0(u)>D_{M-1}(u))\\
&=\sum_{n_0=0}^{\infty} P(D_0(u)=n_0)\prod_{m=1}^{M-1} P(D_m(u)<n_0)\\
&=\sum_{n_0=0}^{\infty} f_{D_0(u)}(n_0|\mathcal{X}_I, X_1(u)=0)\\
&\quad\times\prod_{j=1}^{M-1} P(D_j(u)<n_0|\mathcal{X}_I, X_1(u)=0)\\
&=\sum_{n_0=0}^{\infty}\left[\frac{\Lambda_0^{n_0}(u)e^{-\Lambda_0(u)}}{n_0!}\right]\cdot\prod_{j=1}^{M-1}\left[\sum_{n_m=0}^{n_0-1}\frac{\Lambda_m^{n_m}(u)e^{-\Lambda_m(u)}}{n_m!}\right]
\end{aligned}\tag{2.33}$$

As $D_m(u)$ are discrete random variables, it is possible that $D_0(u)$ is just one of the several maximums. In this cases, the detector randomly and uniformly selects one of the maximums for the final detection. Correspondingly, the conditional probability that the uth symbol of the reference nano-machine is correctly detected is

$$\begin{aligned}
P_c^{(2)}(\mathcal{X}_I, X_1(u)=0)=&\sum_{j=1}^{M-1}\frac{1}{j+1}\binom{M-1}{j}\\
&\times P\Big(D_0(u)=D_{i_1}(u),\ldots,D_0(u)=D_{i_j}(u);\\
&\quad D_0(u)>D_{i_{j+1}}(u),\ldots,D_0(u)>D_{i_{M-1}}(u)\Big)
\end{aligned}\tag{2.34}$$

where $i_j\in\{1,2,\ldots,M-1\}$. Following (2.33), we can derive $P_c^{(2)}(\mathcal{X}_I, X_1(u)=0)$ as

$$\begin{aligned}
P_c^{(2)}(\mathcal{X}_I, X_1(u)=0)=&\sum_{j=1}^{M-1}\frac{1}{j+1}\binom{M-1}{j}\\
&\times\sum_{n_0=0}^{\infty}P(D_0(u)=n_0)\prod_{m_1=i_1}^{i_j}P(D_{m_1}(u)=n_0)\\
&\times\prod_{m_2=i_{j+1}}^{i_{M-1}}P(D_{m_2}(u)<n_0)\\
=&\sum_{j=1}^{M-1}\frac{1}{j+1}\binom{M-1}{j}\sum_{n_0=0}^{\infty}\left[\frac{\Lambda_0^{n_0}(u)e^{-\Lambda_0(u)}}{n_0!}\right]\\
&\times\prod_{m_1=i_1}^{i_j}\left[\frac{\Lambda_{m_1}^{n_0}(u)e^{-\Lambda_{m_1}(u)}}{n_0!}\right]\\
&\times\prod_{m_2=i_{j+1}}^{i_{M-1}}\left[\sum_{n_m=0}^{n_0-1}\frac{\Lambda_{m_2}^{n_m}(u)e^{-\Lambda_{m_2}(u)}}{n_m!}\right]
\end{aligned}\tag{2.35}$$

When we combine (2.33) and (2.35), a compact form expression can be obtained, which is

$$\begin{aligned} &P_c(\mathcal{X}_I, X_1(u)=0) \\ &= \sum_{j=0}^{M-1} \frac{1}{j+1}\binom{M-1}{j} \sum_{n_0=0}^{\infty} \left[\frac{\Lambda_0^{n_0}(u)e^{-\Lambda_0(u)}}{n_0!}\right] \\ &\times \prod_{m_1=i_1}^{i_j} \left[\frac{\Lambda_{m_1}^{n_0}(u)e^{-\Lambda_{m_1}(u)}}{n_0!}\right] \\ &\times \prod_{m_2=i_{j+1}}^{i_{M-1}} \left[\sum_{n_m=0}^{n_0-1} \frac{\Lambda_{m_2}^{n_m}(u)e^{-\Lambda_{m_2}(u)}}{n_m!}\right] \end{aligned} \tag{2.36}$$

where we set $i_0 = 0$ and in this case, $i_{0+1} = 1$. Note that, in the case of $D_0(u) = 0$, the only event for possible correct detection is $D_0(u) = D_1(u) = \ldots = D_{M-1}(u) = 0$, which yields a correct symbol probability of $1/M$.

The average correct symbol probability can be obtained by considering all the possible symbols in $\mathcal{X}_I$, which can be expressed as

$$P_c = \frac{1}{M^{|\mathcal{X}_I|}} \sum_{\mathcal{X}_I} P_c(\mathcal{X}_I, X_1(u)=0) \tag{2.37}$$

However, this is usually impossible to compute, as the ISI is in general very long in DMC. To simplify (2.37), we only consider the average with the symbols sent by the $K-1$ nano-machines during the uth (current) symbol-duration, while the ISI symbols sent before the uth symbol period are averaged out using their statistics. Specifically, when the Poisson-approximation is employed, we approximate $D_{m,l}(u)$ as a Poisson distributed random variable with the PMF given by

$$\begin{aligned} &f_{D_{m,l}(u)}(n|X_1(u)=0, X_2(u), \ldots, X_K(u)) \\ &= \frac{\lambda_{m,l}^n(u)e^{-\lambda_{m,l}(u)}}{n!},\ n=0,1,\ldots, \end{aligned} \tag{2.38}$$

where $\lambda_{m,l}(u)$ still follows (2.30), but with $\lambda_{q,l}(u)$ given by

$$\begin{aligned} &\lambda_{q,l}(u) \\ &= V\sum_{k=1}^{K}\left[\sum_{i=0}^{\min\{I,l\}} \ell_{k,q}^{uL+l-i} c_{k,q}(i) + \frac{1}{M}\sum_{i=L}^{\min\{I,uL+l\}} c(i)\right] \\ &= V\left[\sum_{k=1}^{K}\sum_{i=0}^{\min\{I,l\}} \ell_{k,q}^{uL+l-i} c_{k,q}(i) + \frac{K}{M}\sum_{i=L}^{\min\{I,uL+l\}} c(i)\right] \end{aligned} \tag{2.39}$$

where the second term in the bracket is a constant obtained by assuming that the data symbols obey the uniform distribution in $[0, M-1]$.

With the above approximation, (2.37) can now be re-written as

$$\begin{aligned} P_c = &\frac{1}{M^{K-1}} \sum_{X_2(u),\ldots,X_K(u)\in\{0,\ldots,M-1\}} P_c(X_1(u)=0, \\ &X_2(u), \ldots, X_K(u)) \end{aligned} \tag{2.40}$$

Correspondingly, the BER of the MTS-MoSK DMC system with EGCD can be obtained from the formula [86]

$$P_b = \frac{M/2}{M-1}(1 - P_c). \tag{2.41}$$

In the context of the Gaussian approach, $D_{m,l}(u)$ is approximated as a Gaussian distributed random variable with the PDF given by

$$D_{m,l}(u) \sim \mathcal{N}\left(\lambda_{m,l}(u), \lambda_{m,l}(u)\right) \tag{2.42}$$

where $\lambda_{m,l}(u)$ is the same as the one in (2.29). Furthermore, since the sum of Gaussian distributed random variables is still Gaussian distributed, the PDF of $D_m(u) = \sum_{l=0}^{L-1} D_{m,l}(u)$ is

$$D_m(u) \sim \mathcal{N}\left(\Lambda_m(u), \Lambda_m(u)\right),\ m = 0, 1, \ldots, M-1 \tag{2.43}$$

where $\Lambda_m(u)$ is the same as the one in (2.32). Then, following the derivation of (2.33) and remembering that $D_m(u)$ are continue random variables, we can obtain the conditional correct symbol probability as

$$\begin{aligned} P_c(\mathcal{X}_I, X_1(u) = 0) = &\int_{-\infty}^{\infty} f_{D_0(u)}(x)dx \\ &\times \prod_{m=1}^{M-1} \int_{-\infty}^{x} f_{D_m(u)}(y)dy \end{aligned} \tag{2.44}$$

where $f_{D_m(u)}(x)$ is the Gaussian PDF given by (2.43). Upon applying the PDFs of (2.43) into the above equation, it can be shown that

$$\begin{aligned} P_c(\mathcal{X}_I, X_1(u) = 0) = &\int_{-\infty}^{\infty} \frac{1}{\sqrt{2\pi}\sigma_0} \exp\left(-\frac{[x-\mu_0]^2}{2\sigma_0^2}\right) dx \\ &\times \prod_{m=1}^{M-1} \left(1 - Q\left[\frac{x-\mu_m}{\sigma_m}\right]\right) \end{aligned} \tag{2.45}$$

where $Q(t)$ is the Gaussian Q-function defined as $Q(t) = (2\pi)^{-1/2} \int_t^{\infty} e^{-t^2/2} dt$, and by definition,

$$\begin{aligned} \mu_m = &\sigma_m^2 = \Lambda_m(u) = \sum_{l=0}^{L-1} \lambda_{m,l}(u), \\ &m = 0, 1, \ldots, M-1 \end{aligned} \tag{2.46}$$

Note that, all μ_m and σ_m^2 are dependent on $\mathcal{X}_I$ and $X_1(u) = 0$.

Continuing from (2.44), the average correct symbol probability can in theory be obtained from (2.37). Furthermore, if we apply the $\lambda_{q,l}(u)$ as shown in (2.39), we can obtain for the average correct symbol probability a relatively simplified expression as shown in (2.40). Finally, the BER is given by (2.41). However, even in this case, the computation for the BER is extreme. As shown in (2.45), there are M-ple integrals to compute for every set of the given $(K-1)$ symbols of $\{X_2, \ldots, X_K\}$, not need to mention that $\{X_2, \ldots, X_K\}$ have in total M^{K-1} combinations. For this sake, in Section 2.2.6, we only evaluate the error probability of EGCD, when nano-machines' MTS codes are fixed, i.e., without considering the randomness of MTS codes.

2.2.6 Performance Results and Discussion

In this section, the error performance of the MTS-MoSK DMC systems with respectively the MS-MVD and EGCD is demonstrated against the number of molecules emitted per bit expressed as A_b, when various cases are considered. As in MTS-MoSK DMC systems, each symbol carries $b = \log_2 M$ bits, the total number of molecules emitted for transmitting one symbol is $A_s = b \times A_b$. However, due to the introduction of MTS, each symbol is transmitted using L chips by activating L molecular pulses. Hence, the number of molecules emitted per pulse is $A_h = A_s/L$. Additionally, we note that A_b in the figures is shown in dB values given by $10\log_{10} A_b$.

In our performance studies, unless specifically noted, there are some parameters set to fixed values, which are $D = 2.2 \times 10^{-9}\ m^2/s$ and $V = 4\pi\rho^3/3$ with $\rho = 20$ nm.The bit-duration is set to $T_b = 6 \times 10^{-5}\ s$, hence the symbol-duration is $T_s = b \times (6 \times 10^{-5})\ s$, and furthermore, the chip-duration is $T_h = T_s/L$. Additionally, considering the effect of ISI, we evaluate the effective length of a transmitted molecular pulse according to

$$I \triangleq \arg_i \left\{ \frac{c_{h(i)}}{c_{h(o)}} \leq 0.1\% \right\} \tag{2.47}$$

Assume that a pulse of molecules is emitted at $t = 0$, $c_{h(o)}$ in the above expression is the peak concentration obtained within the first chip-duration, while $c_h(i)$ is the concentration sampled at the ith chip-duration. Expression (2.47) means that only the concentration with the strength above 0.1% of the peak concentration is considered. Additionally, all the MTS codes employed in our studies are random codes.

Fig. 2.11 and Fig. 2.12 demonstrate the potential BER performance of the MTS-MoSK DMC systems with MS-MVD, which were evaluated from the lower-bound formulas derived in Section 2.2.4.1. Specifically in Fig. 2.11, we investigate the idealized error performance (lower-bound BER) versus K of the number of nano-machines supported by the MTS-MoSK DMC system, when $M = 32$ and $L = 4, 6, 8, 16$, respectively. Explicitly, the error performance of the MTS-MoSK DMC system degrades with the increase of the number of nano-machines supported. As shown in Fig. 2.11, as the number of chips used to transmit a symbol increases, the error performance continuously improves. The reason behind the observation is that when more chips per symbol is used, it becomes harder for the interferers to form the same number of entries as the reference nano-machine does. In other words, when the number of chips per symbol increases, the interference between any two nano-machines, i.e., MAI, reduces, hence resulting in the improvement of error performance. Note that for a given chip-duration, data rate reduces as the number of chips per symbol increases, which is also an explanation for the improvement of error performance.

Fig. 2.12 illustrates the impact of the number of molecular types on the BER performance of the MTS-MoSK DMC system with MS-MVD, when $L = 4$ is assumed. From the principles of MTS-MoSK DMC, we can know that when M increases, the modulation level increases and the number of bits conveyed per symbol increases. From the results of Fig. 2.12, we can observe

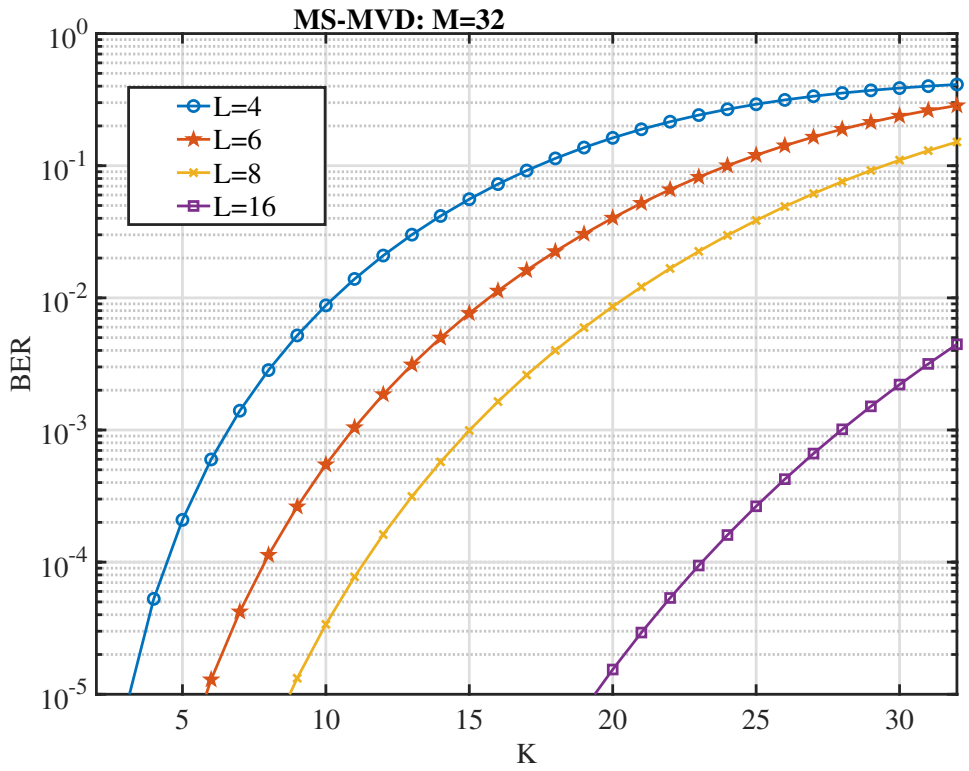

Figure 2.11: Lower-bound BER versus K of the number of nano-machines for the MTS-MoSK DMC system with MS-MVD, when given $M = 32$ and different number of chips per symbol.

that the BER performance improves, as M is increased from $M = 4$ to $M = 32$, respectively, corresponding to 2 to 5 bits per symbol. This observation conforms to the noble characteristics of MoSK modulation for interference mitigation. When given a value of L and a given value of K, as the value of M increases, there are more entries in the observation matrix $\boldsymbol{R}_u$ for the interfering elements to distribute. Hence, the MAI decreases, as the value of M increases, therefore resulting in the improvement of BER performance.

In Figs. 2.13 and 2.14, we compare the BER performance of the MTS-MoSK DMC systems with EGCD, which are obtained respectively from analytical approaches and simulation approaches. Note that, in term of the channel models, the simplified $\lambda_{q,l}(u)$ as shown in (2.39) is used to generate the number of molecules for both analysis and simulation. Furthermore, to make the performance evaluation and simulation manageable, the MTS codes are first randomly generated and then fixed for obtaining both analytical and simulation results.

In detail, in Fig. 2.13, we demonstrate the BER performance of the MTS-MoSK DMC systems employing EGCD, when various symbol-duration T and hence different data rates are considered. To obtain the analytical results in Fig. 2.13, the Poisson approach introduced in Section 2.2.5 is employed, and the results obtained by this approach are compared with that obtained from simulation. Note that, the MTS codes for the $K = 4$ nano-machines are $\boldsymbol{a}_1 = [3, 10, 14, 13, 9, 11, 5, 12]$, $\boldsymbol{a}_2 =$

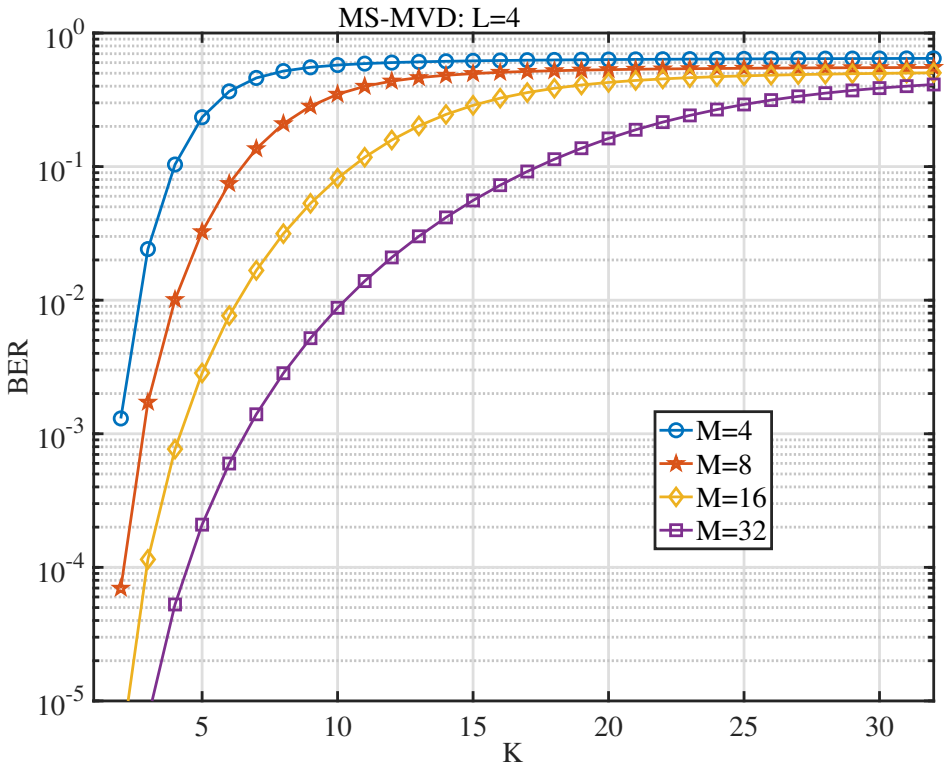

Figure 2.12: Lower-bound BER versus K of the number of nano-machines for the MTS-MoSK DMC system with MS-MVD, when given $L = 4$ and different modulation level.

$[15,3,11,10,6,7,5,0]$, $\boldsymbol{a}_3 = [8,6,9,5,12,4,10,13]$, $\boldsymbol{a}_4 = [4,15,3,5,12,6,1,0]$, and the other parameter values are detailed with the figure. As the results in Fig. 2.13 show, first, the analytical results agree well with the simulation results. Thus, the Poisson analytical approach is valid for performance study of MTS-MoSK DMC systems. Second, when the symbol-duration increases or data rate decreases, the BER performance of the MTS-MoSK DMC systems with EGCD improves, as the result of ISI reduction due to the increase of symbol-duration.

Fig. 2.14 compares the BER performance obtained from the analytical results based respectively on the Poisson approach and Gaussian approach, and that obtained by simulations. We assume that $K = 2$ nano-machines are invoked, and their MTS codes are $\boldsymbol{a}_1 = [2,0,5,6,7,3,4,1]$ and $\boldsymbol{a}_2 = [0,4,2,1,5,7,6,3]$. The results in Fig. 2.14 show that the analytical results obtained from both the approaches are very similar, and their agree well with the simulation results, although the analytical results slightly under estimate the simulation results. Therefore, both the Poisson approach and Gaussian approach can be employed for analyzing the performance of MTS-MoSK DMC systems, and our analytical results obtained in Section 2.2.4 are valid. Additionally, from Fig. 2.14 we can clearly observe that the BER performance of the MTS-MoSK DMC systems degrades as the transmission distance increases. This is because as the transmission distance increases, the ISI increases, and hence the BER performance degrades.

In Fig. 2.15, we compare the BER performance of the MTS-MoSK DMC systems employing

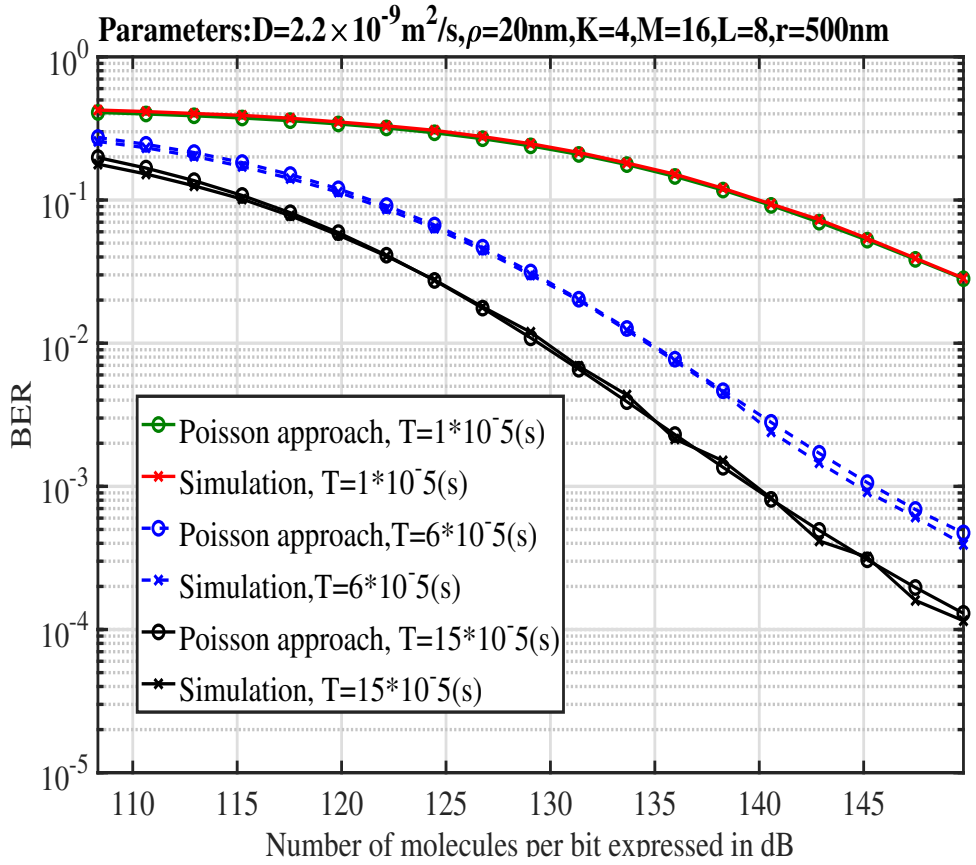

Figure 2.13: BER performance of MTS-MoSK DMC systems with EGCD, where the analytical results were evaluated based on the Poisson-approach.

respectively the MS-MVD and EGCD, when different numbers of nano-machines as shown in the figure are supported, while all the other parameters are fixed with the values shown on the top of the figure. From Fig. 2.15 we can have the following observations. First, for both the MS-MVD and EGCD, the BER performance declines, as the number of nano-machines supported increases, as the result of increased MAI. Second, MS-MVD outperforms EGCD, when A_b is relatively small. This becomes more declared, as the number of nano-machines supported becomes smaller. In other words, the MS-MVD is more desirable, when the number of nano-machines is lower, in particular, if A_b is small. By contrast, when A_b is relatively big, such as higher than 105 dB for $K = 4$, the BER performance achieved by EGCD becomes better than that attainable by MS-MVD. Therefore, MS-MVD is beneficial for operation in the case that the number of molecules emitted per pulse is relatively small, but is less effective than EGCD in MAI dominant environments. To be more specific, when A_b is small, the system performance is dominated by the counting noise, which depends on the transmitted signals. When EGCD is employed, the decision valuables are the sums of the row elements of matrix $\boldsymbol{D}_{k,u}$, as seen in Fig. 2.10. These operations enhance the influence of noise. By contrast, by selecting the largest ones from each column, the MS-MVD is capable of efficiently mitigating the effect of noise, making it outperform the EGCD in low A_b region. On the other side, if A_b is sufficiently high, the system performance becomes dominated by MAI. As

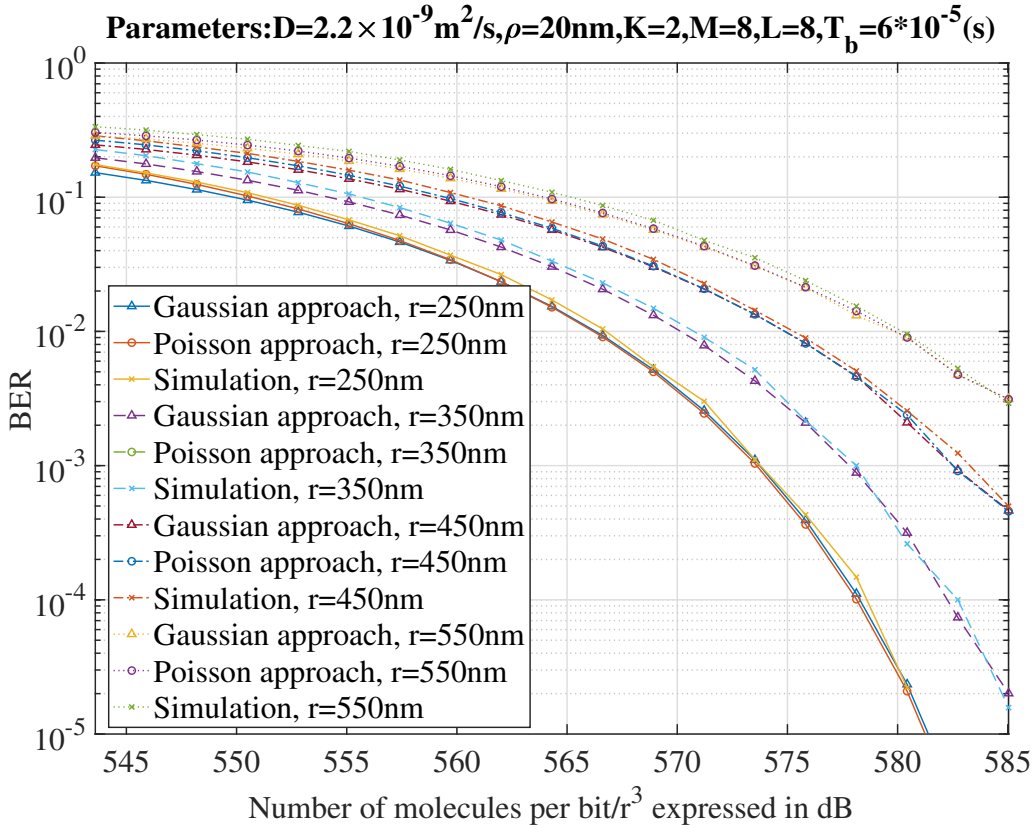

Figure 2.14: BER performance of MTS-MoSK DMC systems with EGCD, where the analytical results were evaluated based on the Poisson-approach and Gaussian approach, respectively.

the sum operation in EGCD is able to smooth the MAI but the MS-MVD is unable to, the EGCD performs better than the MS-MVD. This observation can be further evidenced by the results with the increase of the number of nano-machines. As shown in Fig. 2.15, for a given and low A_b value, the gap between the BER achieved by EGCD and that by MS-MVD becomes smaller, as K increases.

Fig. 2.16 compares the BER performance of MS-MVD with that of the EGCD with respect to different modulation levels, namely, $M = 8$, 16 and 32. We can see that when the modulation level M, i.e., the number of molecular types, increases, the BER performance achieved by both detection schemes improves significantly. The reason behind this observation is that when M increases, both the ISI and MAI reduce. Another observation we can attain from Fig. 2.16 is that MS-MVD becomes more promising than EGCD, as M increases. As the curves in Fig. 2.16 show, when $M = 8$, both BER curves are close to each other and when A_b is relatively small, MS-MVD is in fact outperformed by the EGCD. By contrast, when M is increased to 16 and further to 32, the performance improvement of the MS-MVD with respect to the EGCD enhances, and the performance gap between them becomes bigger.

Given the bit-duration $T_b = 6 \times 10^{-5}$ s and hence, the symbol-duration, Fig. 2.17 compares the

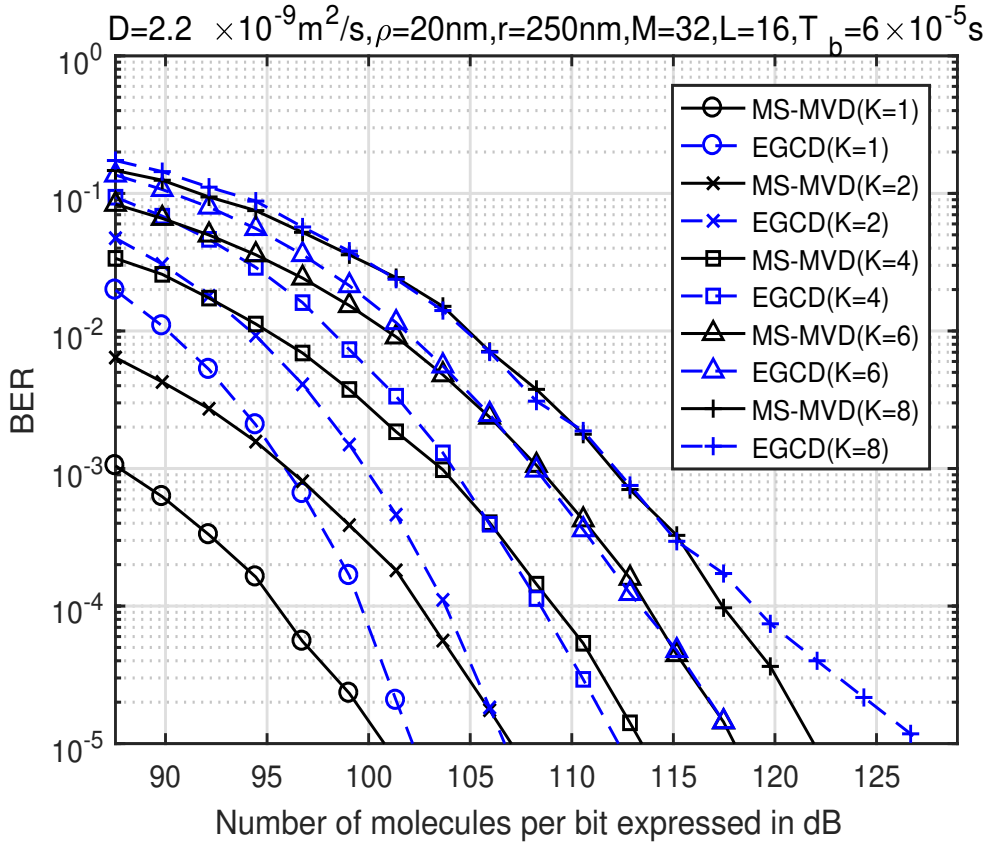

Figure 2.15: Comparison of BER performance of the MTS-MoSK DMC systems employing MS-MVD and EGCD, respectively.

MS-MVD with EGCD, when different values of L are considered. From the results of Fig. 2.17, we observe that the BER performance does not monotonically improves, as the number of chips L per symbol increases. As the results show, for both the MS-MVD and EGCD, $L = 16$ attains the best BER performance over the main SNR region. The only exception is that the EGCD with $L = 32$ achieves the best BER performance, after the A_b is higher than about 110 dB. The reason for the above observation is that the increase of L has two-fold of effect. First, increasing L is capable of averaging out (smoothing) the effect of noise and ISI. However, when L increases, more molecular pulses per symbol are transmitted and for a fixed symbol-duration, the chip-duration is reduced, which therefore, result in the increase of ISI and MAI. The above observations and analysis imply that for given other parameters and a detection scheme (either MS-MVD or EGCD), there is an optimum value of L, which is capable of attaining the lowest BER.

Finally, in order to validate the model-based simulation and our analytical results, particle-based simulation results are compared with that obtained from the model-based simulations or/and analytical results in the following two figures. First, in Fig. 2.18, we compare the BER performance of the MTS-MoSK DMC systems with MS-MVD obtained respectively from the Gaussian-model based Monte-Carlo simulations and the particle-based simulations. In our simulations, we

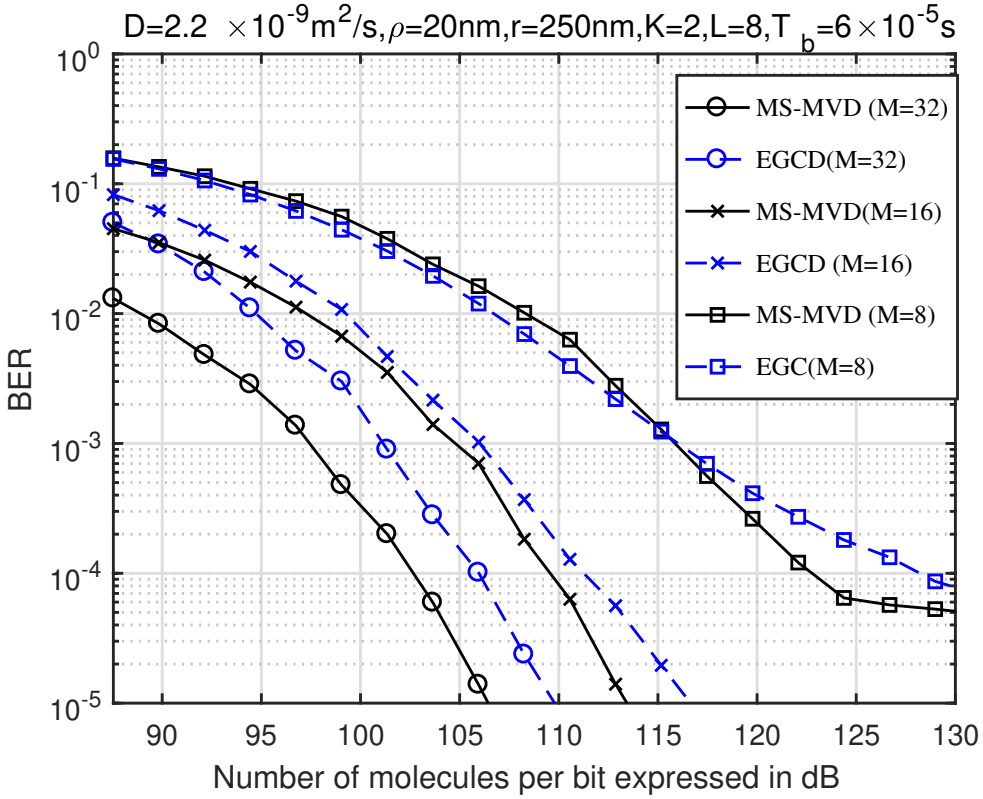

Figure 2.16: Comparison of BER performance of the MTS-MoSK DMC systems employing respectively MS-MVD and EGCD, when different numbers of molecular types are invoked.

assume $K = 2$ nano-machines with their MTS codes of $\boldsymbol{a}_1 = [2,0,5,6,7,3,4,1]$ and $\boldsymbol{a}_2 = [0,4,2,1,5,7,6,3]$, respectively. Furthermore, since different r values are considered, as shown in Fig. 2.18, we use A_b normalized by r^3, i.e., A_b/r^3, for the X-axis. This is because at the sampling point of $t_d = r^2/6D$, the molecular density is $c_{b(o)} = (A_b/r^3)^{-1}(2\pi e/3)^{\frac{3}{2}}$. Hence, for a given value of A_b/r^3, the molecular density is independent of r. In this case, furthermore, the number of received molecules by a detector with volume V is $Vc_{b(o)} = V(A_b/r^3)^{-1}(2\pi e/3)^{\frac{3}{2}}$, which is also a function of A_b/r^3. In other words, regardless of the distance r between the transmitter and receiver, the received power is the same when A_b/r^3 is given. Therefore, the comparison for different r values is done under the same receive power. From the results we can observe that, first, the BER performance degrades when increasing r, as the result of increased interference. Second, the BER obtained from the model based simulations agrees well with that obtained from the particle-based simulations. Furthermore, the BER results obtained from the model-based simulations become closer to that obtained from the particle-based simulations, as the distance r between transmitter and receiver increases. The reason behind is obvious. The spherical receiver (with a radius of $\rho = 20$ nm) is modeled as a point receiver in the model based simulations, but not in the particle-based simulations. Explicitly shown in Fig. 2.18, the approximation to a point receiver becomes more accurate as r increases, or more precisely, as r/ρ increases.

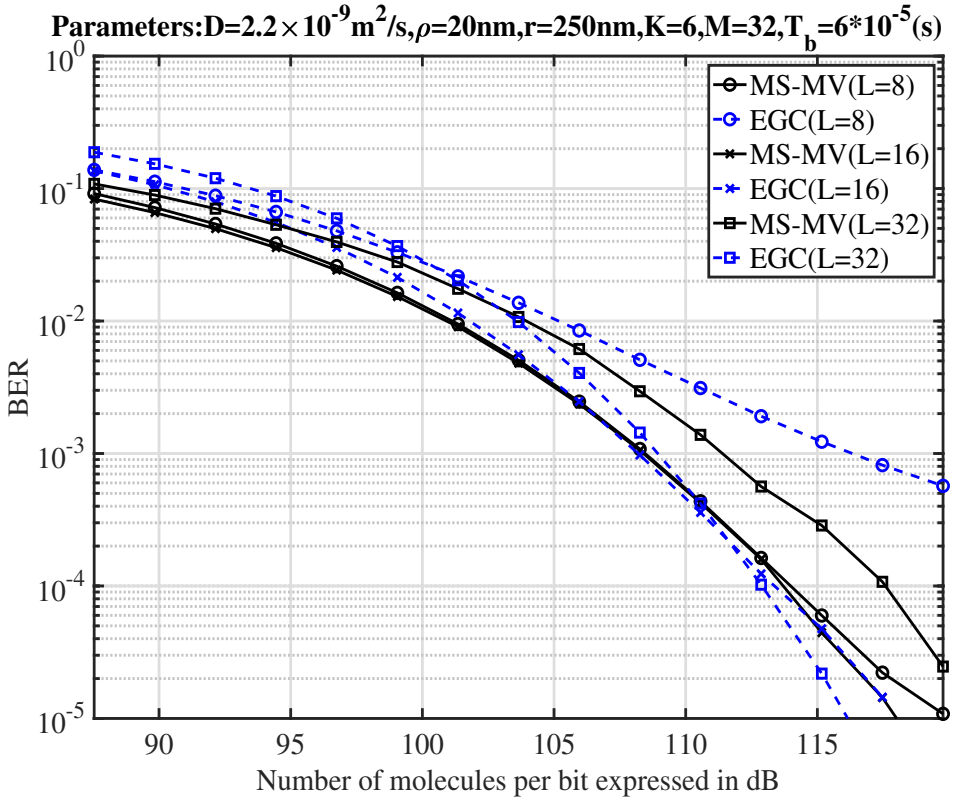

Figure 2.17: Comparison of the BER performance of the MTS-MoSK DMC systems employing respectively MS-MVD and EGCD, when various number of chips per symbol is considered.

In Fig. 2.19, we compare the BER performance of the MTS-MoSK DMC systems with EGCD obtained from different approaches, including the Poisson based analytical approach, Gaussian-based Monte-Carlo simulations and the particle-based simulations. We also assume $K = 2$ nano-machines with the MTS codes of $\boldsymbol{a}_1 = [2,0,5,6,7,3,4,1]$ and $\boldsymbol{a}_2 = [0,4,2,1,5,7,6,3]$. Note that in the figure, the results corresponding to EGCD sim (Gaussian) fully overlap with the results corresponding to EGCD Ana (Poisson). We also compare the BER performance of the MTS-MoSK DMC systems with that of the OOK DMC systems, where each of nano-machines is exclusively supported by one type of molecules. For fair comparison, both systems are set to have the same data rate and the same power budget. The results in Fig. 2.19 demonstrate that when the bit-duration is $T_b = 2 \times 10^{-5}$, implying a relatively high bit rate, the BER performance of the MTS-MoSK DMC systems with EGCD is better than that of the OOK DMC systems. By contrast, when the bit rate is relatively low corresponding to $T_b = 6 \times 10^{-5}$, the OOK DMC slightly outperforms the MTS-MoSK DMC in terms of the BER performance. The reason behind is that OOK DMC does not experience MAI but suffers from ISI, which becomes severer as bit-duration becomes smaller or as data rate becomes higher. By contrast, while MTS-MoSK DMC suffers from MAI, its ISI can be much lower than OOK DMC, which becomes more noticeable as data rate increases. Hence, when data rate is relatively high, MTS-MoSK DMC is capable of achieving better BER performance

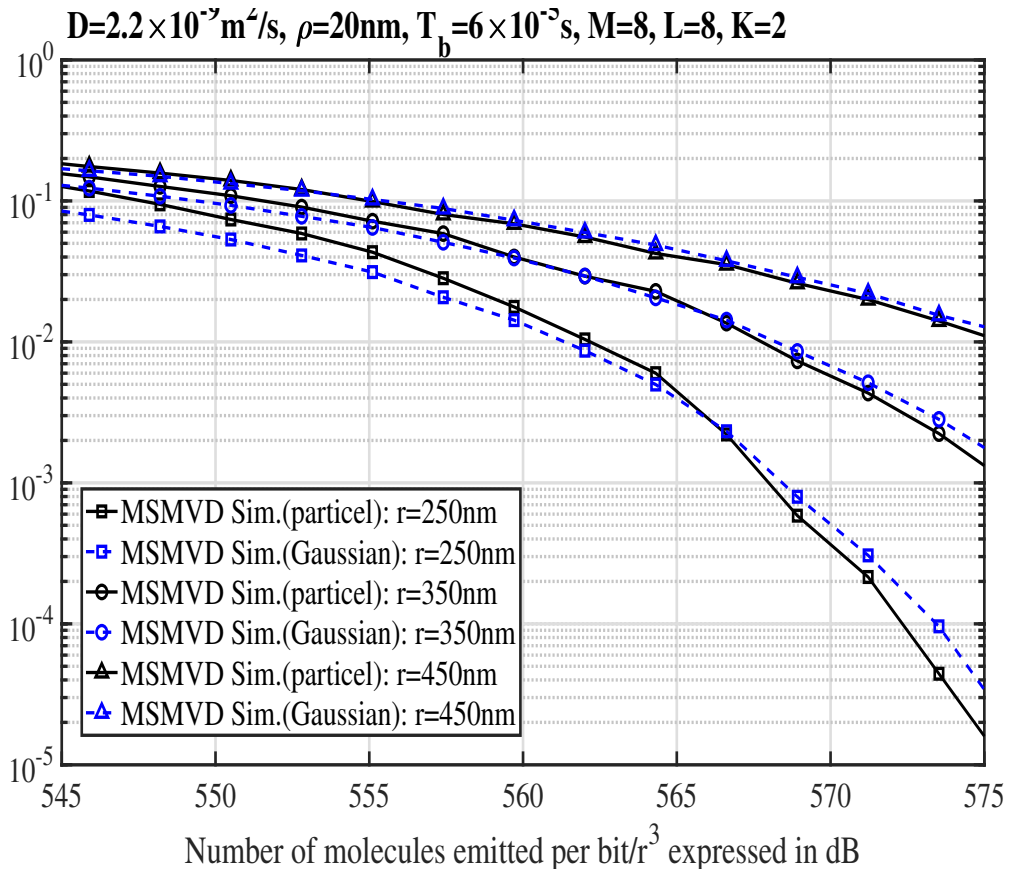

Figure 2.18: BER versus the number of molecules emitted per bit normalized by $/r^3$ for the MTS-MoSK DMC systems with MS-MVD, where results were obtained from the Gaussian-modeling Monte-Carlo simulations or the particle-based simulations.

than OOK DMC. On the other side, when data rate is low, resulting in that the ISI in OOK DMC is insignificant, the BER performance of OOK DMC may become better than that of MTS-MoSK DMC, as in this case the MTS-MoSK DMC may still suffer from MAI. From these observations we may deduce that MTS-MoSK DMC is beneficial to supporting the multiple-access transmission requiring relatively high data rate.

Additionally, the results of Fig. 2.19 show that in both MTS-MoSK DMC and OOK DMC, the result obtained from the particle-based simulation is slightly lower than that obtained from the Poisson-based analysis or Monte-Carlo simulation. The reason is that in the Poisson-based analysis or Monte-Carlo simulation, the molecular density within the observation space is assumed to be uniform. However, in the particle-based simulation, the molecules within the observation space is non-uniform distributed, which results in a slight difference from the uniform distribution based analysis/simulation. Again, we can deduce that the order of difference is depended on the distance between transmitter and receiver relative to the size of the observation space, i.e., on the ratio of ρ/r. Provided that this ratio is sufficiently big, such as$\geq$ 10, the model based Monte-Carlo simulations, which approximate receiver as a point, can be confidently employed for the

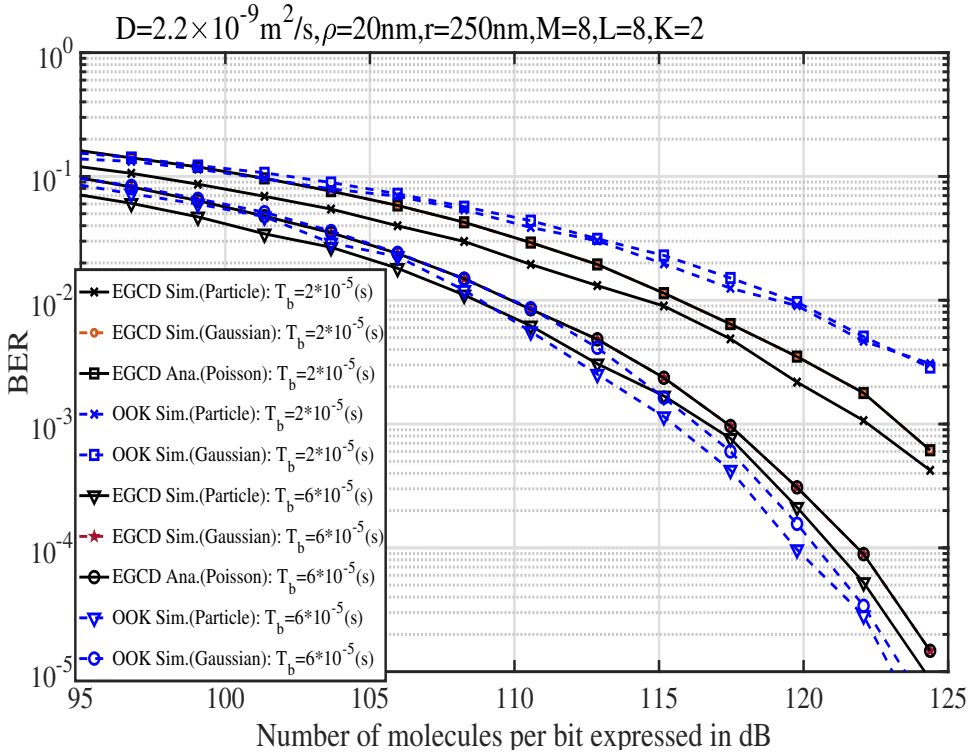

Figure 2.19: Comparison of the BER versus SNR performance of the MTS-MoSK DMC systems with EGCD and that of OOK-DMC systems, where analytical results were evaluated based on the Poisson-approach and simulation results were obtained from Monte-Carlo and particle-based methods, respectively.

performance estimation/prediction of DMC systems, as evidenced by both Fig. 2.18 and Fig. 2.19.

2.2.7 Conclusions

In order for DMC to support multiple access communications, a MTS-MoSK DMC scheme has been proposed. Correspondingly, two low-complexity detection approaches, namely MS-MVD and EGCD, have been proposed. It is shown that both detection approaches are not dependent on thresholds for detection, which are beneficial for implementation, as threshold in DMC is usually difficult to set, due to the transmission-relied noise and strong ISI. In this section, the error performance of MTS-MoSK DMC systems has been investigated based on both analytical results and simulations. It can be shown that the analytical results are valid. Against the conventional radio-based communications where EGCD always outperforms MS-MVD, our studies demonstrate that in a DMC system supporting a small number of nano-machines relative to L, MS-MVD usually outperforms EGCD at relatively low SNR. When the SNR is high, MS-MVD may be outperformed by EGCD. By contrast, when a DMC system supports a big number of nano-machines relative to L, the BER performance achieved by both MS-MVD and EGCD is close to each other, although MS-MVD may slightly outperform (or be outperformed by) EGCD, depending on the SNR region

observed. In terms of the impact of modulation order, it is shown that the error performance improves, as the modulation order M increases. Furthermore, it is shown that for a given number of molecules released per symbol and a given number of nano-machines supported, there is an optimum value for L, which results in the best error performance. Our future research will consider the design of promising MTS codes for MTS-MoSK DMC systems, as well as the low-complexity detection schemes with MAI cancellation capability, in order to enhance the DMC reliability and/or support more nano-machines.

Chapter 3

Interference Cancellation in Type-Spread Molecular Shift Keying Multiple-Access Systems

In the last chapter, we proposed a MTS-MoSK scheme to support multiple-access in DMC, where several NMs are able to communicate with one AP simultaneously via a common DMC channel. However, multiple-access DMC systems suffer from severe Multiple-Access Interference (MAI) and ISI, which should be effectively mitigated at receiver in order to achieve acceptable performance. In this chapter, built on two fundamental single-user detection schemes, namely Threshold assisted Majority Vote Detection (TMVD) and Equal Gain Combination Detection (EGCD), we first propose three low-complexity interference cancellation schemes, which are the TMVD-assisted Iterative Interference Cancellation (TMVD-IIC), TMVD-based Minimum-Distance Decoding assisted Interference Cancellation (TMVD-MDDIC) and the EGCD-assisted N-order Iterative Interference Cancellation (EGCD-NIIC), for operation in the MTS-MoSK DMC systems. Then, following the principle of maximum likelihood detection, we propose a Simplified Approximate Maximum Likelihood (SAML) detection scheme.

3.1 Introduction

Following Moore's law, nano-machines have been becoming smaller and smaller. In practice, nano-machines may find different applications, especially, in biology and healthcare. In literature, there are many novel researches on the health monitor and disease treatment that rely on the implementation of nano-machines [87–89]. However, the manufacture capability of nano-machines puts constraints on the computation or tasks that a nano-machine is able to accomplish [90]. Due to this kind of constraints, Internet of Nano-Machines (IoNM) needs to be constructed to allow var-

ious nano-machines to cooperate via information exchange, so as to complete complex tasks. As an efficient communication technique for IoNM, Molecular Communication (MC) has a range of advantages, including energy saving, biocompatibility, small size, etc. [12, 13, 91]. However, to implement the IoNM that relies on MC, a critical issue is how multiple nano-machines transmit information simultaneously with high-efficiency. For example, in a molecular sensor network, because of limited storage space and computation capability of individual nano-sensors, the observations attained by individual sensors need to be sent to a processing center for fusion. In this network, it is highly challenging for the multiple nano-sensors to propagate their sensed information to the processing center, reliably and efficiently. Even so, to our knowledge, multiple-access MC (MAMC) has received insufficient attention in the MC research communities.

Following the principles of multiple-access wireless communications, some multiple-access schemes have been considered in Diffusion-based Molecular Communication (DMC). More specifically, Molecular Division Multiple-Access (MDMA) proposed by [**?**, 16] straightforwardly allocates one or groups of unique molecules to individual nano-machine. In this way, simultaneous transmissions of different nano-machines can be implemented in one sharing medium without interference imposed on or suffered from each other. [51, 74] proposed the Molecular Code-Division Multiple-Access (MCDMA), which assigns individual nano-machines unique signature codes for them to implement simultaneous transmission to a common receiver, where the signature codes are used to distinguish the information sent by different nano-machines. In [52–54], Molecular Time-Division Multiple-Access (MTDMA) was introduced to support multiple nano-machines communicating with a common receiver. In MTDMA DMC systems, different time slots are assigned to different nano-machines for them to send information so as to mitigate the inter-user interference. Because the molecular concentration impulse received is significantly sensitive to the transmission distance in DMC, [50] and [49] proposed the Molecular Space Division Multiple-Access (MSDMA) to distinguish nano-transmitters via their distances from the receiver. Furthermore, the authors of [75, 92–95] proposed the Molecule Division Multiple Access (MDMA), where individual nano-transmitters use unique types of molecules to build orthogonal channels for information transmission to a common receiver.

Due to the diffusive properties of DMC, multiple-access DMC (MA-DMC) usually experiences various types of interference, especially, Multiple-Access Interference (MAI). Furthermore, due to the slow process of Brownian motion, interference, especially MAI, in MA-DMC systems is likely to be severe. Hence, the designs of multiple-access schemes and transceivers are highly important in mitigating the interference in MA-DMC systems. In literature, there are some works having proposed and investigated the detection schemes for MA-DMC systems [49, 51, 52, 75]. Specifically, considering the MCDMA with On-Off Keying (OOK) modulation, a chip-threshold-based detection scheme was developed in [51], where an adaptive threshold is set according to the concentration values measured with the previous chips around the receiver. For the MoTDMA with Molecular Shift Keying (MoSK) [52], the authors adopted the detection approach presented in [61],

which is also a threshold-based detection scheme. As this MoTDMA scheme employs two types of molecules to transmit binary data, the detector uses the observation of one type of molecules as the decision variable, while the observation of the other type of molecules is used as the adaptive threshold for the decision-making in each signal interval. For the MSDMA systems in [49], the expected shapes of the received molecular pulses corresponding to all the possible transmission cases are estimated, which are then compared respectively with the observation samples to achieve Information detection. Finally, in [75], different types of molecules were straightforwardly exploited for distinguishing the transmissions by different nano-machines.

Inspired by the Fast Frequency-Hopping M-ary Frequency Shift Keying (FFH-MFSK) scheme [76, 77] in the conventional wireless communications, we have proposed a Molecular Type Spread assisted Molecular Shift Keying (MTS-MoSK) scheme to support MA-DMC in [96]. In this MTS-MoSK DMC scheme, different nano-machines are assigned with unique address codes, which are used to implement molecular type hopping at transmitter and assist signal detection at receiver. For signal detection, in [96], two low-complexity single-use detection schemes have been studied, which are the Threshold assisted Majority Vote Detector (TMVD) and Equal Gain Combining Detector (EGCD). Although these detection approaches have low complexity. However, due to the severe interference existing in the MTS-MoSK systems, as above-mentioned, the MTS-MoSK systems with these detectors can only support a low number of nano-machines. Otherwise, the error performance of MTS-MoSK systems will be very poor. To enable a MTS-MoSK system to simultaneously support a relatively high number of nano-machines while attaining practically meaningful reliability, in this chapter, we focus on the MAI mitigation by proposing and comparing a range of interference mitigation schemes for the MTS-MoSK systems. Specifically, four MAI cancellation schemes are proposed, which are the Minimum-Distance Decoding based Interference Cancellation (MDDIC), TMVD-assisted Iterative Interference Cancellation (TMVD-IIC), the EGCD-assisted N-order Iterative Interference Cancellation (EGCD-NIIC) and the EGC-based Interference Mitigation (EGC-IM). We investigate their achievable performance and compare it with that obtained by the TMVD or EGCD. Furthermore, as another bench-marker, we propose a Simplified Approximate Maximum Likelihood (SAML) detection scheme, which has high complexity, to compare it with the interference cancellation assisted detection schemes. Furthermore, we demonstrate the impact of different parameters on the error performance of MTS-MoSK DMC systems. In particular, we show the effect of the thresholds in the TMVD-MDDIC and TMVD-IIC schemes, the number of nano-machines participated in the interference cancellation in the EGCD-NIIC scheme, and the number of entries erased from each row in the EGC-IM scheme. Additionally, we analyze the complexities of all the detection schemes considered and show their performance-complexity trade-off.

The contributions of the paper can be summarized as follows.

- MTS-MoSK assisted MA-DMC systems with various detection schemes are introduced, in-

vestigated and compared, to show the feasibility for supporting multiple-access communications in DMC environments.

- Four detection schemes having MAI mitigation capability are proposed, which are the TMVD-MDDIC, TMVD-IIC, EGCD-NIIC, EGC-IM and SAML. Among these five detection schemes, the TMVD-MDDIC, TMVD-IIC, EGCD-NIIC, and EGC-IM detection schemes rely on interference cancellation to mitigate MAI, while the SAML implements information detection in the principle of ML.

- The performance of the MTS-MoSK assisted MA-DMC systems with respectively these detection schemes and the TMVD and EGCD, which are the single-user detectors without attempting MAI mitigation, is investigated and compared. The impact of the parameters related to system design, channel, and detection schemes on system performance is comprehensively studied. Furthermore, the complexities of the detection schemes are analyzed to show the trade-off between complexity and performance.

The remainder of this chapter is organized as follows. Section 3.2 introduces the MTS-MoSK DMC system model. In Section 3.3, the principles of four MAI mitigation schemes are introduced. Performance results are demonstrated and discussed in Section 3.4. Finally, the main conclusions from research are summarized in Section 3.5.

3.2 System Description

The framework of our MTS-MoSK DMC system is shown in Fig. 3.1, which was firstly introduced in Chapter 2 [96]. The specific system structure and the procedure of operations are detailed in the following subsections.

3.2.1 Description of Transmitter and Channel Model

We assume that M types of information molecules are employed to support $K \leq M$ nano-machines to exchange information with a common access point (AP). The nano-machines and AP are static and their positions do not vary during a communication session. For simplicity, each nano-machine is assumed to have a similar distance from the AP. Note that, this can be a practical case in molecular sensor network (MSN). For example, several sensors monitoring an event may be arranged to have a similar distance from a fusion center, where the sensors upload their sensed data. In Fig. 3.1, the transmission of several bits of binary data from one nano-machine is demonstrated as the upper half of the figure. We assume that each nano-machine uses M types of molecules to transmit information in the form of M-ary symbols. Hence, each nano-machine can send $b = \log_2 M$ bits information per symbol. The symbol-duration is represented as T_s, which is divided into $L = T_s/T_h$ chips. Each chip takes up $T_h = T_s/L$ seconds, referred to as chip-duration. In our system

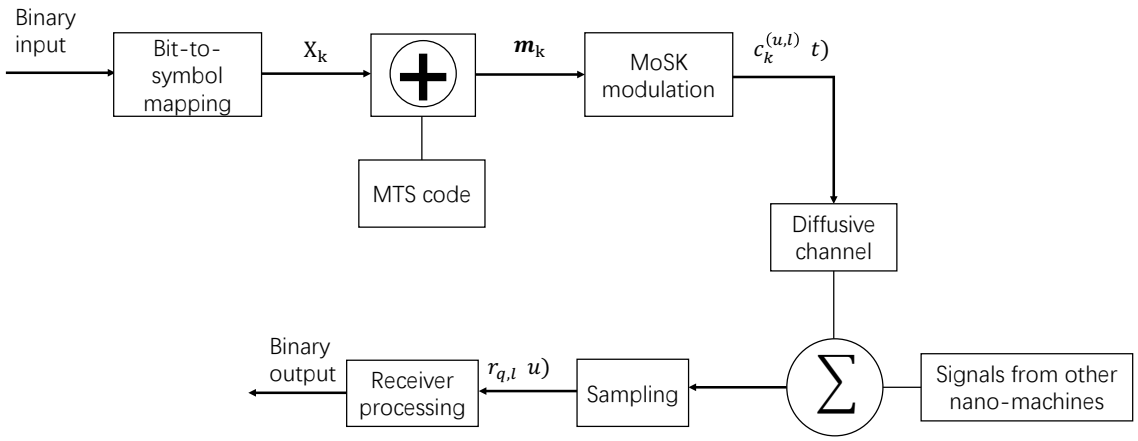

Figure 3.1: System diagram demonstrating the procedures of the MTS-MoSK DMC systems.

model, we also assume that the K nano-machines implement synchronous transmission at chip level. In practice, AP can send periodic pilot signals to the nano-machines for them to synchronize their transmissions. As Fig. 3.1 shows, at the beginning of a T_s-second symbol-duration, b bits of binary data to be transmitted by the kth nano-machine is mapped to a M-ary symbol, which is expressed as $X_k \in \{0,1,\ldots,M-1\}$. Then, the M-ary symbol X_k is signed by the molecular type spreading (MTS) code of the kth nano-machine. The kth nano-machine's MTS code can be expressed as $\boldsymbol{a}_k = [a_k^{(0)}, a_k^{(1)}, \ldots, a_k^{(L-1)}]$, $k = 1,2,\ldots,K$, $a_k^{(i)} \in [0, M-1]$. The signature operation in Fig. 3.1 can be expressed as

$$\begin{aligned}\boldsymbol{m}_k =& [m_k^{(0)}, m_k^{(1)}, \ldots, m_k^{(L-1)}] \\ =& X_k \cdot \mathbf{1}_{(1\times L)} \oplus \boldsymbol{a}_k \\ =& [X_k \oplus a_k^{(0)}, X_k \oplus a_k^{(1)}, \ldots, X_k \oplus a_k^{(L-1)}], \\ & k = 1,2,\ldots,K\end{aligned} \tag{3.1}$$

where $\mathbf{1}_{(1\times L)}$ is a row vector of L ones, which is used to extend the symbol X_k to a row vector with L elements of all being X_k, $\oplus$ is the addition operation in the Galois field GF(M) [83]. The elements of $\boldsymbol{m}_k$ are the symbols signed by the MTS code at chip scale and they are the integer values in $[0, M-1]$. After the signature operation, the MoSK modulation block in Fig. 3.1 controls the emission of the corresponding M types of molecules according to the values in $\boldsymbol{m}_k$ over the L chip-durations.

To explain the transmission process more clearly, let us assume a MTS-MoSK DMC system, which employs $M = 8$ types of molecules and $L = 6$ chips per symbol to support the information transmission of two nano-machines to an AP. Two MTS codes of $\boldsymbol{a}_1 = [4,3,7,6,2,5]$ and $\boldsymbol{a}_2 = [2,0,1,6,4,7]$ are assigned to the two nano-machines, respectively. Data symbols to be transmitted by two nano-machines are assumed to be $X_1 = 5$ and $X_2 = 3$. Then, X_1 and X_2 are extended to the L-length row vectors of $X_1 \cdot \mathbf{1}_{(1\times L)} = [5,5,5,5,5,5]$ and $X_2 \cdot \mathbf{1}_{(1\times L)} = [3,3,3,3,3,3]$, respec-

tively. Then, these two row vectors execute the addition operation in Galois field $GF(8)$ with $\boldsymbol{a}_1$ and $\boldsymbol{a}_2$, yielding $\boldsymbol{m}_1 = X_1 \cdot \mathbf{1}_{(1\times L)} \oplus \boldsymbol{a}_1 = [1,6,2,3,7,0]$ and $\boldsymbol{m}_2 = X_2 \cdot \mathbf{1}_{(1\times L)} \oplus \boldsymbol{a}_2 = [1,3,2,5,7,4]$, respectively, where every element value corresponds to a type of molecules to be emitted within its chip-duration. Note that, the red elements in $\boldsymbol{m}_1$ and $\boldsymbol{m}_2$ indicate that the transmissions from two nano-machines generate collisions, which results in MAI, because the two nano-machines emit the same type of molecules during the same chip duration.

Assume that the MTS-MoSK DMC system employs the M types of isomer molecules, which have similar physical properties, including a similar diffusion coefficient expressed by D, when diffusing in a fluid medium [84]. After the MoSK modulation, a type of molecules are emitted at the beginning of a chip duration. Then, the concentration of this type of molecules around the receiver AP will start arising from the beginning of this chip-duration. We assume that within the lth chip duration of the uth symbol-duration, the qth type of molecules is activated for transmission by the kth nano-machine. According to Fick's second law [42, 69], the concentration observed at the AP varies with time t as

$$\begin{aligned} c_{k,q}^{(u,l)}(t) =& \frac{A}{\left[4\pi D\left(t-uT_s-lT_h\right)\right]^{3/2}} \\ & \times \exp\left(\frac{-r^2}{4D\left(t-uT_s-lT_h\right)}\right), \\ & t \geq (uL+l)\,T_h; u=0,1,\ldots; l=0,1,\ldots,L-1 \end{aligned} \tag{3.2}$$

where r is the transmission distance from the kth nano-machine to AP and A is the total number of molecules emitted per pulse.

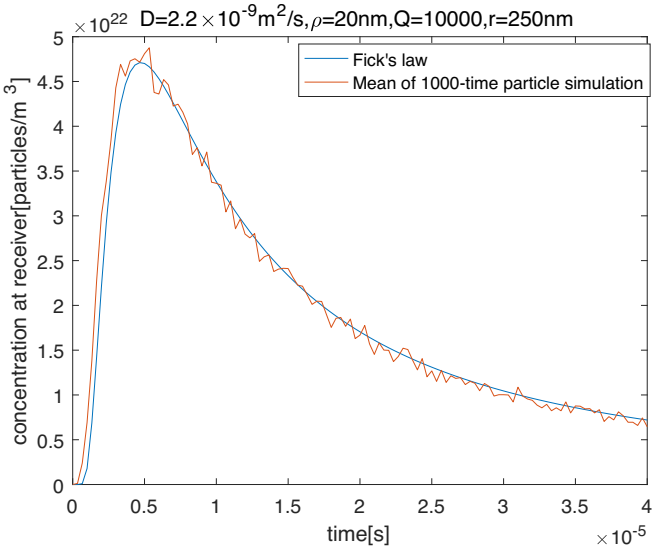

Figure 3.2: Comparison between the expectation of concentration predicated by Fick's law of (3.2) and the average concentration obtained from 1000 particle-based simulations, when assuming that an impulse of 10000 molecules is emitted at $t = 0$.

Fig. 3.2 shows a molecular pulse of concentration generated, when an impulse of $A = 10000$ molecules is emitted at $t = 0$. The smooth curve is computed from (3.2) of Fick's diffusion law. The vibrating curve is the average concentration obtained from 1000 realizations. Explicitly, the estimated concentration agrees well with the concentration predicted by Fick's law of (3.2). However, the estimated concentration slightly fluctuates around the theoretical expectation, which is because of the random noise generated by the Brownian motion of molecules and the limited 1000 realizations. Note that, according to [66], in DMC, we usually treat the expected concentration of (3.2) as the ideal signal, while the expected concentration plus the random noise generated by Brownian motion is the actual observation at receiver.

According to the properties of the free diffusion phenomenon, it can be easily deduced that there are three kinds of interference in the multiple access DMC systems, including the MTS-MoSK DMC system considered in this chapter. First, as mentioned in many references [30, 58], the molecules of a given type generated for transmitting previous symbols may overlap with that for the later symbols, generating ISI. Second, the random Brownian motion of molecules results in background noise, which is also referred to as counting noise [22]. Third, as in the MTS-MoSK DMC system, when a desired nano-machine transmits the type-m molecules at a chip duration, the other nano-machines may also transmit this type of molecules at the same time, which interferes with the desired nano-machine. Furthermore, the mth type of molecules transmitted in the previous chip durations by the other nano-machines also interfere the desired nano-machine in the considered chip-duration. These kinds of interference resulted from the multiple nano-machines' transmissions are referred as MAI. Therefore, to achieve reliable communication in the multiple access DMC systems, the detection scheme must be carefully designed, so that the effect from the various kinds of interference can be minimized. In this chapter, our focus is on the design of the effective interference cancellation schemes, which will be detailed in the forthcoming discourses.

3.2.2 Observations Obtained by Receiver

As Fig. 3.2 shows, when emitting an impulse of molecules at the beginning of a chip, the expected peak of concentration is an appropriate sampling point for the receiver at AP to obtain observations. From (3.2), we can derive that this peak point occurs at $t_d = r^2/(6D)$. Assume that in our MTS-MoSK DMC system, the chip-duration is sufficiently long, so that the extreme point happens within one chip-duration, i.e., $T_h > t_d$. Then, the sampled observation within the lth chip-duration of the uth symbol can be expressed as

$$\begin{aligned} r_{q,l}(u) =& r_q(t = uT_s + lT_h + t_d), \\ & l = 0, 1, \ldots, L-1;\ u = 0, 1, \ldots; \\ & q = 0, 1, \ldots, M-1 \end{aligned} \tag{3.3}$$

When the Brownian motion generated noise, ISI and MAI, as discussed previously, are taken into account, it can be shown that $r_{q,l}(u)$ can be expressed as

$$\begin{aligned} r_{q,l}(u) &= \sum_{k=1}^{K} \sum_{i=0}^{\min\{I,uL+l\}} \ell_{k,q}^{uL+l-i} c_{k,q}(iT_h + t_d) \\ &\quad + n_q(uT_s + lT_h + t_d) \\ &= \sum_{k=1}^{K} \sum_{i=0}^{\min\{I,uL+l\}} \ell_{k,q}^{uL+l-i} c_{k,q}(i) + n_{q,l}(u) \end{aligned} \tag{3.4}$$

where I represents the ISI length in chip-durations, and $\ell_{k,q}^{i}$ makes a logical decision, equating to '1', when the kth nano-machine emits the type-q molecules to transmit information within the ith chip-duration, and otherwise, is '0'. In (3.4), $c_{k,q}(i)$, i.e., $c_{k,q}(iT_h + t_d)$, is the expected concentration of the type-q molecules sampled at $t = iT_h + t_d$, if this type of molecules was emitted at $t = 0$, which is given by (3.2) with $t = iT_h + t_d$. It can be conceived from (3.4) that only the term with $i = 0$ contributes the desired observation for the current chip, while all the other terms with $i \neq 0$ impose interference. Finally, $n_{q,l}(u)$ in (3.4) represents the background noise resulted from the diffusion of the type-q molecules, which can be approximated as a Gaussian distribution [58], with the probability density function (PDF) expressed as

$$n_{q,l}(u) \sim \mathcal{N}\left(0, \frac{1}{V} \sum_{k=1}^{K} \sum_{i=0}^{\min\{I,uL+l\}} \ell_{k,q}^{uL+l-i} c_{k,q}(i)\right) \tag{3.5}$$

where V is the volume of the detection sphere that the AP uses for sensing information particles. As shown in (3.5), the variance of noise is depended on the amplitude of signal, which explains that noise is introduced whenever a signal is transmitted. The higher power of transmitted signal results in the higher power of noise.

3.3 Signal Detection and MAI cancellation in MTS-MoSK DMC Systems

According to the indexes shown in (3.3), it can be inferred that there are in total ML observations sampled by the receiver at AP in every symbol-duration. In order to describe the principles of the detection and MAI mitigation schemes, the observations in one symbol duration are arranged to form a matrix $\boldsymbol{R}_u$, expressed as

$$\boldsymbol{R}_u = \begin{bmatrix} r_{1,1}(u) & r_{1,2}(u) & \cdots & r_{1,l}(u) & \cdots & r_{1,L}(u) \\ r_{2,1}(u) & r_{2,2}(u) & \cdots & r_{2,l}(u) & \cdots & r_{2,L}(u) \\ \vdots & \vdots & \ddots & \vdots & \ddots & \vdots \\ r_{q,1}(u) & r_{q,2}(u) & \cdots & r_{q,l}(u) & \cdots & r_{q,L}(u) \\ \vdots & \vdots & \ddots & \vdots & \ddots & \vdots \\ r_{M,1}(u) & r_{M,2}(u) & \cdots & r_{M,l}(u) & \cdots & r_{M,L}(u) \end{bmatrix} \tag{3.6}$$

where M rows correspond to the M molecular types representing the M possibly transmitted symbols, and L columns correspond to the L chips of a symbol-duration. The (q,l)th element of $\boldsymbol{R}_u$ is $r_{q,l}(u)$ given by (3.4).

Having obtained the observation matrix $\boldsymbol{R}_u$, below we introduce two fundamental detection schemes and four MAI cancellation algorithms for signal detection in MTS-MoSK DMC systems. More specifically, the first one, inspired by a conventional single-user noncoherent detection scheme in radio communication [97], implements the threshold filtering before the majority vote assisted detection, which is named as TMVD. The second one is the proposed TMVD-MDDIC, which implements the minimum-distance decoding assisted interference cancellation followed by TMVD. The third one carries out the iterative interference cancellation after the fundamental TMVD, which is referred to as TMVD-IIC [98]. The forth one is the conventional equal-gain combining assisted detection (EGCD) [78], based on which the final one iteratively implements the EGCD and the N-order interference cancellation, which is referred to as NIIC-EGCD for convenience [99]. The last detection scheme is based on the maximum likelihood (ML) principle, which is a common and optimum signal processing method in wireless communications.

3.3.1 Threshold-Assisted Majority Vote Detection

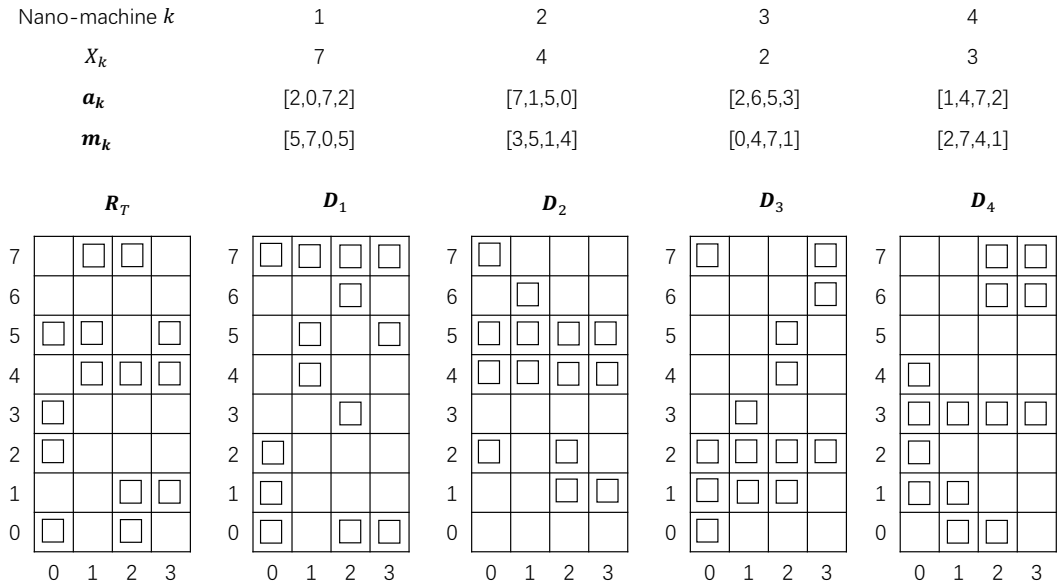

Figure 3.3: An example to explain the TMVD for the MTS-MoSK DMC system supporting $K = 4$ nano-machines and employing $M = 8$ molecular types to transmit one symbol using $L = 4$ chips.

The detection principle of TMVD can be well explained using the example as shown in Fig. 3.3. In detail, the TMVD executes the following operations.

1) Based on the observation matrix $\boldsymbol{R}_u$, the TMVD inspects each of the elements against a preset

threshold, which can be expressed as

$$T_h = \alpha C_h(0) \tag{3.7}$$

where $\alpha > 0$ is a scaling factor and $C_h(0)$ is the expected peak concentration, as shown in Fig. 3.2. The output of this procedure is a threshold-filtered matrix denoted by $\boldsymbol{R}_T$, as shown in Fig. 3.3, which contains the elements of '0' or '1', or 'empty' and 'mark'. Specifically, if an element in $\boldsymbol{R}_u$ is larger than T_h, the corresponding element in $\boldsymbol{R}_T$ is set to '1', representing that the element is marked. It is regarded as that this entry is activated by one or several nano-machines. By contrast, if an element in $\boldsymbol{R}_u$ is less than T_h, the corresponding element in $\boldsymbol{R}_T$ is set to '0', meaning that the receiver believes that no signal was transmitted by nano-machines in this entry.

2) The threshold-filtered matrix $\boldsymbol{R}_T$ is de-spread respectively by invoking the MTS signature codes of the K nano-machines, yielding K de-spread matrices, denoted by $\boldsymbol{D}_1, \boldsymbol{D}_2, \ldots, \boldsymbol{D}_K$. Specifically, based on the subtraction operation in the Galois field $GF(M)$, the (q,l) th element $r(q,l)$ in $\boldsymbol{R}_T$ is shifted to the location $(q \ominus a_k(l), l)$ in $\boldsymbol{D}_k$, i.e.,

$$\begin{aligned} d_{(k)}((q \ominus a_k(l), l)) = r(q,l),\ q = 0,1,\ldots,M-1; \\ l = 0,1,\ldots,L-1;\ k = 1,2,\ldots,K \end{aligned} \tag{3.8}$$

As shown in Fig. 3.3, after de-spreading, we obtain $\boldsymbol{D}_1, \boldsymbol{D}_2, \boldsymbol{D}_3$, and $\boldsymbol{D}_4$.

3) Finally, based on the de-spread matrices $\boldsymbol{D}_1, \boldsymbol{D}_2, \ldots, \boldsymbol{D}_K$, the decisions are made in the principle of majority votes, rendering the index of the row having the maximum number of 1s as the value of the transmitted symbol. Hence, with regard to the example shown in Fig. 3.3, the detected symbols are $\hat{X}_1 \in \{7\}$, $\hat{X}_2 \in \{4\ or\ 5\}$, $\hat{X}_3 \in \{2\}$, $\hat{X}_4 \in \{3\}$, respectively. As shown in Fig. 3.3 , $\boldsymbol{D}_1, \boldsymbol{D}_3$ and $\boldsymbol{D}_4$ each has just one majority row, which gives no confusive decision. By contrast, $\boldsymbol{D}_2$ has two majority rows, the TMVD has to choose randomly one of them as the detected symbol, which results in a symbol error probability of 0.5, even when the transmitted symbol was indeed 4 or 5.

Therefore, even when the channel is free of noise, TMVD may make erroneous detection because of the existence of the various interference as previously analyzed. In order to improve the detection performance, below we introduce the MAI-mitigation assisted detection schemes for MTS-MoSK DMC systems.

3.3.2 Minimum Distance Decoding Assisted Interference Cancellation (MDDIC)

The MDDIC algorithm is proposed to mitigate the interference experienced by TMVD by essentially examining the Hamming distance between the threshold-filtered observation matrix $\boldsymbol{R}_T$ and a range of constructed matrices based on the candidate symbols in detection. MDDIC is carried out

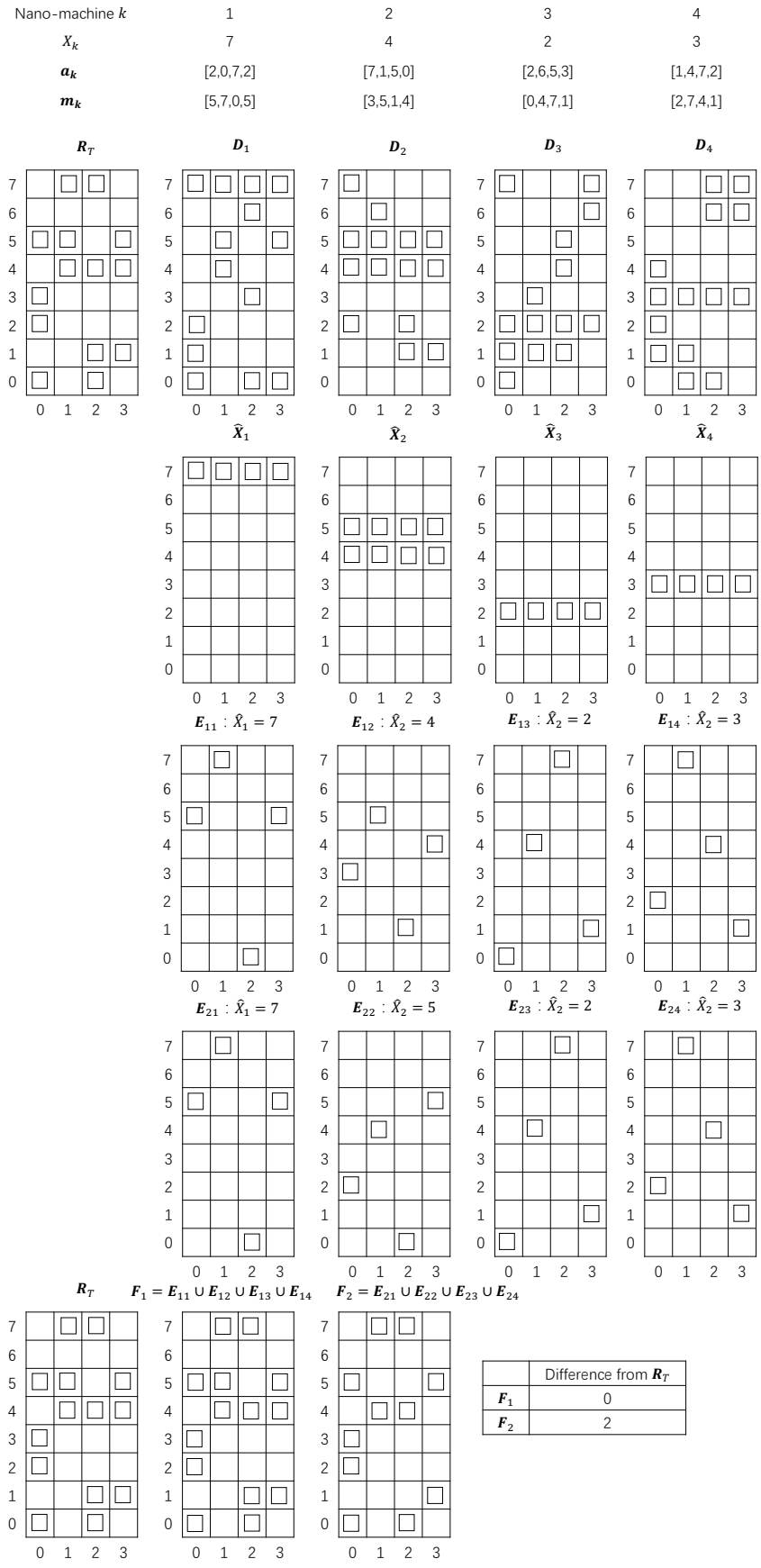

Figure 3.4: Illustration of the TMVD-MDDIC for the MTS-MoSK DMC systems.

after TMVD obtains the candidate symbols for the K nano-machines. In detail, MDDIC first lists all the possible combinations of the candidate symbols of the K nano-machines. Then, for each combination, the candidate symbols are spread by invoking the K nano-machines' MTS codes. In this way, a number of constructed matrices in the structure of $\boldsymbol{R}_T$ can be obtained. Finally, the similarity between any of these constructed matrices and the threshold-filtered observation matrix $\boldsymbol{R}_T$ is measured. On the basis of their Hamming distances, the combination giving the minimum distance from the threshold-filtered observation matrix $\boldsymbol{R}_T$ is selected, whose corresponding candidate symbols yield the finally detected symbols for the K nano-machines.

In detail, the principle of MDDIC can be understood with the aid of Fig 3.4 as follows.

1) TMVD as described in Section 3.3.1 is first carried out to generate the de-spread matrices $\boldsymbol{D}_1, \boldsymbol{D}_2, \boldsymbol{D}_3$ and $\boldsymbol{D}_4$, as shown in Fig 3.4. When only the full rows are considered, the candidate symbols are $\hat{X}_1 \in \{7\}$, $\hat{X}_2 \in \{4, 5\}$, $\hat{X}_3 \in \{2\}$ and $\hat{X}_4 \in \{3\}$. We can see that there are two candidate symbols for nano-machine 2.

2) All the combinations formed by the candidate symbols of K nano-machines are listed. For the example of Fig 3.4, the two combinations of candidate symbols are $\{\hat{X}_1 = 7, \hat{X}_2 = 4, \hat{X}_3 = 2, \hat{X}_4 = 3\}$ and $\{\hat{X}_1 = 7, \hat{X}_2 = 5, \hat{X}_3 = 2, \hat{X}_4 = 3\}$. Then, for each combination, the candidate symbols are respectively spread by invoking the corresponding MTS codes of the $K = 4$ nano-machines. As shown in Fig 3.4, after spreading the symbol of $\{\hat{X}_1 = 7, \hat{X}_2 = 4, \hat{X}_3 = 2, \hat{X}_4 = 3\}$, we obtain the matrices $\{\boldsymbol{E}_{11}, \boldsymbol{E}_{12}, \boldsymbol{E}_{13}, \boldsymbol{E}_{14}\}$. Similarly, for the combination $\{\hat{X}_1 = 7, \hat{X}_2 = 5, \hat{X}_3 = 2, \hat{X}_4 = 3\}$, we have $\{\boldsymbol{E}_{21}, \boldsymbol{E}_{22}, \boldsymbol{E}_{23}, \boldsymbol{E}_{24}\}$.

3) For each of the combinations, a matrix similar to $\boldsymbol{R}_T$ is constructed by adding the spreading matrices using the logical OR addition, forming the constructed observation matrix $\{\boldsymbol{F}_n\}$ for the n-th combination. As shown in Fig 3.4, we have $\boldsymbol{F}_1 = \boldsymbol{E}_{11} \cup \boldsymbol{E}_{12} \cup \boldsymbol{E}_{13} \cup \boldsymbol{E}_{14}$ and $\boldsymbol{F}_2 = \boldsymbol{E}_{21} \cup \boldsymbol{E}_{22} \cup \boldsymbol{E}_{23} \cup \boldsymbol{E}_{24}$.

4) The final step of MDDIC is to compare the constructed observation matrices $\{\boldsymbol{F}_n\}$ with the threshold-filtered observation matrix $\boldsymbol{R}_T$ to select the combination yielding the minimum Hamming distance from $\boldsymbol{R}_T$. Correspondingly, the candidate symbols included in the selected combination represent the final decisions for the K symbols of the K nano-machines. Specifically for the example in Fig 3.4, we find that the distance between $\boldsymbol{F}_1$ and $\boldsymbol{R}_T$ is 0, while that between $\boldsymbol{F}_2$ and $\boldsymbol{R}_T$ is 2. Therefore, the first combination is finally selected, which gives the correctly detected symbols $\hat{X}_1 = 7$, $\hat{X}_2 = 4$, $\hat{X}_3 = 2$, $\hat{X}_4 = 3$.

In summary, the algorithm of TMVD-MDDIC is stated in Algorithm 1.

It can be inferred from above that MDDIC is efficient to cancel MAI and improve the detection performance. More performance improvement is possible when more candidate symbols are tested. However, the computation and complexity may become dramatically high, when the number of candidate symbols is big and when the number of nano-machines supported is high.

Algorithm 1 Minimum Distance Decoding assisted Interference Cancellation (MDDIC)

Input: Observation matrix $\boldsymbol{R}_u$.

Output: Symbols transmitted by K nano-machines within the uth symbol duration, expressed as $\hat{\boldsymbol{X}}(u)$.

1. **TMVD:** Execute TMVD as stated in Section 3.3.1 based on $\boldsymbol{R}_u$ to generate the threshold-filtered matrix $\boldsymbol{R}_T$ and the de-spread matrices $\{\boldsymbol{D}_k\}$. The row indices of each de-spread matrix $\boldsymbol{D}_k$ with the maximum number of activated entries are classified as the candidate symbols. The candidate symbols of kth nano-machine are collected to $\hat{\boldsymbol{X}}_k$.

2. **Combinations of candidate symbols:** Pick one element from each nano-machine's candidate symbol set $\hat{\boldsymbol{X}}_k$ to form all the possible combinations expressed as $\boldsymbol{P}_1, \boldsymbol{P}_2, \ldots, \boldsymbol{P}_n, \ldots, \boldsymbol{P}_N$, where N is the number of possible combinations and $\boldsymbol{P}_n = \{\hat{X}_{n1}, \hat{X}_{n2}, \ldots, \hat{X}_{nK}\}$.

3. **MDDIC:**

   For $i = 1, 2, \ldots, N$, execute the following steps:

   (a) **Initialization:** The matrices $\boldsymbol{E}_{ik}$ are set as $(M \times L)$ all zero matrices.

   (b) The candidate symbols of a combination $\boldsymbol{P}_i$ are respectively re-spread by invoking the corresponding MTS codes and then stored into the matrices $\boldsymbol{E}_{ik}$. The operation can be expressed as $e_{ik}\left(\hat{X}_{1k} \oplus a_k(l), l\right) = 1$, where $e_{ik}(m, l)$ is the (m, l)th element in $\boldsymbol{E}_{ik}$.

   (c) $\boldsymbol{E}_{ik}$ are added based on the logical OR addition, giving $\boldsymbol{F}_i = \boldsymbol{E}_{i1} \cup \boldsymbol{E}_{i2} \cup \ldots \cup \boldsymbol{E}_{iK}$.

   (d) Find the Hamming distance between $\boldsymbol{R}_T$ and $\boldsymbol{F}_i$ as $H_i = L_0(\boldsymbol{R}_T - \boldsymbol{F}_i)$, where $L_0(\boldsymbol{A})$ returns the number of nonzero elements of $\boldsymbol{A}$.

   End For

4. Find the $\boldsymbol{P}_n$ yielding the minimum Hamming distance, which is expressed as $n = \arg\min_n \{H_1, H_2, \ldots, H_N\}$.

5. **Output:** $\hat{\boldsymbol{X}}(u) = \boldsymbol{P}_n$.

3.3.3 TMVD-based Iterative Interference Cancellation (TMVD-IIC)

Since the MDDIC-assisted detector demands a high computation, when a MTS-MoSK system supports a large number of nano-machines, an IIC algorithm is proposed based on TMVD, so as to attain a good trade-off between complexity and reliability. This detector is referred to as the TMVD-IIC. Its operation principle is detailed as Algorithm 2 associated with the explanation as follow.

The principle of the TMVD-IIC can be explained with the aid of the example shown in Fig. 3.5. As Fig. 3.5 demonstrates, after the initial stage of TMVD, the transmitted symbols of three nano-machines, namely $k = 1, 3, 4$, can be detected as $\hat{X}_1 = 7$, $\hat{X}_3 = 2$ and $\hat{X}_4 = 3$, because their de-spread matrices $\boldsymbol{D}_1, \boldsymbol{D}_3, \boldsymbol{D}_4$ all have only one majority row. By contrast, the 2nd nano-machine has two candidate symbols $\{4, 5\}$. Therefore, during the IIC stage, the three re-spreading matrices of the nano-machines 1, 3 and 4, namely $\boldsymbol{E}_1, \boldsymbol{E}_3, \boldsymbol{E}_4$, are added in logical OR, yielding the interference matrix $\boldsymbol{R}_I$. Then, according to the interference matrix $\boldsymbol{R}_I$, the received matrix $\boldsymbol{R}_T$ is updated to $\boldsymbol{R}^{(1)}$ by operating the interference cancellation, which removes the elements in $\boldsymbol{R}_T$ according to the marked elements in $\boldsymbol{R}_I$. Finally, the detector de-spreads the updated matrix $\boldsymbol{R}^{(1)}$ using the 2nd nano-machine's MTS code $\boldsymbol{a}_2 = [7, 1, 5, 0]$, yielding the new de-spread matrix $\boldsymbol{D}_2^{(1)}$. Based on $\boldsymbol{D}_2^{(1)}$, the symbol transmitted by the 2nd nano-machine can be detected, which is $\hat{X}_2 = 4$, yielding the correct detection.

From the above description, we can infer that the TMVD-IIC algorithm is capable of improving the error performance of TMVD. It can be shown that the complexity of TMVD-IIC only increases linearly with the number of nano-machines supported.

3.3.4 Equal-Gain Combining Detection (EGCD)

When the EGCD is employed, the detector first carries out de-spreading on $\boldsymbol{R}_u$ in the context of each nano-machine, generating the de-spread matrix $\boldsymbol{D}_{k,u}$ for the kth nano-machine. Specifically, the de-spreading process shifts the elements in $\boldsymbol{R}_u$ according to the rule of

$$d^{(k)}_{(q\ominus a_k(l),l)}(u) = r_{q,l}(u),\ q = 0, 1, \ldots, M-1; \\ l = 0, 1, \ldots, L-1;\ k = 1, 2, \ldots, K \tag{3.9}$$

where $\ominus$ represents the subtraction in $GF(M)$. Eq.(3.9) means that, after the de-spreading, the (q, l)th element $r_{q,l}(u)$ in $\boldsymbol{R}_u$ is shifted to the location of $(q \ominus a_k(l), l)$ in $\boldsymbol{D}_{k,u}$.

Based on the de-spread matrix $\boldsymbol{D}_{k,u}$, the detector executes the equal-gain combining (EGC) to form M decision variables for the kth nano-machine as

$$Z_q^{(k)}(u) = \sum_{l=0}^{L-1} d^{(k)}_{(q,l)}(u),\ q = 0, 1, \ldots, M-1; \\ k = 1, 2, \ldots, K \tag{3.10}$$

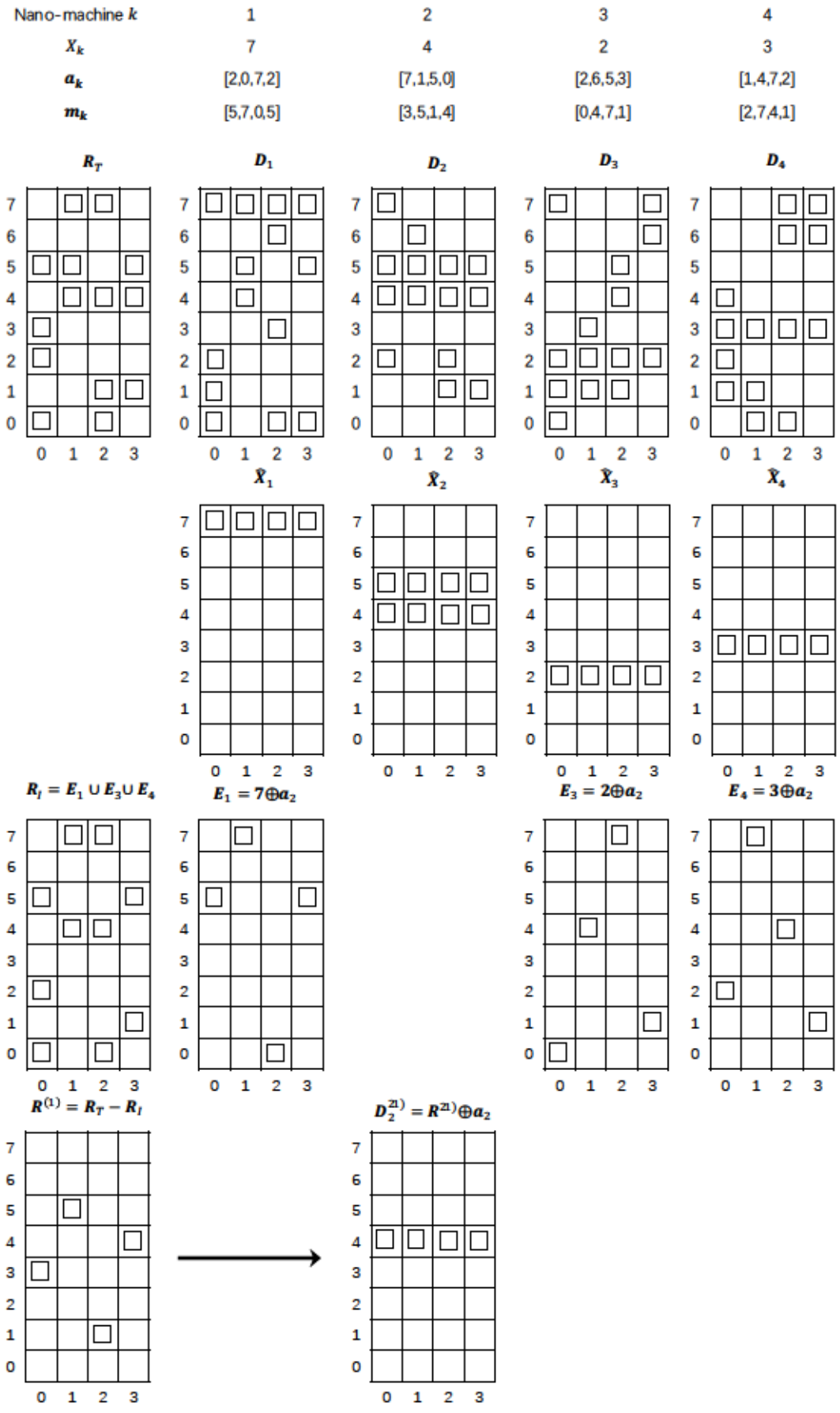

Figure 3.5: Example to illustrate the operations of TMVD-IIC.

Algorithm 2 TMVD-based Iterative Interference Cancellation (TMVD-IIC)

Input: Observation matrix $\boldsymbol{R}_u$.

Output: Symbols transmitted by K nano-machines within the uth symbol duration $\hat{\boldsymbol{X}}(u)$.

1. Execute TMVD to generate the de-spread matrices $\boldsymbol{D}_1, \ldots, \boldsymbol{D}_K$ corresponding to the individual nano-machines. In each of the de-spread matrices, the rows with the maximum number of entries are identified, whose indices represent the candidate symbols.

2. **If** a detection matrix contains only one majority row, the detector directly makes the decision to provide an estimate to the transmitted symbol in the principle of TMVD.
   Else: If detection matrix contains more than one majority row, the decision on the transmitted symbol is delayed to the later stages of the IIC, as explained below.

3. **Initialization:** $\boldsymbol{R}^{(0)} = \boldsymbol{R_T}$.

4. **For** $j = 1, 2, \ldots$, execute:

   a) The symbols detected by the nano-machines unambiguously at the $(j-1)$th iteration are respectively spreaded using the MTS codes of the nano-machines to form the re-spreading matrices.

   b) These re-spreading matrices are added element-by-element in logical OR to generate an interference matrix $\boldsymbol{R}_I$.

   c) The received matrix $\boldsymbol{R}^{(j-1)}$ is then updated to $\boldsymbol{R}^{(j)}$ by erasing the elements in $\boldsymbol{R}^{(j-1)}$ that have the same locations as those non-empty elements in the interference matrix $\boldsymbol{R}_I$.

   d) For each of the nano-machines whose transmitted symbols have not been detected, a new de-spread matrix as $\boldsymbol{D}_k^{(j)}$ is formed by de-spreading the updated matrix $\boldsymbol{R}^{(j)}$ using the nano-machine's MTS code. The majority rows of these de-spread matrices are then identified.

   If there are detection matrices without ambiguous rows, the decisions are made to provide the detected symbols.

   Else if there are no further symbols detected at the jth iteration or the maximum number of iterations is reached, randomly select a row as the detected symbol. Then, iteration **Stops**.

   Else: the detections for those nano-machines with ambiguous rows are left to the $(j+1)$th iteration.

End For

Finally, the largest decision variable in $\{Z_0^{(k)}(u), Z_1^{(k)}(u), \ldots, Z_{M-1}^{(k)}(u)\}$ is selected and its subscript represents the estimate to the symbol transmitted by the kth nano-machine. This decision making can be expressed as

$$\hat{X}_k(u) = \arg\max_q \{Z_q^{(k)}(u)\},\ k = 1, 2, \ldots, K \tag{3.11}$$

When there is severe MAI in the MTS-MoSK DMC system, the EGCD's performance may be poor. In this case, MAI mitigation technique may be introduced to enhance the performance at relatively practical complexity. Let us now consider a NIIC algorithm for the purpose.

3.3.5 EGCD-assisted N-order Iterative Interference Cancellation (EGCD-NIIC)

EGCD-NIIC tries to detect the transmitted symbols of K nano-machines in the order from the most reliable one to the least reliable one by carrying out EGCD and NIIC iteratively. Once a symbol of a nano-machine is detected, the detector attempts to remove its effect on the following detections via interference cancellation. Hence, in EGCD-NIIC, efficiently measuring the reliabilities of the symbols to be detected is critical. In this chapter, a simple but efficient reliability measurement approach is introduced by making use of the decision variables in $\mathbf{Z}^{(k)} = \left\{Z_0^{(k)}(u), Z_1^{(k)}(u), \ldots, Z_{M-1}^{(k)}(u)\right\}$ obtained by EGCD, which can be expressed as [100]

$$E^{(k)} = \frac{\max_2\{\mathbf{Z}^{(k)}\}}{\max_1\{\mathbf{Z}^{(k)}\}},\ k = 1, 2, \ldots, K \tag{3.12}$$

where $\max_1\{\mathbf{Z}^{(k)}\}$ chooses the maximum of the decision variables in $\{Z_0^{(k)}(u), Z_1^{(k)}(u), \ldots, Z_{M-1}^{(k)}(u)\}$, while $\max_2\{\mathbf{Z}^{(k)}\}$ selects the second maximum from them. The nano-machine with a lower value of $E^{(k)}$ is rendered to be more reliable, as the result that the decision variable matching to the transmitted symbol has a significant difference from the other decision variables not matching to the transmitted symbol.

In detail, the EGCD-NIIC detector can be described as Algorithm 3.

From Algorithm 3 we know that EGCD-NIIC algorithm only attempts to mitigate the interference imposed by the first N most reliable nano-machines, while the symbols transmitted by the other nano-machines are detected by the conventional EGCD. Note that, for given values of K, L, signal-to-noise ratio, transmission distance r and data rate $1/T_b$, there is an optimal value for N to result in the best error performance, as shown by our performance results in Section 3.4.

3.3.6 EGC-based Interference Mitigation (EGC-IM)

The proposed EGC-IM scheme is an enhanced single-user detection scheme. In comparison with the conventional EGC scheme, EGC-IM requires a slightly increased computation. However, as the results in Section 3.4 illustrate, it has the potential to mitigate the MAI and ISI existing in

Algorithm 3 EGCD-assisted N-order Iterative Interference Cancellation (EGCD-NIIC)

Input: Observation matrix $\boldsymbol{R}_u$, Number of iterations: N $(N < K)$.

Output: Detected symbols transmitted by K nano-machines within the uth symbol duration $\hat{\boldsymbol{X}}(u)$.

Initialization: $\boldsymbol{R}^{(0)} = \boldsymbol{R}_u$.

For $j = 1, 2, \ldots, N$, execute:

1. Corresponding to the $(K - j + 1)$ undetected nano-machines, their de-spread matrices $\boldsymbol{D}_j^{(1)}, \boldsymbol{D}_j^{(2)}, \ldots, \boldsymbol{D}_j^{(K-j+1)}$ are generated by applying their MTS codes, as done in (3.9).

2. Apply the EGC rule to these de-spread matrices, as shown in (3.10), yielding the M-length decision variable vectors $\boldsymbol{Z}^{(1)}, \boldsymbol{Z}^{(2)}, \ldots, \boldsymbol{Z}^{(K-j+1)}$.

3. Using (3.12) to measure the reliabilities for detecting these nano-machines, yielding $E_j^{(1)}, E_j^{(2)}, \ldots, E_j^{(K-j+1)}$.

4. Find the most reliable nano-machine from the $(K - j + 1)$ undetected nano-machines, expressed as

$$\tilde{k} = \arg\min_{k} \{E_j^{(1)}, E_j^{(2)}, \ldots, E_j^{(k)}, \ldots, E_j^{(K-j+1)}\}$$

5. The symbol transmitted by the most reliable nano-machine $\tilde{k}$ is detected as the index of the maximum decision variable in $\boldsymbol{Z}^{(\tilde{k})}$. The detected symbol is expressed as $\hat{X}^{\tilde{k}}$.

6. Interference cancellation: the detector erases the $(\hat{X}^{\tilde{k}} \oplus a_{\tilde{k}}(l), l)$th, $l = 1, 2, \ldots, L$, elements in $\boldsymbol{R}^{(j-1)}$ to update $\boldsymbol{R}^{(j-1)}$ to $\boldsymbol{R}^{(j)}$, if these elements in $\boldsymbol{R}^{(j-1)}$ are not empty.

End For

Completion: Symbols transmitted by the remaining $K - N$ nano-machines are detected using $\boldsymbol{R}^{(N+1)}$ based on the conventional EGCD, as introduced in Section 3.3.4. Then, detection **Stops**.

our MTS-MoSK system and hence, achieves performance improvement when compared with the conventional EGC scheme.

According to (3.3), within one symbol duration, we can obtain in total $M \times L$ observations, consisting of the signals transmitted by K nano-machines during the current symbol duration, the interference from previous symbol durations and background noise.

Having obtained the observation matrix $\boldsymbol{R}_u$, next, we can invoke the MTS address code $\boldsymbol{a}_k$ of the desired nano-machine k (to be detected) to de-spread the observation matrix $\boldsymbol{R}_u$, same as the operation (3.9) in conventional EGCD. Then, we generate the detection matrix $\boldsymbol{D}_{k,u}$ corresponding to nano-machine k.

It can be inferred that the elements activated by the interfering nano-machines should be expected to have higher energy than the elements containing only interference plus noise. Hence, in the EGC-IM assisted detection, we may make use of this property to mitigate MAI. Specifically, to

detect a nano-machine's information, we first identify the J $(J < L)$ largest elements in each row of $\boldsymbol{D}_{k,u}$ and substitute them with zeros. Following the above analysis, this operation will most probably remove the elements activated by the interfering nano-machines, or the elements experiencing high interference due to ISI and MAI. This can be understood with the aid of the example shown in Fig. 2.10 in Chapter 2. For principle, we assume that there is no ISI and one maximum element of each row is removed. Then, we can know that all the interfering elements in rows 0, 1, 2, 4 and 6 will be removed. At the same time, the maximum of Row 5 is removed, which will reduce the output of final combining, as shown below. However, Row 5 still has 5 elements containing the desired signal and the symbol of nano-machine 1 can be detected free from interference.

Let the detection matrix of nano-machine k after the IM operations be expressed as $\boldsymbol{D}'_{k,u}$ with its elements as $\bar{d}^{(k)}_{(q,l)}(u)$. Then, based on $\boldsymbol{D}'_{k,u}$, EGC is implemented to form M decision variables as

$$D^{(k)}_q(u) = \sum_{l=0}^{L-1} \bar{d}^{(k)}_{(q,l)}(u),\ q = 0, 1, \ldots, M-1;$$
$$k = 1, 2, \ldots, K \tag{3.13}$$

for each of $u = 0, 1, \ldots$. The last step of the EGC-IM assisted detection is to select the largest of the M decision variables $\{D^{(k)}_0(u), D^{(k)}_1(u), \ldots, D^{(k)}_{M-1}(u)\}$ provided by (3.13), whose index for q represents the detected M-ary symbol transmitted by the desired nano-machine k. This is expressed as

$$\hat{X}_k(u) = \arg\max_q \{D^{(k)}_q(u)\},\ k = 1, 2, \ldots, K \tag{3.14}$$

where $D^{(k)}_q(u) \in \{D^{(k)}_0(u), D^{(k)}_1(u), \ldots, D^{(k)}_{M-1}(u)\}$.

Note that, as mentioned above, the erasure operation can mitigate MAI/ISI, while also reduce the output value of the desired decision variable, yielding a trade-off between the value of J and the achievable performance. Hence, for a given Signal-to-Noise (SNR), a given number K of nano-machines and a given number L of chips per symbol duration, there exists an optimum value for J, which results in the best performance, as to be demonstrated in Section 3.4.

3.3.7 Simplified Approximate Maximum Likelihood Detection

In the MTS-MoSK DMC systems with ISI, the optimum detector is a sequential detector. Let us assume a MTS-MoSK DMC system with the ISI being $(I+1)$ length. Then, the detection of the uth $(u > I)$ symbol depends on the former IK transmitted symbols. As the MTS-MoSK DMC system employs MoSK modulation, there are in total M^{IK} transmission states affecting the current symbol's detection. Hence, when the optimum Maximum Likelihood (ML) detection is employed, the detection complexity should be extremely high. To reduce the complexity, a simplified approximate ML (SAML) detector is proposed to detect the symbols of K nano-machines. In our SAML

detection, the previously detected symbols are assumed to be correct, which reduces the detection complexity from $O\left(M^{IK}\right)$ to $O\left(M^{K}\right)$, which is explicitly only suitable for the system with a small K value.

The SAML detector estimates the K symbols transmitted by the K nano-machines during the uth symbol duration by maximizing the joint probability density function (pdf) of the K candidate symbols and the received signal samples, which can be expressed as

$$\hat{\boldsymbol{X}}(u) = \arg\max_{\boldsymbol{X}(u)} f(\boldsymbol{R}_u, \boldsymbol{X}(u)) \tag{3.15}$$

where $\boldsymbol{R}_u$ is the observation matrix of (3.6) and $\boldsymbol{X}(u)$ represents the set of K candidate symbols of the K nano-machines possibly transmitted during the uth symbol duration. Upon applying the Bayes rule, and the fact that the symbols transmitted by different nano-machines are independent, we have

$$\begin{aligned} f(\boldsymbol{R}_u, \boldsymbol{X}(u)) =& P(\boldsymbol{X}(u)) f(\boldsymbol{R}_u \big| \boldsymbol{X}(u)) \\ =& \prod_{k=1}^{K} P(X_k(u)) \prod_{q=1}^{M} \prod_{l=1}^{L} f(r_{q,l}(u) \big| \boldsymbol{X}(u)) \end{aligned} \tag{3.16}$$

where the observations of the different types and of the different chips are also independent, when $\boldsymbol{X}(u)$ is given.

To maximize the joint pdf of (3.16), it is usually more convenient to minimize the negative logarithm of it. Thus, the SAML detector of Eq.(3.15) can be converted to

$$\begin{aligned} \hat{\boldsymbol{X}}(u) &= -\arg\min_{\boldsymbol{X}(u)} \ln \left[\prod_{k=1}^{K} P(X_k(u)) \prod_{q=0}^{M-1} \prod_{l=0}^{L-1} f(r_{q,l}(u) | \boldsymbol{X}(u)) \right] \\ &= -\arg\min_{\boldsymbol{X}(u)} \left[\sum_{k=1}^{K} \ln P(X_k(u)) + \sum_{q=0}^{M-1} \sum_{l=0}^{L-1} \ln f(r_{q,l}(u) \big| \boldsymbol{X}(u)) \right] \end{aligned} \tag{3.17}$$

Furthermore, if the probability of each transmitted symbol is the same, i.e., $P(X_k(u)) = 1/M$, the first term in the bracket of (3.17) is common and can be removed. Therefore, only the conditional pdf (the second term) in (3.17) needs to be minimized. Consequently, the SAML detector can be described as

$$\hat{\boldsymbol{X}}(u) = -\arg\min_{\boldsymbol{X}(u)} \sum_{q=0}^{M-1} \sum_{l=0}^{L-1} \ln f(r_{q,l}(u) \big| \boldsymbol{X}(u)) \tag{3.18}$$

From (3.4) and (3.5), we can know that $r_{q,l}(u)$ follows the Gaussian distribution expressed as

$$r_{q,l}(u) \sim \mathcal{N}\left(\mu_{q,l}(u), \sigma^2_{q,l}(u)\right) \tag{3.19}$$

where the mean and variance are

$$\begin{aligned} \mu_{q,l}(u) =& \sum_{k=1}^{K} \sum_{i=0}^{\min\{I, uL+l\}} \ell_{k,q}^{uL+l-i} c_{k,q}(i); \\ \sigma^2_{q,l}(u) =& \frac{1}{V} \mu_{q,l}(u) \end{aligned} \tag{3.20}$$

Explicitly, the pdf of $r_{q,l}(u)$ on the condition of $\boldsymbol{X}(u)$ can be expressed as

$$f(r_{q,l}(u)|\boldsymbol{X}(u)) = \frac{1}{\sqrt{2\pi\sigma_{q,l}^2(u)}} \exp\left[-\frac{(r_{q,l}(u)-\mu_{q,l}(u))^2}{2\sigma_{q,l}^2(u)}\right] \tag{3.21}$$

Substituting this pdf into the objective function of (3.18), we obtain

$$\begin{aligned}\Lambda^{ML}(\boldsymbol{R}_u, \boldsymbol{X}(u)) =& -\sum_{q=0}^{M-1}\sum_{l=0}^{L-1} \ln f(r_{q,l}(u)|\boldsymbol{X}(u)) \\ =& \frac{1}{2}\sum_{q=0}^{M-1}\sum_{l=0}^{L-1} \ln\left(2\pi\sigma_{q,l}^2(u)\right) \\ &+ \sum_{q=0}^{M-1}\sum_{l=0}^{L-1} \frac{(r_{q,l}(u)-\mu_{q,l}(u))^2}{\sigma_{q,l}^2(u)}\end{aligned} \tag{3.22}$$

From the above analysis, we can see that the SAML detector has the complexity of $O(M^k)$. Hence, it is only practical for application, when the number of nano-machines is relatively small and when the value of M is not big.

3.3.8 Complexity of Detection Schemes

Now we analyze the complexity of the detection schemes considered above. In order to describe the complexity of different operations, we assume that the arithmetic operation of individual elements in a matrix has the complexity of $\mathcal{O}(1)$. Since some detection algorithms are joint multiuser detectors, for convenience of comparison, the complexity is expressed in terms of K symbols simultaneously transmitted by K nano-machines.

Let us first analyze the complexity of TMVD. First, its threshold-based decision operation has the complexity of $\mathcal{O}(ML)$, as all the $(M \times L)$ elements in $\boldsymbol{R}_u$ need to be compared with the threshold. Assume that after the threshold-based decision operations, there are Q_a out of the ML elements marked. Then, de-spreading these elements by invoking K MTS codes requires the total complexity of $\mathcal{O}(KQ_a)$. Finally, the majority voting requires $\mathcal{O}(K(L-1)M)$ additions to count the numbers of entries activated in the M rows and $\mathcal{O}(K(M-1))$ comparisons to identify the majority rows. Hence, the total complexity of TMVD is $\mathcal{O}(ML + K(Q_a + ML - 1))$. Having obtained the complexity of TMVD, the TMVD-MDDIC can be analyzed as follows. For the analysis, we assume that the numbers of candidate rows in de-spread matrices $\{\boldsymbol{D}_1, \ldots, \boldsymbol{D}_K\}$ are $\{Q_b^{(1)}, \ldots, Q_b^{(K)}\}$. Then, the number of possible combinations N_{MDD} in Section 3.3.2 is $N_{MDD} = \prod_{k=1}^{K} Q_b^{(k)}$, meaning that there are N_{MDD} iterations. In every iteration, the complexity of re-spreading the candidate symbols is $\mathcal{O}(KL)$ and also, there are in total $ML(K-1)$ logical OR additions for processing $\boldsymbol{E}_{ik}$. To obtain the Hamming distance between $\boldsymbol{R}_T$ and $\boldsymbol{F}_i$, the complexity is $\mathcal{O}(2ML-1)$ in an iteration. After the iterations, the complexity for the comparisons to select the most likely combination is $\mathcal{O}(N_{MDD}-1)$. After considering all the above operations,

Table 3.1: Complexity of Post-processing and that of Detection for various Detection Schemes.

Detector	Complexity
TMVD	$\mathcal{O}(ML + K(Q_a + ML - 1))$
TMVD-MDDIC	$\mathcal{O}(K(Q_a + ML - 1) + N_{MDD}L(K + MK + M) + ML - 1)$
TMVD-IIC (upper bond)	$\mathcal{O}(2LK^2 + (Q_a + ML + L - 1)K + ML + 3L(Q_b^{(1)} + \ldots + Q_b^{(K)}))$
EGCD	$\mathcal{O}(K(2ML - M - L))$
EGCD-NIIC	$\mathcal{O}(N_{NIIC}[(\frac{2K+1-N_{NIIC}}{2})(M^2 + 2ML - 4M + 4) - 2ML + M + 2L - 1] + K(2ML - M - L))$
SAML	$\mathcal{O}(M^K(L + 3ML + KI + 1))$

the complexity of MDDIC can be found to be $\mathcal{O}(N_{MDD}L(K + MK + M) - 1)$. With the complexity of TMVD, the complexity of TMVD-IIC can also be straightforwardly analyzed. As the complexity of TMVD-IIC is related to the number of symbols detected in every iteration, which is uncertain, we instead analyze the complexity upper-bound of the TMVD-IIC. Note that, from our simulations, we find that, typically, three iterations are sufficient. When all the candidate rows are considered in each iteration, it can be shown that the complexity upper-bound is about $\mathcal{O}(2LK^2 + (Q_a + ML + L - 1)K + ML + 3L(Q_b^{(1)} + \ldots + Q_b^{(K)}))$. However, we should note that the real computation required is much lower than this bound, as the symbols detected in the previous iterations are not required to be considered in the following iterations.

The complexity of EGCD can be readily derived, which is $\mathcal{O}(K(2ML - M - L))$. To analyze the complexity of EGCD-NIIC, we first calculate the complexity of the NIIC invoked. When given N_{NIIC} iterations for detecting the N_{NIIC} most reliable nano-machines, according to Algorithm 3, the complexity of each iteration can be analyzed step-by-step as follows. 1) The de-spreading invoking $(K - j + 1)$ nano-machines' signature codes costs $\mathcal{O}((K - j + 1)ML)$ $j = 1, 2, \ldots, N_{NIIC}$ of computations. 2) The complexity of EGC on the de-spread matrices is $\mathcal{O}(M(L - 1)(K - j + 1))$. 3) The measurement of $(K - j + 1)$ nano-machines' reliabilities requires the complexity of $\mathcal{O}([(M - 1)(M - 2) + 1](K - j + 1))$. 4) The complexity of finding the most reliable nano-machine is $\mathcal{O}(K - j)$. 5) The erasure operation of the L entries activated by the most reliable nano-machine requires the complexity of $\mathcal{O}(L)$. Therefore, the total complexity of N_{NIIC} iterations is $\mathcal{O}(N_{NIIC}[(\frac{2K+1-N_{NIIC}}{2})(M^2 + 2ML - 4M + 4) + L - 1])$. Then, the detection of the symbols sent by the rest $K - N_{NIIC}$ nano-machines requires $\mathcal{O}((K - N_{NIIC})(2ML - M - L))$ calculations. Consequently, the overall complexity of EGCD-NIIC is $\mathcal{O}(N_{NIIC}[(\frac{2K+1-N_{NIIC}}{2})(M^2 + 2ML - 4M + 4) - 2ML + M + 2L - 1] + K(2ML - M - L))$.

Finally, the complexity of SAML can be analyzed as follows. First, spreading the M^K pos-

sible combinations of symbols sent by K nano-machines requires the complexity of $\mathcal{O}(M^K L)$. Then, to obtain the means and variances of the received signals of all the possible combinations, the complexity is $\mathcal{O}(M^K KI)$, where I is the ISI length considered. Finally, the complexity for decision-making is approximately $\mathcal{O}(M^K(3ML+1))$. Hence, the overall complexity of SAML is $\mathcal{O}(M^K(L+3ML+KI+1))$.

The complexities of all the considered detection schemes are summarized in Table 3.1. Explicitly, provided that $K \geq 3$, SAML has the highest complexity followed by the TMVD-MDDIC, whose complexity is related to $N_{MDD} = \prod_{k=1}^{K} Q_b^{(k)}$. The value of N_{MDD} can be a big value if the threshold in TMVD is set to be a low value. On the contrary, if the threshold in TMVD is relatively big, N_{MDD} can be small. In practice, the threshold should be appropriately set to make both the false-alarm and miss probabilities sufficiently small. Subsequently, EGCD-NIIC has a higher complexity than TMVD-IIC, as TMVD-IIC can usually complete the detection in three iterations. Fundamentally, TMVD has the lowest complexity followed by EGCD having a slightly higher complexity than TMVD.

3.4 Performance Results and Discussion

In this section, the error performance of the MTS-MoSK DMC systems with respectively the TMVD, TMVD-IIC, MDDIC, EGCD, EGCD-NIIC and SAML is demonstrated against the signal-to-noise ratio (SNR) per bit, SNR_b, in the context of some cases. The performance results were obtained from the Monte-Carlo simulations with random data generated by statistical models. To carry out a fair comparison between different settings, we consider the error performance against SNR_b. Following [70], SNR_b is defined as the ratio between the power (number of molecules) received from a pulse of molecules emitted for transmitting one isolated bit and the corresponding noise power. Assume that within the observation space with a volume V, the expected concentration at the sampling time is $c_{b(o)}$. Then, according to [66], the number of molecules presenting in the observation space follows the Poisson distribution with the mean and variance both given by $Vc_{b(o)}$. Hence, the SNR_b is

$$\text{SNR}_b = \frac{(Vc_{b(o)})^2}{Vc_{b(o)}} = Vc_{b(o)}. \tag{3.23}$$

Based on the above definition, when given SNR_b and volume V, we can obtain $c_{b(o)}$ from (3.23). If the communication distance r_k between a nano-machine and AP is known, according to (3.2), the number of molecules A_b for transmitting one bit can be calculated. As in MTS-MoSK DMC systems, each symbol conveys $b = \log_2 M$ bits, the total number of molecules emitted for transmitting one symbol is $A_s = b \times A_b$. On the other side, due to the introduction of MTS, the transmission of a symbol is split into L chips to transmit L pulses of molecules. Hence, the number of molecules emitted by each chip pulse is $A_h = A_s/L = b \times A_b/L$.

In our demonstration of performance result, unless specifically stated, some of the parameters in our simulations are fixed, which include $D = 2.2 \times 10^{-9}\ m^2/s$ and $V = 4\pi\rho^3/3$ with $\rho = 20$ nm. The duration of one bit is set to $T_b = 6 \times 10^{-5}\ s$, so one symbol duration is $T_s = b \times (6 \times 10^{-5})\ s$. Moreover, to take the effect of ISI into consideration, we evaluate the effective length of a transmitted molecular pulse according to

$$I \triangleq \arg_i \left\{ \frac{c_{h(i)}}{c_{h(o)}} \leq 0.1\% \right\} \tag{3.24}$$

where $c_{h(o)}$ in (3.24) is the maximun concentration expected within the first chip's duration, when a molecular pulse is started transmitting at $t = 0$, and $c_h(i)$ is the residue concentration of this molecular pulse sampled at the ith chip-duration. From (3.24) we are implied that only the residue concentration in the following chip-durations with the strength above 0.1% of the peak concentration in the initial chip-duration is counted. This is reasonable because in Fig. 3.6, both 0.1% and

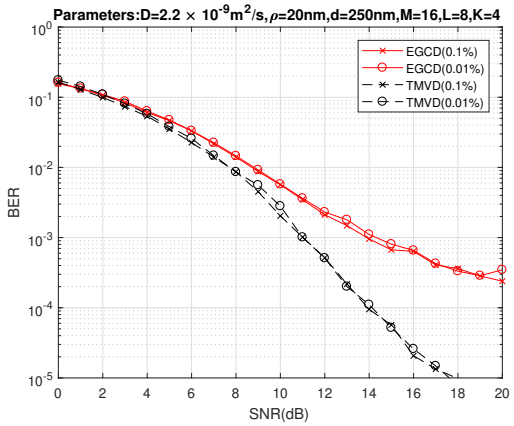

Figure 3.6: BER vs SNR performance of MTS-MoSK DMC systems detected by TMVD/EGCD with different ISI lengths counted.

0.01% thresholds are adopted to determine the length of I and the BER performance of both MTS-MoSK DMC systems coincides with each other no matter what detector is employed. It indicates that the length of ISI I decided by the 0.1% threshold is sufficient to approximate the effect of infinitely long ISI. Additionally, we assume the random MTS codes in all simulations.

Fig. 3.7 demonstrates that the probabilities of error, false-alarm and miss of TMVD vary with the normalized threshold α, as seen in (3.7), when SNR$= 15dB$ or $5dB$. We can see that as the threshold increases, the probability of false-alarm decreases while that of miss increases. Therefore, a trade-off exists between the probabilities of false-alarm and miss. As shown in Fig. 3.7, if the general error probability is considered, there is an optimum value for α, which results in that the MTS-MoSK DMC system achieves the lowest error probability. Furthermore, as SNR increases from $5dB$ to $15dB$, the optimum threshold reduces. However, we should note that the optimum threshold is dependent on SNR and is usually hard to derive an analytical solution. In Fig. 3.8, we show the probabilities of error, false-alarm and miss of TMVD versus the normalized threshold

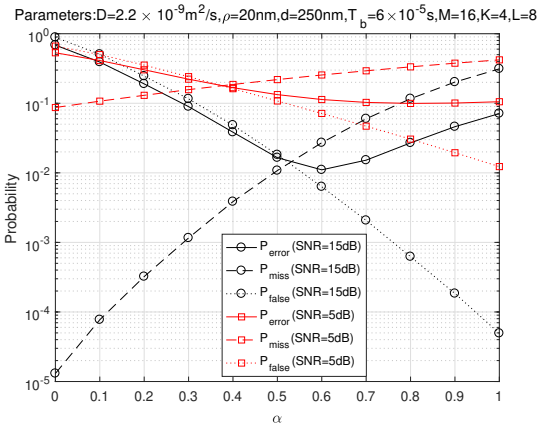

Figure 3.7: Probability of error, miss and false-alarm versus α performance of MTS-MoSK DMC systems detected by TMVD with different SNR.

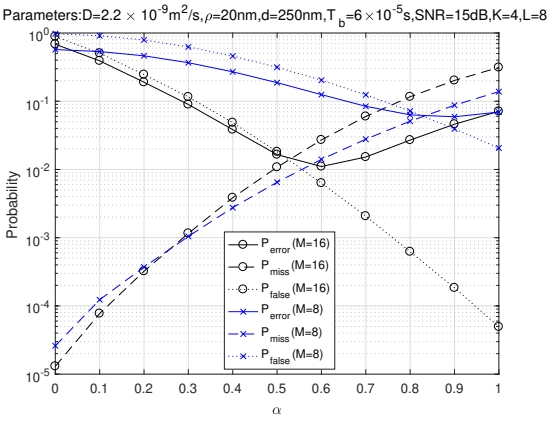

Figure 3.8: Probability of error, miss and false-alarm versus α performance of MTS-MoSK DMC systems detected by TMVD.

α, when $M = 16$ and 8 types of molecules are respectively employed. From Fig. 3.8 we can observe that the miss probability typically reduces and the false probability increases significantly as the number of molecular types employed decreases from $M = 16$ to $M = 8$. The reason behind is that the reduction of M results in severer ISI and MAI, which enhances the molecular concentration around AP. Therefore, the miss probability reduces while the false-alarm probability increases. Again, if the general error probability is considered, there is an optimum value of α that is M-dependent, which makes the error probability minimum.

Below we specifically consider BER. First, Fig. 3.9 shows that the optimum normalized threshold α is around 0.4 in a MTS-MoSK DMC system that employs $M = 16$ types of molecules and $L = 8$ chips per symbol for supporting $K = 4$ nano-machines, wherever the SNR is $10dB$ or $15dB$. The reason behind the above observations is that the normalized threshold α is proportional to the maximum concentration of a molecular pulse. Therefore, to demonstrate the performance of the MDDIC and IIC that are based on TMVD, later, the normalized coefficient α is set to 0.5 in our

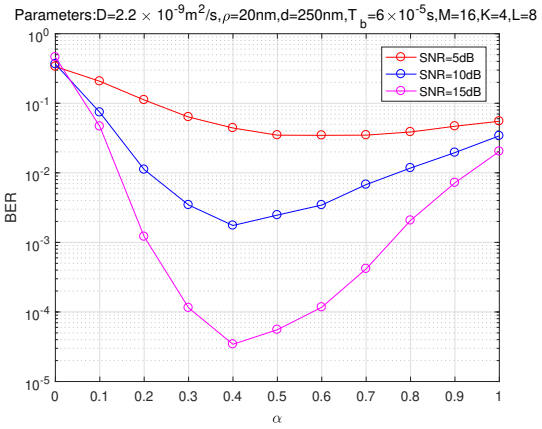

Figure 3.9: BER versus α performance of MTS-MoSK DMC systems detected by TMVD, when different SNRs are considered.

simulations.

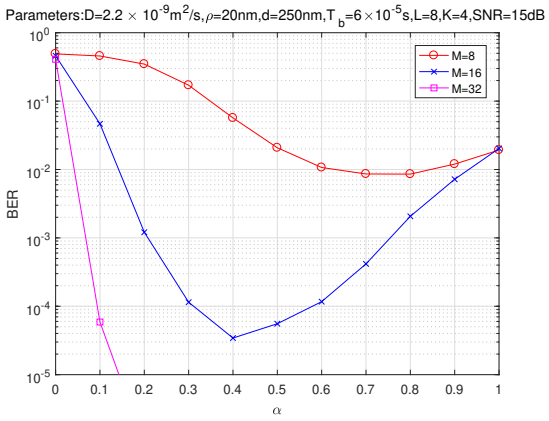

Figure 3.10: BER versus α performance of MTS-MoSK DMC systems detected by TMVD, when different numbers of molecular types M are employed.

In Fig. 3.10, the optimum normalized threshold α is shifted to left as the number of molecular types increases. This is because for given K and L, the increase of molecular types leads to the reduced MAI and ISI, due to the reduction of concentration at AP. Therefore, when the DMC system employs the larger number, such as $M = 32$, of molecular types to transmit information, the miss probability dominates the error performance and hence the normalized threshold reduces.

Fig. 3.11 demonstrates the impact of the number of chips per symbol on the bit error performance of the MTS-MoSK DMC systems detected by TMVD. It can be observed that when using more chips per symbol, the optimum normalized threshold α is shifted to right. This is because when L increases, ISI increases as the result of the increased concentration at AP. In this case, the false-alarm becomes dominant of the error performance.

Fig. 3.12 compares the BER performance of the MTS-MoSK DMC systems with TMVD,

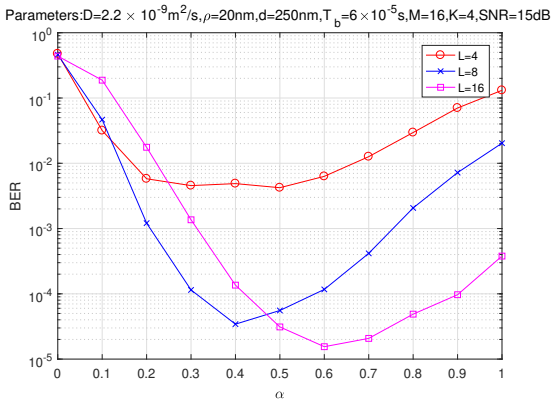

Figure 3.11: BER versus α performance of MTS-MoSK DMC systems detected by TMVD, when different length of chips L per symbol duration are considered.

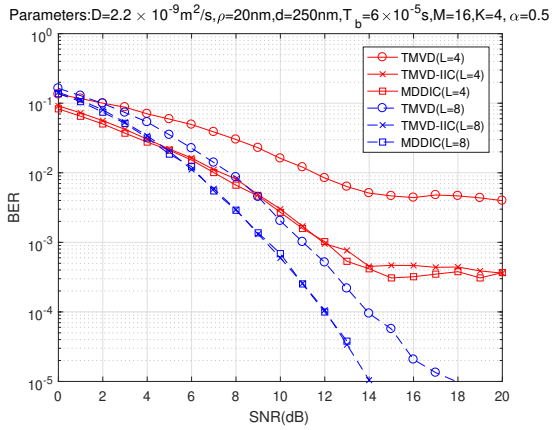

Figure 3.12: Comparison of BER versus SNR performance of MTS-MoSK DMC systems detected by TMVD, TMVD-IIC and TMVD-MDDIC, when different L is considered.

TMVD-IIC and TMVD-MDDIC, when the different numbers of chips per symbol are considered. From the results of Fig. 3.12, we observe that in comparison with TMVD, both the interference cancellation assisted methods are capable of improving the bit error performance of the MTS-MoSK DMC systems. This is more significant, when L is small. When compared to TMVD-IIC, TMVD-MDDIC only has a very slight improvement on the BER performance. Hence, when taking both the computation complexity and communication reliability into account, TMVD-IIC is more desirable for application. Additionally, as Fig. 3.12 shows, the BER performance improves as L is increased from $L = 4$ to $L = 8$, when SNR is sufficiently high. This is because, increasing the value of L can bring more diversity to the detection, which helps to average out the noise and ISI effect.

Fig. 3.13 illustrates the BER versus SNR performance of the MTS-MoSK DMC systems employing TMVD, TMVD-IIC and TMVD-MDDIC, when different numbers of molecular types, i.e., M, are employed. Explicitly, increasing the value of M results in significant improvement of BER performance for all the detection schemes considered, owing to the fact that MAI and ISI decreases

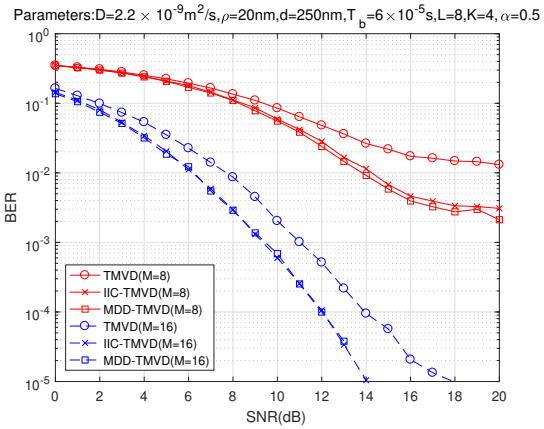

Figure 3.13: Comparison of BER versus SNR performance of the MTS-MoSK DMC systems detected by TMVD, TMVD-IIC and TMVD-MDDIC detection schemes, when different numbers of molecular types are employed.

with the increase of M.

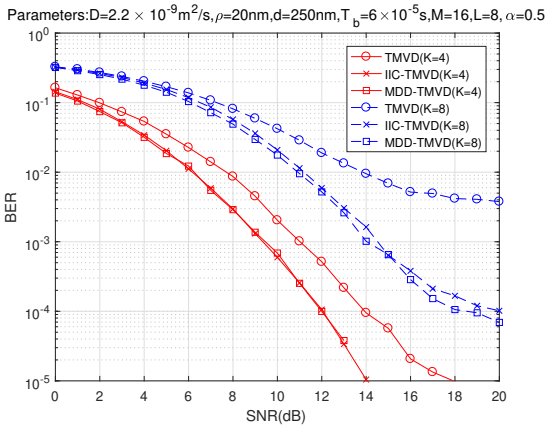

Figure 3.14: Comparison of BER versus SNR performance of the MTS-MoSK DMC systems detected by TMVD, TMVD-IIC and TMVD-MDDIC, when different numbers of nano-machines are supported.

In Fig. 3.14, we compare the BER performance of the MTS-MoSK DMC systems with TMVD, TMVD-IIC and TMVD-MDDIC, when the systems support different numbers of nano-machines. As Fig. 3.14 shows, when the number of nano-machines increases, yielding the increasing MAI, the BER performance of MTS-MoSK DMC systems degrades. The results also show that when multiple nano-machines are supported, both TMVD-MDDIC and TMVD-IIC have a similar efficiency and achieve similar BER performance, which is much better than the BER performance attained by TMVD. Therefore, both TMVD-MDDIC and TMVD-IIC are efficient for MAI mitigation, especially, in the relatively high SNR region, where MAI dominates the BER performance.

Fig. 3.15 shows the transmission rate on the BER performance of the MTS-MoSK DMC sys-

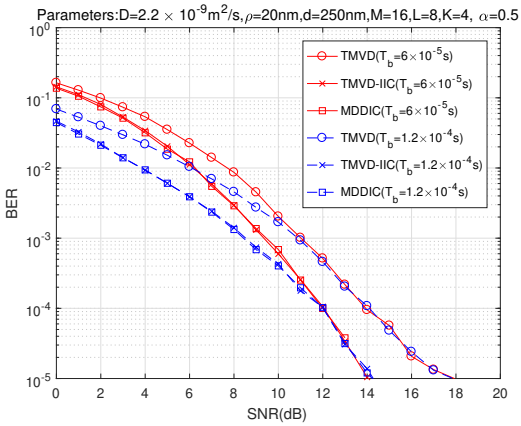

Figure 3.15: Comparison of BER versus SNR performance of the MTS-MoSK DMC systems employing TMVD, TMVD-IIC and TMVD-MDDIC, when transmitting at different bit rates of $1/T_b$.

tems with TMVD, TMVD-IIC and TMVD-MDDIC. Here, the bit rate is given by $R_b = 1/T_b$ and hence, a higher data rate corresponds to a lower value of T_b. Therefore, as shown in Fig. 3.15, when the bit rate reduces, the BER performance improves, especially, when SNR is low, which is due to the reduction of ISI, when T_b increases. By contrast, when SNR increases, the performance attained in two cases converge. This is because the threshold applied in TMVD is adjusted according to the bit interval. When SNR is high, the error performance of TMVD is insensitive to the bit rate, provided that it satisfies the assumption for sampling stated in Section 3.2.2.

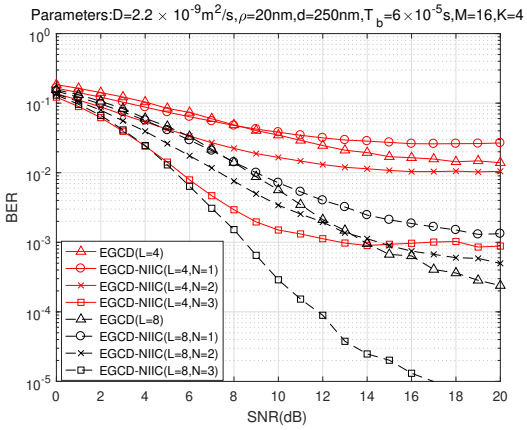

Figure 3.16: Comparison of BER versus SNR performance of the MTS-MoSK DMC systems detected by EGCD and EGCD-NIIC, when different values of L are considered.

In Fig. 3.16, the BER performance of MTS-MoSK DMC systems detected by EGCD and EGCD-NIIC is compared, when different length of chips L per symbol duration are considered. Furthermore, for the EGCD-NIIC, the impact of the number of iterations for IIC, i.e. N, on the achievable BER performance is investigated. As Fig. 3.16 shows, the error performance for both

L values improves as the value of N increases. It can be expected that the best BER performance is achieved in the case of $N = K - 1$. However, increasing the number of iterations of IIC results in the increase of detection complexity. Hence, the EGCD-NIIC detection scheme can provide a trade-off between BER performance and detection complexity. Additionally, as seen in Fig. 3.16, in both cases, the EGCD-NIIC with $N = 1$ achieves worse BER performance than the EGCD, when SNR is relatively high. The reason for the observation is that the EGCD-NIIC is more efficient, when signals appear more like Gaussian signals. When SNR is high, interference dominates, making the EGCD-NIIC less efficient. This is also the reason that in Fig. 3.16 the BER curves with $N \geq 1$ present error floors, when SNR is high.

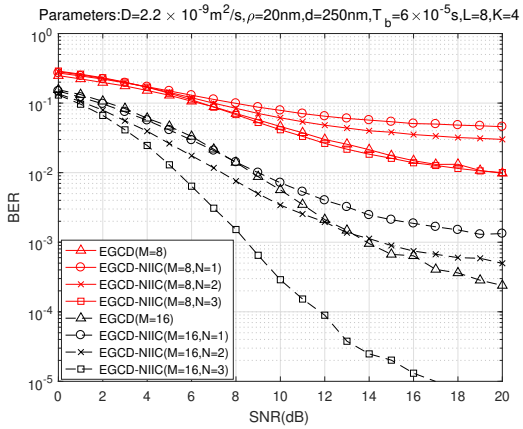

Figure 3.17: Comparison of BER versus SNR performance of the MTS-MoSK DMC systems employing EGCD and EGCD-NIIC, when different numbers of molecular types M are employed.

Fig. 3.17 compares the BER performance of the MTS-MoSK DMC systems detected by EGCD and EGCD-NIIC with respect to different values of M. Explicitly, when the value of M increases, the BER performance attained by both the detection schemes significantly improve. Furthermore, for a given SNR, the EGCD-NIIC with a sufficient number of IIC stages can significantly outperform the EGCD without the attempt of interference mitigation. For instance, in Fig. 3.17, when N increases from 2 to 3, the BER performance gain is significant. It indicates that the erasure operation in NIIC makes signals in $\boldsymbol{R}_u$ no longer independent, it would better continue to detect from more reliable NM to less reliable nano-machine.

In Fig. 3.18, we compare the BER performance of the MTS-MoSK DMC systems employing EGCD and EGCD-NIIC, when the systems support different numbers of nano-machines associated with using different numbers of iterations in the NIIC. It is shown that when K is too big ($K = 8$), the application of NIIC is unable to gain any performance improvement. This is because when K is large resulting in high interference, the reliability measurement by (3.12) is unable to identify the most reliable nano-machine. In this case, interference cancellation in fact introduces extra interference, which results in performance degradation. Therefore, by also considering the results

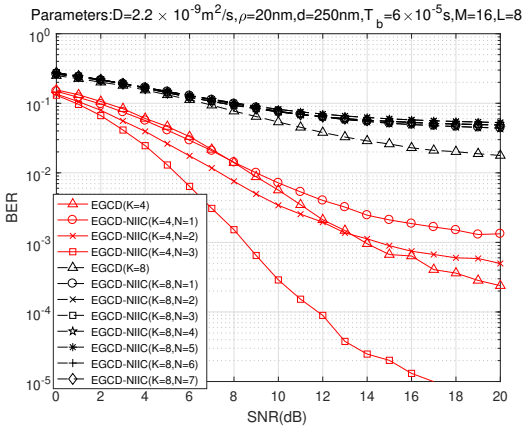

Figure 3.18: Comparison of BER versus SNR performance of the MTS-MoSK DMC systems employing EGCD and EGCD-NIIC, when different number of nano-machines is supported.

in Fig. 3.17, we can know that the EGCD-NIIC scheme requires a relatively high budget of M/K to gain the benefit of performance improvement.

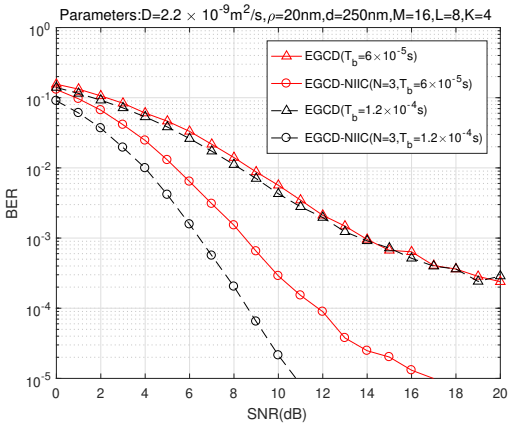

Figure 3.19: Comparison of BER versus SNR performance of the MTS-MoSK DMC systems employing EGCD and EGCD-NIIC, when different bit rate of $1/T_b$ is transmitted.

The BER performance of the MTS-MoSK DMC systems employing respectively EGCD and EGCD-NIIC to support different transmission rates is compared in Fig. 3.19. As the results of Fig. 3.19 show, for the two bit rates considered, EGCD achieves nearly the same BER performance. By contrast, when the EGCD-NIIC with $N = 3$ is employed, significant performance improvement is observed, when the bit rate is reduced from about 16.7K to about 3.3K. Therefore, when the symbol duration becomes longer, resulting the reduction of ISI, the interference cancellation in the EGCD-NIIC becomes more efficient and hence, the BER performance improves.

Fig. 3.20 compares the error performance of our MTS-MoSK DMC systems employing various detectors we propose with the BER performance of a classified MDMA DMC system based on

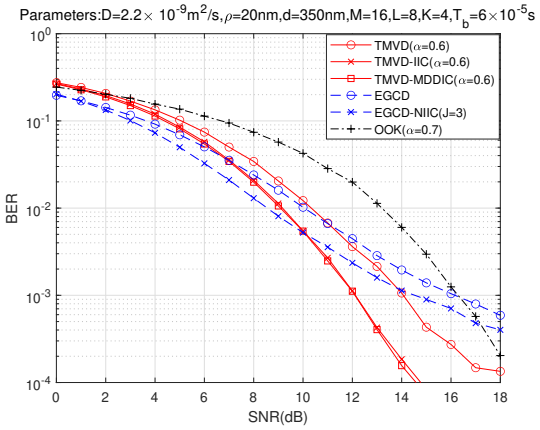

Figure 3.20: Comparison of BER performance of the MTS-MoSK DMC systems employing TMVD-series or EGCD-series detection schemes and that of an orthogonal MDMA DMC system based on OOK, where transmission distance $d = 350nm$ is considered.

OOK modulation scheme to support a longer transmission distance $d = 350nm$. Note that in this OOK-based MDMA DMC system, each nano-machine is straightforwardly assigned a unique type of molecule to transmit information while suffering and imposing no MAI. For a fair comparison of both systems, they are allocated the same bit rate $T_b = 6 \times 10^{-5}$ and the same SNR per-bit budget. It is also worth noting that all special parameters in individual detectors are set to be nearly optimal, such as, the activation threshold $0.6c_h(0)$ in TMVD-series detectors, the number of iterations in EGCD-NIIC, and the decision threshold $0.7c_b(0)$ in OOK demodulation. The results in Fig. 3.20 show that our MTS-MoSK DMC systems outperform OOK-based MDMA DMC systems in the relatively low SNR region no matter which detector is employed in MTS-MoSK DMC systems. This is because OOK-based MDMA systems experience severe ISI though they are equipped with completely orthogonal multiple-access channels especially when the transmission distance increases resulting in the flatter shape of molecular impulses. By contrast, our MTS-MoSK DMC systems employ groups of stochastic molecular types to transmit information that mitigates ISI in nature. We can observe that EGCD-series detectors assisting MTS-MoSK DMC systems are outperformed by OOK-based MDMA DMC systems in the high SNR region eventually, due to error floors resulting from collisions of the same sequence of molecular types emitted by two or more than two nano-machines simultaneously. However, the MTS codes can be carefully designed to prevent this type of collision from occurring frequently which has been well-developed in conventional wireless communication.

Finally, in Fig. 3.21, we compare the BER performance of the MTS-MoSK DMC systems employing the various detection schemes introduced in this chapter, when $K = 2$ nano-machines are supported. In addition to the detection schemes considered in the previous figures, explicitly, the SAML detector achieves the best BER performance, while at the cost of the highest detection complexity. Furthermore, we can observe that even for the SAML, the BER curves appear error

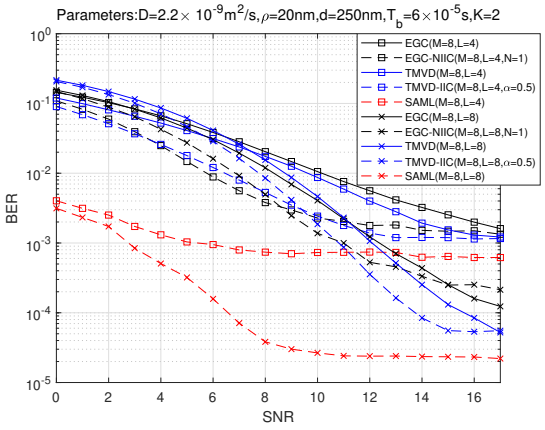

Figure 3.21: Comparison of BER versus SNR performance of the MTS-MoSK DMC systems employing EGCD, EGCD-NIIC, TMVD, TMVD-IIC and SAML, when different values of L are considered.

floors in high SNR region. The reason behind is that the SAML assumes that all the previously detected symbols are correct, which is practically not true. Therefore, when there are erroneously detected symbols, they impose interference on the following detections but the SAML detector ignores and hence, it results in error floor.

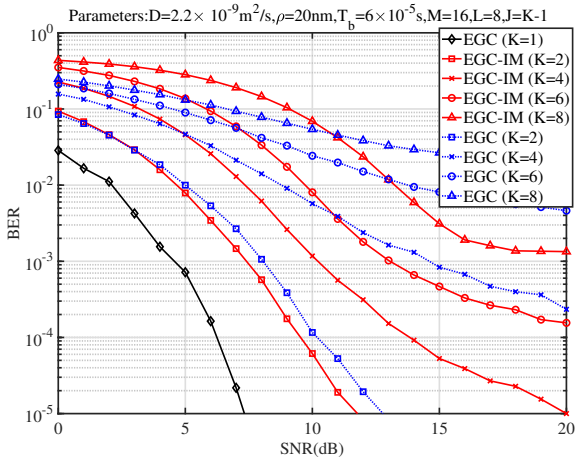

Figure 3.22: Comparison of BER versus SNR performance of the MTH-MoSK DMC systems with EGC-IM and with conventional EGC, when different numbers of nano-machines are supported.

Subsequently, we demonstrate the result of BER improvement EGC-IM brings.[1] First, in Fig. 3.22, we demonstrate and compare the BER versus SNR performance of the MTH-MoSK DMC systems employing the proposed EGC-IM and the conventional EGC, respectively, when $K = 1, 2, 4, 6$ or 8 nano-machines are supported. When EGC-IM is employed, we assume $J = K - 1$ elements are removed from each row of the detection matrix $\boldsymbol{D}_{k,u}$. From the results show we

[1]The numerical result of EGC-IM is provided separately because its content was published in an individual journal.

have the following observations. First, the BER performance of the MTH-MoSK DMC systems employing either detection schemes degrades with the increase of the number of nano-machines, as the result of MAI. When $K \geq 2$, the EGC-IM scheme outperforms the conventional EGC scheme, provided that SNR is sufficiently high. This observation becomes more declared, when K is larger and SNR is higher. However, if SNR is low, the EGC-IM may be outperformed by the conventional EGC scheme. The reason behind is that when SNR is low, system performance is dominated by background noise. In this case, combining more samples encourages to smooth noise and hence improve BER performance. By contrast, when SNR is relatively high, system performance is dominated by MAI. Hence, the proposed EGC-IM scheme having the capability of MAI mitigation outperforms the conventional EGC detection.

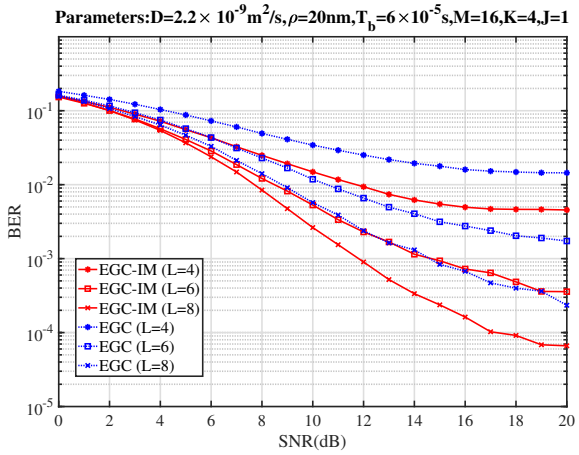

Figure 3.23: BER versus SNR performance of the MTH-MoSK DMC systems with the conventional EGC and the proposed EGC-IM schemes, when one symbol is transmitted using $L = 4$, 6 or 8 chips.

Second, we investigate the effect of L on the performance of the considered detection schemes in Fig. 3.23. Given $K = 4$ nano-machines supported and $J = 1$ entry per row removed from detection matrix, the proposed EGC-IM always outperforms the conventional EGC within the considered SNR region for all the L values. Furthermore, the results show that for both the EGC-IM and EGC, the BER performance improve, as the value of L increases. This is the result that MAI decreases as L increases.

Fig. 3.24 demonstrates the impact of the number of molecular types on the BER performance of the MTH-MoSK DMC systems supporting $K = 4$ nano-machines. As shown in the figure, when EGC-IM scheme is employed, $J = 1$ entry is removed from each row of detection matrix. The results in Fig. 3.24 demonstrate that as more types of molecules are employed, the BER performance of MTH-MoSK DMC systems improves, in addition to the increased data rate[2]. The reason behind is that for a given value of K, MAI reduces as M increases. This is because the MAI entries are more sparsely distributed in the detection matrix, as implied in Fig. 2.10, when M becomes larger.

[2]When $M = 8$, 16 and 32, the data rates are 3, 4, and 5 bits per symbol, respectively.

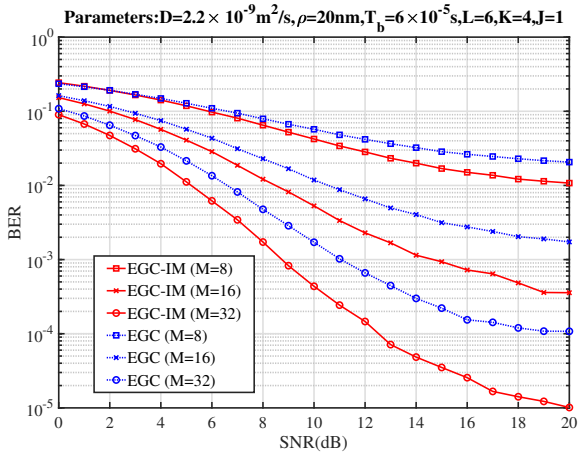

Figure 3.24: BER versus SNR performance of the MTH-MoSK DMC systems with the conventional EGC and proposed EGC-IM, when the number of molecular types is $M = 8$, 16 or 32.

Again, as shown by Fig. 3.24, the EGC-IM detection scheme outperforms the conventional EGC scheme and furthermore, the performance gain at a given SNR increases with the increase of M.

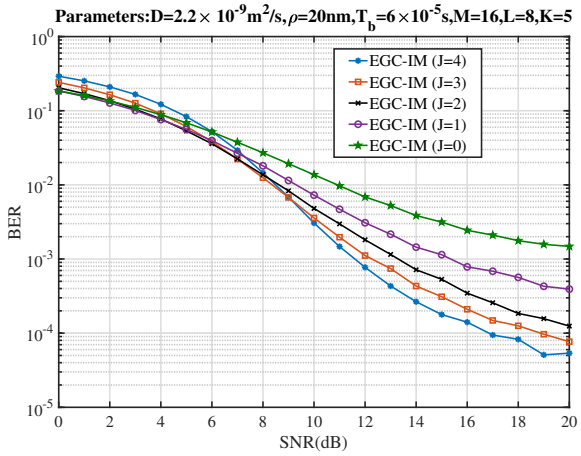

Figure 3.25: BER versus SNR performance of the MTH-MoSK DMC systems with the EGC-IM, when different number of elements per row are removed from the detection matrix.

Finally, Fig. 3.25 demonstrates the effect of the number of elements removed from each of the rows in the detection matrix $\boldsymbol{D}_{k,u}$ on the BER performance of the MTH-MoSK DMC systems with the proposed EGC-IM. In the considered MTH-MoSK DMC systems, we assume that there are $K = 5$ nano-machines supported. Note that, when $J = 0$, the EGC-IM is reduced to the conventional EGC. The results of Fig. 3.25 show that the BER drops, as the value of J increases, provided that the SNR is sufficiently high. This observation implies that MAI can be efficiently mitigated by deleting an appropriate number of entries from the detection matrix. However, at the low SNR region, the EGC-IM with more elements removed from each row of the detection matrix

might not result in BER performance improvement. In other words, for a given SNR and a given value of K, there is an optimum value of J to attain the best possible error performance.

3.5 Conclusions

This chapter has focused on comparing the performance of the MTS-MoSK DMC systems with various detection schemes, which include four proposed interference cancellation relied schemes, namely, TMVD-IIC, TMVD-MDDIC, EGCD-NIIC and EGC-IM, a proposed SAML detector, and two legacy single-user detection schemes, namely TMVD and EGCD. The impacts of the various parameters involved in system design, signal propagation and detector design have been comprehensively investigated and demonstrated via simulations. The studies and performance results show that both TMVD-IIC and TMVD-MDDIC are efficient to mitigate MAI and achieve the similar BER performance, which is much better than that attainable by TMVD and EGCD. In particular, TMVD-IIC has the advantage of a lower complexity than TMVD-MDDIC. When a proper number, i.e., N, is used for interference cancellation, EGCD-NIIC can significantly outperform EGCD. However, the complexity of EGCD-NIIC increases with N, but a very small value of N yields limited performance gain. By contrast, the proposed EGC-IM scheme is efficient for MAI mitigation. Furthermore, the proposed EGC-IM is low complexity. In comparison with the conventional EGC scheme, the extra operations required by the EGC-IM scheme are only identifying some largest elements in each row and deleting them. In addition, for given values of M, L, K and SNR, there is an optimum number of deleted elements from each row to achieve the best BER performance. Among the detection schemes considered, SAML is capable of achieving the best error performance, but it also has the impractically high complexity. Therefore, when the performance-complexity trade-off is concerned, TMVD-IIC is the most promising detection scheme for the MTS-MoSK DMC systems. Our future work will be extended to study the efficient interference cancellation schemes in the MTS-MoSK DMC systems where transmit nano-machines are distributed at different distances away from the AP.

Chapter 4

Molecular Code-Division Multiple-Access: Signaling, Detection and Performance

In the last chapter, we proposed a range of MAI cancellation-assisted detectors for the MTS-MoSK DMC systems, which can further mitigate the effect of MAI and enable significant performance improvement at the slightly increased complexity. However, there are some system settings in our MTS-MoSK DMC systems, which are hypercritical for implementation on some occasions. For instance, MTS-MoSK DMC systems may require a large number of molecular types and the transmission distances between nano-machines (NMs) and AP need to be similar. In order to relax these constraints, in this chapter, relying on two types of molecules, a molecular code-division multiple-access (MoCDMA) scheme is designed for multiple NMs to simultaneously send information to a fusion center (FC) in DMC environments. In our considered MoCDMA system, different NMs may have different distances from FC, which generates 'near-far' effect. Correspondingly, the uniform and channel-inverse based molecule-emission schemes are proposed for NMs to emit information molecules. To facilitate signal detection, the received signals by FC are represented in different forms, based on which a range of detection schemes are derived. Specifically, by considering the limited computational power of nano-machines, a range of relatively low complexity detectors are derived in the principles of matched-filtering (MF), zero-forcing (ZF) and minimum mean-square error (MMSE). Furthermore, the noise characteristics in MoCDMA systems and the complexity of various detection schemes are analyzed.

4.1 Introduction

With the global outbreak of COVID-19, human's well-being has attracted intensive research interest of the researchers various all fields. Nanotechnologies involving the manufacture of nano-material and nano-devices have revolutionized the ways for disease diagnostics and treatment [11, 101]. Though nano-devices like bio-sensors have the advantages of, such as, tiny size, energy saving, and biocompatibility, making them suitable for medical and healthcare applications, an individual nano-machine (NM) is usually incapable of completing complex tasks, due to its low-energy storage and low computation capability [96, 102]. To accomplish more complicated biomedical tasks, including targeted drug delivery [8, 9], health monitoring [12, 13], tissue engineering [103], and tumor diagnosis [10], etc, a recent revolution trend is to envision the concept of Internet of Things (IoT) at the nano-scale, which is referred to the Internet of Bio-Nano Things (IoBNT) [87–89, 104]. There are a range of communication technologies that may be the candidate technologies for designing the nano-networks, including molecular communication (MC) [17, 105], electromagnetic communication at terahertz band [106, 107], acoustic and mechanical communication. Among them, the MC belonging to a bio-inspired communication paradigm has the most biocompatibility [16], which enables molecules to convey information from one nano-transmitter, such as a NM/sensor, to another access point (AP), like a fusion centre, which are separated with a certain distance [108].

Because free diffusion is a common propagation mechanism in nature [28], molecular communication via diffusion, or diffusive molecular communication (DMC) can be facilitated by the movements of information-embedded molecules solely driven by the diffusion process in liquid or gas media. Owing to this, DMC systems are energy-efficient, which benefits the durability of IoBNT. In DMC systems, information can be conveyed via modifying the concentration levels of molecules at transmitter. Correspondingly, the receiver decodes the information according to the concentration levels obtained from its detection space [109]. However, due to the random diffusive movements of molecules, DMC usually experiences long transmission delay and strong inter-symbol interference (ISI) [90], in addition to the noise generated from the random movements of information molecules as well as from the other noisy sources in the communications environment [22].

For implementation of the collaboration among individual NMs, a significant challenge in IoBNT is to enable multiple NMs to share a common DMC medium, namely multiple-access DMC, in order for them to send information to an AP for further processing or fusion [17]. As in the conventional radio-based wireless communication, in principle, multiple-access DMC can be implemented in different domains. The most straightforward one is the molecular division multiple-access (MDMA) [45, 109], which is in parallel with the frequency division multiple-access (FDMA) in wireless communications. With MDMA, different NMs sharing a common environment simultaneously communicate with a common receiver via orthogonal channels consisting of different types of information molecules. MDMA is simple. However, when there are many NMs

communicating at the same time, many types of molecules are required, which is highly challenging in terms of the synthesis and storage of molecules as well as the design of nano-transceivers. For instance, as many types of molecules are required to be sensed, the receiver is required to be equipped with many types of receptors, correspondingly, which may demand a high complexity. Multiple-access DMC can also be achieved in the time-domain using molecular time-division multiple-access (MoTDMA) [46–48]. To implement MoTDMA, the time axis can be divided into frames, and a frame is further divided into a number of time slots. In this way, messages of different NMs can be delivered to the common receiver using only one type of molecules via scheduling different NMs to transmit on different time slots of a frame. It is well-known that a crucial requirement for implementing TDMA is that all the transmitted signals should be well synchronized. However, this is often challenging to achieve in DMC, unless all the transmit NMs have the same distance from their common receiver. This is because in DMC, the channel impulse response (CIR) is non-linear, which is highly sensitive to the transmission distance, making both the amplitude and width of the received pulses from different nano-transmitters very different, if they have different distances from the receiver [56]. Furthermore, by exploiting the tremendous impact of transmission distance on the CIR in DMC, multiple-access DMC may also be achieved via space division multiple-access, forming the MoSDMA, which distinguishes different transmit NMs based on their shapes of CIR corresponding to different locations relative to the receiver [49, 50]. However, MoSDMA relies very much on the instantaneous channels from different NMs, which are hard to estimate due to the multiple-access interference (MAI) among different transmissions.

Furthermore, multiple-access DMC can also be achieved in the principles of CDMA, forming the MoCDMA [51, 52]. In MoCDMA, different NMs are assigned different signatures to spread messages, which can then be invoked by the receiver to de-spread and detect the information conveyed by the NMs. Additionally, a physical experiment for MoCDMA systems has been conducted in [74]. Explicitly, MoCDMA has the advantage that it only requires a small (typically 1 or 2) number of molecular types. Furthermore, depending on DMC scenarios, MoCDMA may be operated in synchronous mode or asynchronous mode, and even in the scenarios where different NMs have different distances from their common receiver or/and transmit at different data rates. In detail, in [51], a MoCDMA scheme has been proposed on the basis of a single type of molecules with the aid of the on-off keying (OOK) modulation. Correspondingly, in this type of MoCDMA, the optical spreading sequences having their elemental values in the additive group of $\{0, 1\}$ are used. Due to the on-off nature of signature sequences, the performance results in [51] show that the achievable error performance of this MoCDMA system is in general poor, even when the number of NMs supported is as low as 2 or 4 for a spreading factor of 10. By contrast, the authors in [52] have proposed a MoCDMA scheme based on two types of molecules and the binary molecule-shift keying (MoSK) modulation. The comparison between this MoSK-based MoCDMA with the OOK-based MoCDMA shows that the former one has the potential to significantly outperform the latter one. However, the studies in [52] are very specific, which assume only the Walsh codes for spreading

and the adaptive threshold detection. Furthermore, the system model is not sufficiently generalized for use, due to the assumption of the same transmission distance between nano-transmitters and the common receiver.

Based on the above observations, in this chapter, we propose a MoCDMA scheme, where the transmission distances between NMs and the AP receiver are different. For molecular transmission at NMs, we consider two emission schemes, namely, the uniform emission and channel-inverse emission. With uniform emission, each NM emits the same number of molecuels per symbol according to the required signal-to-noise ratio (SNR). By contrast, for the channel-inverse emission, the number of molecules emitted by a NM is proportional to the cube of its distance from the AP. Explicitly, the channel-inverse emission strategy achieves fair communication quality (FoCQ) among 'near-far' NMs. In our MoCDMA system, in order to implement the antipodal signalling, as in [52], two types of molecules, which constitute a pair of isomers with the same diffusion coefficient [84], are introduced. One type (Type-A) is for sending $+1$ signed signals and one type (Type-B) is for sending -1 signed signals. At the AP receiver, we assume a passive observer, which is capable of counting the numbers of molecules of both Type-A and Type-B within a detection space at chip level. We examine in detail the observations and show that the received signals in our MoCDMA can be represented in the forms fully equivalent to that in the conventional RdCDMA systems with binary phase shift keying (BPSK) modulation [78]. Based on this observation, then, we derive the representations for the observations.

Due to the slow diffusive propagation of DMC channels, MoCDMA systems may suffer from different types of interference, including, inter-chip interference (ICI), inter-symbol interference (ISI) and multiple-access interference (MAI), as well as the background noise that increases with the number of molecules emitted in the system. Therefore, in MoCDMA systems, the AP receiver should be carefully designed to efficiently suppress the above-mentioned interference. However, the transceiver design in nano-network is usually constrained by a tight computation budget, only allowing relatively low-complexity techniques. Hence, in this chapter, we consider three low-complexity linear detection schemes, which are the matched-filtering (MF), zero-forcing (ZF) and minimum mean-square error (MMSE) detectors. Furthermore, we consider only the low complexity symbol by symbol detection. We analyze their complexity, as well as investigate and compare their error performance. Our numerical studies demonstrate the achievable performance and analyze the performance-complexity trade-off of the MoCDMA systems with two molecular emission strategies and three detection schemes.

In summary, the novelties of this chapter are as follows:

- In analogy with the conventional RdCDMA system with BPSK modulation, an equivalent MoCDMA system based on binary MoSK (BMoSK) modulation is introduced to take the advantages of the well-developed signal processing techniques in the conventional BPSK-modulated RdCDMA systems, such as, signal representation, interference mitigation, signal

detection, etc.

- Different transmission distances between NMs and FC are assumed to make the DMC system model more practical. Correspondingly, a synchronization scheme is proposed to align the expected maximum concentration points of different NMs.

- Considering that the performance of MoCDMA systems is highly sensitive to the transmission distances of different NMs, in analogy with the power-control in conventional Rd-CDMA, two molecular emission schemes, namely, the uniform emission and channel-inverse emission, are proposed and compared. The performance results show that the channel-inverse emission is capable of improving the reliability of the NMs further away from FC. This allows the detection of differently located NMs to achieve a similar BER performance and, hence, mitigate the near-far problem.

- Three linear multiuser detection schemes in the principles of MF, ZF, and MMSE are proposed for signal detection in MoCDMA systems. Our studies and performance results show that all these detection schemes are low-complexity detection schemes, while the ZF- and MMSE-detectors are capable of achieving more reliable detection than the MF-detector.

The rest of the paper is organized as follows. First, the system model, including transmitter, channel model, emission approaches and received signals, as well as the research assumptions are stated in Section 4.2. The different representations of the received signals in the perspective of symbol-level are derived in Section 4.3. Section 4.4 presents the derivation of three signal detection schemes, i.e., MF, ZF and MMSE at the symbol-level. In addition, the complexities of different detectors are provided in Section 4.4. The bit error rate (BER) performance of the MoCDMA systems with different detectors and molecular emission schemes are compared in Section 4.5. Finally, the concluding summary is made in Section 4.6.

4.2 System Model

We consider a multiple-access DMC system that consists of K point nano-machines (NMs) (transmitters) and one spherical passive nano-type AP (receiver) with a radius ρ, as illustrated in Fig. 4.1. The locations of the AP and of all NMs are fixed. Unlike the assumption made in [52] for the multiple-access MC systems, this chapter takes different transmission distances from NMs into consideration. Without any loss of generality, the transmission distances from NMs to AP are sorted as $d_1 \leq d_2 \leq \ldots \leq d_K$. Because the concentration of information molecules at AP is highly sensitive to the transmission distance, two emission strategies will be introduced after the channel model description in this section. Here, we generally denote $Q^{(k)}$ as the number of molecules emitted by the kth NM for transmitting a symbol. Following the CDMA concept, a symbol of information is further transmitted via emitting N impulses of each having $Q_c^{(k)} = Q^{(k)}/N$ molecules, where N

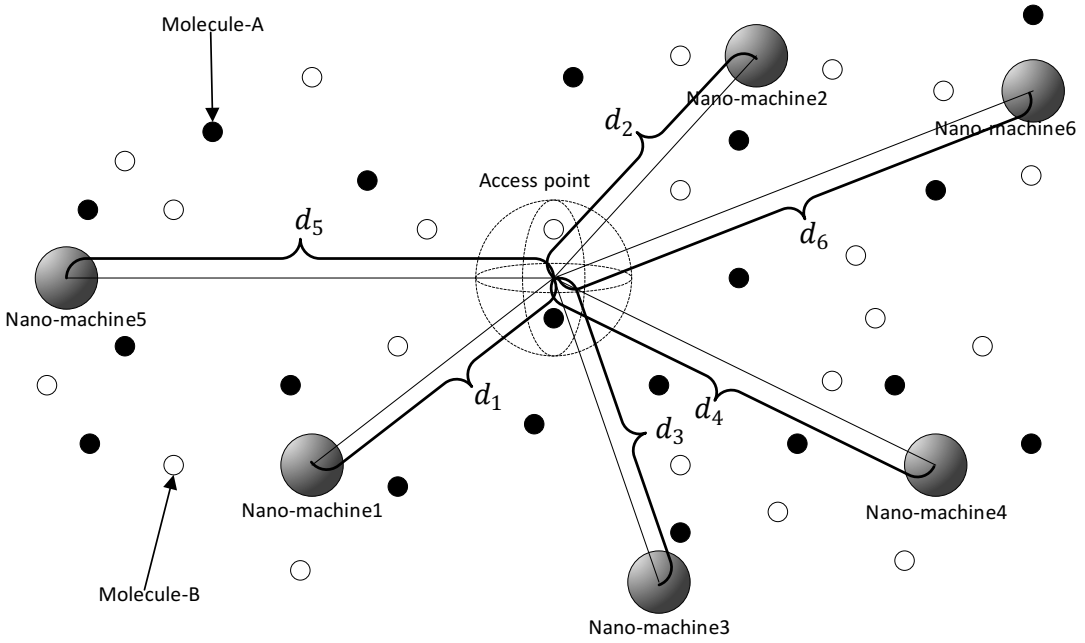

Figure 4.1: System model for MoCDMA DMC systems, where nano-machines have different transmission distances to a common access point.

can be understood as the spreading factor or the number of chips within one symbol-duration of T_s. The interval between any two adjacent impulses is a fixed chip-duration of T_c. Hence, we have $T_s = NT_c$, when BMoSK modulation is employed, $T_s = T_b$, where T_b is the bit-duration. Below we describe the transmitter, channel model, emission strategies and receiver for the MoCDMA systems in detail.

4.2.1 Transmitter

We assume that in the considered MoCDMA system, information transmitted by the kth NM is expressed as $\boldsymbol{B}_k = \{b_{k,0}, b_{k,1}, \ldots, b_{k,j}, \ldots\}$, where $b_{k,j} \in \{1, -1\}$. According to the methodology of MoCDMA, the uth bit of NM k is spread by a N length spreading sequence [110] denoted by $\boldsymbol{s}_k = [s_{k,0}, s_{k,1}, \ldots, s_{k,N-1}]^T$, where $s_{k,n} \in \{1, -1\}$, and again, $N = T_s/T_c$. In our MoCDMA system, as the NMs have different distances from AP, we define a common and fixed T_s to allow all NMs to simultaneously transmit information to AP under the basic principle of DMC, which will become apparent in the forthcoming discourses. Moreover, to make sure that AP can obtain a good observation for all NMs, when only one sample in each chip duration is taken, a time offset (delay) denoted by $T_o^{(k)}$ is introduced for the kth NM to emit. Note that this time offset of an NM is dependent on its pulse peak presenting at AP, which will be detailed after describing the channel model. Then, when assuming that BMoSK modulation is employed, $Q_c^{(k)}$ molecules per pulse are emitted for the activated type (Type-A or Type-B) of molecules. Note that, Type-A and Type-B molecules are assumed to be a pair of isomers, whose diffusion coefficients are generally the same.

Therefore, the transmitted signal for the uth bit of NM k can be expressed as

$$s_k(t) = \sum_{n=0}^{N-1} \left[\frac{1 + b_{k,u} s_{k,n}}{2} Q_c^{(k)} \delta_A(t - uT_s - nT_c - T_o^{(k)}) + \frac{1 - b_{k,u} s_{k,n}}{2} Q_c^{(k)} \delta_B(t - uT_s - nT_c - T_o^{(k)}) \right]$$
$$k = 1, 2, \ldots, K; u = 0, 1, \ldots, \tag{4.1}$$

where $\delta_A(t)$ and $\delta_B(t)$ denote the impulses of Type-A and Type-B molecules, respectively, which are defined as $\delta_A(0) = 1$ and $\delta_B(0) = 1$, and $\delta_A(t) = 0$ and $\delta_B(t) = 0$ for all $t \neq 0$.

4.2.2 Channel Model

Let us assume that the diffusion channel environment is a fluid medium without any flow and that the fluid environment is unchanged during a session of communication. Therefore, the diffusion coefficient D of isomers is constant during transmission. On the other side, the AP is assumed to be able to measure the concentration of molecules inside the spherical detection space. We assume that precise synchronization can be achieved between NMs and AP. Based on these assumptions, and when an impulse of $Q_c^{(k)}$ molecules is released by a NM at $t = T_o^{(k)}$, the concentration measured inside AP at $t > T_o^{(k)}$ follows Fick's Law, which can be expressed as [56]

$$c_k(t) = \frac{Q_c^{(k)}}{[4\pi D(t - T_o^{(k)})]^{\frac{3}{2}}} \exp\left[-\frac{d_k^2}{4D(t - T_o^{(k)})} \right], t > T_o^{(k)} \tag{4.2}$$

As shown in (4.2), the molecular concentration $c_k(t)$ is a time(T)-domain pulse function, the shape of which can be defined as the channel impulse response (CIR) [111]

$$h_k(t) = \frac{1}{[4\pi D(t - T_o^{(k)})]^{\frac{3}{2}}} \exp\left[-\frac{d_k^2}{4D(t - T_o^{(k)})} \right], t > T_o^{(k)} \tag{4.3}$$

It can be shown that in (4.3), when d_k is given, the maximum value of pulse or pulse peak, can be attained at $t_d^{(k)} = d_k^2/6D$ which has a value of $h_{k,max} = \left(\frac{3}{2\pi e}\right)^{\frac{3}{2}} \frac{1}{d_k^3}$. In principle, this extreme point is an ideal sampling point, which results in the highest power for signal detection. However, the pulse peak value $h_{k,\max}$ decreases with d_k^3, making DMC system is highly sensitive to transmission distance. Therefore, emission strategies need to be designed for MoCDMA systems to handle the 'near-far' issue.

4.2.3 Emission Control

In our MoCDMA system with different transmission distances for NMs, the distance from the furthest NM to AP is denoted as d_K. This distance parameter is assumed to be known to AP and all NMs. In this case, the peak point of the pulse due to the furthest NM occurs at $t_d^{(K)} = d_K^2/6D$. Correspondingly, the maximum magnitude of the CIR is $h_{K,max} = \left(\frac{3}{2\pi e}\right)^{\frac{3}{2}} \frac{1}{d_K^3}$. With the above information, to synchronize the peak points of different NMs to the same time at AP, each NM emits pulses according to its distance d_k from AP. Note that, this can be achieved as follows.

Before NM's transmission, AP can send some pilot signals, such as, some pulses of other types of molecules to NMs. Based on the measurements of pilots, each NM can identify its distance from AP and hence its emitting time, so that it can be synchronized with the other NM's signals, as above-mentioned. In detail, when NMs are assumed to be equipped with accurate clocks [112–114], then, at the beginning of the first chip, the emission time delay of NM k can be obtained to be $T_o^{(k)} = t_d^{(K)} - t_d^{(k)}$, relative to the NM farthest from AP. When all NMs emit molecular pulses at the corresponding moments, the AP can sample at the maximum magnitudes of the CIRs of different NMs.

In terms of the numbers of molecules emitted by different NMs, we proposed two approaches with low complexity to monitor them. The first approach is uniform emission, which allocates the same number of molecules to all NM. Specifically, for a given one-bit budget of molecules denoted by Q, the number of molecules emitted by NM k to transmit a chip pulse is

$$Q_c^{(k)} = Q/N. \tag{4.4}$$

However, this approach generates the 'near-far' problem, yielding that the CIR peak of a closer NM is higher than that of a further away NM.

Therefore, with the second approach, the channel-inverse emission based is implemented, which adjusts the number of molecules emitted by a NM according to its CIR. From (4.2) and (4.3) we know that $c_{k,max}$ and $h_{k,max}$ are related by $c_{k,max} = Q_c^{(k)} h_{k,max}$. Then, with the channel-inverse based emission approach, the NMs emit the numbers of molecules per chip to achieve

$$c_{1,max} = c_{2,max} = \ldots = c_{K,max} \tag{4.5}$$

where $c_{K,max}$ is obtained by assuming that the maximum number of molecules emitted per chip by the furthest NM, which is according to Q/N. Hence, the number of molecules emitted per chip by NM k can be formed to be

$$Q_c^{(k)} = \frac{Q}{N} \cdot \frac{h_{K,max}}{h_{k,max}} = \frac{Q}{N} \cdot \left(\frac{d_k}{d_K}\right)^3 \leq \frac{Q}{N}. \tag{4.6}$$

Compared to the uniform emission approach, the channel-inverse based emission approach can save a considerable number of molecules of the system while keeping that the signals sent by different NMs have a similar reliability. Otherwise, the NMs closer to AP will impose significant interference on the NMs farther away from AP.

4.2.4 Receiver

Assume that AP is able to identify the two types of molecules (Type-A and Type-B) without absorbing them. Then, when K NMs emit molecular impulses in the form of (4.1) to AP, the sampled observation difference at t between Type-A and Type-B molecules corresponding to the nth chip,

$n = 0, 1, \ldots N-1$, within the uth bit-duration can be expressed as

$$\begin{aligned} z(t) =& z_A(t) - z_B(t) \\ =& \sum_{k=1}^{K} \sum_{j=0}^{uN+n} \frac{1 + b_{k,\lfloor j/N \rfloor} s_{k,j\%N}}{2} \left[c_k(t - jT_c) + n_{A,k,j}(t) \right] \\ & - \sum_{k=1}^{K} \sum_{j=0}^{uN+n} \frac{1 - b_{k,\lfloor j/N \rfloor} s_{k,j\%N}}{2} \left[c_k(t - jT_c) + n_{B,k,j}(t), \right] \\ & (uN+n)T_c + T_o^{(k)} \leq t < (uN+n+1)T_c + T_o^{(k)} \end{aligned} \tag{4.7}$$

where $\lfloor \cdot \rfloor$ is the floor operation, $j \,\%\, N$ is the reminder of j/N, $n_{A,k,j}(t)$ and $n_{B,k,j}(t)$ are the Brownian motion noise caused respectively by the Type-A and Type-B molecules emitted by the NM k within the jth chip duration [22]. To be more specific, according to [22, 115], when the average number of molecules per pulse is sufficiently large, we can employ the Gaussian-approximation to the Brownian motion noise $n_{A,k,j}(t)$ and $n_{B,k,j}(t)$, with the mean being zero and variance being

$$\begin{aligned} \sigma^2_{A,k,j}(t) =& \frac{1 + b_{k,\lfloor j/N \rfloor} s_{k,j\%N}}{2V} c_k(t - jT_c), \\ \sigma^2_{B,k,j}(t) =& \frac{1 - b_{k,\lfloor j/N \rfloor} s_{k,j\%N}}{2V} c_k(t - jT_c), \end{aligned} \tag{4.8}$$

respectively, where $V = \frac{4}{3}\pi\rho^3$ is the volume of the spherical detection space with a radius of ρ. For convenient expression, these distributions are denoted as $n_{A,k,j}(t) \sim \mathcal{N}\left(0, \sigma^2_{A,k,j}(t)\right)$ and $n_{B,k,j}(t) \sim \mathcal{N}\left(0, \sigma^2_{B,k,j}(t)\right)$, respectively.

As illustrated in (4.2), after NM k emits an pulse of molecules at $t = T_o^{(k)}$, the expected peak concentration of $c(t)$ at AP is at $t = t_d^{(K)}$, which is the same for all the K NMs. Therefore, to detect the uth bits of K NMs, AP samples for the concentrations at $t = (uN+n)T_c + t_d^{(K)}$, where $n = 0, 1, \ldots, N-1$. Correspondingly, the observation difference between two types of molecules can be expressed as

$$\begin{aligned} Z_{u,n} &= z_A(t = (uN+n)T_c + t_d^{(K)}) - z_B(t = (uN+n)T_c + t_d^{(K)}) \\ &= \sum_{k=1}^{K} \sum_{j=0}^{uN+n} \frac{1 + b_{k,\lfloor j/N \rfloor} s_{k,j\%N}}{2} \left[c_k\Big((uN+n-j)T_c + t_d^{(K)}\Big) \right. \\ &\qquad \left. + n_{A,k,j}\Big((uN+n)T_c + t_d^{(K)}\Big) \right] \\ &\quad - \sum_{k=1}^{K} \sum_{j=0}^{uN+n} \frac{1 - b_{k,\lfloor j/N \rfloor} s_{k,j\%N}}{2} \left[c_k\Big((uN+n-j)T_c + t_d^{(K)}\Big) \right. \\ &\qquad \left. + n_{B,k,j}\Big((uN+n)T_c + t_d^{(K)}\Big) \right] \\ &\quad u = 0, 1, \ldots;\ n = 0, 1, \ldots, N-1 \end{aligned} \tag{4.9}$$

As (4.9) shows, the terms with index $j \neq 0$, representing the previous pulses sent before the $(uN+n)$th impulse, imposes inter-chip interference (ICI) on the current chip. However, from the characteristics of $c(t)$ we know that ICI reduces significantly with time. Thus, we set the maximum

length of ICI to L chips in our analysis, by assuming that the ICI yielded by a previously sent pulse exceeding L chips is negligible. In this case, $Z_{u,n}$ in (4.9) can be denoted in the form of

$$\begin{aligned} Z_{u,n} = &\sum_{k=1}^{K} \sum_{j=\max\{0,uN+n-L\}}^{uN+n} \frac{1+b_{k,\lfloor j/N \rfloor} s_{k,j\%N}}{2} \left[c_k(uN+n-j) + n_{A,k,j}(uN+n)\right] \\ &- \sum_{k=1}^{K} \sum_{j=\max\{0,uN+n-L\}}^{uN+n} \frac{1-b_{k,\lfloor j/N \rfloor} s_{k,j\%N}}{2} \left[c_k(uN+n-j) + n_{B,k,j}(uN+n)\right] \\ &u = 0,1,\ldots;\ n = 0,1,\ldots,N-1 \end{aligned} \tag{4.10}$$

where $c_k(uN+n-j)$ corresponds to $c_k\left((uN+n-j)T_c + t_d^{(K)}\right)$ and $n_{X,k,j}(uN+n)$ corresponds to $n_{X,k,j}\left((uN+n)T_c + t_d^{(K)}\right)$ in (4.9), X represents A or B.

In (4.10), when the specific kth NM and jth pulse are considered, we have either $\frac{1}{2}\left(1+b_{k,\lfloor j/N \rfloor} s_{k,j\%N}\right) = 1$ and $\frac{1}{2}\left(1-b_{k,\lfloor j/N \rfloor} s_{k,j\%N}\right) = 0$ if $b_{k,\lfloor j/N \rfloor} s_{k,j\%N} = 1$, or $\frac{1}{2}\left(1+b_{k,\lfloor j/N \rfloor} s_{k,j\%N}\right) = 0$ and $\frac{1}{2}\left(1-b_{k,\lfloor j/N \rfloor} s_{k,j\%N}\right) = 1$ if $b_{k,\lfloor j/N \rfloor} s_{k,j\%N} = -1$. Furthermore, $n_{A,k,j}(uN+n)$ for $b_{k,\lfloor j/N \rfloor} s_{k,j\%N} = 1$ and $n_{B,k,j}(uN+n)$ for $b_{k,\lfloor j/N \rfloor} s_{k,j\%N} = -1$ have the same statistical property. Hence, (4.10) can be expressed in an equivalent form of

$$\begin{aligned} Z_{u,n} = &\sum_{k=1}^{K} \sum_{j=\max\{0,uN+n-L\}}^{uN+n} b_{k,\lfloor j/N \rfloor} s_{k,j\%N} \left[c_k(uN+n-j) + n_{k,j}(uN+n)\right] \\ &u = 0,1,\ldots;\ n = 0,1,\ldots,N-1 \end{aligned} \tag{4.11}$$

where $n_{k,j}(uN+n)$ is approximately Gaussian distribution as $\mathcal{N}\left(0, \sigma_{k,j}^2(u,n)\right)$ with $\sigma_{k,j}^2(u,n) = V^{-1}c_k(uN+n-j)$.

Let $i = uN+n-j$. Then, we can represent (4.11) in a more convenient form of

$$\begin{aligned} Z_{u,n} &= \sum_{k=1}^{K} \sum_{i=0}^{\min\{L,uN+n\}} b_{k,\lfloor (uN+n-i)/N \rfloor} s_{k,(n-i)\%N} \left[c_k(i) + n_{k,uN+n-i}(uN+n)\right] \\ &= \sum_{k=1}^{K} \sum_{i=0}^{\min\{L,uN+n\}} c_k(i) s_{k,(n-i)\%N} b_{k,\lfloor (uN+n-i)/N \rfloor} + N_{u,n} \\ &\quad u = 0,1,\ldots;\ n = 0,1,\ldots,N-1 \end{aligned} \tag{4.12}$$

where $N_{u,n} = \sum_{k=1}^{K} \sum_{i=0}^{\min\{L,uN+n\}} b_{k,\lfloor (uN+n-i)/N \rfloor} s_{k,(n-i)\%N} n_{k,uN+n-i}(uN+n)$, which is a Gaussian distributed as $\mathcal{N}\left(0,\sigma^2\right)$, where $\sigma^2 = V^{-1}\sum_{k=1}^{K}$ $\sum_{i=0}^{\min\{L,uN+n\}} c_k(i)$. It is worth noting that one advantage of the BMoSK modulation employed in our MoCDMA systems is that the Brownian motion noise can be approximated by the Gaussian noise irrelevant to the information bits transmitted.

As Eq. (4.12) demonstrates, in MoCDMA systems, the transmission suffers from ISI, ICI as well as MAI between NMs. Hence, the detector at AP should be designed carefully in order to achieve reliable detection. Furthermore, as shown in the above representation of $Z_{u,n}$, though the noise in MoCDMA systems modulated by BMoSK is not directly related to the transmitted information, any emitted molecule simultaneously results in the increase of noise power, in addition to

its role in conveying information. This is because the Brownian motions of molecules contribute to the noise in DMC systems, which is referred to as the counting noise. Counting noise leads to unintentional perturbations to the concentration (or number of molecules) expected from the Fick's second rule within the detection sphere of AP [22]. Thus, we should note that in a MoCDMA system, the noise power increases with the number of NMs supported by the system via ISI, ICI and MAI. This is very different from that in the conventional radio-based communication systems, where the environment noise is usually the additive white Gaussian noise (AWGN), which is completely independent of the transmitted signals, including various types of interfering signals, such as, ISI, MAI, etc.

Having obtained the equivalent representation for the observations, as demonstrated in (4.12), now we represent the received signals in different forms in 4.3 for easily explaining the various detection schemes in 4.4.

4.3 Representation of Received Signals

Considering the challenges of transceiver implementation in MoCDMA systems, in this chapter, we only consider the symbol-by-symbol detectors. In this case, AP carries out detections based on N-length observation vector corresponding to one bit, such as bit $u > 1$. Then, it can be shown that from (4.12) we have an expression of

$$\begin{aligned}\boldsymbol{z}_u &= \sum_{k=1}^{K} \boldsymbol{C}_{k2}\boldsymbol{S}_{k2}\boldsymbol{b}_{k2} + \boldsymbol{n}_u \\ &= \sum_{k=1}^{K} \left(\boldsymbol{C}_{k0}\boldsymbol{s}_k b_{k,u} + \boldsymbol{C}_{k-1}\boldsymbol{s}_k b_{k,u-1}\right) + \boldsymbol{n}_u \end{aligned} \tag{4.13}$$

where $\boldsymbol{z}_u = [Z_{u,0}, Z_{u,1}, \ldots, Z_{u,N-1}]^T$, $\boldsymbol{n}_u = [N_{u,0}, N_{u,1}, \ldots, N_{u,N-1}]^T$, $\boldsymbol{C}_{k2}$ is a $(N \times 2N)$ matrix whose last row is constituted by zeros and $\text{Rev}(\boldsymbol{c}_k^T) = [c_k(L), c_k(L-1), \ldots, c_k(0)]$, and $c_k(0)$ is located at the position of $(N-1, 2N-1)$. In the other $(N-1)$ rows, the parts of non-zero elements are just the shifts of these $(L+1)$ elements, and the left shift of the ith row is $(N-1-i)$ for $i = 0, 1, \ldots, N-2$. In (4.13), $\boldsymbol{S}_{k2} = \boldsymbol{I}_2 \otimes \boldsymbol{s}_k$, where $\boldsymbol{I}_2$ is a (2)-element identity matrix and $\otimes$ represents the Kronecker product operation, and $\boldsymbol{b}_{k2} = [b_{k,u-1}, b_{k,u}]^T$. Note that, to obtain (4.13), we assumed that the uth bit experiences interference only from a previous bit $(u-1)$. Correspondingly, the second equation in (4.13) explicitly represents the two bits separately, where $\boldsymbol{C}_{k-1}$ consists of the first N columns of $\boldsymbol{C}_{k2}$, while $\boldsymbol{C}_{k0}$ is structured by the other N columns of $\boldsymbol{C}_{k2}$.

It can be shown that the second equation in (4.13) has another form of

$$\boldsymbol{z}_u = \sum_{k=1}^{K} \left(\tilde{\boldsymbol{S}}_{k,0}\boldsymbol{c}_k b_{k,u} + \tilde{\boldsymbol{S}}_{k,-1}\boldsymbol{c}_k b_{k,u-1}\right) + \boldsymbol{n}_u \tag{4.14}$$

where $\boldsymbol{c}_k = [c_k(0), c_k(1), \ldots, c_k(L)]^T$, $\tilde{\boldsymbol{S}}_{k,0}$ is a $N \times (L+1)$ lower diagonal matrix structured as: a) $s_{k,0}$ is on diagonal; b) the first column is occupied by $\boldsymbol{s}_k$ and otherwise zeros; and c) the other

columns are constituted by the downshifts of the first column after deleting the elements that are shifted outside the matrix. $\tilde{\boldsymbol{S}}_{k,-1}$ is also a $N \times (L+1)$ matrix, which has only L non-zero rows starting from the top (row 0) of the matrix. These non-zero rows are structured as follows: a) from left to right, the first row has the elements of $\{0, s_{k,N-1}, s_{k,N-2}, \ldots, s_{k,N-L}\}$; and b) the other rows are obtained from right shifting this row by adding zeros to the left and deleting non-zero elements from the right, if they are shifted beyond the Lth column. For instance, the second row is $\{0, 0, s_{k,N-1}, s_{k,N-2}, \ldots, s_{k,N-L+1}\}$ and the final non-zero row is $\{0, 0, \ldots, 0, s_{k,N-1}\}$; and c) except the above, all the other locations are occupied by zeros.

In addition, when writing in a more compact form, (4.14) can be represented as

$$\boldsymbol{z}_u = \tilde{\boldsymbol{S}}_0 \tilde{\boldsymbol{C}} \boldsymbol{b}_u + \tilde{\boldsymbol{S}}_{-1} \tilde{\boldsymbol{C}} \boldsymbol{b}_{u-1} + \boldsymbol{n}_u \tag{4.15}$$

where $\tilde{\boldsymbol{S}}_0 = \left[\tilde{\boldsymbol{S}}_{1,0}, \tilde{\boldsymbol{S}}_{2,0}, \ldots, \tilde{\boldsymbol{S}}_{K,0}\right]$, $\tilde{\boldsymbol{S}}_{-1} = \left[\tilde{\boldsymbol{S}}_{1,-1}, \tilde{\boldsymbol{S}}_{2,-1}, \ldots, \tilde{\boldsymbol{S}}_{K,-1}\right]$, $\boldsymbol{b}_u = [b_{1,u}, b_{2,u}, \ldots, b_{K,u}]^T$, $\boldsymbol{b}_{u-1} = [b_{1,u-1}, b_{2,u-1}, \ldots, b_{K,u-1}]^T$, and $\tilde{\boldsymbol{C}}$ is a $(LK \times K)$ matrix constructed as

$$\tilde{\boldsymbol{C}} = \begin{bmatrix} c_1(0) & c_1(1) & \cdots & c_1(L) & 0 & 0 & \cdots & 0 & \cdots & 0 & 0 & \cdots & 0 \\ 0 & 0 & \cdots & 0 & c_2(0) & c_2(1) & \cdots & c_2(L) & \cdots & 0 & 0 & \cdots & 0 \\ \vdots & \vdots & \ddots & \vdots & \vdots & \vdots & \ddots & \vdots & \ddots & \vdots & \vdots & \ddots & \vdots \\ 0 & 0 & \cdots & 0 & 0 & 0 & \cdots & 0 & \cdots & c_K(0) & c_K(1) & \cdots & c_K(L) \end{bmatrix}^T. \tag{4.16}$$

With the representations prepared, as shown in (4.13) - (4.15), the detection schemes are now derived in Section 4.4.

4.4 Signal Detection

Due to the computation limits of nano-devices in DMC, it is impractical to implement the detection schemes with high-complexity non-linear computation. Hence, our study focuses on three linear detectors with low complexity that are applicable for operation with the terminals in DMC systems. Specifically, we consider the matched-filtering (MF) detection, also named correlation detection, zero-forcing (ZF) detection, and minimum mean-square error (MMSE) detection.

It is well known that for linear detectors, the decision variable for the uth bit of the kth NM can be general expressed as

$$\varepsilon_{k,u} = \boldsymbol{w}_{k,u}^T \boldsymbol{z}_u, \; u = 0, 1, \ldots; \; k = 1, 2, \ldots, K \tag{4.17}$$

where $\boldsymbol{w}_{k,u}$ is a weight vector, to be derived in the following subsections when different detection schemes are respectively considered.

Based on the decision variable $\varepsilon_{k,u}$, the decision for the uth bit of the kth NM is simply made

as

$$\hat{b}_{k,u} = \begin{cases} 1, & \text{if } \varepsilon_{k,u} > 0 \\ 0 \text{ (or } -1), & \text{else} \end{cases}, \ u = 0,1,\ldots; \ k = 1,2,\ldots,K. \tag{4.18}$$

In the following subsections, we detail the principles of different detection schemes and derive $\boldsymbol{w}_{k,u}$ of them, respectively.

4.4.1 Matched-Filtering Detection

The MF detection scheme is derived based on (4.14). When employing MF-detector, the AP is not aimed at mitigating any interference but attempts to maximize the received energy with the aid of the knowledge about CIR as well as spreading sequence. We assume that AP attempts to detect the uth bit $b_{k,u}$ transmitted by a reference NM k with the knowledge of corresponding spreading code $\boldsymbol{s}_k$ and the channel information $\boldsymbol{c}_k$, which consists of the expected concentration of a pulse at different sampling times within the ICI length. According to the principle of MF, the weight vector can be formed as

$$\boldsymbol{w}_{k,u} = \tilde{\boldsymbol{S}}_{k,0}\boldsymbol{c}_k \tag{4.19}$$

Upon substituting it into (4.17), the decision variable $\varepsilon_{k,u}$ can be expressed as

$$\begin{aligned} \varepsilon_{k,u} =& \boldsymbol{w}_{k,u}^T \boldsymbol{z}_u \\ =& \|\tilde{\boldsymbol{S}}_{k,0}\boldsymbol{c}_k\|^2 b_{k,u} + \sum_{l\neq k}^{K} \boldsymbol{c}_k^T \tilde{\boldsymbol{S}}_{k,0}^T \tilde{\boldsymbol{S}}_{l,0}\boldsymbol{c}_k b_{l,u} + \sum_{l=1}^{K} \boldsymbol{c}_k^T \tilde{\boldsymbol{S}}_{k,0}^T \tilde{\boldsymbol{S}}_{l,-1}\boldsymbol{c}_k b_{l,u-1} + \boldsymbol{c}_k^T \tilde{\boldsymbol{S}}_{k,0}^T \boldsymbol{n}_u \end{aligned} \tag{4.20}$$

On the right-hand side of (4.20), the first term is the desired signal part, the second term represents the MAI imposed by the other $(K-1)$ interfering NMs, the third term is the ISI of the previous $(u-1)$th bits transmitted by all the K NMs and the final term is noise.

In the case that the channel information $\boldsymbol{c}_k$ is not available to AP, $\boldsymbol{c}_k$ in (4.19) is replaced by a $(L+1)$-length all-one vector expressed as $\mathbf{1}$, yielding

$$\boldsymbol{w}_{k,u} = \tilde{\boldsymbol{S}}_{k,0}\mathbf{1} \tag{4.21}$$

Correspondingly, we have

$$\varepsilon_{k,u} = \mathbf{1}^T \tilde{\boldsymbol{S}}_{k,0}^T \tilde{\boldsymbol{S}}_{k,0}\boldsymbol{c}_k b_{k,u} + \sum_{l\neq k}^{K} \mathbf{1}^T \tilde{\boldsymbol{S}}_{k,0}^T \tilde{\boldsymbol{S}}_{l,0}\boldsymbol{c}_k b_{l,u} + \sum_{l=1}^{K} \mathbf{1}^T \tilde{\boldsymbol{S}}_{k,0}^T \tilde{\boldsymbol{S}}_{l,-1}\boldsymbol{c}_k b_{l,u-1} + \mathbf{1}^T \tilde{\boldsymbol{S}}_{k,0}^T \boldsymbol{n}_u \tag{4.22}$$

Referring to some concepts used in radio-based communications [86], the detector of (4.20) carries out the maximal ratio combining (MRC), which is referred to as the MRC-detector, while (4.22) executes the equal-gain combining (EGC), which is referred to as the EGC-detector for convenience.

The MRC-detector attempts to maximize the signal-to-noise ratio (SNR), while all the interference is treated as Gaussian noise, as shown below. Upon substituting $\boldsymbol{z}_u$ from (4.14) into (4.17), the decision variable can be formed as

$$\begin{aligned}\varepsilon_{k,u} =& \boldsymbol{w}_{k,u}^T \left(\sum_{k=1}^{K} \left(\tilde{\boldsymbol{S}}_{k,0} \boldsymbol{c}_k b_{k,u} + \tilde{\boldsymbol{S}}_{k,-1} \boldsymbol{c}_k b_{k,u-1} \right) + \boldsymbol{n}_u \right) \\ =& \boldsymbol{w}_{k,u}^T \tilde{\boldsymbol{S}}_{k,0} \boldsymbol{c}_k b_{k,u} + n_{k,u} \end{aligned} \tag{4.23}$$

where $n_{k,u} = \boldsymbol{w}_{k,u}^T \left(\sum_{l \neq k}^{K} \tilde{\boldsymbol{S}}_{l,0} \boldsymbol{c}_k b_{l,u} + \sum_{l=1}^{K} \tilde{\boldsymbol{S}}_{l,-1} \boldsymbol{c}_k b_{l,u-1} + \boldsymbol{n}_u \right)$ is the weighted sum of interference and noise. When we approximate this weighted sum as a random variable following Gaussian distribution of $\mathcal{N}(0, \boldsymbol{w}_{k,u}^T \boldsymbol{R}_I \boldsymbol{w}_{k,u})$, where $\boldsymbol{R}_I$ is the autocorrelation matrix of interference-plus-noise, i.e., of $\boldsymbol{I}_n = \sum_{l \neq k}^{K} \tilde{\boldsymbol{S}}_{l,0} \boldsymbol{c}_k b_{l,u} + \sum_{l=1}^{K} \tilde{\boldsymbol{S}}_{l,-1} \boldsymbol{c}_k b_{l,u-1} + \boldsymbol{n}_u$, the SNR for detection of $b_{k,u}$ can be expressed as

$$\begin{aligned}\gamma_{k,u} =& \frac{\| \boldsymbol{w}_{k,u}^T \tilde{\boldsymbol{S}}_{k,0} \boldsymbol{c}_k \|^2}{\boldsymbol{w}_{k,u}^T \boldsymbol{R}_I \boldsymbol{w}_{k,u}} \\ =& \frac{\| (\boldsymbol{R}_I^{1/2} \boldsymbol{w}_{k,u})^T (\boldsymbol{R}_I^{-1/2} \tilde{\boldsymbol{S}}_{k,0} \boldsymbol{c}_k) \|^2}{\boldsymbol{w}_{k,u}^T \boldsymbol{R}_I \boldsymbol{w}_{k,u}} \\ \leq& \frac{\| (\boldsymbol{R}_I^{1/2} \boldsymbol{w}_{k,u})^T \|^2 \| (\boldsymbol{R}_I^{-1/2} \tilde{\boldsymbol{S}}_{k,0} \boldsymbol{c}_k) \|^2}{\boldsymbol{w}_{k,u}^T \boldsymbol{R}_I \boldsymbol{w}_{k,u}} \end{aligned} \tag{4.24}$$

where '$\leq$' is satisfied due to the Cauchy-Schwarz inequality [116, 117]. It is well known that the equality in (4.24) is satisfied, if and only if

$$\boldsymbol{R}_I^{1/2} \boldsymbol{w}_{k,u} = \alpha \boldsymbol{R}_I^{-1/2} \tilde{\boldsymbol{S}}_{k,0} \boldsymbol{c}_k \tag{4.25}$$

where α is a constant. Hence,

$$\boldsymbol{w}_{k,u} = a \boldsymbol{R}_I^{-1} \tilde{\boldsymbol{S}}_{k,0} \boldsymbol{c}_k, \; u = 0, 1, \ldots, M-1; \; k = 1, 2, \ldots, K \tag{4.26}$$

The detector with the weight vector of (4.26) is capable of maximizing the signal to interference-plus-noise ratio (SINR), after mitigating the interference in $\boldsymbol{I}_n$ [42]. However, computing (4.26) requires knowledge about the spreading sequences employed by all NMs, as well as the CIR $\boldsymbol{c}$ of all NMs. If the receiver only has the knowledge about the reference NM to be detected, i.e., only knows $\boldsymbol{s}_k$ (or $\tilde{\boldsymbol{S}}_{k,0}$) and $\boldsymbol{c}_k$, the detector is reduced to a MRC-detector. In this case, the detector has to approximate $\boldsymbol{I}_n$ as a Gaussian noise vector, which has a covariance matrix of $\sigma_I^2 \boldsymbol{I}_N$. Consequently, the weight vector of (4.26) is reduced to

$$\boldsymbol{w}_{k,u} = \frac{a}{\sigma_I^2} \tilde{\boldsymbol{S}}_{k,0} \boldsymbol{c}_k \equiv \tilde{\boldsymbol{S}}_{k,0} \boldsymbol{c}_k \tag{4.27}$$

which is (4.19). Therefore, the MRC-detector maximizes SNR, after approximating the interference as Gaussian noise.

4.4.2 Zero-Forcing Detection

Based on equation (4.15), the ZF-detector can be derived. The conditions for implementation of the ZF detection include that the AP employs the knowledge of the spreading sequences employed by the K NMs, and their CIRs to AP, so that the detector can construct $\tilde{\boldsymbol{C}}$ and $\tilde{\boldsymbol{S}}_0$ seen in (4.15). If these requirements are satisfied, according to (4.15), the decision variables of ZF-detector for the K NMs can be obtained as

$$\begin{aligned}\boldsymbol{\varepsilon}_u &= \left(\tilde{\boldsymbol{S}}_0\tilde{\boldsymbol{C}}\right)^{\dagger}\boldsymbol{z}_u \\ &= \left(\tilde{\boldsymbol{C}}^T\tilde{\boldsymbol{S}}_0^T\tilde{\boldsymbol{S}}_0\tilde{\boldsymbol{C}}\right)^{-1}\tilde{\boldsymbol{C}}^T\tilde{\boldsymbol{S}}_0^T\boldsymbol{z}_u,\ u=0,1,\ldots,M-1\end{aligned} \tag{4.28}$$

where $\boldsymbol{A}^{\dagger}$ denotes the pseudo-inverse of $\boldsymbol{A}$ [117]. Upon substituting $\boldsymbol{z}_u$ from (4.15) into (4.28), we have

$$\boldsymbol{\varepsilon}_u = \boldsymbol{b}_u + \underbrace{\left(\tilde{\boldsymbol{C}}^T\tilde{\boldsymbol{S}}_0^T\tilde{\boldsymbol{S}}_0\tilde{\boldsymbol{C}}\right)^{-1}\tilde{\boldsymbol{C}}^T\tilde{\boldsymbol{S}}_0^T\left(\tilde{\boldsymbol{S}}_{-1}\tilde{\boldsymbol{C}}\boldsymbol{b}_{u-1}+\boldsymbol{n}_u\right)}_{\text{ISI and noise}} \tag{4.29}$$

From (4.29) we can see that the MAI is fully removed. However, there is still ISI.

Specifically, the weight vector for detecting the uth bit of the k NM is given by the kth column of $\left(\tilde{\boldsymbol{S}}_0\tilde{\boldsymbol{C}}\right)^{\dagger}$ in (4.28), which can be expressed in detail as

$$\boldsymbol{w}_{k,u} = \left(\tilde{\boldsymbol{S}}_0\tilde{\boldsymbol{C}}\left(\tilde{\boldsymbol{C}}^T\tilde{\boldsymbol{S}}_0^T\tilde{\boldsymbol{S}}_0\tilde{\boldsymbol{C}}\right)^{-1}\right)(:,k),\ k=1,2,\ldots,K \tag{4.30}$$

where $\boldsymbol{A}(:,k)$ represents the kth column of $\boldsymbol{A}$.

4.4.3 Minimum Mean-Square Error Detection

We first derive the MMSE-detector based on (4.14) to detect the information transmitted by a NM.

The MMSE-detector is derived by attempting to minimize the mean-square error (MSE) between the estimated data and the actual data, which can be obtained from the optimization problem of

$$\begin{aligned}\boldsymbol{w}_{k,u} &= \arg\min_{\boldsymbol{w}}\left\{E\left[\|b_{k,u}-\varepsilon_{k,u}\|^2\right]\right\} \\ &= \arg\min_{\boldsymbol{w}}\left\{E\left[\|b_{k,u}-\boldsymbol{w}^T\boldsymbol{z}_u\|^2\right]\right\}\end{aligned} \tag{4.31}$$

Let us define the cost function as

$$\begin{aligned}J_{k,u}(\boldsymbol{w}) &= E\left[\|b_{k,u}-\boldsymbol{w}^T\boldsymbol{z}_u\|^2\right] \\ &= 1-2\boldsymbol{r}_{ku}^T\boldsymbol{w}+\boldsymbol{w}^T\boldsymbol{R}_{\boldsymbol{z}_u}\boldsymbol{w}\end{aligned} \tag{4.32}$$

where $\boldsymbol{R}_{\boldsymbol{z}_u}$ is the auto-correlation matrix of $\boldsymbol{z}_u$, which can be derived from (4.14) and expressed as

$$\boldsymbol{R}_{\boldsymbol{z}_u} = \sum_{k=1}^{K}\left(\tilde{\boldsymbol{S}}_{k,0}+\tilde{\boldsymbol{S}}_{k,-1}\right)\boldsymbol{c}_k\boldsymbol{c}_k^T\left(\tilde{\boldsymbol{S}}_{k,0}+\tilde{\boldsymbol{S}}_{k,-1}\right)^T+\sigma^2\boldsymbol{I}_N \tag{4.33}$$

In (4.32), $\boldsymbol{r}_{ku}$ is the cross-correlation between $\boldsymbol{z}_u$ and $b_{k,u}$, which is

$$\boldsymbol{r}_{k,u} = \tilde{\boldsymbol{S}}_{k,0}\boldsymbol{c}_k \tag{4.34}$$

Upon taking the derivatives of $J_{k,u}(\boldsymbol{w})$ with respect to $\boldsymbol{w}$ and equating the result to zero, we obtain

$$\frac{\partial J_{k,u}(\boldsymbol{w})}{\partial(\boldsymbol{w})} = -2\boldsymbol{r}_{k,u} + 2\boldsymbol{R}_{\boldsymbol{z}_u}\boldsymbol{w} = 0 \tag{4.35}$$

from which we obtain the optimum weight vector implementing MMSE detection as

$$\begin{aligned}\boldsymbol{w}_{k,u} =& \boldsymbol{R}_{\boldsymbol{z}_u}\boldsymbol{r}_{k,u} \\ =& \left(\sum_{k=1}^{K}\left(\tilde{\boldsymbol{S}}_{k,0} + \tilde{\boldsymbol{S}}_{k,-1}\right)\boldsymbol{c}_k\boldsymbol{c}_k^T\left(\tilde{\boldsymbol{S}}_{k,0} + \tilde{\boldsymbol{S}}_{k,-1}\right)^T + \sigma^2\boldsymbol{I}_N\right)^{-1}\tilde{\boldsymbol{S}}_{k,0}\boldsymbol{c}_k, \\ & u = 0,1,\ldots,M-1;\ k = 1,2,\ldots,K\end{aligned} \tag{4.36}$$

From (4.36), it can be inferred that for implementing the MMSE-detector, AP requires the knowledge about the spreading sequences employed by all NMs and their CIRs to the AP, so that AP can construct the matrices/vectors as shown in the formula. Furthermore, AP requires to know the noise power denoted by σ^2. In this case, the MMSE-detector is capable of achieving the best trade-off between interference (including both MAI and ISI) suppression and noise suppression. Note that due to the BMoSK modulation employed, the noise power can be calculated, as shown in (4.12).

Additionally, when AP does not have the knowledge of all the spreading sequences of the K NMs, but only that of the desired NM, AP has to approximate $\boldsymbol{R}_u$ as a constant diagonal matrix, making (4.36) be reduced to the weight vector of the MRC-detector. On the other side, AP can estimate $\boldsymbol{R}_{\boldsymbol{z}_u}$ using received observations as $\bar{\boldsymbol{R}}_{\boldsymbol{z}_u} = \frac{1}{M}\sum_{u=1}^{M}\boldsymbol{z}_u\boldsymbol{z}_u^T$ provided that M is sufficiently large, we can have $\bar{\boldsymbol{R}}_{\boldsymbol{z}_u} \approx \boldsymbol{R}_{\boldsymbol{z}_u}$.

The above MMSE detector detects one NM after another. We can also derive an MMSE detector based on (4.15) to detect all NMs simultaneously. In this case, let $\boldsymbol{W}_u$ be the $(N \times K)$ weight matrix. Then, the decision variable vector is given by

$$\boldsymbol{\varepsilon}_u = \boldsymbol{W}^T\boldsymbol{z}_u \tag{4.37}$$

where the weight matrix in the MMSE principle is obtained from solving the optimization problem:

$$\begin{aligned}\boldsymbol{W}_u &= \arg\min_{\boldsymbol{W}}\left\{E\left[\|\boldsymbol{b}_u - \boldsymbol{\varepsilon}_u\|^2\right]\right\} \\ &= \arg\min_{\boldsymbol{W}}\left\{E\left[\|\boldsymbol{b}_u - \boldsymbol{W}^T\boldsymbol{z}_u\|^2\right]\right\}\end{aligned} \tag{4.38}$$

where $\boldsymbol{z}_u$ is given by (4.15).

Let us define the cost function as

$$J_u(\boldsymbol{W}) = E\left[\|\boldsymbol{b}_u - \boldsymbol{W}^T\boldsymbol{z}_u\|^2\right] \tag{4.39}$$

Then, when assuming that data bits are uniform random variables, we can obtain the covariance matrix of $\boldsymbol{b}_u - \boldsymbol{W}^T\boldsymbol{z}_u$ as

$$\boldsymbol{J}_u(\boldsymbol{W}) = \boldsymbol{I}_K - \boldsymbol{R}^T_{\boldsymbol{z}_u\boldsymbol{b}_u}\boldsymbol{W} - \boldsymbol{W}^T\boldsymbol{R}_{\boldsymbol{z}_u\boldsymbol{b}_u} + \boldsymbol{W}^T\boldsymbol{R}_{\boldsymbol{z}_u}\boldsymbol{W} \tag{4.40}$$

where $\boldsymbol{R}_{\boldsymbol{z}_u} = E\left[\boldsymbol{z}_u\boldsymbol{z}_u^T\right]$ and $\boldsymbol{R}_{\boldsymbol{z}_u\boldsymbol{b}_u} = E\left[\boldsymbol{z}_u\boldsymbol{b}_u^T\right]$, which are given by

$$\begin{aligned}\boldsymbol{R}_{\boldsymbol{z}_u} =& \tilde{\boldsymbol{S}}_0\tilde{\boldsymbol{C}}\tilde{\boldsymbol{C}}^T\tilde{\boldsymbol{S}}_0^T + \tilde{\boldsymbol{S}}_{-1}\tilde{\boldsymbol{C}}\tilde{\boldsymbol{C}}^T\tilde{\boldsymbol{S}}_{-1}^T + \sigma_n^2\boldsymbol{I}_N,\\ \boldsymbol{R}_{\boldsymbol{z}_u\boldsymbol{b}_u^T} =& \tilde{\boldsymbol{S}}_0\tilde{\boldsymbol{C}}\end{aligned} \tag{4.41}$$

Note that, it can be shown that $\boldsymbol{R}_{\boldsymbol{z}_u}$ in (4.41) is the same as the $\boldsymbol{R}_{\boldsymbol{z}_u}$ in (4.33).

The optimum weight matrix $\boldsymbol{W}_u$ can be obtained by differentiating the trace of $\boldsymbol{J}_u(\boldsymbol{W})$ with respect to $\boldsymbol{W}$ and equating the result to zero, i.e.,

$$\frac{\partial \mathrm{Tr}(\boldsymbol{J}_u(\boldsymbol{W}))}{\partial(\boldsymbol{W})} = -2\boldsymbol{R}_{\boldsymbol{z}_u\boldsymbol{b}_u^T} + 2\boldsymbol{R}_{\boldsymbol{z}_u}\boldsymbol{W} = 0 \tag{4.42}$$

the solution of which is the optimal solution, given as

$$\boldsymbol{W}_u = \boldsymbol{R}^{-1}_{\boldsymbol{z}_u}\boldsymbol{R}_{\boldsymbol{z}_u\boldsymbol{b}_u^T} \tag{4.43}$$

Upon substituting the results in (4.41) into (4.43), we obtain

$$\boldsymbol{W}_u = \left(\tilde{\boldsymbol{S}}_0\tilde{\boldsymbol{C}}\tilde{\boldsymbol{C}}^T\tilde{\boldsymbol{S}}_0^T + \boldsymbol{R}_I\right)^{-1}\tilde{\boldsymbol{S}}_0\tilde{\boldsymbol{C}} \tag{4.44}$$

where by definition, $\boldsymbol{R}_I = \tilde{\boldsymbol{S}}_{-1}\tilde{\boldsymbol{C}}\tilde{\boldsymbol{C}}^T\tilde{\boldsymbol{S}}_{-1}^T + \sigma_n^2\boldsymbol{I}_N$.

Furthermore, after applying the matrix inverse lemma, we can obtain another representation for $\boldsymbol{W}_u$, which is

$$\boldsymbol{W}_u = \boldsymbol{R}_I^{-1}\tilde{\boldsymbol{S}}_0\tilde{\boldsymbol{C}}\left(\tilde{\boldsymbol{C}}^T\tilde{\boldsymbol{S}}_0^T\boldsymbol{R}_I^{-1}\tilde{\boldsymbol{S}}_0\tilde{\boldsymbol{C}} + \boldsymbol{I}_K\right)^{-1}, u = 1, 2, \ldots, M \tag{4.45}$$

Additionally, when there is no ISI, making $\boldsymbol{R}_I = \sigma_n^2\boldsymbol{I}_N$, we can easily show that (4.45) is reduced to the formula

$$\boldsymbol{W}_u = \tilde{\boldsymbol{S}}_0\tilde{\boldsymbol{C}}\left(\tilde{\boldsymbol{C}}^T\tilde{\boldsymbol{S}}_0^T\tilde{\boldsymbol{S}}_0\tilde{\boldsymbol{C}} + \sigma_n^2\boldsymbol{I}_K\right)^{-1}, u = 1, 2, \ldots, M \tag{4.46}$$

4.4.4 Complexity of Detection Schemes

In this section, we analyze the complexity of the detection schemes described above. Considering that the weight vector $\boldsymbol{w}_{k,u}$ in symbol-by-symbol detection is fixed in one session of detection, we separate the computation at the AP into the preparation of $\boldsymbol{w}_{k,u}$ and the process of detection. The complexities of these two procedures are investigated respectively. Furthermore, in order to describe the complexity of the different cases, we assume that the arithmetic operation of individual elements in a vector or matrix has the complexity of $\mathcal{O}(1)$. Additionally, the complexity is analyzed in terms of one bit and one NM.

Table 4.1: Complexity of Computing Weight Vectors and that of Detection for various Detection Schemes.

Detector	Computing weight vector	Detection
MF	$\mathcal{O}(N(L+1))$	$\mathcal{O}(N)$
ZF	$\mathcal{O}(N(L+1)+2NK+K^2)$	$\mathcal{O}(N)$
MMSE	$\mathcal{O}(N^3/K+2N^2+3N(L+1)+N/K)$	$\mathcal{O}(N)$

As shown in Section 4.4.1, 4.4.2 and 4.4.3, all the detection schemes proposed have their corresponding decision variables respectively for detecting one bit in the form of (4.17). Thus, once the N-length weight vector is constructed, the detection complexity of all the detectors, i.e., the MF-(MRC,EGC), ZF- and MMSE-detectors, is the same and is $\mathcal{O}(N)$ per bit of one NM. By contrast, the complexity of computing the weight vectors of different detectors is probably different. First, for the MF-detector, $\boldsymbol{w}_{k,u}$ is given by (4.19) for the MRC-detector, and by (4.21) for the EGC-detector, both of which have the complexity of $\mathcal{O}(N(L+1))$. For the ZF-detector, corresponding to (4.15), the weight vectors are given by (4.30). It is known that the complexity for obtaining the inverse of a $(K \times K)$ dimensional matrix is $\mathcal{O}(K^3)$ [118]. Hence, we can readily derive that the complexity for computing the weight vector for the ZF-detector based on (4.30) is $\mathcal{O}(N(L+1)+2NK+K^2)$. Finally, the complexity for preparing the weight vector based on (4.36) for the MMSE-detector can be similarly analyzed, which is $\mathcal{O}(N^3/K+2N^2+3N(L+1)+N/K)$.

The complexity of the different detection schemes is summarized in Table 4.1. Given $K \leq N$, it is shown that computing the weight vector for MMSE-detector demands the highest complexity, followed by the ZF-detector. MF-detector has the lowest complexity. However, we should note that provided that the positions of nano-machines do not change, the weight vectors also keep unchanged, and are not required to be updated.

4.5 Performance Results and Discussion

In this section, we demonstrate the performance of the MoCDMA systems with different settings. In our simulations, when there is no specific notification, the default assumptions and parameters are shown as Table 4.2. Note that in our study, spreading sequences are generated from the maximum length sequences (MLS). However, they are periodic sequences, one of them can be obtained from another one with a certain number of shifts [110]. Hence, they cannot be directly applied to the MoCDMA experiencing severe ISI and ICI. This is because, if the number of NMs supported exceeds some upper limit, the ICI in the current symbol duration and the ISI in the following durations may be fully despread by another sequence assigned to another NM, generating high MAI. Based on the above observation and in order to prevent interference, we set the length of spreading sequence as $N = 31$ to support maximum $K = 6$ NMs, when employing MLS in our MoCDMA

Table 4.2: Parameters for performance study

Parameter	Value
Bit duration T_b	$0.06s$ or $0.03s$
ISI length L	10
Length of (MLS) spreading sequence N	31
Radius of AP sensing space ρ	$0.4\ \mu m$
Diffusion coefficient D	$4.5 \times 10^{-9}\ m^2/s$
Distance between AP and NM 1 d_1	$2.2\ \mu m$
Distance between AP and NM 2 d_2	$2.4\ \mu m$
Distance between AP and NM 3 d_3	$2.6\ \mu m$
Distance between AP and NM 4 d_4	$2.8\ \mu m$
Distance between AP and NM 5 d_5	$3.3\ \mu m$
Distance between AP and NM 6 d_6	$3.5\ \mu m$

systems. We use this setting because for the MLSs with $N = 31$ chips, there are only a maximum of 6 sequences that cannot be overlapped by up to 9 shifts, as the result of $L = 10$. Besides MLS, we also investigate the performance of the MoCDMA systems with gold sequence or Walsh code as the spreading sequences [110] in order to support more NMs.

Let us first compare the two emission control ways addressed in this chapter in Fig. 4.2, where all the detection schemes described in Section 4.4 are respectively considered. The MoCDMA system in Fig. 4.2 supports 6 NMs with the details listed in Table 4.2. It is worth noting that specifically in Fig. 4.2, $\mathcal{Q}$ represents the maximum number of molecules available to transmit for one bit. As Section 4.2.3 describes, in the uniform emission case, all NMs emit the maximum number of molecules for one bit, while NM k in the channel-inverse emission case emits the number of molecules according to $Q_b^{(k)} \propto d_k^3$ for one-bit transmission. Hence, in the channel-inverse emission case, for the NMs relatively close to AP, their actually emitted molecule numbers are lower than $\mathcal{Q}$ as shown in Fig. 4.2(d). Explicitly, when a NM is closer to AP, it can save more molecules, where the channel-inverse based emission is employed. In addition to this, another advantage of the channel-inverse emission is that by reducing the number of molecules, a NM closer to AP also reduces the interference on the NMs further away from AP.

As shown in Fig. 4.2(a), when the NMs adopt the uniform molecule emission and AP employs MRC-detector, the distance between an NM and AP has a significant influence on the BER performance of MoCDMA systems. The communication reliabilities of the NMs with different distances from AP are in great differences. Specifically, for the NMs 5 and 6, furthest away from AP, their information is completely undetectable in both uniform form and channel-inverse case. By contrast, NM 1, which is the one closest to AP, achieves a promising error performance that is only slightly lagging behind the corresponding one in Fig. 4.2(c) with MMSE-detector. This is

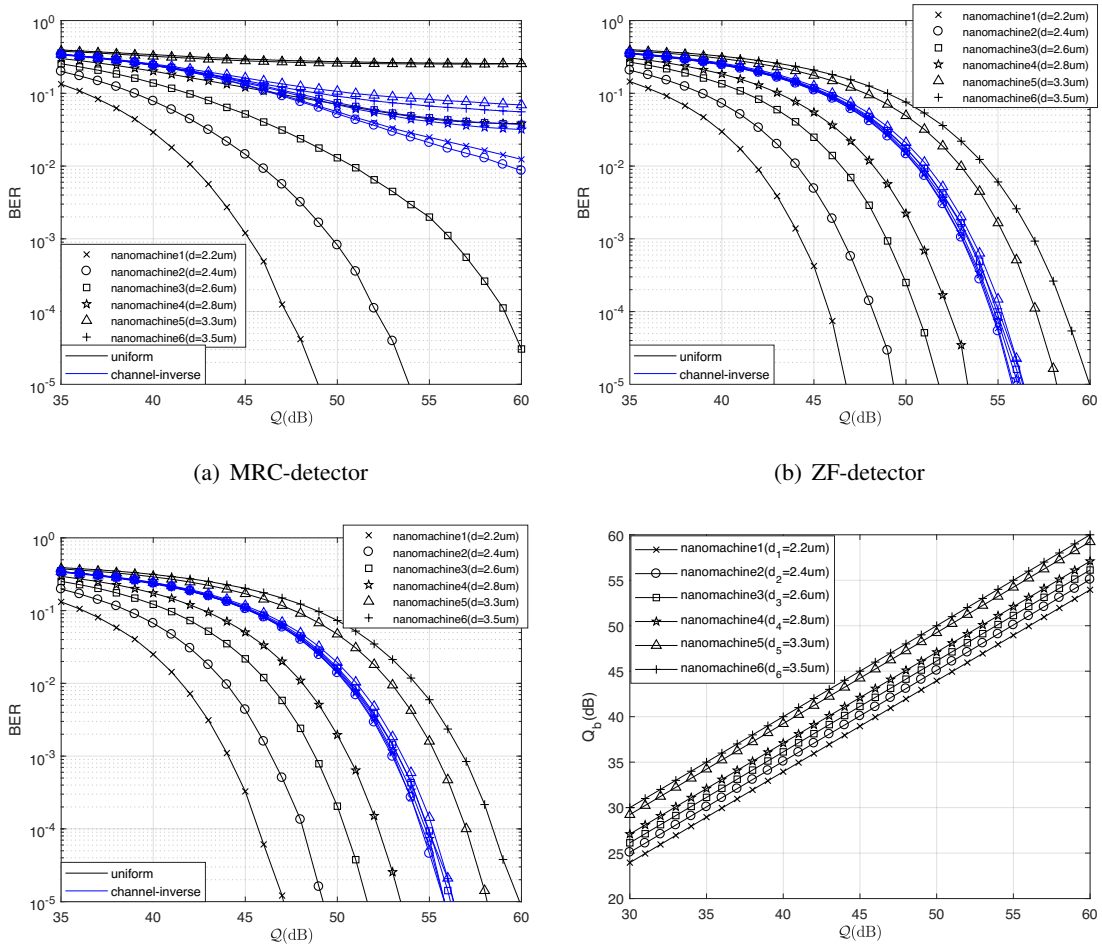

(a) MRC-detector

(b) ZF-detector

(c) MMSE-detector

(d) Real number of molecules emitted for one bit

Figure 4.2: Comparison of BER performance of the MoCDMA systems with various detection schemes, when $T = 6 \times 10^{-2}s$, $L = 10$, $N = 31$ and where two emission ways are considered.

because the MRC-detector amplifies the impact of CIR, which causes a polarization among NMs. When the channel-inverse emission is employed as shown in Fig. 4.2(a), the BER performance of the far away NMs like No.5 and 6 is improved, while that of the NMs close AP like No.1 and 2 is degraded. The reason behind this is that the decrease in the number of molecules emitted by the close AP NMs can reduce the severe MAI on the far away NMs, which hence benefits the detection of the far away NM. However, as the results in Fig. 4.2(a) illustrate, the channel-inverse emission cooperating with MRC-detection can hardly provide a reasonable BER performance, as the result of the severe interference, incluing ISI/ICI and MAI.

Compared to the MRC-detector, both the ZF-detector and MMSE-detector are highly efficient, when they are operated with either the uniform or channel-inverse emission. As shown in Fig. 4.2(b) and Fig. 4.2(c), even when NMs emit molecules in the uniform way, the BER curves emerge in the water-falling form, inferring that a low BER can be attainable, provided that SNR is sufficiently high. If the channel-inverse emission is adopted by NMs, the BER performance of

all NMs with different transmission distances is reasonably similar, guaranteeing the FoCQ among NMs. This phenomenon can be explained as follows. First, the quality of MLS assigned to different NMs is quite similar. Second, according to the principle of ZF-detector, it is capable of cancelling MAI while the channel-inverse emission provides the same received signal power for all NMs. Consequently, the post-processed SINR of all NMs can be nearly the same. Third, because the MMSE-detector can suppress interference and noise in the best trade-off, the most unfavorable factor can be mitigated. Therefore, AP can also make the detections of all NMs at similar SINRs. In addition, a similar observation as that in Fig. 4.2(a) can also be obtained, i.e., though the channel-inverse emission results in some reliability loss of the close AP NMs, it can improve the BER performance of the far away NMs. Finally, when comparing the ZF-detector with the MMSE-detector, we can see that the MMSE-detector slightly outperforms the ZF-detector.

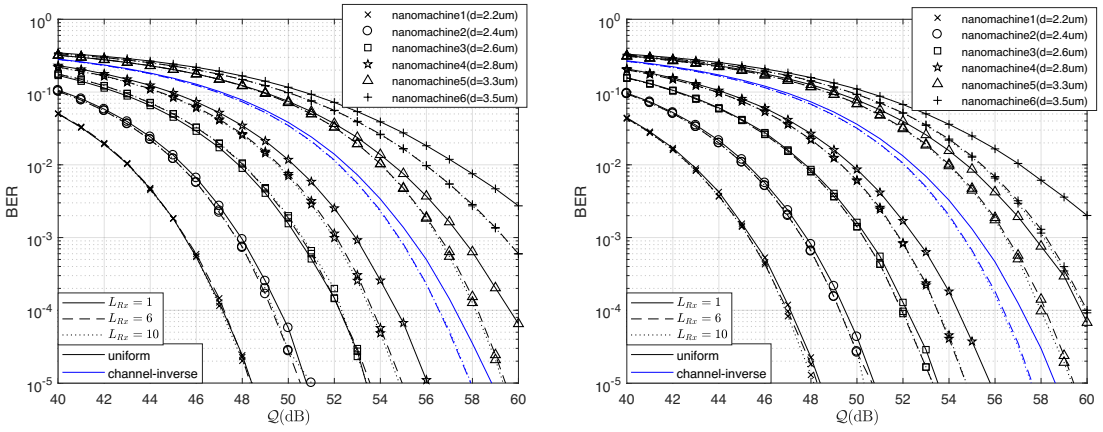

(a) ZF-detector

(b) MMSE-detector

Figure 4.3: Impact of the ISI-length exploited by AP on the BER performance of MoCDMA systems with ZF- and MMSE-detectors, when $T_b = 0.03s$, $L = 10$, $N = 31$ and where two emission ways are considered.

In the second set of figures shown in Fig. 4.3, we demonstrate the impact of the ISI length exploited by AP on the BER performance of the MoCDMA systems with respectively ZF- and MMSE-detectors, when $T_b = 0.03s$ and the other parameters are shown in Table. 4.2. In our investigation, we assume that the ISI length is $L = 10$, and the ISI length exploited by AP is $L_{Rx} = 1, 6$ or 10. When the channel-inverses emission cooperates with ZF- or MMSE-detector, due to the proximity of the BER performance of different NMs, the average BER of an individual NM is demonstrated as the blue-colored curves in Fig. 4.3, instead of the BER curves of all the 6 NMs. As the results in Fig. 4.3 show, for both the emission methods and both detectors considered, a better BER performance is generally achieved, as longer ISI is exploited by AP for carrying out detection. Specifically, when the uniform emission is employed, the NMs located further away from AP achieve more explicit improvement in the BER performance, as the ISI length exploited increases. This is because as the distance increases, the pulse of the received molecular concentration becomes wider, resulting in that the peak value of the pulse becomes similar to that of the residual

concentration from previous transmissions, and hence, yielding severer interference and counting noise. In this case, exploiting more ISI by AP is helpful for the ZF- or MMSE-detector to mitigate interference and background noise. However, as shown in Fig. 4.3, provided that $L_{Rx} \geq 6$, the BER performance achieved by both the ZF- and MMSE-detectors aided by the uniform or channel-inverse emission is nearly the same. This observation infers that although there is still ISI beyond $L_{Rx} = 6$, the ISI is generally ignorable, as the result that the number of residual molecular is reduced to a very low level after about 6 chip durations.

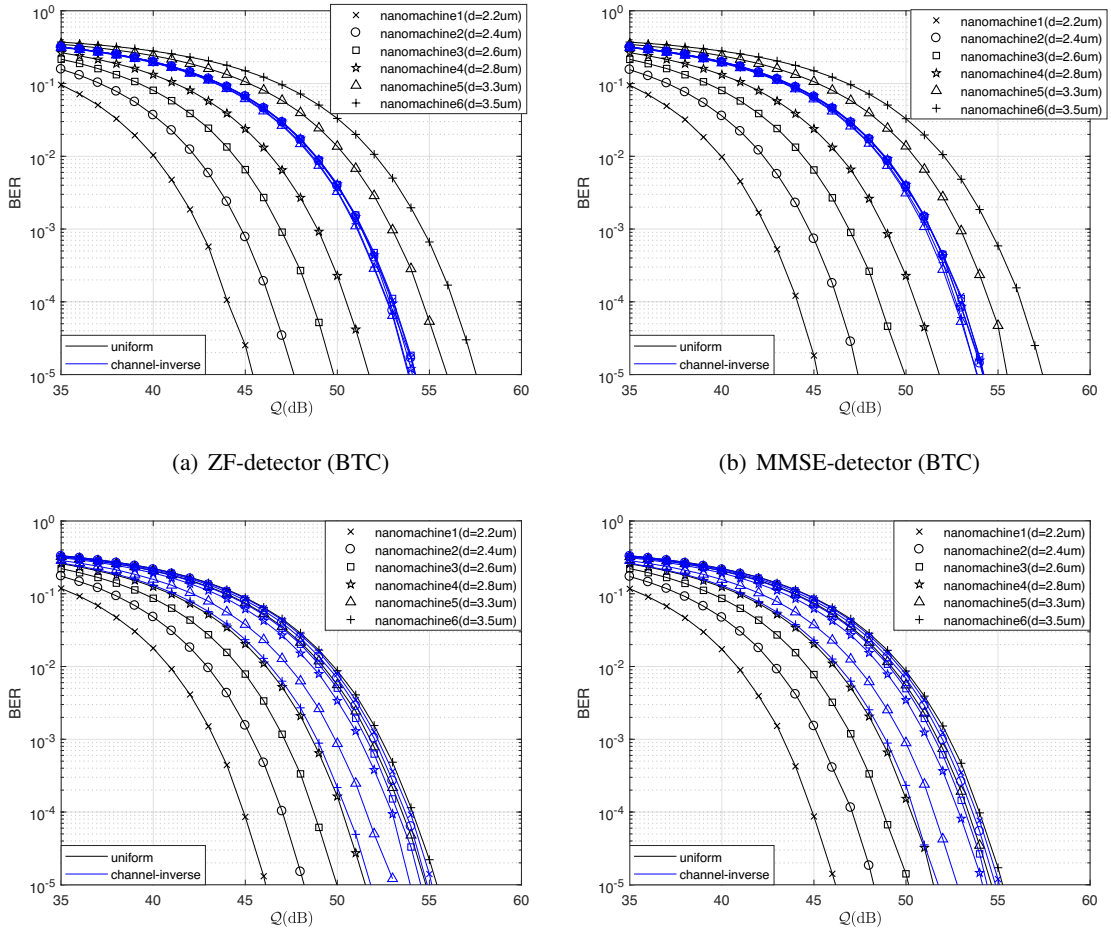

(a) ZF-detector (BTC)

(b) MMSE-detector (BTC)

(c) ZF-detector (BTF)

(d) MMSE-detector (BTF)

Figure 4.4: Comparison of BER performance of the MoCDMA systems with the parameters of $T = 6 \times 10^{-2}s$, $L = 10$, Walsh codes of $N = 32$, supporting 6 NMs as specified in Table. 4.2, when different emission methods and detection schemes are considered.

In the context of Fig. 4.4, the settings are the same as that for Fig. 4.2, expect that in Fig. 4.4 the $N = 32$ Walsh codes are employed. Compared to the results in Fig. 4.2 utilizing MLS, employing Walsh codes can improve the BER performance of MoCDMA systems for both the emission methods and also the ZF- and MMSE-detectors, thanks to the orthogonality of Walsh codes. However, it is worth noting that the assignment of Walsh codes to nano-machines has a considerable impact on the BER performance of MoCDMA systems. This is because the locations of '-1's and '1's in the

assigned Walsh codes result in different ICI, which hence affect the BER performance. Specifically, the Walsh code with '1's occupying the first half and '-1's occupying the other half of the sequence is in favour of boosting the received signal power. By contrast, the Walsh code having '-1' and '1' evenly distributed results in larger ICI. Thus, two Walsh code assignment methods are implemented in Fig. 4.4, namely the best-to-closest (BTC) and best-to-furthest (BTF). Specifically, according to the locations of '-1's and '1's in a sequence, BTC assigns the best sequence to the NMs closest to AP, the second best to the second closest, and so on; while BTF carries out the assignment in the way opposite to BTC, i.e., the best sequence to the NM furthest away from AP, and so on. By comparing Fig. 4.4(a)(b) with (c)(d), it can be shown that the BTF scheme enhances the reliability of the NMs further away from AP at the cost of slightly degraded performance of the NMs closer to AP, when the uniform emission is employed. When the channel-inverse emission is employed, the BTF scheme makes the error performance of different NMs be distributed not as dense as that of the cases considered before in Fig. 4.4(a)(b). Furthermore, the NM furthest away from AP achieves the best BER performance, while the one closest to AP obtains the worst BER performance. The reason for the above observation is that the best Walsh code not only boosts the signal power of the desired NM, but also generates severe interference on the other NMs, especially when the kind of Walsh codes are assigned to the furthest NMs, whose concentration tails can keep relatively large values for long time. On the other hand, the worst Walsh code with evenly distributed '-1's and '1's results in severe ICI to the desired NM, if it is assigned to the NM closest to AP, whose concentration decreases quickly. In the case of channel-inverses emission, the above influences of BTF on the BER performance can also be visualized.

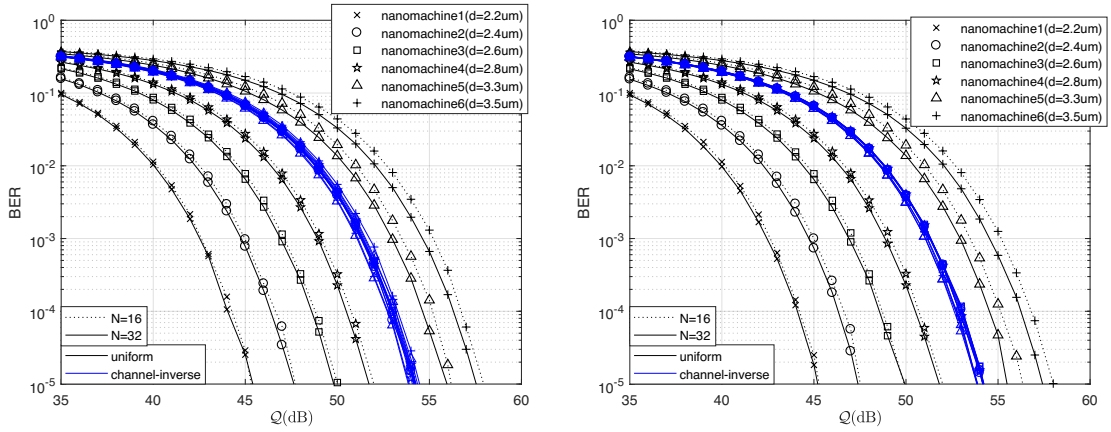

(a) ZF-detector (BTC)

(b) MMSE-detector (BTC)

Figure 4.5: Impact of different spreading factors on the BER performance of the MoCDMA systems employing the Walsh codes assigned by following the BTC schemes, when the parameters are $T = 6 \times 10^{-2}s$, $L = 10$, and supporting 6 NMs specified in Table. 4.2.

As the $N = 31$ length MLSs only have six preferred pairs which can support only $K = 6$ NMs in a MoCDMA DMC system. By contrast, $N = 32$ length Walsh codes can support many more

NMs. Therefore, in Fig. 4.5, we investigate the impact of the spreading factor N of the Walsh codes assigned based on the BTC scheme on the BER performance of the MoCDMA systems employing respectively the ZF- and MMSE-detectors cooperating, when both the uniform and channel-inverse emission schemes are implemented. Compared to the results shown in Fig. 4.4(a) and (b), Fig. 4.5 demonstrates that the decrease of spreading factor from $N = 32$ to 16 does not yield explicit degradation on the BER performance of the MoCDMA systems. It is well known that in the conventional radio-based CDMA (RdCDMA) systems, the BER performance is usually explicitly dependent on the value of K/N. However, as shown in Fig. 4.5, for both the detectors and also both the emission ways, the BER performance is only slightly dependent on the spreading factor N. The reason behind is that in MoCDMA, the noise power is coupled with the number of NMs simultaneously supported and the interference generated by all NMs, regardless of what spreading factor is used. The noise power increases with the increase of the number of NMs, and furthermore, the noise power is unable to be reduced solely by the spreading and de-spreading operations. Therefore, we can be inferred that in MoCDMA systems, the BER performance is more dependent on the number of NMs, instead of the spreading factor.

4.6 Conclusion

A MoCDMA system relying on two types of molecules for supporting multiple NMs to transmit binary information to one FC (or AP) was designed and studied. Our MoCDMA scheme can be seen as an analogy to the conventional RdCDMA with BPSK modulation. Therefore, the well developed signal processing algorithms for the signal detection in the conventional RdCDMA systems can be adopted/extended to the MoCDMA systems after addressing the unique characteristics of DMC. Specifically, it was found that in the MoCDMA systems employing BMoSK, although the background noise is still signal-dependent, it is stationary and its statistics is not related to the specific information transmitted. Owing to this property, it was shown that the low-complexity MF, ZF and MMSE detection schemes are similarly effective as in the conventional RdCDMA systems. The DMC scenario where NMs have different transmission distances to FC was also considered and, correspondingly, the uniform and channel-inverse based molecule-emission schemes were introduced and compared. The performance results illustrated that the channel-inverse emission is capable of improving the reliability of the NMs relatively 'far away' from FC. This allows the detection of differently located NMs to achieve a similar BER performance and, hence, mitigate the near-far effect. Furthermore, our complexity analysis and performance comparison revealed that the MF-, ZF-, and MMSE detectors are all low-complexity detection schemes, although the ZF- and MMSE-detectors require slightly higher computations than the MF-detector. Furthermore, these detectors provide the promising options for MoCDMA systems to attain a good trade-off between computational complexity of computation and information transmission reliability.

Chapter 5

Frequency-Domain Detection and Interference Cancellation for Molecular Code-Division Multiple-Access

In the last chapter, we proposed and studied a MoCDMA scheme, which is designed based on BMoSK modulation assisted by pseudo-sequence spreading, for supporting the uplink information transmission from multiple NMs to a FC via DMC channels. Considering the computational complexity constraint of nano-devices, a range of low-complexity detection schemes were introduced and compared. In this chapter, we extend the research in Chapter 4 by introducing a range of frequency-domain equalizers (FDEs) so as to more efficiently mitigate ICI, while still achieving low-complexity signal detection. Furthermore, a decision-feedback successive interference cancellation (DF-SIC) scheme is proposed to mitigate multiple-access interference (MAI) and, hence, improve the detection reliability.

5.1 Introduction

Recently, the Nobel prize in Chemistry 2022 has drawn significant attention from numerous fields including molecular communication (MC), which exploits chemical signals as information carrier to conduct intra-body communication. Because human body or organism is a complex biological environment, the chemical reactions occurring in the MC environment are likely to affect the propagation of information molecules [28]. Bertozzi et al. [1] have developed the bioorthogonal chemistry, which can bring the current MC channel model further to practice. Meldal and Barry Sharpless et al. [1] have provided catalytic click reactions, which are able to facilitate the synthesis of various information molecules that can be used by MC transmitter without byproducts. Owing

[1] The news is available at https://www.nobelprize.org/frequently-asked-questions.

to the above processes, MC has become more feasible and has research the value as a promising alternative communication paradigm for ultra-short distance and a candidate for constructing the Internet of Bio-Nano Things (IoBNT).

Compared to conventional communication based on electromagnetic waves, MC has a range of advantages for information exchange between biological nano-sensors and a fusion centre (FC): 1) small size [15] 2) low energy consumption [18] 3) biocompatibility [17]. Thanks to these advantages, MC is suitable for nano-devices to exchange information within biological organisms for, such as, medical applications.

Nowadays, nano-devices like nano-machines and nano-sensors have been widely used in the healthcare applications, such as, diagnosing and treating diseases [11, 101]. However, the tiny nano-devices usually have only limited storage space, power supplementation, and computational capability. As a result, individual nano-device is incompetent for accomplishing complicated tasks [96, 102]. However, MC, as a promising bio-inspired communication method, is able to be envisioned to implement the IoBNT for the coordination of multiple nano-devices, in order to accomplish the advanced work, such as, monitoring health [12, 13], drug delivery [8, 9], etc. Therefore, multiple-access techniques in MC play an important role in the implementation of IoBNT. In literature, there are various multiple access techniques having been proposed based on different criteria [44–52]. To be more specific, inspired by neural network, the authors of [53–55] proposed to use the mechanism of neurons to implement multiple access. On the other hand, most research has considered multiple access schemes based on diffusive MC (DMC), owing to the fact that free diffusion is the most common propagation way in biological environments. In DMC, the molecular division multiple-access (MDMA) [45, 109] is the most straightforward way to support multiple nano-machines (NMs) for simultaneous transmission via assigning different NMs with different types of molecules. In [46–48], the molecular time-division multiple-access (MoTDMA) was proposed to implement multiple-access DMC in the time-domain. To achieve multiple-access transmission, different NMs are scheduled to transmit within different time-slots. The molecular space-division multiple-access (MoSDMA) is another scheme to support multiple-access DMC [49, 50]. With MoSDMA, the receiver distinguishes information pulses corresponding to different nano-machines based on their shapes of channel impulse response (CIR) related to their locations as in DMC the CIR is significantly impacted by the transmission distance. Furthermore, the principle of CDMA can also be introduced to implement multiple-access DMC, yielding MoCDMA [51, 52]. In MoCDMA, different nano-machines are assigned different signatures to spread messages, which are also utilized by the receiver to de-spread and distinguish the information transmitted by different NMs.

DMC relies on the slow diffusion process for information delivery. Correspondingly, the transmission of information in multiple-access DMC systems experiences both severe inter-symbol interference (ISI) and MAI. In terms of the signal detection at FC or access point (AP), the mitigation of ISI has been a hotspot investigated by different researchers. In principle, many existing signal

processing approaches inspired by radio-based communications, such as, maximum *a-posteriori* (MAP), maximum likelihood (ML), etc., have been introduced to DMC systems to conduct signal detection [30, 57, 58]. The studies show that although MAP or ML can achieve optimal detection, its complexity increases exponentially with the length of ISI, which is impractical for implementation with the nano-devices lacking ofsufficient computing capability. Instead, they are usually deemed as a criterion to appraise the other detection schemes. In literature, adaptive decision-feedback equalizer (DFE) and minimum mean-square error (MMSE) equalizer having lower complexity than MAP and ML equalizers for implementation have also been considered [30, 59]. Additionally, matched-filtering (MF), zero-forcing (ZF), and MMSE equalizers have been proposed to mitigate the ISI in molecular shift keying (MoSK) DMC systems [119]. All the above-mentioned references considered the signal processings operated in time-domain. On the other hand, there are also some frequency-domain equalizers (FDEs) proposed for DMC [120–122]. Specifically, the FDEs based on ZF and MMSE principles were investigated in [120] and [121], respectively, while [122] provided rigorous proof and analysis in the frequency-domain for the DMC with ZF and MMSE equalizers. The performance analysis in [122] shows that compared to time-domain equalizers (TDEs), FDEs have lower computational complexity and better error performance, when transmitting at a high rate. In addition,the authors of [123] applied the principle of orthogonal frequency division multiplexing (OFDMA) in optical communications to DMC, so as to eliminate the ISI by introducing a sufficiently long cyclic prefix (CP).

Although there are numerous methods proposed for ISI mitigation and signal detection in single-user DMC systems, limited research has been conducted on MAI mitigation and single-/multiple-user detection for multiple-access DMC. In literature, a Reed-Solomon (RS) error correction coding assisted method was proposed to combat the MAI and ISI in [63], which belongs to a channel coding method. Recently, the authors of [64] proposed a novel modulation scheme, referred to as the binary direction shift keying (BDSK), which encodes one-bit data in two different pumping directions. With the BDSK modulation, adjacent NMs are able to pump the same type of information molecules in two opposite nano-receivers to mitigate MAI. However, the system considered in [64] puts strict requirements on transceivers, including, the spherical transceivers of considerably large sizes relative to the transmission distance, the fixed pair of non-rotatable transceivers, and the reflective surfaces of transmitters and fully absorbing receivers. However, little attention has been paid to the receiver design for detection schemes and interference cancellation in multiple-access DMC systems.

Based on the above retrospection, in this chapter, we study a MoCDMA scheme, which employs the spreading sequences with the chip-elements taking values in the multiplicative group of $\{+1, -1\}$. Because in the well-developed radio-based CDMA (RdCDMA), there are different types of spreading sequences executing operations in $\{+1, -1\}$ [124], which include, such as, Walsh codes, m-sequences or called maximum-length sequences (MLS), Kasami sequences, Gold sequences, etc. Some of these sequences have good orthogonality and are proper for operation in

multiple-access communications scenarios. Specifically, in our MoCDMA system, in order to generate the antipodal signal of differential concentration, as in [52], a pair of isomers with the same diffusive coefficient are employed, where one type (Type-A) is mapped for $+1$ transmission and the other type (Type-B) is mapped for -1 transmission. An important advantage of this setting is that the counting noise in the MoCDMA system can be deemed as Gaussian additive noise with a constant variance, when the time-invariant channel is considered. At the receiver of MoCDMA system, we assume a transparent observer, which is able to sense and measure the concentrations of both Type-A and Type-B molecules within a sphere detection space at chip level. Moreover, we assume that data are sent in blocks with CP, so that low-complexity FDE algorithms can be introduced for interference mitigation and signal detection.

Due to the slow propagation of molecules in DMC, MoCDMA signals experience various types of interference, including ISI, inter-chip interference (ICI) and MAI, in addition to the counting noise, which increases with the number of NMs. Therefore, in MoCDMA systems, it is desirable that the receiver is capable of mitigating the interference as above-mentioned and achieve the best possible performance. However, the nano-scale transceivers are usually limited by their computational capability, making only low-complexity algorithms be feasible for implementation. Hence, in this chapter, we introduce the signal processing and detection schemes in the frequency-domain with relatively low-complexity. Specifically, we introduce the MF, ZF, and MMSE assisted FDEs to mainly combat ICI. Furthermore, the decision-feedback successive interference cancellation (DF-SIC) schemes are integrated with these equalizers to further cancel MAI and hence, improve the detection performance. In this chapter, we analyze the complexity of the considered detection schemes and compare their achievable performance. Our studies will clearly demonstrate the potential of the MoCDMA and the performance-complexity trade-off of the different detection schemes.

In summary, the contributions of this chapter are stated as follows:

- Inspired by the RdCDMA with BPSK modulation, a MoCDMA system with BMoSK modulation is proposed which relies on two types of molecules for multiple NMs to simultaneously transmit information to a FC (or AP).
- The proposed MoCDMA system transmits data block-by-block with the aid of CP to avoid inter-block interference (IBI) and equalize signals parallelly in the frequency-domain.
- Three FDE schemes, namely MF-, ZF-, and MMSE-FDE are proposed to equalize the received signals so as to mitigate ICI for reliable detection. Furthermore, based on MF-, ZF-, and MMSE-FDE, one/two-stage DF-SIC schemes are proposed to further mitigate MAI, which allows to attain some further performance gain. Our studies show that all these detection schemes are low-complexity schemes and are efficient to achieve reliable communication.

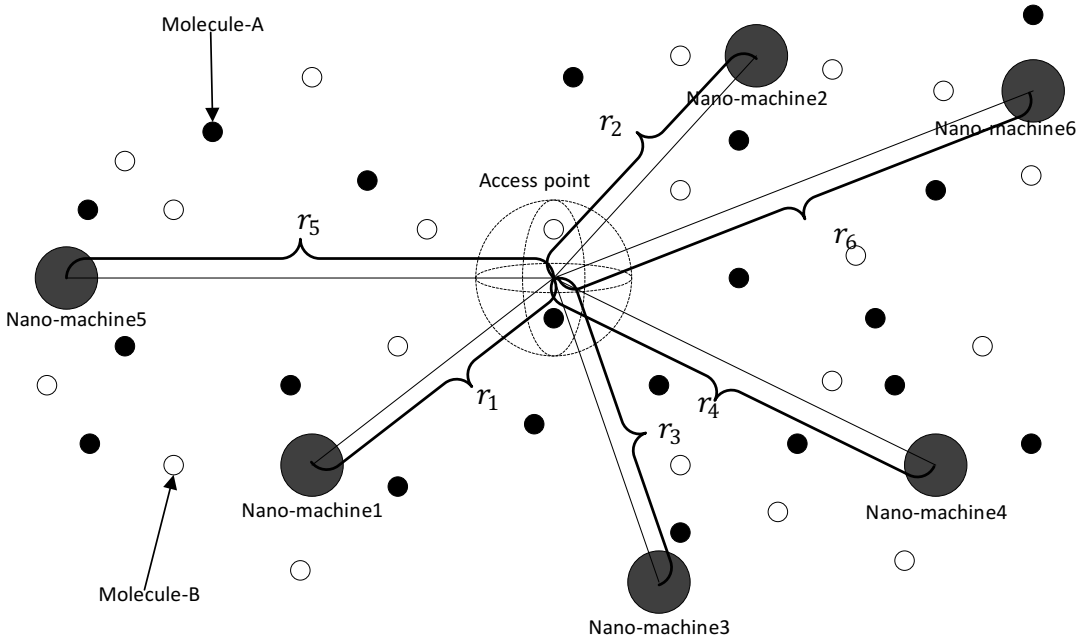

Figure 5.1: Diagram of a multiple-access DMC system.

- The error performance of the MoCDMA systems with different detection schemes and three types of spreading sequences, namely, Walsh codes, MLS, and Gold sequences is studied and compared.

The remainder of this chapter is structured as follows. First, the main assumptions for DMC systems and the system model, including transmitter, channel model, and receiver, are presented in Section 5.2. The representations for the received block signals with or without CP are derived in Section 5.3. In Section 5.4, the various equalization and detection schemes operated in the frequency-domain are derived. Furthermore, the computational complexity of the various detection schemes is analyzed in this section. Section 5.5 presents the performance results reflected mainly by the bit error rate (BER) of the MoCDMA systems with various detection schemes. Finally, our concluding summary is provided in Section 5.6.

5.2 System Model

As the intuitive diagram shown in Fig. 5.1, we consider a DMC uplink communication system, which is composed of K point-source nano-sensors (transmitters) and a spherical transparent fusion center (receiver). The nano-machines (NMs) release two types of information molecules into a three-dimensional fluid medium with infinite space. The fusion center (FC) is capable of sampling and detecting molecular signals with a detection space of radius ρ. Both NMs and FC are immobile, and the diffusive medium is uniform and stable. Furthermore, to focus our attention on the principles, we assume that synchronization is achieved between NMs and FC, which ensures

that sampling can always happen at the maximum point of the individual molecular concentration pulse.

Following the principles of RdCDMA, in MoCDMA, a NM transmits one-bit information via releasing N molecular pulses of each having $Q_c = Q/N$ molecules with respect to N chips, which have a fixed chip duration of T_c seconds. As the convention, N is the spreading factor, and $T_s = NT_c$ is symbol-duration, or bit duration if binary data modulation, i.e., BMoSK, is employed. When NMs with different transmission distances from FC are considered, in order to align ideally sampling instant, i.e., maximum points of the molecular pulses corresponding to different NMs, the transmission times of NMs are scheduled according to their transmission distances. Below we analyze the transmitter, channel model and the receiver of MoCDMA systems in detail.

5.2.1 Transmitter

Let us assume that in the MoCDMA system, the kth NM's information to be transmitted is expressed as $\boldsymbol{b}_k = \{b_{k,0}, b_{k,1}, \ldots, b_{k,j}, \ldots\}$, where $b_{k,j} \in \{1, -1\}$. In the principle of MoCDMA, a N length spreading sequence [110] is introduced to spread the uth bit sent by NM k, which can be expressed as $\boldsymbol{s}_k = [s_{k,0}, s_{k,1}, \ldots, s_{k,N-1}]^T$, where $s_{k,n} \in \{1, -1\}$, and $N = T_s/T_c$. If the transmission distances between NMs and the FC are quite different, a constant T_s is defined for the whole MoCDMA systems in order to conduct synchronous transmissions among different NMs. Furthermore, no matter what the distance is from FC, we assume that FC samples at the expected maximum of the concentration pulse. To achieve this, a straightforward solution is to schedule the initial emission times of different NMs via the time delays expressed as $T_0^{(k)}$, so as to align the peak times of all received molecular concentration pulses by different NMs. Then, when the BMSK modulation is employed, Q_c number of (Type-A or Type-B) molecules per pulse are emitted for sending '1' or '-1'. Consequently, the molecular signal transmitted by nano-user k for sending the uth bit can be expressed as

$$s_k(t) = \sum_{q=0}^{N-1} \left(\frac{1 + b_{k,u} s_{k,q}}{2} Q_c \delta_A t_e(u, q, T_0^{(k)}) + \frac{1 - b_{k,u} s_{k,q}}{2} Q_c \delta_B t_e(u, q, T_0^{(k)}) \right),$$
$$k = 1, 2, \ldots, k, u = 0, 1, \ldots \tag{5.1}$$

where $t_e(u, q, T_0^{(k)}) = t - uT_s - qT_c - T_0^{(k)}$ is the emission moment. The impulses of Type-A and Type-B molecules are respectively represented by $\delta_A(t)$ and $\delta_B(t)$, which are defined as $\delta_A(0) = 1$ ($\delta_B(0) = 1$), and $\delta_A(x) = 0$ ($\delta_B(x) = 0$) for $x \neq 0$.

5.2.2 Channel Model

As we assumed before, molecules freely diffuse in a fluid medium without boundaries, there is no flow, and the medium environment is uniform and stable. Hence, the fluid medium's diffusion coefficient D is constant. Based on these assumptions and considering that NM k emits an impulse

of Q_c molecules at $t = T_0^{(k)}$, the concentration sampled by the FC at $t > T_0^{(k)}$ follows Fick's second law, which is given by [56]

$$c_k(t) = \frac{Q_c^{(k)}}{[4\pi D(t - T_o^{(k)})]^{\frac{3}{2}}} \exp\left[-\frac{r_k^2}{4D(t - T_o^{(k)})}\right], t > T_o^{(k)} \tag{5.2}$$

As shown in [56], molecular concentration $c_k(t)$ is a time(T)-domain pulse function or called channel state information (CSI), whose shape is dependent on the distance r between NM and FC. For a given distance r_k, the maximum concentration can be formed to occur at $t_d^{(k)} = r_k^2/6D$, which is given by $c_{k,\max} = \left(\frac{3}{2\pi e}\right)^{\frac{3}{2}} \frac{Q_c}{r_k^3}$. Hence, to make sure that the maximum expected concentrations arrive at FC from different NMs at the same time, a common sampling time at the maximums can be predefined as $t_d^{(\Re)} \geq t_d^{\text{farthest NM}}$, provided that the emission delay $T_o^{(k)}$ is given by $T_o^{(k)} = t_d^{(\Re)} - t_d^{(k)}$. Note that as $c_{k,\max}$ decreases with r_k^3, DMCs are usually only suitable for information transmission over a very short distance in the fluid environments without flow.

5.2.3 Receiver

We assume that FC is capable of recognizing the two types, namely, Type-A and Type-B, of molecules. Then, when assuming that there are K NMs sending signals in the form of (5.1) to FC, the concentration difference between Type-A and Type-B molecules in the context of the nth chip, $n = 0, 1, \ldots N-1$, of the uth bit can be derived to be

$$\begin{aligned} z(t) =& z_A(t) - z_B(t) \\ =& \sum_{k=1}^{K} \sum_{j=0}^{uN+n} \frac{1 + b_{k,\lfloor j/N \rfloor} s_{k,j\%N}}{2} \left[c_{A,k}(t - jT_c) + n_{A,k,j}(t)\right] \\ & - \sum_{k=1}^{K} \sum_{j=0}^{uN+n} \frac{1 - b_{k,\lfloor j/N \rfloor} s_{k,j\%N}}{2} \left[c_{B,k}(t - jT_c) + n_{B,k,j}(t)\right], \\ & (uN+n)T_c + T_o^{(k)} \leq t < (uN+n+1)T_c + T_o^{(k)} \end{aligned} \tag{5.3}$$

where $\lfloor \cdot \rfloor$ is the floor operation, % is the modulo operation, while $n_{A,k,m}(t)$ and $n_{B,k,m}(t)$ are the particle counting noise caused by the corresponding types of molecules emitted by the kth NM sending the mth pulse of molecules [22]. Specifically, for one particular type of molecules, according to [22, 115], when the number of molecules Q_c per chip or $Q = NQ_c$ per symbol is sufficiently large, both $n_{A,k,j}(t)$ and $n_{B,k,j}(t)$ can be approximated as the Gaussian noise with zero mean and the variances of $\sigma_{A,k,j}^2(t) = \frac{1+b_{k,\lfloor j/N \rfloor} s_{k,j\%N}}{2V_R} c_{A,k}((t-j)T_c$ and $\sigma_{B,k,j}^2(t) = \frac{1-b_{k,\lfloor j/N \rfloor} s_{k,j\%N}}{2V_R} c_{B,k}((t-j)T_c)$, respectively, where $V_R = \frac{4}{3}\pi\rho^3$ is the volume of the FC's spherical detector with a radius of ρ. Consequently, these counting noises follow the normal distribution, given as $n_{A,k,j}(t) \sim \mathcal{N}\left(0, \sigma_{A,k,m}^2(t)\right)$ and $n_{B,k,j}(t) \sim \mathcal{N}\left(0, \sigma_{B,k,m}^2(t)\right)$, respectively.

According to the properties of $c(t)$ as shown in (5.2), after a pulse of molecules is released by a NM at $t = T_0^{(k)}$, the expected concentration at FC reaches maximum at $t = t_d^{(\Re)}$. Therefore, for detection of the uth bits of K NMs, the receiver samples for the concentrations at $t =$

$(uN+n)T_c + \hat{t}_d^{\Re}$ for $n = 0, 1, \ldots, N-1$, where $\hat{t}_d^{(\Re)}$ is the estimated $t_d^{(\Re)}$. Correspondingly, the concentration difference between Type-A and Type-B molecules at the sampling times can be expressed as

$$\begin{aligned} z_{u,n} &= z_A(t = (uN+n)T_c + \hat{t}_d^{(\Re)}) - z_B(t = (uN+n)T_c + \hat{t}_d^{(\Re)}) \\ &= \sum_{k=1}^{K} \sum_{j=0}^{uN+n} \frac{1 + b_{k,\lfloor j/N \rfloor} s_{k,j\%N}}{2} \Big[c_{A,k}\Big((uN+n-j)T_c + \hat{t}_d^{(\Re)}\Big) \\ &\qquad + n_{A,k,j}\Big((uN+n)T_c + \hat{t}_d^{(\Re)}\Big)\Big] \\ &\quad - \sum_{k=1}^{K} \sum_{j=0}^{uN+n} \frac{1 - b_{k,\lfloor j/N \rfloor} s_{k,j\%N}}{2} \Big[c_{B,k}\Big((uN+n-j)T_c + \hat{t}_d^{(\Re)}\Big) \\ &\qquad + n_{B,k,j}\Big((uN+n)T_c + \hat{t}_d^{(\Re)}\Big)\Big] \\ &\quad u = 0, 1, \ldots;\ n = 0, 1, \ldots, N-1 \end{aligned} \tag{5.4}$$

From the above equation, we can know that, even when there is just one nano-user in the system, the detection of bit u experiences ISI from the bits sent in the front of bit u, via the index of j. Furthermore, due to multiple pulses are transmitted for each bit, there is also inter-chip interference (ICI) imposed by the chips sent within the same bit duration. However, from the properties of the pulse $c(t)$ we can readily observe that both ISI and ICI reduce significantly with time. Hence, our analysis below assumes that the maximum length of ISI is L chips. In this case, $z_{u,n}$ in (5.4) can be represented in the form of

$$\begin{aligned} z_{u,n} &= \sum_{k=1}^{K} \sum_{j=\max\{0,uN+n-L\}}^{uN+n} \frac{1 + b_{k,\lfloor j/N \rfloor} s_{k,j\%N}}{2} \left[c_{A,k}(uN+n-j) + n_{A,k,j}(uN+n) \right] \\ &\quad - \sum_{k=1}^{K} \sum_{j=\max\{0,uN+n-L\}}^{uN+n} \frac{1 - b_{k,\lfloor j/N \rfloor} s_{k,j\%N}}{2} \left[c_{B,k}(uN+n-j) + n_{B,k,j}(uN+n) \right] \\ &\quad u = 0, 1, \ldots;\ n = 0, 1, \ldots, N-1 \end{aligned} \tag{5.5}$$

where $c_{X,k}(uN+n-j) = c_{X,k}\left((uN+n-j)T_c + \hat{t}_d^{(\Re)}\right)$ and $n_{X,k,j}(uN+n) = n_{X,k,j}\left((uN+n)T_c + \hat{t}_d^{(\Re)}\right)$, X is for A or B.

After carefully examining (5.5), we can conceive that, for given indices of k and j, we have either $(1 + b_{k,\lfloor j/N \rfloor} s_{k,j\%N})/2 = 1$ and $(1 - b_{k,\lfloor j/N \rfloor} s_{k,j\%N})/2 = 0$ when $b_{k,\lfloor j/N \rfloor} s_{k,j\%N} = 1$, or $(1 + b_{k,\lfloor j/N \rfloor} s_{k,j\%N})/2 = 0$ and $(1 - b_{k,\lfloor j/N \rfloor} s_{k,j\%N})/2 = 1$ when $b_{k,\lfloor j/N \rfloor} s_{k,j\%N} = -1$. Furthermore, in (5.5), $c_{A,k}(uN+n-j)$ and $c_{B,k}(uN+n-j)$ have the same statistical properties, the same are $n_{A,k,j}(uN+n)$ and $n_{B,k,j}(uN+n)$. Therefore, we can represent (5.5) by an equivalent form of

$$\begin{aligned} z_{u,n} &= \sum_{k=1}^{K} \sum_{j=\max\{0,uN+n-L\}}^{uN+n} b_{k,\lfloor j/N \rfloor} s_{k,j\%N} \left[c_k(uN+n-j) + n_{k,j}(uN+n) \right] \\ &\quad u = 0, 1, \ldots;\ n = 0, 1, \ldots, N-1 \end{aligned} \tag{5.6}$$

where $c_k(uN+n-j)$ is a sample obtained either from $c_{A,k}(t)$ or from $c_{B,k}(t)$, while $n_{k,j}(uN+n)$ has the distribution of $\mathcal{N}\left(0,\sigma^2_{k,j}(u,n)\right)$ with $\sigma^2_{k,j}(u,n) = V_R^{-1}c_k(uN+n-j)$.

Let $i = uN+n-j$. Then, (5.6) can be written in a more convenient form as

$$\begin{aligned} z_{u,n} &= \sum_{k=1}^{K}\sum_{i=0}^{\min\{L,uN+n\}} b_{k,\lfloor (uN+n-i)/N\rfloor} s_{k,(n-i)\%N}\left[c_k(i) + n_{k,uN+n-i}(uN+n)\right] \\ &= \sum_{k=1}^{K}\sum_{i=0}^{\min\{L,uN+n\}} c_k(i) s_{k,(n-i)\%N} b_{k,\lfloor (uN+n-i)/N\rfloor} + n'_{u,n} \\ &\quad u = 0,1,\ldots;\ n = 0,1,\ldots,N-1 \end{aligned} \tag{5.7}$$

where $n'_{u,n} = \sum_{k=1}^{K}\sum_{i=0}^{\min\{L,uN+n\}} b_{k,\lfloor uN+n-i/N\rfloor} s_{k,n-i\%N} n_{k,uN+n-i}(uN+n)$, which can be well approximated by a Gaussian noise with the distribution of $\mathcal{N}\left(0,\sigma^2\right)$, where $\sigma^2 = V_R^{-1}\sum_{k=1}^{K}\sum_{i=0}^{\min\{L,uN+n\}} c_k(i)$. Note here that our MoCDMA systems with BMoSK has a benefit that the counting noise can be approximated as the additive Gaussian noise uncorrelated to the bits transmitted.

Equation (5.7) shows that in the MoCDMA system, there exists ISI, ICI as well as multiple access interference (MAI), which the FC should be handled properly in order to achieve desirable detection performance. Furthermore, we should draw readers attention that, as shown in the previous formulas for $z_{u,n}$, noise in DMC is related to the CSI, and any transmitted molecule contributes to the increase of noise power, along with its duty to carry information. This is because noise, referred to as *counting noise*, in DMC is the result of molecules' (random) Brownian motions, which cause an unwanted perturbation to the concentration (or number of particles) predicted from Fick's diffusive law [22]. Therefore, in MoCDMA systems, the noise power is enhanced with the increasing number of NMs supported, and also enhanced with the ISI, ICI and MAI experienced by a NM.

Having obtained the equivalent formula for the observations, as shown in (5.7), below we consider the signal processing and detection schemes at FC. Fig. 5.2 demonstrates the structure of step-by-step signal processing at FC, which will be further elaborated in the following sections.

5.3 Representation of Received Signals

5.3.1 Continuous Block Transmission

For facilitating the detection, we assume that data are transmitted in blocks of each having a length of M. A data block transmitted by the kth NM is expressed as $\boldsymbol{b}_k = [b_{k,0}, b_{k,1}, \ldots, b_{k,M-1}]^T$. In this case, for a given block transmitted, the transmitted signals are spread over MN observations, from $Z_{0,0}$ to $Z_{M-1,N-1}$.

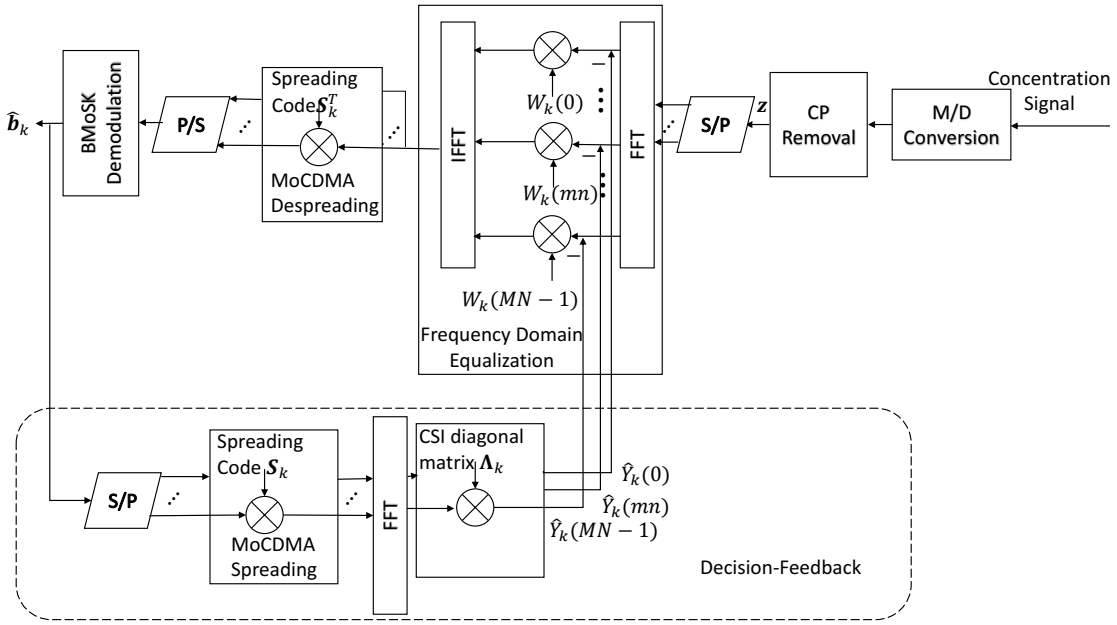

Figure 5.2: Structure diagram showing the operations at FC.

Let

$$\begin{aligned} \boldsymbol{z} &= \left[z_{0,0},\ldots,z_{0,N-1};\ldots,z_{M-1,0},\ldots,z_{M-1,N-1}\right]^T, \\ \boldsymbol{n} &= \left[n_{0,0},\ldots,n_{0,N-1};\ldots,n_{M-1,0},\ldots,n_{M-1,N-1}\right]^T. \end{aligned} \tag{5.8}$$

Then, if the inter-block interference (IBI) is taken into account, the first L observations in $\boldsymbol{z}$ should plus the interference from $\lceil L/N \rceil$ bits, expressed as $\boldsymbol{b}_{k,-1} = \left[b_{k,-\lceil L/N \rceil}, b_{k,-\lceil L/N \rceil+1},\ldots,b_{k,-1}\right]^T$, in the previous block. It can be shown that we can write all the observations corresponding to the MN sampling time in the current block as

$$\boldsymbol{z} = \sum_{k=1}^{K} \boldsymbol{C}_k \tilde{\boldsymbol{S}}_k \tilde{\boldsymbol{b}}_k + \boldsymbol{n}, \tag{5.9}$$

where $\boldsymbol{C_k}$ is a $(MN \times [\lceil L/N \rceil N + MN])$ matrix, in the form of

$$\left[\begin{array}{ccccc|ccccccc} 0 & \cdots & c_k(L) & c_k(L-1) & \cdots & c_k(0) & 0 & \cdots & 0 & 0 & \cdots & 0 \\ 0 & \cdots & 0 & c_k(L) & c_k(L-1) & \cdots & c_k(0) & \cdots & 0 & 0 & \cdots & 0 \\ \vdots & \ddots & \vdots & \vdots & \vdots & \ddots & \vdots & \ddots & \vdots & \vdots & \ddots & \vdots \\ 0 & \cdots & 0 & 0 & 0 & \cdots & 0 & \cdots & c_k(L) & c_k(L-1) & \cdots & c_k(0) \end{array}\right]. \tag{5.10}$$

The left block of matrix (5.10) is a $(MN \times \lceil L/N \rceil N)$ matrix starting with $MN \times [\lceil L/N \rceil]N - L]$ zeros. In (5.9), $\tilde{\boldsymbol{S}}_k = \boldsymbol{I}_{M+\lceil L/N \rceil} \otimes \boldsymbol{s}_k$, where $\otimes$ denotes the Kronecker product operation. Hence, $\tilde{\boldsymbol{S}}_k$ is a $([M+\lceil L/N \rceil]N \times [M+\lceil L/N \rceil])$ matrix. $\tilde{\boldsymbol{b}}_k$ includes all the bits $\begin{bmatrix} \boldsymbol{b}_{k,-1} \\ \boldsymbol{b}_k \end{bmatrix}$ affecting the observations in $\boldsymbol{z}$. Additionally, because all these MN observations experience the whole length L of ICI, $\boldsymbol{n}$ is Gaussian distributed with zero mean and a covariance matrix of $\sigma^2 \boldsymbol{I}_{MN}$.

5.3.2 Cyclic Prefix (CP) Assisted Transmission

In order to eliminate IBI and introduce the circulant property into the CSI matrix for frequency-domain detection, a cyclic prefix (CP) is inserted as a guard interval (GI) between two adjacent data blocks. Because the length of CP should be longer than L of the length of ICI to fully counteract the IBI, it can be set as the last $\lceil L/N \rceil N$ values after the spreading. To be more specific, after spreading, the last $\lceil L/N \rceil N$ chips of $\boldsymbol{S}_k \boldsymbol{b}_k$ are copied and prefixed in the front of a data block. Subsequently, the NM transmits a block including $\lceil L/N \rceil N$ CP chips and MN normal data chips. At the FC, the first $\lceil L/N \rceil N$ chip observations are removed and the rest MN observations are employed for signal processing, as in the radio-based OFDM system [125]. Consequently, due to the above CP insertion, the CSI $\boldsymbol{C}_k$ is transformed into an $(MN \times MN)$ circulant matrix $\tilde{\boldsymbol{C}}_k$ [117] having the diagonal elements being $c_k(0)$, which is denoted by

$$\tilde{\boldsymbol{C}}_k = \begin{bmatrix} c_k(0) & 0 & \cdots & c_k(L) & \cdots & c_k(1) \\ c_k(1) & c_k(0) & 0 & \vdots & \ddots & \vdots \\ \vdots & \ddots & \ddots & \ddots & \ddots & c_k(L) \\ c_k(L) & \cdots & c_k(1) & c_k(0) & 0 & 0 \\ \vdots & \ddots & \vdots & \ddots & c_k(0) & 0 \\ 0 & \cdots & c_k(L) & \cdots & c_k(1) & c_k(0) \end{bmatrix}. \tag{5.11}$$

Consequently, the observation equation (5.9) can now be written as

$$\boldsymbol{z} = \sum_{k=1}^{K} \tilde{\boldsymbol{C}}_k \boldsymbol{S}_k \boldsymbol{b}_k + \boldsymbol{n}, \tag{5.12}$$

where $\boldsymbol{S}_k$ is a $(MN \times M)$ matrix constructed by $\boldsymbol{I}_M \otimes \boldsymbol{s}_k$, i.e., $\boldsymbol{S}_k = \boldsymbol{I}_M \otimes \boldsymbol{s}_k$.

5.4 Signal Detection and Complexity Analysis

Time domain signal detection in DMC systems has been widely investigated. However, the complexity of time-domain detectors increases rapidly with the increase of ISI/ICI length. Owing to the introduction of CP, the frequency-domain detectors require lower computational complexity. In this section, we introduce a range of signal-detection algorithms that are operated in the frequency domain.

To facilitate frequency-domain detection, as illustrated in Fig. 5.2, at FC, the received time-domain discrete signal $\boldsymbol{z}$ in (5.12) is transformed to the frequency-domain by a MN-point FFT with the FFT matrix given by

$$\boldsymbol{\mathcal{F}} = \frac{1}{\sqrt{MN}} \begin{bmatrix} 1 & 1 & 1 & \cdots & 1 \\ 1 & e^{-\frac{j2\pi}{MN}} & e^{-\frac{j4\pi}{MN}} & \cdots & e^{-\frac{j2\pi(MN-1)}{MN}} \\ \vdots & \vdots & \vdots & \ddots & \vdots \\ 1 & e^{-\frac{j2\pi(MN-1)}{MN}} & e^{-\frac{j4\pi(MN-1)}{MN}} & \cdots & e^{-\frac{j2\pi(MN-1)^2}{MN}} \end{bmatrix}, \tag{5.13}$$

where the (p,q)th element $(p,q \in [0, MN-1])$ is $F_{pq} = \frac{1}{\sqrt{MN}} e^{-\frac{j2\pi pq}{MN}}$. $\boldsymbol{\mathcal{F}}$ is a unitary matrix satisfying $\boldsymbol{\mathcal{F}}\boldsymbol{\mathcal{F}}^H = \boldsymbol{\mathcal{F}}^H\boldsymbol{\mathcal{F}} = \boldsymbol{I}$ [78], where $[\cdot]^H$ denotes the conjugate transpose operation, and $\boldsymbol{\mathcal{F}}^H$ is called as the IFFT matrix. Consequently, upon executing the FFT operation to transform (5.12) to the frequency-domain, we obtain

$$\tilde{\boldsymbol{z}} = \boldsymbol{\mathcal{F}}\boldsymbol{z} = \sum_{k=1}^{K} \boldsymbol{\Lambda}_k \boldsymbol{\mathcal{F}} \boldsymbol{S}_k \boldsymbol{b}_k + \tilde{\boldsymbol{n}} = [\tilde{z}_0, \ldots, \tilde{z}_p, \ldots, \tilde{z}_{MN-1}]^T, \tag{5.14}$$

which gives the observations of the MN subcarriers [78]. In (5.12) , $\boldsymbol{\Lambda}_k$ is a diagonal matrix, obtained by diagonalising the circulant matrix $\tilde{\boldsymbol{C}}_k$, which can be expressed as

$$\boldsymbol{\Lambda}_k = \boldsymbol{\mathcal{F}}\tilde{\boldsymbol{C}}_k\boldsymbol{\mathcal{F}}^H = \mathrm{diag}\{\lambda_{k,0}, \ldots, \lambda_{k,p}, \ldots, \lambda_{k,MN-1}\}. \tag{5.15}$$

For processing, the CSI matrix $\tilde{\boldsymbol{C}}_k$ can be constructed via by channel estimation in advance which is time-invariant when the channel environment does not change. Hence, the subcarriers' channel gains in $\boldsymbol{\Lambda}_k$ are also stationary. Moreover, we can express the frequency domain spread block as $\boldsymbol{B}_k = \boldsymbol{\mathcal{F}}\boldsymbol{S}_k\boldsymbol{b}_k = [B_{k,0}, \ldots, B_{k,p}, \ldots, B_{k,MN-1}]^T$, where

$$B_{k,p} = \frac{1}{\sqrt{MN}} \sum_{q=0}^{MN-1} (\boldsymbol{S}_k\boldsymbol{b}_k)_q e^{-\frac{j2\pi pq}{MN}}. \tag{5.16}$$

In (5.16), $(\boldsymbol{S}_k\boldsymbol{b}_k)_q$ represents the qth chip of the spread vector $(\boldsymbol{S}_k\boldsymbol{b}_k)$ transmitted by the kth NM. Besides, the frequency-domain noise vector in (5.14) is $\tilde{\boldsymbol{n}} = \boldsymbol{\mathcal{F}}\boldsymbol{n} = [\tilde{n}_0, \ldots, \tilde{n}_p, \ldots, \tilde{n}_{MN-1}]^T$, whose pth entry is the noise on the pth subcarrier, which is

$$\tilde{n}_p = \frac{1}{\sqrt{MN}} \sum_{q=0}^{MN-1} n_q e^{-\frac{j2\pi pq}{MN}}. \tag{5.17}$$

It can be shown that $\tilde{n}_p$ has zero mean and the variance σ^2, owing to the unitary transform of FFT/IFFT.

5.4.1 Frequency-Domain Equalization Detection

As Fig. 5.2 illustrates, after obtaining the frequency-domain representation of the received signals, the frequency-domain equalization is carried out to mitigate ISI/ICI before signal detection. Considering the computational complexity constraint of nano-devices in DMC, in this chapter, three linear equalizer options that have relatively low complexity are first considered to facilitate the detection in our MoCDMA DMC systems. Hence, upon following the principles of linear frequency-domain equalization [78, 126–128], the equalized signal $\bar{\boldsymbol{z}}_k$ derived from (5.14) can be formed as

$$\begin{aligned} \bar{\boldsymbol{z}}_k =& \boldsymbol{W}_k^H \tilde{\boldsymbol{z}} \\ =& \boldsymbol{W}_k^H \boldsymbol{\mathcal{F}} \boldsymbol{z} \\ =& \boldsymbol{W}_k^H \sum_{k=1}^{K} \boldsymbol{\Lambda}_k \boldsymbol{\mathcal{F}} \boldsymbol{S}_k \boldsymbol{b}_k + \boldsymbol{W}_k^H \boldsymbol{\mathcal{F}} \boldsymbol{n}, \end{aligned} \tag{5.18}$$

where $\boldsymbol{W}_k$ is a diagonal equalization matrix, which can be expressed as $\boldsymbol{W}_k = \text{diag}\{W_0, \ldots, W_p, \ldots, W_{MN-1}\}$ with element W_p for equalization of the pth subcarrier.

Inspired by the various frequency-domain equalization schemes available in wireless communications [78, 126–128], the low-complexity (MF-FDE, ZF-FDE and MMSE-FDE) are taken into consideration. Correspondingly, the equalization-processing matrices are provided below.

5.4.1.1 MF-FDE

The MF-based equalizer aims to maximize the received energy of the desired signals transmitted by the kth NM by exploiting the channel knowledge $\boldsymbol{\Lambda}_k$ in the frequency domain, instead of attempting to suppress any interference. As the gain of the pth subcarrier is the pth entry on the diagonal of $\boldsymbol{\Lambda}_k$, expressed as

$$W_{k,p}(\text{MF}) = \lambda_{k,p},\ p = 0, 1, \ldots, MN-1. \tag{5.19}$$

Furthermore, we can write

$$\boldsymbol{W}_k(\text{MF}) = \boldsymbol{\Lambda}_k = \text{diag}\{\lambda_{k,0}, \ldots, \lambda_{k,p}, \ldots, \lambda_{k,MN-1}\}. \tag{5.20}$$

The MF-FDE has the merit that, when given the constant distance between the kth NM and FC, $\boldsymbol{\Lambda}_k$ is fixed. Thus, it only needs to be completed once and hence is in low complexity.

5.4.1.2 ZF-FDE

The ZF-FDE inverts the channel of the desired kth NM based on the frequency-domain CSI $\boldsymbol{\Lambda}_k$, which can eliminate ICI. correspondingly, we have

$$W_{k,p}(\text{ZF}) = \frac{1}{\lambda^*_{k,p}}, \tag{5.21}$$

and

$$\boldsymbol{W}_k(\text{ZF}) = \left(\boldsymbol{\Lambda}_k^{-1}\right)^H = \text{diag}\left\{\frac{1}{\lambda^*_{k,0}}, \ldots, \frac{1}{\lambda^*_{k,p}}, \ldots, \frac{1}{\lambda^*_{k,MN-1}}\right\}. \tag{5.22}$$

Compared to the MF-FDE, the additional computation required by the ZF-FDE is the matrix inverse operation. However, as the MF-FDE, if the locations of NM and FC are fixed, $\boldsymbol{W}_k(\text{ZF})$ is also fixed. Hence, ZF-FDE has nearly the same complexity as MF-FDE, if the channel keeps unchanged for a relatively long time.

5.4.1.3 MMSE-FDE

To minimize the mean square error, the MMSE-FDE is derived by finding the solution to an optimization problem of

$$W_{k,p}(\text{MMSE}) = \arg\min_{W} \left\{ E\left[\|B_{k,p} - W^* Z_p\|^2\right]\right\}, \tag{5.23}$$

which it can be shown gives the solution of

$$W_{k,p}(\text{MMSE}) = \frac{\lambda_{k,p}}{|\lambda_{k,p}|^2 + \sigma^2}. \tag{5.24}$$

Correspondingly, we express

$$\boldsymbol{W}_k(\text{MMSE}) = \text{diag}\left\{ \frac{\lambda_{k,0}}{|\lambda_{k,0}|^2 + \sigma^2}, \ldots, \frac{\lambda_{k,p}}{|\lambda_{k,p}|^2 + \sigma^2}, \ldots, \frac{\lambda_{k,MN-1}}{|\lambda_{k,MN-1}|^2 + \sigma^2} \right\}, \tag{5.25}$$

which is also a fixed matrix when the channel does not vary. Hence, it is also low-complexity.

MF-FDE maximizes the received energy without attempting interference suppression. By contrast, ZF-FDE has the capability to fully remove ICI but it has the disadvantages of noise amplification [78]. In comparison with these two, MMSE-FDE is capable of striking a trade-off between interference suppression and noise suppression and achieving better error performance than both MF- and ZF-FDE schemes.

5.4.2 Signal Detection

As Fig. 5.2 illustrates, after FDE is operated by multiplying $\boldsymbol{W}_k^H$ on $\tilde{\boldsymbol{z}}$ in (5.18), the IFFT matrix $\boldsymbol{\mathcal{F}}^H$ is multiplied on the FDE results to transform signals from frequency-domain to time-domain. Subsequently, despreading is achieved by multiplying $\boldsymbol{S}_k^T$, yielding the decision variables for detecting the M bits of the kth NM. Consequently, we obtain

$$\begin{aligned}
\boldsymbol{d}_k =& \boldsymbol{S}_k^T \boldsymbol{\mathcal{F}}^H \tilde{\boldsymbol{z}}_k \\
=& \boldsymbol{S}_k^T \boldsymbol{\mathcal{F}}^H \boldsymbol{W}_k^H \tilde{\boldsymbol{z}} \\
=& \boldsymbol{S}_k^T \boldsymbol{\mathcal{F}}^H \boldsymbol{W}_k^H \boldsymbol{\mathcal{F}} \boldsymbol{z} \\
=& \boldsymbol{S}_k^T \boldsymbol{\mathcal{F}}^H \boldsymbol{W}_k^H \boldsymbol{\Lambda}_k \boldsymbol{\mathcal{F}} \boldsymbol{S}_k \boldsymbol{b}_k + \sum_{l \neq k}^{K} \boldsymbol{S}_k^T \boldsymbol{\mathcal{F}}^H \boldsymbol{W}_k^H \boldsymbol{\Lambda}_l \boldsymbol{\mathcal{F}} \boldsymbol{S}_l \boldsymbol{b}_l + \boldsymbol{n}',
\end{aligned} \tag{5.26}$$

where $\boldsymbol{n}' = \boldsymbol{S}_k^T \boldsymbol{\mathcal{F}}^H \boldsymbol{W}_k^H \boldsymbol{\mathcal{F}} \boldsymbol{n}$.

When the MRC-FDE is employed by substituting $\boldsymbol{W}_k = \boldsymbol{\Lambda}_k$ into (5.26), the M-length decision variable block can be expressed as

$$\boldsymbol{d}_k(\text{MF}) = \boldsymbol{S}_k^T \boldsymbol{\mathcal{F}}^H |\boldsymbol{\Lambda}_k|^2 \boldsymbol{\mathcal{F}} \boldsymbol{S}_k \boldsymbol{b}_k + \sum_{l \neq k}^{K} \boldsymbol{S}_k^T \boldsymbol{\mathcal{F}}^H \boldsymbol{\Lambda}_k^H \boldsymbol{\Lambda}_l \boldsymbol{\mathcal{F}} \boldsymbol{S}_l \boldsymbol{b}_l + \boldsymbol{S}_k^T \boldsymbol{\mathcal{F}}^H \boldsymbol{\Lambda}_k^H \boldsymbol{\mathcal{F}} \boldsymbol{n}. \tag{5.27}$$

Similarly, by multiplying the ZF-based weight matrix $\boldsymbol{\Lambda}_k^{-1}$, IFFT matrix $\boldsymbol{\mathcal{F}}^H$, and despreading sequence $\boldsymbol{S}_k^T$ of the kth NM, the M decision variables in the case of ZF-FDE can be formed as

$$\begin{aligned}
\boldsymbol{d}_k(\text{ZF}) =& \boldsymbol{S}_k^T \boldsymbol{\mathcal{F}}^H \boldsymbol{\mathcal{F}} \boldsymbol{S}_k \boldsymbol{b}_k + \sum_{l \neq k}^{K} \boldsymbol{S}_k^T \boldsymbol{\mathcal{F}}^H \boldsymbol{\Lambda}_k^{-1} \boldsymbol{\Lambda}_l \boldsymbol{\mathcal{F}} \boldsymbol{S}_l \boldsymbol{b}_l + \boldsymbol{S}_k^T \boldsymbol{\mathcal{F}}^H \boldsymbol{\Lambda}_k^{-1} \boldsymbol{\mathcal{F}} \boldsymbol{n} \\
=& \boldsymbol{S}_k^T \boldsymbol{\mathcal{F}}^H \boldsymbol{\mathcal{F}} \boldsymbol{S}_k \boldsymbol{b}_k + \sum_{l \neq k}^{K} \boldsymbol{S}_k^T \boldsymbol{\mathcal{F}}^H \boldsymbol{\mathcal{F}} \tilde{\boldsymbol{C}}_k^{-1} \boldsymbol{\mathcal{F}}^H \boldsymbol{\Lambda}_l \boldsymbol{\mathcal{F}} \boldsymbol{S}_l \boldsymbol{b}_l + \boldsymbol{S}_k^T \boldsymbol{\mathcal{F}}^H \boldsymbol{\mathcal{F}} \tilde{\boldsymbol{C}}_k^{-1} \boldsymbol{\mathcal{F}}^H \boldsymbol{\mathcal{F}} \boldsymbol{n} \\
=& \boldsymbol{S}_k^T \boldsymbol{S}_k \boldsymbol{b}_k + \sum_{l \neq k}^{K} \boldsymbol{S}_k^T \tilde{\boldsymbol{C}}_k^{-1} \tilde{\boldsymbol{C}}_l \boldsymbol{S}_l \boldsymbol{b}_l + \boldsymbol{S}_k^T \tilde{\boldsymbol{C}}_k^{-1} \boldsymbol{n}.
\end{aligned} \tag{5.28}$$

From (5.28) we can readily show that if ZF-FDE is employed, as well as when orthogonal spreading codes are assigned to different NMs and when the transmission distances from different NMs to FC are the same, when have $\tilde{\boldsymbol{C}}_1 = \tilde{\boldsymbol{C}}_2 = \ldots = \tilde{\boldsymbol{C}}_K$, and furthermore we have

$$\boldsymbol{d}_k = N\boldsymbol{b}_k + \boldsymbol{S}_k^T \tilde{\boldsymbol{C}}_k^{-1} \boldsymbol{n}, \tag{5.29}$$

where $\boldsymbol{S}_k^T \boldsymbol{S}_k = N\boldsymbol{I}_M$ is applied. Therefore, the ICI and MAI are fully removed. However, we should mention that while in this case, the ZF-FDE can fully remove ICI and MAI, the operation amplifies noise, i.e., the noise power in (5.29) is higher than σ^2.

Finally, when MMSE-FDE is considered, $\boldsymbol{W}_k = \boldsymbol{W}_k(\text{MMSE})$ is substituted into (5.26). Then, the M-length block of decision variables after IFFT and despreading can be expressed as

$$\boldsymbol{d}_k(\text{MMSE}) = \boldsymbol{S}_k^T \boldsymbol{\Theta}_k \tilde{\boldsymbol{C}}_k \boldsymbol{S}_k \boldsymbol{b}_k + \sum_{l \neq k}^{K} \boldsymbol{S}_k^T \boldsymbol{\Theta}_k \tilde{\boldsymbol{C}}_l \boldsymbol{S}_l \boldsymbol{b}_l + \boldsymbol{S}_k^T \boldsymbol{\Theta}_k \boldsymbol{n}, \tag{5.30}$$

where $\boldsymbol{\Theta}_k$ denotes the circulant matrix $\boldsymbol{\mathcal{F}}^H \boldsymbol{W}_k^H(\text{MMSE}) \boldsymbol{\mathcal{F}}$.

In general, for decision-making, the decision variable for the uth bit of the kth NM can be expressed as $d_{k,u}$, which is the uth element in the M-length vector $\boldsymbol{d}_k$. Based on $d_{k,u}$, the uth bit of the kth NM is able to be recovered as

$$\hat{b}_{k,u} = \begin{cases} 1, & \text{if } d_{k,u} > 0 \\ 0 \text{ (or } -1), & \text{else} \end{cases} \tag{5.31}$$

for $u = 0, 1, \ldots, M-1$ and $k = 1, 2, \ldots, K$.

5.4.3 Decision-Feedback Interference Cancellation

The above FDE-assisted detection mainly aims at mitigating the effect of ICI, without putting attention on the MAI mitigation. To mitigate MAI, a decision-feedback-based successive interference cancellation (DF-SIC) scheme is introduced. The basic principle of DF-SIC is that, after an NM is correctly detected, its interference on the other undetected NMs can be removed with the aid of knowledge about the detected NM.

As Fig. 5.2 demonstrates, the DF-SIC can be explained as follows. After the M bits transmitted by the 1st NM are detected in the principle described in the last subsection, a copy of signals received from it can be formed as

$$\hat{\boldsymbol{y}}_1 = \boldsymbol{\Lambda}_1 \boldsymbol{\mathcal{F}} \boldsymbol{S}_1 \hat{\boldsymbol{b}}_1, \tag{5.32}$$

where $\hat{\boldsymbol{y}}_1$ is a MN-length vector expressed as $[\hat{Y}_1(0), \hat{Y}_1(1), \ldots, \hat{Y}_1(MN-1)]^T$, which are the estimates to the signals received from the 1st NM on the MN subcarriers.

Subsequently, the estimated $\hat{\boldsymbol{y}}_1$ is subtracted from the MN-length frequency-domain observations to mitigate the interference from the 1st NM on the other NMs, yielding $\tilde{\boldsymbol{z}}^{(1)} = \tilde{\boldsymbol{z}} - \hat{\boldsymbol{y}}_1$. Then,

Algorithm 4 One-Stage Decision Feedback Successive Interference Cancellation

Input: Frequency-domain observation matrix $\tilde{\boldsymbol{z}}$.

Output: M detected bits transmitted by each of the K NMs.

Initialization: $\tilde{\boldsymbol{z}}^{(0)} = \tilde{\boldsymbol{z}}$.

Sort: Ordering NMs according to $r_1 \leq r_2 \leq \cdots \leq r_K$.

For $k = 1, 2, \ldots, K-1$, execute:

1. $\hat{\boldsymbol{b}}_k = f_{decision}\left(\boldsymbol{S}_k^T \boldsymbol{\mathcal{F}}^H \boldsymbol{W}_k \tilde{\boldsymbol{z}}^{(k-1)}\right)$, where $\boldsymbol{W_k}$ depends on which FDE is employed.
2. $\hat{\boldsymbol{y}}_k = \boldsymbol{\Lambda}_k \boldsymbol{\mathcal{F}} \boldsymbol{S}_k \hat{\boldsymbol{b}}_k$.
3. $\tilde{\boldsymbol{z}}^{(k)} = \tilde{\boldsymbol{z}}^{(k-1)} - \hat{\boldsymbol{y}}_k$.

End For

Detection of NM-K: $\hat{\boldsymbol{b}}_K = f_{decision}\left(\boldsymbol{S}_K^T \boldsymbol{\mathcal{F}}^H \boldsymbol{W}_K \tilde{\boldsymbol{z}}^{(K-1)}\right)$.

by executing equalization, spreading, and decision-making as described in Section 5.4.2, the M bits sent by the 2nd NM can be detected as

$$\hat{\boldsymbol{b}}_2 = f_{decision}\left(\boldsymbol{S}_2^T \boldsymbol{\mathcal{F}}^H \boldsymbol{W}_2 \tilde{\boldsymbol{z}}^{(1)}\right), \tag{5.33}$$

where $f_{decision}(x)$ denotes the decision making defined in (5.31).

Similarly, the M bits sent by the 3rd NM can be detected based on the updated observation vector $\tilde{\boldsymbol{z}}^{(2)} = \tilde{\boldsymbol{z}} - \hat{\boldsymbol{y}}_1 - \hat{\boldsymbol{y}}_2 = \tilde{\boldsymbol{z}}^{(1)} - \hat{\boldsymbol{y}}_2$, where $\hat{\boldsymbol{y}}_2 = \boldsymbol{\Lambda}_2 \boldsymbol{\mathcal{F}} \boldsymbol{S}_2 \hat{\boldsymbol{b}}_2$. In general, the detection of the kth NM can be deduced, which can be represented as

$$\begin{aligned} \hat{\boldsymbol{y}}_{k-1} &= \boldsymbol{\Lambda}_{k-1} \boldsymbol{\mathcal{F}} \boldsymbol{S}_{k-1} \hat{\boldsymbol{b}}_{k-1}, \\ \tilde{\boldsymbol{z}}^{(k-1)} &= \tilde{\boldsymbol{z}}^{(k-2)} - \hat{\boldsymbol{y}}_{k-1}, \\ \hat{\boldsymbol{b}}_k &= f_{decision}\left(\boldsymbol{S}_k^T \boldsymbol{\mathcal{F}}^H \boldsymbol{W}_k \tilde{\boldsymbol{z}}^{(k-1)}\right). \end{aligned} \tag{5.34}$$

The above DF-SIC is summarized in Algorithm 4, which is referred to as the one-stage DF-SIC.

It can be shown that if $\hat{b}_{k-1}(m)$ in $\hat{\boldsymbol{b}}_{k-1}$ is detected correctly, the MAI caused by the mth bit sent by the $(k-1)$th NM can be completely canceled. Otherwise, if $\hat{b}_{k-1}(m)$ is detected by mistake, the interference resulted from $\hat{b}_{k-1}(m)$ is doubled. Thus, the errors made in a previous detection will be spread to the following detection of the other NMs. In order to reduce the occurrences of error spreading, the detection of NMs should be ordered according to their received power at FC from high to low. In MoCDMA, the received power is very sensitive to distance. Hence, when the numbers of molecules per pulse emitted by NMs are the same, a NM close to FC should have high reliability to be detected. Consequently, its strong interference on the other NMs can be efficiently mitigated. Therefore, as shown in Algorithm 4, the NM closer to FC has a higher priority to be detected than the NM farther away from FC.

Algorithm 5 Two-Stage Decision Feedback Successive Interference Cancellation

Input: Frequency-domain observation matrix $\tilde{\boldsymbol{z}}$.

Output: M detected bits transmitted by each of the K NMs.

Initialization: $\tilde{\boldsymbol{z}}^{(0)} = \tilde{\boldsymbol{z}}$.

Sort: Ordering NMs according to $r_1 \leq r_2 \leq \cdots \leq r_K$.

For $k = 1, 2, \ldots, K-1$, execute:

1. $\hat{\boldsymbol{b}}_k = f_{decision}\left(\boldsymbol{S}_k^T \boldsymbol{\mathcal{F}}^H \boldsymbol{W}_k \tilde{\boldsymbol{z}}^{(k-1)}\right)$, where $\boldsymbol{W_k}$ depends on which FDE is employed.
2. $\hat{\boldsymbol{y}}_k = \boldsymbol{\Lambda}_k \boldsymbol{\mathcal{F}} \boldsymbol{S}_k \hat{\boldsymbol{b}}_k$.
3. $\tilde{\boldsymbol{z}}^{(k)} = \tilde{\boldsymbol{z}}^{(k-1)} - \hat{\boldsymbol{y}}_k$.

End For

Detection of NM-K: $\hat{\boldsymbol{b}}_K = f_{decision}\left(\boldsymbol{S}_K^T \boldsymbol{\mathcal{F}}^H \boldsymbol{W}_K \tilde{\boldsymbol{z}}^{(K-1)}\right)$.

For $k = K, K-1, \ldots, 2$, execute:

1. $\hat{\boldsymbol{y}}_k = \boldsymbol{\Lambda}_k \boldsymbol{\mathcal{F}} \boldsymbol{S}_k \hat{\boldsymbol{b}}_k$.
2. $\tilde{\boldsymbol{z}}^{(k-2)} = \tilde{\boldsymbol{z}}^{(k-2)} - \hat{\boldsymbol{y}}_k$.
3. $\hat{\boldsymbol{b}}_{k-1} = f_{decision}\left(\boldsymbol{S}_k^T \boldsymbol{\mathcal{F}}^H \boldsymbol{W}_k \tilde{\boldsymbol{z}}^{(k-2)}\right)$

End For

By contrast, when the transmission distances between all NMs and FC are the same and the reliability of detection is unknown, the multistage successive interference cancellation (MSIC) can be implemented to improve the detection reliability. MSIC cancels interference several times. which yields the trade-off between complexity and performance gain. Specifically, for the considered MoCDMA, a two-stage DF-SIC is proposed to cancel the estimated MAI from the other NMs on the detection of a desired NM.

Specifically, after the one-stage SIC, it can be inferred that $\hat{\boldsymbol{b}}_K$ is the most reliable one detected because at this time, the detection of all the other NMs has been completed and their interference on $\boldsymbol{b}_K$ can be canceled. By contrast, $\hat{\boldsymbol{b}}_1$ is the most unreliable one detected, as there was no interference cancellation attempt before its detection. Thus, with the two-stage FD-SIC, the FC detects the $(K-1)$th NM first by canceling the interference from the Kth NM, yielding $\tilde{\boldsymbol{z}}^{(K-2)} - \hat{\boldsymbol{y}}_K$. Then, the estimated interference $\hat{\boldsymbol{y}}_{K-1}$ of the $(K-1)$th NM on the other NMs is updated based on the modified $\hat{\boldsymbol{b}}_{K-1}$. Then, the $(K-2)$th NM is detected based on $\tilde{\boldsymbol{z}}^{(K-3)} - \hat{\boldsymbol{y}}_K - \hat{\boldsymbol{y}}_{K-1}$. This procedure proceeds until the first NM is detected. Specifically, the two-stage DF-SIC is summarized as Algorithm 5.

5.4.4 Complexity of Detection Schemes

In this section, we analyse the complexity of the FDE-assisted detection and DF-SIC schemes described in the previous subsections. Because the weight matrix $\boldsymbol{W}_k^H$ is fixed when a specific type of FDE is employed, we consider the complexity of pre-processing and the complexity of equalization and detection separately. In addition, the computational complexity is measured in terms of M bits and K NMs.

As Fig. 5.2 shows, different FDEs have the same complexity for equalization and detection and only slight difference for computing $\boldsymbol{W}_k^H$. Specifically for pre-processing, FC needs to compute $\boldsymbol{\Lambda} = \boldsymbol{\mathcal{F}}\tilde{\boldsymbol{C}}\boldsymbol{\mathcal{F}}^H$. It is known that the FFT and IFFT on a MN-length vector have the complexity of $\mathcal{O}(MN\log_2(MN))$. For detection, we analyze the three FDEs first, since DF-SIC is based on them. According to (5.26), the FDE includes the operations of FFT, frequency-domain multiplication, IFFT, and despread. In addition to FFT and IFFT, multiplying a $(MN \times MN)$ diagonal matrix on a MN-length vector has the complexity of $\mathcal{O}(MN)$. Moreover, as $\boldsymbol{s}_{k,u}$ has only N essential elements, multiplying $\boldsymbol{S}_k^T$ with a MN-length vector has the complexity of $\mathcal{O}(MN)$. Therefore, the total computation for the FDE-assisted detection is $K(MN\log_2(MN) + 2MN) + MN\log_2(MN)$. Hence, the detection complexity of the three fundamental FDE-assisted detectors is $\mathcal{O}(K(MN\log_2(MN) + 2MN))$ for detecting the M-bit blocks of K NMs.

Subsequently, the complexity of the DF-SIC is dependent on which FDE is utilized. The one-stage DF-SIC consists of the sort, $K-1$ times interference cancellation and decision-making, as Fig. 5.2 depicts. If the bubble sort [129] is employed, its complexity is $\mathcal{O}(K^2)$ for K NMs. For one iteration of decision feedback interference cancellation, the complexity of re-spreading to compute $\boldsymbol{S}_k\hat{\boldsymbol{b}}_k$ is $\mathcal{O}(MN)$. The complexity of FFT on a MN-vector is $MN\log_2(MN)$. The complexity of multiplying $\boldsymbol{\Lambda}$ on a frequency-domain MN-vector is $\mathcal{O}(MN)$. Eventually, the complexity of subtraction in terms of MN subcarriers is $\mathcal{O}(MN)$. Consequently, the one-stage DF-SIC has the total complexity of $\mathcal{O}(K(2MNlog_2(MN) + 4MN) + K^2)$ for the stage of detection. For the two-stage DF-SIC, it repeats reversely the $(K-1)$ times of interference cancellation of the one-stage DF-SIC. Explicitly, its detection complexity is $\mathcal{O}(2K(2MNlog_2(MN) + 4MN) + K^2)$.

The complexity of the different detectors is summarized in Table 5.1. It can be shown that all the detection schemes are low complexity schemes, with the complexity depending linearly on K when M and N are given. The complexity of the DF-SIC schemes is similar as that of the FDE-assisted detectors, although DF-SIC schemes need several times more computation in practice.

5.5 Performance Results and Discussion

This section demonstrates the bit error rate (BER) performance of the DMC MoCDMA systems equalized by MF-, ZF-, and MMSE-FDE with/without DF-SIC. The label for the X-axis in most BER result figures is Q_b expressed in dB, which is the number of molecules emitted by an NM

Table 5.1: Complexity of detection schemes.

Detection scheme	Detection
MF-FDE	$\mathcal{O}(K(MN\log_2(MN)+2MN))$
ZF-FDE	$\mathcal{O}(K(MN\log_2(MN)+2MN))$
MMSE-FDE	$\mathcal{O}(K(MN\log_2(MN)+2MN))$
One-stage DF-SIC	$\mathcal{O}(2K(MN\log_2(MN)+2MN+K))$
Two-stage DF-SIC	$\mathcal{O}(4K(MN\log_2(MN)+2MN+K))$

for one-bit transmission. Throughout our simulations, besides some special assumptions and parameters that are notified in the context or detailed in the figure caption, the common parameters are as follows: Walsh codes length is $N = 16$, data block length is $M = 100$, number of NMs supported is $K = 4$, diffusion coefficient is $D = 4.5 \times 10^{-9}$ nm/s, and the radius of receiver is $\rho = 0.4\ \mu m$. In addition, for convenient demonstration of error performance, we assume the same distance $r = 2.2\mu m$ between any NM and FC in some simulations. Following [111], the length of ICI is defined as

$$L = \arg\max_i \left\{ \frac{c_k(i)}{c_k(0)} \geq 1\% \right\}, \tag{5.35}$$

where $c_k(i)$ is the residual concentration sampled at the ith chip and the kth NM is the farthest NM away from FC, which yields the severest ICI on the other NMs. The definition of (5.35) indicates that the ICI less than 1% of the concentration of the current chip impulse is neglected, as its impact on BER performance is insignificant.

First, Fig. 5.3 compares the BER performance of the MoCDMA systems employing the various detection schemes considered and when different spreading sequences, including, MLS, Gold sequences, and (orthogonal) Walsh codes, are respectively employed. It is worth noting that in our simulation, the chip duration is set to $T_c = t_d$ to fix the length of ICI, which is $L = 57$ based on (5.35). Due to the characteristics of various spreading codes, we set $N = 31$ for MLS and Gold sequences, while $N = 32$ for Walsh codes. Though the bit rate $R_b = 1/T_b = 1/(NT_c)$ in the case of Walsh codes is slightly lower than that in the situations of MLS and Gold sequences, the comparison of their error performance is still nearly fair. From Fig. 5.3 we can see that, explicitly, different types of sequences may yield different performances, as they generate different levels of interference. In more detail, for all the three FDE schemes and the three cases of interference cancellation, Walsh codes provide the best BER performance, owing to the merit that Walsh codes allow orthogonal signal transmission, after the employment of FDE. From the results, we can deduce that ZF- and MMSE-FDE are highly efficient for ICI cancellation and orthogonal sequences are promising for our MoCDMA systems to prevent MAI. Thus, in the following figures, we will mainly consider the MoCDMA systems deploying Walsh codes.

As Fig. 5.3(a) shows, when the Walsh codes are employed, the performance gain by the two-stage DF-SIC becomes insignificant, which means that the one-stage DF-SIC is capable of re-

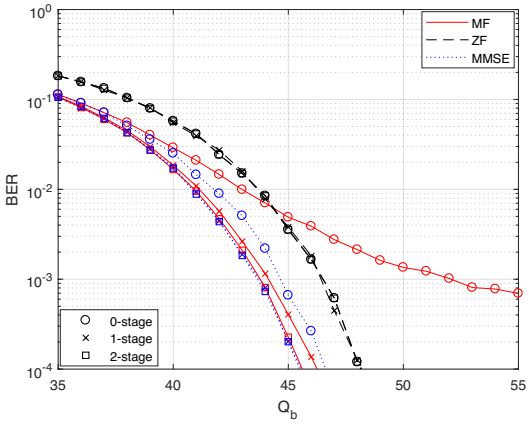

(a) Walsh codes $(N = 32)$

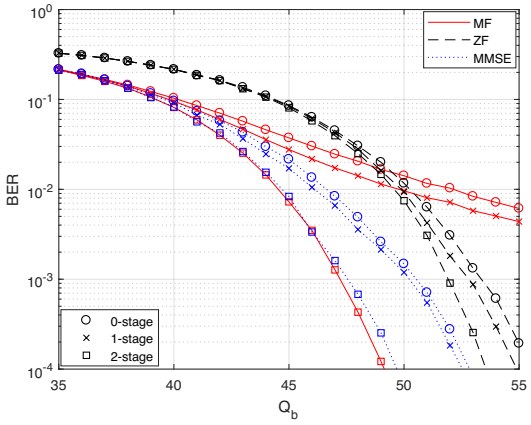

(b) Gold sequences $(N = 31)$

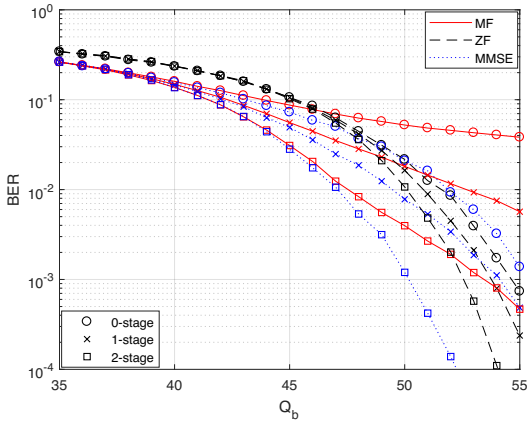

(c) MLS $(N = 31)$

Figure 5.3: Comparison of BER performance of the MoCDMA systems with various detection schemes, when Walsh codes, Gold sequences or MLS are employed and when $T_c = t_d$, $K = 4$.

moving most of the interference. Furthermore, both the one-stage ZF-SIC and two-stage ZF-SIC are unable to improve further the BER performance of the ZF-FDE. This is because after the ZF-FDE, the signals from different NMs become orthogonal, yielding zero ICI and MAI. By contrast, when the non-orthogonal spreading address sequences are employed, as seen in Fig. 5.3(b) and Fig. 5.3(c), the two-stage DF-SIC can attain a significant gain in the error performance, especially, where the MF- or MMSE-FDE is invoked. The reason behind this observation is that the MF- and MMSE-FDE are unable to eliminate ICI completely. Hence, the DF-SICs need not only cancel MAI but also ICI of the signals equalized by these two FDEs. However, although ZF-FDE is able to ideally remove ICI, it amplifies noise power. Therefore, as seen in these figures, provided that Q_b is small, in other words, the signal-to-noise ratio (SNR) is low, the ZF-FDE exhibits the worst BER performance in all the figures in Fig. 5.3. As illustrated in Fig. 5.3(a) and Fig. 5.3(b), when Q_b is relatively low, the BER curves of the two-stage MF-SIC appear in the water-falling form, close to that of the two-stage MMSE-SIC. This indicates that the two-stage DF-SIC is able to provide

significant assistance for interference mitigation, yielding a significant performance gain.

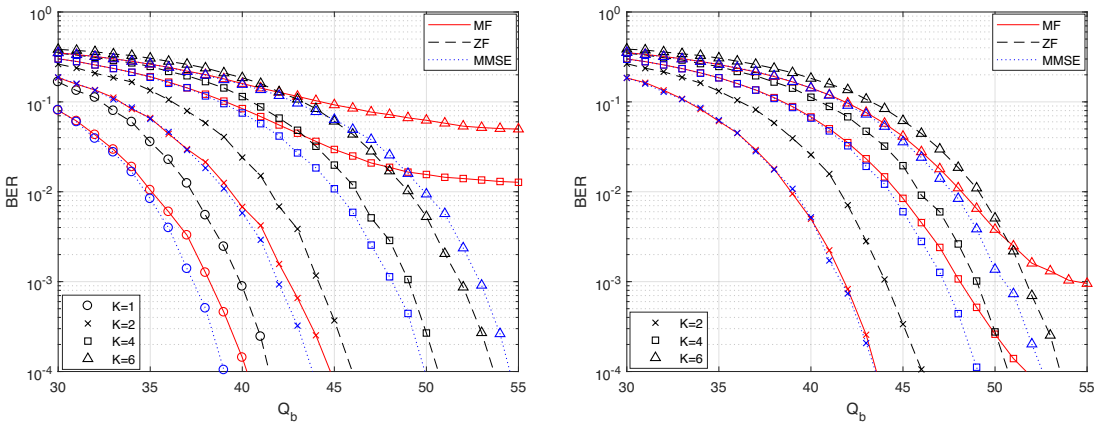

(a) Without DF-SIC

(b) With One-stage DF-SIC

Figure 5.4: Comparison of BER performance of the MoCDMA systems with the various detection schemes with/without one-stage DF-SIC, when $T_c = t_d$ and supporting $K = 1,\ 2,\ 4$, or 6 NMs.

In the second set of results shown in Fig. 5.4, the BER performance of the MoCDMA systems employing the three detectors described in Section 5.4.1 is demonstrated when one-stage DF-SIC is or is not employed. Following the studies in Fig. 5.3, here Walsh codes are used as the spreading sequence and $K = 1, 2, 4$, or 6 NMs are supported, respectively. Note that, as employing two-stage SIC does not bring explicit gain over the one-stage DF-SIC, when Walsh codes are employed, the results of the two-stage DF-SIC are omitted in these and the following figures, whenever Walsh codes are employed.

Explicitly, due to the severe interference, which includes ISI, ICI and MAI, the MF-FDE without DF-SIC can hardly provide reasonable performance, as shown in Fig. 5.4(a), when multiple NMs are supported. Specifically, the MF-FDE is unable to support more than $K = 2$ NMs to achieve practically meaningful performance. Compared to the MF-FDE, both ZF- and MMSE-FDE are much more efficient. As shown in Fig. 5.4(a), even when the number of NMs supported is as high as $K = 6$, the BER curves appear in the water-falling form, and a low BER can be attainable, provided that the Q_b is sufficiently high. When comparing ZF-FDE with MMSE-FDE, we can see that the BER performance gap between MMSE-FDE and ZF-FDE decreases, as the number of NMs supported increases. Moreover, when $K = 6$ NMs are supported, ZF-FDE surprisingly outperforms MMSE-FDE, which is never the case in RdCDMA. The underlying reason is that although MMSE-FDE outperforms ZF-FDE in the single-carrier case, this is not necessary the case, when all the subcarriers are considered. As a result that the spreading sequences are not exploited by the equalizers operated with the individual subcarriers, after FDE, the despreading of the ZF-equalized signals yields zero ISI/ICI and zero MAI. By contrast, the despreading of the MMSE-equalized signals returns significant interference, as MMSE-FDE yields the subcarriers

with different gains.

The interference experienced by MoCDMA systems can be mitigated by the DF-SIC, as shown in Fig. 5.4(b). However, the amplified noise resulted from ZF-FDE is unable to be mitigated by the DF-SIC. Thus, in the following figures depicting the BER performance of the MoCDMA systems employing Walsh codes and DF-SIC, ZF-SIC is not further considered. Another observation from Fig. 5.4(b) is that when the MoCDMA system supports a relatively large number of NMs, i.e., $K = 6$, the MF-assisted DF-SIC is still incapable of eliminating the BER's error-floor, although the achieved performance has a significant improvement compared to the corresponding results in Fig. 5.4(a). This means that there is still interference not removable by the MF-assisted DF-SIC.

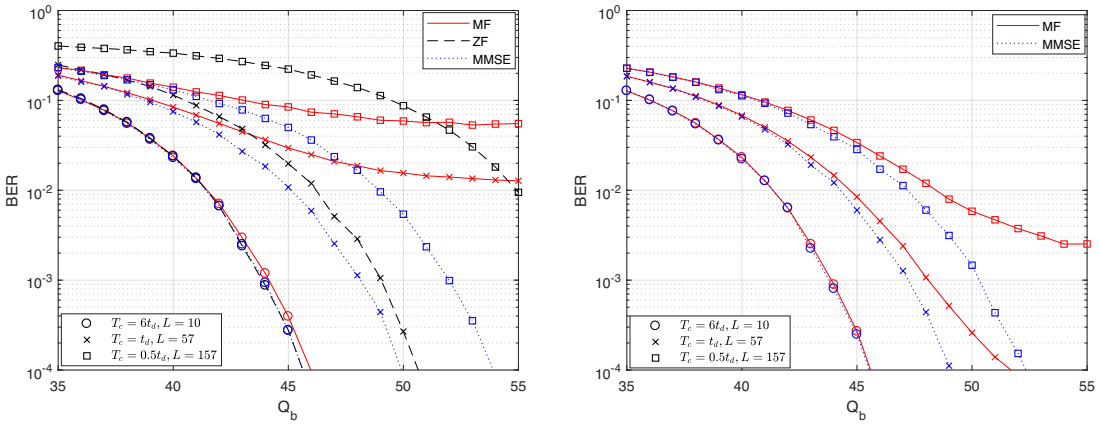

(a) Without DF-SIC (b) With one-stage SIC

Figure 5.5: Comparison of BER performance of the MoCDMA systems with the various detection schemes with/without one-stage DF-SIC, when chip-duration is $T_c = 6t_d,\ t_d$, or $0.5t_d$, respectively.

Fig.5.5 demonstrates the impact of different transmission rates on the BER performance of the MoCDMA systems with various detection schemes. As the number of chips per bit is kept to $N = 16$, the bit duration corresponding to $T_c = 6t_d,\ t_d$, and $0.5t_d$ is $T_b = 96t_d,\ 6t_d$, and $8t_d$, respectively. Correspondingly, the lengths of ICI are $L = 10,\ 57$, and 157, respectively.

As shown in Fig.5.5(a), the three detectors achieve a similar BER performance, when chip/bit duration is large, resulting in little ICI. By contrast, at a higher transmission rate of $2/t_d$, MMSE-FDE is the most promising equalization scheme, while MF-FDE does not work properly and ZF-FDE can achieve a reasonable reliability but at the cost of significantly increased Q_b, inferring an enormously increased number of molecules emitted by an NM. The reason behind this observation is that the short chip duration of $T_c = t_d/2$ is unable to cover the whole rising edge of the received molecular pulse. Consequently, the sampling point is always at the end of a chip, which results in that the desired concentration sampled is even lower than the residual concentration of a previous chip, resulting in strong interference. In this case, the valid signal is overwhelmed by the severe ICI. When comparing Fig.5.5(a) and Fig.5.5(b), it can be seen that the MAI generated by the Walsh-

code is relevant to the ICI, which makes that the DF-SIC exhibits the observable performance improvement over the corresponding FDE schemes, especially when the equalized signals still experience severe ICI.

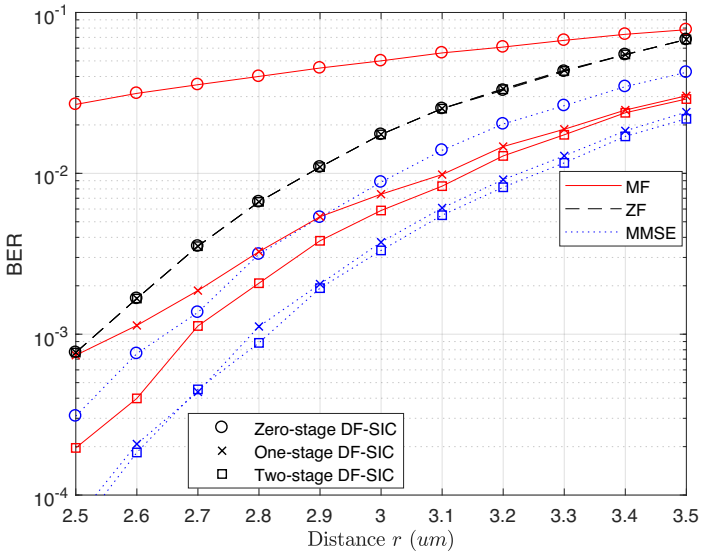

Figure 5.6: BER performance versus transmission distance of the MoCDMA systems employing various detection schemes, when $Q_b = 52dB$, $T_b = 2.97ms$.

Fig. 5.6 depicts the BER performance of the MoCDMA systems versus the transmission distance r, when different detection schemes are respectively employed, and when each NM emits $Q_b = 52dB$ molecules. From the results, we have the following observations. First, as the transmission distance increases, the BER performance achieved by all detectors becomes worse. This is because as the distance increases, the received pulse of molecular concentration becomes wider, resulting in that the pulse peak becomes lower, and hence, lower signal gain, stronger interference and higher noise power. Second, when MF-FDE is considered, as the transmission distance increases, the improvement in the BER performance provided by the two-stage DF-SIC declines. This is because the increase in transmission distance reduces the number of information molecules received and MF-FDE yields lower SNR. As DF-SIC's capability is relied on the performance achieved by MF-FDE, and hence little performance improvement. In terms of the MMSE series, we can see that the two-stage MMSE-assisted FD-SIC always has a slight BER improvement over the other schemes in the distance range as considered.

Finally, in the set of results shown in Fig. 5.7, we investigate the impact of spreading factor N on the BER performance of the MoCDMA systems employing the different detectors with/without the one-stage DF-SIC, when two different bit durations of $T_b = 16t_d$ and $T_b = 96t_d$ are respectively considered. Note that the chip duration T_c and its ICI length L corresponding to different combinations of T_b and N are provided in the legend of curves. Furthermore, in these figures,

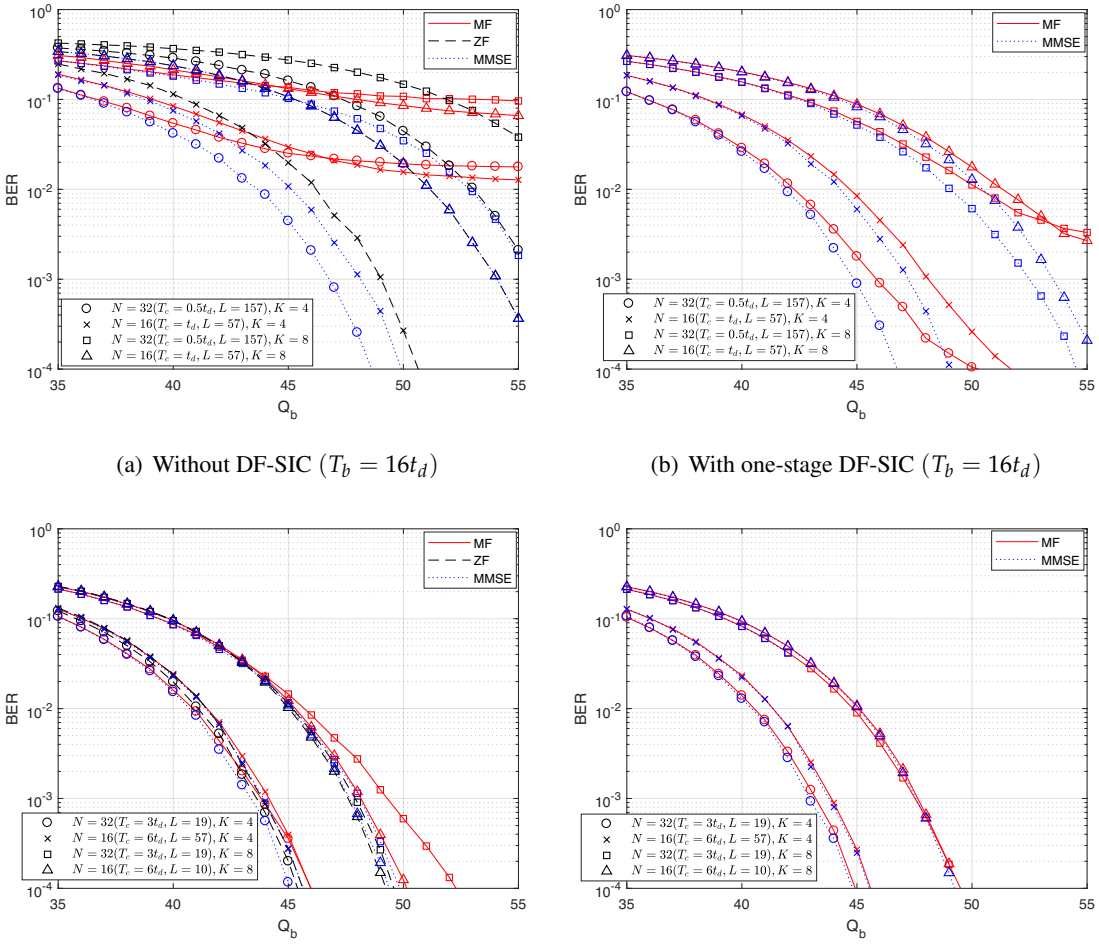

(a) Without DF-SIC $(T_b = 16t_d)$

(b) With one-stage DF-SIC $(T_b = 16t_d)$

(c) Without DF-SIC $(T_b = 96t_d)$

(d) With one-stage DF-SIC $(T_b = 96t_d)$

Figure 5.7: Impact of different spreading factors and different number of NMs $(K = 4 \text{ or } 8)$ on the BER performance of the MoCDMA systems using the MF-, ZF-, and MMSE-FDEs with/without the one-stage DF-SIC, when assuming two different bit durations $T_b = 16t_d$ or $96t_d$.

rather than considering solely the impact of N, we investigate the impact of K/N on the BER performance of MoCDMA systems. It is known that in the conventional radio-based CDMA (RdCDMA) systems, the BER performance of multiuser detectors usually slightly improves, as K/N is kept a constant, while K and N simultaneously increase. However, as shown in Fig. 5.7, for all the three FDE schemes, the BER performance is more dependent on the number of NMs K supported by the MoCDMA systems. Particularly in Fig. 5.7(c) and (d), when the MoCDMA systems supporting the same number of NMs sending at a relatively low rate, all detection schemes obtain similar BER performance. The reason behind this observation, which is distinctively different from that in the conventional RdCDMA, is that in MoCDMA, the noise power is coupled with the number of NMs simultaneously supported as well as with the different types of interference generated by all the NMs. Therefore, regardless of what spreading factor is used, the noise power increases with the increase of the number of NMs. Furthermore, the noise power is unable to be reduced by

the spreading and de-spreading operations in the MoCDMA systems.

Furthermore, when the bit rate is high, as shown in Fig. 5.7(a), the BER performance of the case of $N = 32,\ K = 8$ is worse than that of the case of $N = 16,\ K = 8$. This is because as the spreading factor increases while the bit duration is fixed, the ICI effect is enhanced. However, when one-stage DF-SIC is employed, the BER performance of the MF-assisted DF-SIC and MMSE-assisted DF-SIC in the case $N = 32$ becomes better than that in the case of $N = 16$. This implies that the increase of the spreading factor for a given bit-duration is beneficial to DF-SIC.

5.6 Conclusion

This chapter motivated to design low-complexity signal detection schemes for ICI and MAI suppression. To this purpose, we introduced the concept of FDE so that interference can be suppressed in parallel in the frequency domain. Specifically, we firstly developed three block-based FDE schemes in the principles of MF, ZF, and MMSE. It can be shown that all these equalizers have low-complexity and the capability to mitigate ICI. In more detail, MF-FDE is capable of maximizing a NM's SNR without being aware of the interference. The ZF-FDE with Wash codes can fully remove the ICI but amplifies noise. By contrast, the MMSE-FDE can take the advantages of both MF-FDE and ZF-FDE while avoiding their shortcomings, and hence, often achieves the best performance among these three FDE schemes. While these FDE schemes, especially, the ZF-FDE and MMSE-FDE, are efficient for ICI mitigation, their capability of MAI mitigation is limited. Then, in order to further mitigate MAI, the one- and two-stage DF-SIC schemes are proposed. Our studies show that while the complexity of the DS-SIC schemes is slightly higher than that of the corresponding FDE schemes, they are capable of providing significant performance gain for signal detection. Therefore, the detection schemes considered in this chapter can provide us with the design options to obtain a good trade-off between complexity and performance for the DMC systems required to support multiple-access transmissions. Additionally, from the performance comparison of the MoCDMA systems with different classes of spreading sequences, we found that the orthogonal spreading sequences result in the best performance. This result implies that by introducing a CP in transmission, the orthogonality of the received signals can be efficiently recovered with the aid of the FDE, especially, ZF- or MMSE-FDE, scheme, resulting in the effective reduction of ICI and MAI.

Chapter 6

Conclusions and Future Work

In this chapter, we first provide the conclusion summary of the thesis. Subsequently, several open issues for future research are presented.

6.1 Conclusions

This thesis has motivated to propose and investigate the multiple-access schemes for operation in DMC environments and to design the low-complexity detection schemes for the proposed multiple-access schemes. In more details, the research issues and conclusions can be summarized as follows.

In Chapter 2, a TS-MoSK modulation scheme has been firstly proposed to improve the BER performance of the original MoSK modulation scheme by employing more molecular types. We have introduced a passive ISIM at receiver and an active ISIM at transmitter to further mitigate ISI. The BER performance of the MoSK DMC systems with these schemes has been respectively investigated. Our comparison and studies demonstrated that TS operation can provide some reliability improvement and both ISIM schemes can enhance the ISIM achievement when proper design and system settings were given. Compared with the active ISIM, the passive ISIM is usually more efficient in terms of reliability achievement. However, active ISIM has the advantage of molecule-saving, whose influence on the communication environment is less than passive ISIM.

Then, in order to support multiple-access DMC, we have extended the TS-MoSK scheme to a multiple-access MTS-MoSK scheme. Correspondingly, low-complexity MS-MVD and EGCD have been proposed for detection in MTS-MoSK DMC systems. The error performance of MTS-MoSK DMC systems based on both analytical results and simulations has been compared and analyzed. The results show that MS-MVD usually outperforms EGCD at relatively low SNR, when a MTS-MoSK DMC system supports few NMs relative to chip-length L. Their BER performance is close to each other in a system supporting a large number of NMs. In terms of the impact of modulation order, more molecular types employed improves the error performance. Furthermore,

the optimum value for the length of chips per symbol duration depends on several other parameters like molecules released per symbol and number of NMs supported.

In Chapter 3, we have first proposed four interference cancellation relied detection schemes based on two fundamental single-user detection schemes (TMVD and EGCD), namely, TMVD-IIC, TMVD-MDDIC, EGCD-NIIC and EGC-IM. The impacts of the various parameters related to system design, signal propagation and detector design have been comprehensively investigated and demonstrated via simulations. Our studies demonstrate that both TMVD-IIC and TMVD-MDDIC are efficient to cancel MAI and attain very similar and improved BER performance, compared to that achieved by TMVD and EGCD. In addition, TMVD-IIC requires a lower complexity than TMVD-MDDIC. EGCD-NIIC can only significantly mitigate MAI in EGCD, when a large number of iterations is set, which results in high complexity. By contrast, the proposed EGC-IM scheme can solidly mitigate MAI at the cost of low complexity. Furthermore, we have proposed a SAML to provide a near-optimal BER performance criterion, whose complexity is however too high to be implemented in practical DMC environments.

In Chapter 4, a MoCDMA system based on BMoSK modulation that mirrors the conventional RdCDMA with BPSK modulation has been proposed. This multiple-access DMC system has been designed to be more practical because its information carrier is a pair of isomers and distances between NMs and AP are different. Our studies have revealed that in the MoCDMA systems employing BMoSK, although the background noise is still signal-dependent, it is stationary and its statistics is not related to the specific information transmitted. Owing to this property, the low-complexity MF, ZF and MMSE detection schemes are found to be similarly effective as in the conventional RdCDMA systems. We have considered the DMC scenario where NMs have different transmission distances to FC and, correspondingly, the uniform and channel-inverse based molecule-emission schemes have been introduced and compared. The performance results illustrate that the channel-inverse emission is capable of improving the reliability of the NMs relatively 'far away' from FC. This allows the detection of differently located NMs to achieve a similar BER performance and, hence, mitigate the near-far effect. Furthermore, our complexity analysis and performance comparison have revealed that the MF-, ZF-, and MMSE detectors are all low-complexity detection schemes, although the ZF- and MMSE-detectors require slightly higher computations than the MF-detector. Furthermore, these detectors provide the promising options for MoCDMA systems to attain a good trade-off between computational complexity of computation and information transmission reliability.

Finally in Chapter 5, we have first proposed three block-based FDE schemes, namely, MF-, ZF-, and MMSE-FDE for our MoCDMA systems to suppress ICI in parallel with lower complexity in the frequency domain. Our studies and results show that all detectors based on these equalizers require low-complexity and achieve acceptable detection reliability. Then, in order to further mitigate MAI, we have proposed the one- and two-stage DF-SIC schemes. It is shown that the DS-SIC schemes are capable of achieving significant performance improvement for signal detection at the

cost of several times higher complexity than that of the corresponding FDE schemes. Therefore, we can obtain a good trade-off between complexity and performance for the MoCDMA DMC systems by employing the promising options of detection schemes proposed in Chapter 5. In addition, comparing the BER performance of the MoCDMA systems employing different classes of spreading sequences, our studies show that the orthogonal spreading sequences like Walsh codes render the best performance. This observation implies that by inserting a CP in the transmission block, the orthogonality of received signals can be efficiently recovered with the assistance of the FDE, especially, ZF- or MMSE-FDE scheme, resulting in the effective suppression of ICI and MAI.

6.2 Future Work

Molecular communications (MC), as an interdisciplinary research hotspot, is still in its infancy. There are many research issues and a lot of challenges ahead. Specifically related to the studies in this thesis, there are some open issues as follows.

1. In Chapters 2 and 3, we studied the MTS-MoSK DMC systems with various non-coherent detection schemes. In the studies, we assumed that NMs are immobile and have the same distance from AP. In practice, both NMs and APs are likely to diffuse as molecules do and NMs may distribute in random locations. Hence, one important future research issue is to study the signaling, power-control, and the design of the interference cancellation schemes that are efficient for operation in MTS-MoSK DMC systems with mobile NMs and different transmission distances between NMs and AP. Considering these practical factors, the non-coherent detection schemes studied in Chapters 2 and 3 mat not be robust enough to achieve promising performance.

2. In the MoCDMA system model studied in Chapters 4 and 5 and also in most references, the medium diffusion coefficient is typically assumed to be constant and the locations of transceivers are also fixed. However, on many practical occasions, such as organisms and inter/intra cells, the channel environments are complicated and dynamic. In these DMC environments, the coherent detection schemes highly relying on the knowledge of CSI may not be efficient, as the CSI may be difficult to obtain in time-variant channels. Therefore, it is important to develop the low-complexity detectors that are efficient and robust to the time-varying channels or to investigate the high-efficiency channel estimation schemes to obtain the sufficiently reliable CSI for supporting the coherent detection.

3. Furthermore, in the MoCDMA systems studied in this thesis, only the BMoSK modulation scheme relying on two types of molecules is considered. Explicitly, system's data rate is limited by BMoSK. In order to increase the data rate of the BMoSK modulated MoCDMA, the BMoSK can be extended to design a joint modulation scheme by combining BMoSK with M-ary CSK (MCSK), forming a signaling scheme that mirrors the conventional multiple amplitude shift-keying (MASK). For instance, if BMoSK is integrated with 4CSK, there will still be two types

of molecules needed and the received signals can still be obtained as the difference of their concentration observations. However, the modulation scheme will have in total 8 modulation levels, the same as the 8MSK, which hence can convey 3 bits/symbol. In this way, the data rate of the individual NMs in MoCDMA systems can be increased, without significant increase of detection complexity.

4. Additionally, multiple input multiple output (MIMO) techniques have been intensively studied in the conventional radio-based communications. Inspired by the concept of MIMO, multiple receivers can also be adopted in the MTS-MoSK and MoCDMA systems to improve performance and mitigate interference. It is well-known that DMC is very sensitive to distance. Then, when there are several distributed receivers, each of them will only receive a few of strong signals from its nearby NMs, while the other NMs located relatively far away impose only small interference on these nearby NMs. Hence, information transmitted by the nearby NMs can be detected with higher reliability. On the other side, if there are several receivers having a similar distance from one NM, they may cooperate to detect this NM to enhance the detection reliability.

Bibliography

[1] I. F. Akyildiz, F. Fekri, R. Sivakumar, C. R. Forest, and B. K. Hammer, "Monaco: fundamentals of molecular nano-communication networks," *IEEE Wireless Communications*, vol. 19, pp. 12–18, Oct 2012.

[2] F. Al-Turjman and B. Deebak, "Privacy-aware energy-efficient framework using the internet of medical things for covid-19," *IEEE Internet of Things Magazine*, vol. 3, no. 3, pp. 64–68, 2020.

[3] Z. Ning, P. Dong, X. Wang, X. Hu, L. Guo, B. Hu, Y. Guo, T. Qiu, and R. Y. K. Kwok, "Mobile edge computing enabled 5g health monitoring for internet of medical things: A decentralized game theoretic approach," *IEEE Journal on Selected Areas in Communications*, vol. 39, no. 2, pp. 463–478, 2021.

[4] O. B. Akan, H. Ramezani, T. Khan, N. A. Abbasi, and M. Kuscu, "Fundamentals of molecular information and communication science," *Proceedings of the IEEE*, vol. 105, no. 2, pp. 306–318, 2017.

[5] J. M. Jornet and I. F. Akyildiz, "Information capacity of pulse-based wireless nanosensor networks," in *2011 8th Annual IEEE Communications Society Conference on Sensor, Mesh and Ad Hoc Communications and Networks*, pp. 80–88, June 2011.

[6] B. Atakan and O. B. Akan, "Carbon nanotube-based nanoscale ad hoc networks," *IEEE Communications Magazine*, vol. 48, pp. 129–135, June 2010.

[7] Z. Zhang, Y. Xiao, Z. Ma, M. Xiao, Z. Ding, X. Lei, G. K. Karagiannidis, and P. Fan, "6g wireless networks: Vision, requirements, architecture, and key technologies," *IEEE Vehicular Technology Magazine*, vol. 14, no. 3, pp. 28–41, 2019.

[8] R. A. Freitas, "Pharmacytes: An ideal vehicle for targeted drug delivery," *Journal of Nanoscience and Nanotechnology*, vol. 6, no. 9-10, pp. 2769–2775, 2006.

[9] B. P. Timko, T. Dvir, and D. S. Kohane, "Remotely triggerable drug delivery systems," *Advanced materials*, vol. 22, no. 44, pp. 4925–4943, 2010.

[10] G. Pan and L. Wang, "Swallowable wireless capsule endoscopy: Progress and technical challenges," *Gastroenterology research and practice*, vol. 2012, 2011.

[11] P. K. D. Pramanik, A. Solanki, A. Debnath, A. Nayyar, S. El-Sappagh, and K.-S. Kwak, "Advancing modern healthcare with nanotechnology, nanobiosensors, and internet of nano things: Taxonomies, applications, architecture, and challenges," *IEEE Access*, vol. 8, pp. 65230–65266, 2020.

[12] S. Ghavami, "Anomaly detection in molecular communications with applications to health monitoring networks," *IEEE Transactions on Molecular, Biological and Multi-Scale Communications*, vol. 6, no. 1, pp. 50–59, 2020.

[13] T. Nakano, Y. Okaie, S. Kobayashi, T. Hara, Y. Hiraoka, and T. Haraguchi, "Methods and applications of mobile molecular communication," *Proceedings of the IEEE*, vol. 107, no. 7, pp. 1442–1456, 2019.

[14] U. A. K. Chude-Okonkwo, R. Malekian, B. T. Maharaj, and A. V. Vasilakos, "Molecular communication and nanonetwork for targeted drug delivery: A survey," *IEEE Communications Surveys & Tutorials*, vol. 19, no. 4, pp. 3046–3096, 2017.

[15] I. Llatser, C. Kremers, D. N. Chigrin, J. M. Jornet, M. C. Lemme, A. Cabellos-Aparicio, and E. Alarcón, "Characterization of graphene-based nano-antennas in the terahertz band," in *2012 6th European Conference on Antennas and Propagation (EUCAP)*, pp. 194–198, 2012.

[16] X. Chen, M. Wen, C.-B. Chae, L.-L. Yang, F. Ji, and K. K. Igorevich, "Resource allocation for multiuser molecular communication systems oriented to the internet of medical things," *IEEE Internet of Things Journal*, vol. 8, no. 21, pp. 15939–15952, 2021.

[17] T. Nakano, M. J. Moore, F. Wei, A. V. Vasilakos, and J. Shuai, "Molecular communication and networking: Opportunities and challenges," *IEEE Transactions on NanoBioscience*, vol. 11, pp. 135–148, June 2012.

[18] N. Farsad, H. B. Yilmaz, A. Eckford, C. B. Chae, and W. Guo, "A comprehensive survey of recent advancements in molecular communication," *IEEE Communications Surveys Tutorials*, vol. 18, pp. 1887–1919, thirdquarter 2016.

[19] S. Iwasaki, J. Yang, and T. Nakano, "A mathematical model of non-diffusion-based mobile molecular communication networks," *IEEE Communications Letters*, vol. 21, no. 9, pp. 1969–1972, 2017.

[20] A. Ahmadzadeh, V. Jamali, A. Noel, and R. Schober, "Diffusive mobile molecular communications over time-variant channels," *IEEE Communications Letters*, vol. 21, no. 6, pp. 1265–1268, 2017.

[21] H. Unterweger, J. Kirchner, W. Wicke, A. Ahmadzadeh, D. Ahmed, V. Jamali, C. Alexiou, G. Fischer, and R. Schober, "Experimental molecular communication testbed based on magnetic nanoparticles in duct flow," in *2018 IEEE 19th International Workshop on Signal Processing Advances in Wireless Communications (SPAWC)*, pp. 1–5, 2018.

[22] M. Pierobon and I. F. Akyildiz, "Diffusion-based noise analysis for molecular communication in nanonetworks," *IEEE Transactions on Signal Processing*, vol. 59, no. 6, pp. 2532–2547, 2011.

[23] M. Pierobon and I. F. Akyildiz, "Noise analysis in ligand-binding reception for molecular communication in nanonetworks," *IEEE Transactions on Signal Processing*, vol. 59, no. 9, pp. 4168–4182, 2011.

[24] S. Kadloor, R. S. Adve, and A. W. Eckford, "Molecular communication using brownian motion with drift," *IEEE Transactions on NanoBioscience*, vol. 11, no. 2, pp. 89–99, 2012.

[25] M. Moore, A. Enomoto, T. Nakano, R. Egashira, T. Suda, A. Kayasuga, H. Kojima, H. Sakakibara, and K. Oiwa, "A design of a molecular communication system for nanomachines using molecular motors," in *Fourth Annual IEEE International Conference on Pervasive Computing and Communications Workshops (PERCOMW'06)*, pp. 6 pp.–559, 2006.

[26] A. O. Bicen, I. F. Akyildiz, S. Balasubramaniam, and Y. Koucheryavy, "Linear channel modeling and error analysis for intra/inter-cellular ca2+ molecular communication," *IEEE Transactions on NanoBioscience*, vol. 15, no. 5, pp. 488–498, 2016.

[27] M. Gregori and I. F. Akyildiz, "A new nanonetwork architecture using flagellated bacteria and catalytic nanomotors," *IEEE Journal on Selected Areas in Communications*, vol. 28, no. 4, pp. 612–619, 2010.

[28] V. Jamali, A. Ahmadzadeh, W. Wicke, A. Noel, and R. Schober, "Channel modeling for diffusive molecular communication—a tutorial review," *Proceedings of the IEEE*, vol. 107, no. 7, pp. 1256–1301, 2019.

[29] A. Noel, K. C. Cheung, and R. Schober, "Optimal receiver design for diffusive molecular communication with flow and additive noise," *IEEE Transactions on NanoBioscience*, vol. 13, no. 3, pp. 350–362, 2014.

[30] D. Kilinc and O. B. Akan, "Receiver design for molecular communication," *IEEE Journal on Selected Areas in Communications*, vol. 31, pp. 705–714, December 2013.

[31] A. Ahmadzadeh, H. Arjmandi, A. Burkovski, and R. Schober, "Comprehensive reactive receiver modeling for diffusive molecular communication systems: Reversible binding, molecule degradation, and finite number of receptors," *IEEE Transactions on NanoBioscience*, vol. 15, no. 7, pp. 713–727, 2016.

[32] Y. Deng, A. Noel, M. Elkashlan, A. Nallanathan, and K. C. Cheung, "Modeling and simulation of molecular communication systems with a reversible adsorption receiver," *IEEE Transactions on Molecular, Biological and Multi-Scale Communications*, vol. 1, no. 4, pp. 347–362, 2015.

[33] A. Noel, D. Makrakis, and A. Hafid, "Channel impulse responses in diffusive molecular communication with spherical transmitters," *arXiv preprint arXiv:1604.04684*, 2016.

[34] H. Arjmandi, A. Ahmadzadeh, R. Schober, and M. Nasiri Kenari, "Ion channel based bio-synthetic modulator for diffusive molecular communication," *IEEE Transactions on NanoBioscience*, vol. 15, no. 5, pp. 418–432, 2016.

[35] K. Aghababaiyan, V. Shah-Mansouri, and B. Maham, "Direction shift keying modulation for molecular communication," in *ICC 2020 - 2020 IEEE International Conference on Communications (ICC)*, pp. 1–6, 2020.

[36] R. Mosayebi, A. Ahmadzadeh, W. Wicke, V. Jamali, R. Schober, and M. Nasiri-Kenari, "Early cancer detection in blood vessels using mobile nanosensors," *IEEE Transactions on NanoBioscience*, vol. 18, no. 2, pp. 103–116, 2019.

[37] W. Wicke, A. Ahmadzadeh, V. Jamali, R. Schober, H. Unterweger, and C. Alexiou, "Molecular communication using magnetic nanoparticles," in *2018 IEEE Wireless Communications and Networking Conference (WCNC)*, pp. 1–6, 2018.

[38] A. Noel, K. C. Cheung, and R. Schober, "Improving receiver performance of diffusive molecular communication with enzymes," *IEEE Transactions on NanoBioscience*, vol. 13, no. 1, pp. 31–43, 2014.

[39] M. Pierobon and I. F. Akyildiz, "Diffusion-based noise analysis for molecular communication in nanonetworks," *IEEE Transactions on Signal Processing*, vol. 59, no. 6, pp. 2532–2547, 2011.

[40] N. Farsad, N. R. Kim, A. W. Eckford, and C. B. Chae, "Channel and noise models for nonlinear molecular communication systems," *IEEE Journal on Selected Areas in Communications*, vol. 32, pp. 2392–2401, Dec 2014.

[41] M. S. Kuran, H. B. Yilmaz, T. Tugcu, and I. F. Akyildiz, "Modulation techniques for communication via diffusion in nanonetworks," in *2011 IEEE International Conference on Communications (ICC)*, pp. 1–5, June 2011.

[42] I. Llatser, A. Cabellos-Aparicio, M. Pierobon, and E. Alarcon, "Detection techniques for diffusion-based molecular communication," *IEEE Journal on Selected Areas in Communications*, vol. 31, pp. 726–734, December 2013.

[43] F.-L. A. Lau, F. Büther, and B. Gerlach, "Computational requirements for nano-machines: there is limited space at the bottom," in *Proceedings of the 4th ACM International Conference on Nanoscale Computing and Communication*, pp. 1–6, 2017.

[44] L. P. Giné and I. F. Akyildiz, "Molecular communication options for long range nanonetworks," *Computer Networks*, vol. 53, no. 16, pp. 2753–2766, 2009.

[45] M. C. Gursoy, A. E. Pusane, and T. Tugcu, "Molecule-as-a-frame: A frame based communication approach for nanonetworks," *Nano Communication Networks*, vol. 16, pp. 45–59, 2018.

[46] J. Suzuki, S. Balasubramaniam, and A. Prina-Mello, "Multi-objective TDMA optimization for neuron-based molecular communication," in *BODYNETS*, 2012.

[47] M. J. Moore, Y. Okaie, and T. Nakano, "Diffusion-based multiple access by nano-transmitters to a micro-receiver," *IEEE Communications Letters*, vol. 18, pp. 385–388, March 2014.

[48] H. K. Rudsari, N. Mokari, M. R. Javan, E. A. Jorswieck, and M. Orooji, "Drug release management for dynamic tdma-based molecular communication," *IEEE Transactions on Molecular, Biological and Multi-Scale Communications*, vol. 5, no. 3, pp. 233–246, 2019.

[49] M. J. Moore and T. Nakano, "Multiplexing over molecular communication channels from nanomachines to a micro-scale sensor device," in *2012 IEEE Global Communications Conference (GLOBECOM)*, pp. 4302–4307, 2012.

[50] Y. Okaie, T. Nakano, M. Moore, and J.-Q. Liu, "Information transmission through a multiple access molecular communication channel," in *2013 IEEE International Conference on Communications (ICC)*, pp. 4030–4034, 2013.

[51] Y. Zamiri-Jafarian, S. Gazor, and H. Zamiri-Jafarian, "Molecular code division multiple access in nano communication systems," in *2016 IEEE Wireless Communications and Networking Conference*, pp. 1–6, April 2016.

[52] S. Korte, M. Damrath, M. Damrath, and P. A. Hoeher, "Multiple channel access techniques for diffusion-based molecular communications," in *SCC 2017; 11th International ITG Conference on Systems, Communications and Coding*, pp. 1–6, Feb 2017.

[53] H. Tezcan, S. Oktug, and F. N. Kok, "Neural delay lines for tdma based molecular communication in neural networks," in *2012 IEEE International Conference on Communications (ICC)*, pp. 6209–6213, June 2012.

[54] R. Yu, M. S. Leeson, and M. D. Higgins, "Multiple-access scheme optimisation for artificial neuronal networks," in *2014 9th International Symposium on Communication Systems, Networks Digital Sign (CSNDSP)*, pp. 428–433, July 2014.

[55] H. Tezcan, S. Oktug, and F. N. Kok, "Statistical multiplexing for neural nanonetworks in case of neuron specific faults," in *2014 6th International Congress on Ultra Modern Telecommunications and Control Systems and Workshops (ICUMT)*, pp. 254–259, 2014.

[56] I. Llatser, A. Cabellos-Aparicio, M. Pierobon, and E. Alarcon, "Detection techniques for diffusion-based molecular communication," *IEEE Journal on Selected Areas in Communications*, vol. 31, pp. 726–734, December 2013.

[57] C. T. Chou, "Maximuma-posterioridecoding for diffusion-based molecular communication using analog filters," *IEEE Transactions on Nanotechnology*, vol. 14, pp. 1054–1067, Nov 2015.

[58] L. Meng, P. Yeh, K. Chen, and I. F. Akyildiz, "On receiver design for diffusion-based molecular communication," *IEEE Transactions on Signal Processing*, vol. 62, pp. 6032–6044, Nov 2014.

[59] B. Tepekule, A. E. Pusane, H. B. Yilmaz, C. Chae, and T. Tugcu, "Isi mitigation techniques in molecular communication," *IEEE Transactions on Molecular, Biological and Multi-Scale Communications*, vol. 1, pp. 202–216, June 2015.

[60] N. Farsad and A. Goldsmith, "Neural network detection of data sequences in communication systems," *IEEE Transactions on Signal Processing*, vol. 66, no. 21, pp. 5663–5678, 2018.

[61] M. Damrath and P. A. Hoeher, "Low-complexity adaptive threshold detection for molecular communication," *IEEE Transactions on NanoBioscience*, vol. 15, pp. 200–208, April 2016.

[62] Z. Wei, W. Guo, B. Li, J. Charmet, and C. Zhao, "High-dimensional metric combining for non-coherent molecular signal detection," *IEEE Transactions on Communications*, vol. 68, no. 3, pp. 1479–1493, 2020.

[63] M. B. Dissanayake, Y. Deng, A. Nallanathan, M. Elkashlan, and U. Mitra, "Interference mitigation in large-scale multiuser molecular communication," *IEEE Transactions on Communications*, vol. 67, no. 6, pp. 4088–4103, 2019.

[64] K. Aghababaiyan, H. Kebriaei, V. Shah-Mansouri, B. Maham, and D. Niyato, "Enhanced modulation for multi-users molecular communication in internet of nano things," *IEEE Internet of Things Journal*, pp. 1–1, 2022.

[65] N. Garralda, I. Llatser, A. Cabellos-Aparicio, and M. Pierobon, "Simulation-based evaluation of the diffusion-based physical channel in molecular nanonetworks," in *2011 IEEE Conference on Computer Communications Workshops (INFOCOM WKSHPS)*, pp. 443–448, April 2011.

[66] M. Pierobon, I. F. Akyildiz, *et al.*, "Diffusion-based noise analysis for molecular communication in nanonetworks," *IEEE Transactions on Signal Processing*, vol. 59, no. 6, pp. 2532–2547, 2011.

[67] B. Atakan and O. B. Akan, "Deterministic capacity of information flow in molecular nanonetworks," *Nano Communication Networks*, vol. 1, no. 1, pp. 31–42, 2010.

[68] A. Zare, A. Jamshidi, and A. Keshavarz-Haddad, "Receiver design for pulse position modulation technique in diffusion-based molecular communication," in *2017 IEEE 4th International Conference on Knowledge-Based Engineering and Innovation (KBEI)*, pp. 0729–0733, Dec 2017.

[69] L. Shi and L. Yang, "Diffusion-based molecular communications: Inter-symbol interference cancellation and system performance," in *2016 IEEE/CIC International Conference on Communications in China (ICCC)*, pp. 1–6, July 2016.

[70] L. Shi and L. Yang, "Error performance analysis of diffusive molecular communication systems with on-off keying modulation," *IEEE Transactions on Molecular, Biological and Multi-Scale Communications*, pp. 1–1, 2018.

[71] A. W. Eckford, "Achievable information rates for molecular communication with distinct molecules," in *2007 2nd Bio-Inspired Models of Network, Information and Computing Systems*, pp. 313–315, Dec 2007.

[72] E. L. Cussler, *Diffusion: mass transfer in fluid systems*. Cambridge university press, 2009.

[73] D. Arifler, "Connectivity properties of free diffusion-based molecular nanoscale communication networks," *IEEE Transactions on Communications*, vol. 65, pp. 1686–1695, April 2017.

[74] L. Wang and A. W. Eckford, "Nonnegative code division multiple access techniques in molecular communication," in *2017 15th Canadian Workshop on Information Theory (CWIT)*, pp. 1–5, June 2017.

[75] G. Aminian, M. Farahnak-Ghazani, M. Mirmohseni, M. Nasiri-Kenari, and F. Fekri, "On the capacity of point-to-point and multiple-access molecular communications with ligand-receptors," *IEEE Transactions on Molecular, Biological and Multi-Scale Communications*, vol. 1, pp. 331–346, Dec 2015.

[76] A. Pouttu, H. Saarnisaari, and S. Glisic, "Noncoherent m mcsk-m mfsk modulation in rayleigh fading channel," in *MILCOM 2006 - 2006 IEEE Military Communications conference*, pp. 1–5, Oct 2006.

[77] S. Ahmed, R. G. Maunder, L. Yang, and L. Hanzo, "Iterative detection of unity-rate precoded ffh-mfsk and irregular variable-length coding," *IEEE Transactions on Vehicular Technology*, vol. 58, pp. 3765–3770, Sep. 2009.

[78] L.-L. Yang, *Multicarrier communications*. John Wiley & Sons, 2009.

[79] A. Ahmadzadeh, A. Noel, and R. Schober, "Analysis and design of multi-hop diffusion-based molecular communication networks," *IEEE Transactions on Molecular, Biological and Multi-Scale Communications*, vol. 1, pp. 144–157, June 2015.

[80] H. Arjmandi, A. Gohari, M. N. Kenari, and F. Bateni, "Diffusion-based nanonetworking: A new modulation technique and performance analysis," *IEEE Communications Letters*, vol. 17, pp. 645–648, April 2013.

[81] M. U. Mahfuz, D. Makrakis, and H. T. Mouftah, "A comprehensive analysis of strength-based optimum signal detection in concentration-encoded molecular communication with spike transmission," *IEEE Transactions on NanoBioscience*, vol. 14, pp. 67–83, Jan 2015.

[82] M. U. Mahfuz and D. Makrakis and H. T. Mouftah, "A comprehensive study of sampling-based optimum signal detection in concentration-encoded molecular communication," *IEEE Transactions on NanoBioscience*, vol. 13, pp. 208–222, Sep. 2014.

[83] D. J. Goodman, P. S. Henry, and V. K. Prabhu, "Frequency-hopped multilevel fsk for mobile radio," *The Bell System Technical Journal*, vol. 59, pp. 1257–1275, Sept 1980.

[84] N. Kim and C. Chae, "Novel modulation techniques using isomers as messenger molecules for nano communication networks via diffusion," *IEEE Journal on Selected Areas in Communications*, vol. 31, no. 12, pp. 847–856, 2013.

[85] W. Press and *et.al*, *Numerical Recipes in C: The Art of Scientific Computing*. Cambridge University Press, 2 ed., 1992.

[86] J. G. Proakis, *Digital Communications*. McGraw Hill, 5 ed., 2007.

[87] I. F. Akyildiz, M. Pierobon, S. Balasubramaniam, and Y. Koucheryavy, "The internet of bio-nano things," *IEEE Communications Magazine*, vol. 53, no. 3, pp. 32–40, 2015.

[88] B. Atakan, O. B. Akan, and S. Balasubramaniam, "Body area nanonetworks with molecular communications in nanomedicine," *IEEE Communications Magazine*, vol. 50, no. 1, pp. 28–34, 2012.

[89] M. Kuscu and O. B. Akan, "The internet of molecular things based on fret," *IEEE Internet of Things Journal*, vol. 3, no. 1, pp. 4–17, 2016.

[90] W. Gao, T. Mak, and L.-L. Yang, "Type-spread molecular communications: Principles and inter-symbol interference mitigation," in *ICC 2019 - 2019 IEEE International Conference on Communications (ICC)*, pp. 1–6, 2019.

[91] L. Felicetti, M. Femminella, and G. Reali, "A molecular communications system for live detection of hyperviscosity syndrome," *IEEE Transactions on NanoBioscience*, vol. 19, no. 3, pp. 410–421, 2020.

[92] A. Ghasempour, "Using a genetic-based algorithm to solve the scheduling optimization problem for long-range molecular communications in nanonetworks," in *2015 IEEE 26th Annual International Symposium on Personal, Indoor, and Mobile Radio Communications (PIMRC)*, pp. 1825–1829, 2015.

[93] N. Farsad, H. B. Yilmaz, C.-B. Chae, and A. Goldsmith, "Energy model for vesicle-based active transport molecular communication," in *2016 IEEE International Conference on Communications (ICC)*, pp. 1–6, 2016.

[94] B. Atakan and O. B. Akan, "Single and multiple-access channel capacity in molecular nanonetworks," in *International Conference on Nano-Networks*, pp. 14–23, Springer, 2009.

[95] M. C. Gursoy, A. E. Pusane, and T. Tugcu, "Molecule-as-a-frame: A frame based communication approach for nanonetworks," *Nano Commun. Networks*, vol. 16, pp. 45–59, 2018.

[96] W. Gao, T. Mak, and L.-L. Yang, "Molecular type spread molecular shift keying for multiple-access diffusive molecular communications," *IEEE Transactions on Molecular, Biological and Multi-Scale Communications*, vol. 7, no. 1, pp. 51–63, 2021.

[97] D. J. Goodman, P. Henry, and V. Prabhu, "Frequency-hopped multilevel fsk for mobile radio," *The Bell System Technical Journal*, vol. 59, no. 7, pp. 1257–1275, 1980.

[98] U.-C. Fiebig, "Iterative interference cancellation for ffh/mfsk ma systems," *IEE Proceedings-Communications*, vol. 143, no. 6, pp. 380–388, 1996.

[99] F. Yang and L.-l. Yang, "Low-complexity noncoherent fusion rules for wireless sensor networks monitoring multiple events," *IEEE Transactions on Aerospace and Electronic Systems*, vol. 50, no. 3, pp. 2343–2353, 2014.

[100] F. Yang and L.-L. Yang, "Frequency-hopping/m-ary frequency-shift keying wireless sensor network monitoring multiple source events," in *2012 IEEE 75th Vehicular Technology Conference (VTC Spring)*, pp. 1–5, 2012.

[101] I. Khan, K. Saeed, and I. Khan, "Nanoparticles: Properties, applications and toxicities," *Arabian Journal of Chemistry*, vol. 12, no. 7, pp. 908–931, 2019.

[102] A. Galal and X. Hesselbach, "Nano-networks communication architecture: Modeling and functions," *Nano Communication Networks*, vol. 17, pp. 45–62, 2018.

[103] J. Li, T. Peng, and Y. Peng, "A cholesterol biosensor based on entrapment of cholesterol oxidase in a silicic sol-gel matrix at a prussian blue modified electrode," *Electroanalysis: An International Journal Devoted to Fundamental and Practical Aspects of Electroanalysis*, vol. 15, no. 12, pp. 1031–1037, 2003.

[104] S. Zafar, M. Nazir, T. Bakhshi, H. A. Khattak, S. Khan, M. Bilal, K.-K. R. Choo, K.-S. Kwak, and A. Sabah, "A systematic review of bio-cyber interface technologies and security issues for internet of bio-nano things," *IEEE Access*, vol. 9, pp. 93529–93566, 2021.

[105] L. Felicetti, M. Femminella, G. Reali, T. Nakano, and A. V. Vasilakos, "Tcp-like molecular communications," *IEEE Journal on Selected Areas in Communications*, vol. 32, no. 12, pp. 2354–2367, 2014.

[106] I. F. Akyildiz and J. M. Jornet, "The internet of nano-things," *IEEE Wireless Communications*, vol. 17, no. 6, pp. 58–63, 2010.

[107] Akyildiz, Ian F and Jornet, Josep Miquel, "Electromagnetic wireless nanosensor networks," *Nano Communication Networks*, vol. 1, no. 1, pp. 3–19, 2010.

[108] I. F. Akyildiz, F. Brunetti, and C. Blázquez, "Nanonetworks: A new communication paradigm," *Comput. Netw.*, vol. 52, pp. 2260–2279, Aug. 2008.

[109] L. Parcerisa Giné and I. F. Akyildiz, "Molecular communication options for long range nanonetworks," *Comput. Netw.*, vol. 53, pp. 2753–2766, Nov. 2009.

[110] R. E. Ziemer and R. L. Peterson, *Digital Communications and Spread Spectrum Systems*. New York: Macmillan Publishing Company, 1985.

[111] Y. Tang, Y. Huang, C.-B. Chae, W. Duan, M. Wen, and L.-L. Yang, "Molecular-type permutation shift keying in molecular mimo communications for iobnt," *IEEE Internet of Things Journal*, vol. 8, no. 21, pp. 16023–16034, 2021.

[112] M. J. Moore and T. Nakano, "Oscillation and synchronization of molecular machines by the diffusion of inhibitory molecules," *IEEE Transactions on Nanotechnology*, vol. 12, no. 4, pp. 601–608, 2013.

[113] M. J. Moore, T. Nakano, A. Enomoto, and T. Suda, "Measuring distance from single spike feedback signals in molecular communication," *IEEE Transactions on Signal Processing*, vol. 60, no. 7, pp. 3576–3587, 2012.

[114] H. ShahMohammadian, G. G. Messier, and S. Magierowski, "Blind synchronization in diffusion-based molecular communication channels," *IEEE Communications Letters*, vol. 17, no. 11, pp. 2156–2159, 2013.

[115] L. S. Meng, P. C. Yeh, K. C. Chen, and I. F. Akyildiz, "On receiver design for diffusion-based molecular communication," *IEEE Transactions on Signal Processing*, vol. 62, pp. 6032–6044, Nov 2014.

[116] X. Wang and H. V. Poor, *Wireless Communication Systems - Advanced Techniques for Signal Reception*. Prentice Hall, 2003.

[117] H. L. V. Trees, *Optimum Array Processing*. Wiley Interscience, 2002.

[118] G. Golub and C. Loan, *Matrix Computations*. Baltimore and London: The Johns Hopkins University Press, 3 ed., 1996.

[119] L. Shi and L.-L. Yang, "Equalisation and performance of diffusive molecular communication systems with binary molecular-shift keying modulation," *IET Communications*, vol. 14, no. 4, pp. 549–555, 2020.

[120] A. Sohail and Y. Sanada, "Novel approximated zero forcing pre-coding technique with threshold for diffusion based molecular communication," *IEICE Communications Express*, vol. 9, no. 7, pp. 348–353, 2020.

[121] Sohail, Ahsan and Sanada, Yukitoshi, "Novel frequency domain equalization with threshold for molecular communication," *IEICE Communications Express*, vol. 9, no. 2, pp. 36–41, 2020.

[122] Y. Huang, F. Ji, Z. Wei, M. Wen, X. Chen, Y. Tang, and W. Guo, "Frequency domain analysis and equalization for molecular communication," *IEEE Transactions on Signal Processing*, vol. 69, pp. 1952–1967, 2021.

[123] M. Damrath, J. J. Koshy, and P. A. Hoeher, "Application of ofdm in diffusion-based molecular communication," *IEEE Transactions on Molecular, Biological and Multi-Scale Communications*, vol. 3, no. 4, pp. 254–258, 2017.

[124] L. Hanzo, L.-L. Yang, E.-L. Kuan, and K. Yen, *Single- and Multi-carrier DS-CDMA*. Chichester, United Kingdom: John Wiley and IEEE Press, 2003.

[125] B. Muquet, Z. Wang, G. Giannakis, M. de Courville, and P. Duhamel, "Cyclic prefixing or zero padding for wireless multicarrier transmissions?," *IEEE Transactions on Communications*, vol. 50, no. 12, pp. 2136–2148, 2002.

[126] D. Garg and F. Adachi, "Packet access using DS-CDMA with frequency-domain equalization," *IEEE Journal on Selected Areas in Communications*, vol. 24, pp. 161–170, Jan 2006.

[127] F. Adachi, T. Sao, and T. Itagaki, "Performance of multicode DS-CDMA using frequency domain equalisation in frequency selective fading channel," *Electronics Letters*, vol. 39, pp. 239–241, Jan 2003.

[128] K. Takeda and F. Adachi, "Joint transmit/receive one-tap minimum mean square error frequency-domain equalisation for broadband multicode direct-sequence code division multiple access," *IET Communications*, vol. 4, pp. 1752–1764, Sep. 2010.

[129] D. A. Bell, "The principles of sorting," *The Computer Journal*, vol. 1, no. 2, pp. 71–77, 1958.